Reconstruction of the Holocene climate using an atmosphere-ocean-biosphere model and proxy data

Dissertation

zur Erlangung des Doktorgrades der Naturwissenschaften
im Department Geowissenschaften der Universität Hamburg

vorgelegt von

Kerstin Haberkorn

aus

Lübeck

Hamburg

2013

Als Dissertation angenommen
vom Department Geowissenschaften der Universität Hamburg

auf Grund der Gutachten von
Prof. Dr. Klaus Fraedrich
und
Dr. Richard Blender

Hamburg, den 30. Januar 2013
Prof. Dr. Jürgen Oßenbrügge
Leiter des Departments Geowissenschaften

“Ihrer wahren Wesensbestimmung nach
ist die Wissenschaft das Studium der Schönheit der Welt.
Simone Weil (1909-43)

Abstract

The Holocene climate and vegetation evolution over Europe is investigated using different simulations performed with the general circulation model Planet Simulator. By doing so, the climatic boundary conditions are determined which have caused the early migration of humans over Europe and the beginning of farming-societies instead of hunters-gatherers. Whereas the latter part is not explicitly covered in this study, it is the larger framework and the leading motivation of this thesis. As a verification of the simulation results, they are compared to other climate and vegetation reconstructions obtained from models and proxy data. This study includes a detailed model validation to present-day climate as an essential prerequisite to the investigations of palaeoclimate. It is carried out for all variables which are important in the further progress of this thesis.

Besides seasonal differences, the results of the Holocene climate simulations clearly show regional variations in Europe, which are more pronounced in the precipitation trends. A general Holocene cooling trend can be observed over nearly the whole Europe, being strongest during the summer season. However, this is confirmed by proxy data only in the northern regions, whereas they show the opposite trend in the southern regions. Concerning the hydrological conditions, a weak drying trend can be observed in the northerly regions during summer as well as in the annual mean, and a moistening trend in the southern European summer, whereas the annual mean also shows a drying trend. Again, the trend is confirmed by the proxy data mainly in the northern regions.

The second, and most decisive part of this study is dedicated to the assimilation of proxy time series into the climate model. A new methodology is developed in this context and introduced using various applications. The dynamical method aims at the adjustment of the model climate to the proxy climate, thus the resimulation of the proxy given climate. Using a linear sensitivity relationship between the sea surface temperatures and the adjacent land temperatures, the model climate is approximated to the proxy climate. In total three different applications of this method are shown. Starting with pure time slice reconstructions of the early, mid- and late Holocene it is proceeded with a millennial-scale, full Holocene reconstruction. The last refinement is made up by an interactive reconstruction of climatological time periods of 40 years. Whereas the first alternative aims at showing the general applicability with regard to past climates including the emerging discrepancies, the other two are set up to improve the overall trend as well as the variability pattern. The reconstructed climates of all three approaches are then related to each other and compared to other reconstruction sources. It can be clearly concluded that this new methodology is applicable and may indeed be a promising new procedure to achieve a synthesis between climate models and proxy data.

In the context of the vegetation studies, the Planet Simulator is used to force the dynamic vegetation model CARAIB which is applied diagnostically in a very high resolution. The outcome is a detailed pattern of the European vegetation evolution over the Holocene. The results clearly indicate the effects of a changing climate on the vegetation. In selected regions, as for example Spain, a transition from drier, at the beginning of the Holocene, to wetter types at the late Holocene can be observed. Beyond that, the northward shift of the treeline as a direct consequence of the increased solar insolation during the early Holocene is very distinct, which relocates to the south in the further evolution of the Holocene.

However, the northerly shift as well as the general vegetation distribution in the northern regions of Europe may be a bit overestimated with regard to warmer types because of the missing land ice in the model. Additional aspects in the context of the vegetation studies are experiments which aim at the investigation of extreme land cover conversions on the climate. Assuming both a forest and a desert world, the influence on the large-scale circulation and the hydrological budget is analyzed. Using two phenomenological quantities, the Koeppen climate classification and the Budyko-Lettau dryness index, the impact of the changing climatic conditions on the global vegetation distribution as well as on the water and energy balance is investigated. In particular two regions are revealed to react very sensitively on external perturbations which can be seen as a proof that these static climate classifications can already give an estimate about potential modifications in the vegetation distribution. This feature is of special importance for the final point where, in the future, it is aimed at an inclusion of changes in land cover, via the modified parameters albedo and roughness length, into the climate model. Hereby, the focus is clearly set on the integration of anthropogenic land cover conversions.

Zusammenfassung

Mittels verschiedener Ansätze werden in dieser Arbeit die Entwicklung des Klimas und der Vegetation in Europa während des Holozäns untersucht. Dies impliziert verschiedene Simulationen mit dem Planet Simulator, einem Globalen Zirkulationsmodell der Atmosphäre. Auf diesem Wege sollen die klimatischen Randbedingungen ermittelt werden, die zu der frühen Besiedelung Europas und dem Beginn der landwirtschaftlichen Nutzung beigetragen haben. Obwohl letzteres nicht Bestandteil dieser Studie ist, sondern extern analysiert und daher hier nicht weiter berücksichtigt wird, dient es vor allem der Einordnung in einen wissenschaftlichen Kontext und somit der allgemeinen Zielsetzung dieser Arbeit. Zur Verifizierung der Simulationen werden die Ergebnisse mit denen anderer Modellstudien und Proxy-Rekonstruktionen verglichen. Am Anfang erfolgt eine Modell-Validierung in Bezug auf das heutige Klima und die im weiteren Verlauf dieser Arbeit benötigten Variablen.

Neben saisonalen Unterschieden zeigen die Ergebnisse der Klima-Simulationen des Holozäns klare regionale Variationen innerhalb Europas, vor allem im Niederschlagstrend. Eine nahezu generelle Abkühlung ist über das gesamte Holozän festzustellen, welche im Sommer am stärksten ist, jedoch nur in den nördlichen Regionen auch von den Proxy-Daten widergespiegelt wird, wohingegen diese in den südlichen Regionen einen entgegengesetzten Verlauf zeigen. Bezogen auf den Wasserhaushalt läßt sich sagen, daß die nördlichen Gebiete vornehmlich durch eine leichte Niederschlagsabnahme sowohl während des Sommers als auch im Jahresmittel gekennzeichnet sind, wohingegen im Süden eine Niederschlagszunahme festgestellt wird. Dieser Trend wandelt sich im Jahresmittel jedoch in eine Niederschlagsabnahme. Die stärkste Übereinstimmung mit den Proxy-Daten tritt auch hier über den nördlichen Regionen Europas auf.

In einem zweiten und dem zugleich wichtigsten Abschnitt dieser Arbeit geht es um die Einbeziehung von Proxy-Zeitserien in den Planet Simulator. Eine dafür entwickelte Methode wird vorgestellt und verschiedene Anwendungen gezeigt. Diese dynamische Methode zielt darauf ab, das Modell-Klima an das Proxy-Klima anzupassen, also das von den Proxies wiedergegebene Klima nachzusimulieren. Mittels einer linearen Sensitivitätsrelation zwischen der Meeresoberflächentemperatur und der Temperatur über den angrenzenden Landregionen werden Modell- und Proxy-Klima angenähert. Insgesamt werden drei verschiedene Anwendungen dieses Verfahrens gezeigt. Angefangen mit voneinander unabhängigen Rekonstruktionen einzelner Zeitscheiben für das frühe, mittlere und späte Holozän folgt im Anschluss eine Rekonstruktion jeder einzelnen Zeitscheibe von 11000 Jahren vor heute bis in die vorindustrielle Zeit. Als weitere Verfeinerung wird eine transiente Anpassung des Modell-Klimas vorgenommen, und zwar in klimatologischen Abschnitten von 40 Jahren. Während die erste Variante primär darauf abzielt, die generelle Durchführbarkeit der Methode und eventuelle Probleme aufzuzeigen, dienen die folgenden zwei Anpassungen einer Verbesserung im Hinblick auf den allgemeinen Trend und die Variabilitätsmuster. Das rekonstruierte Klima aller drei Varianten wird miteinander und mit anderen Datenquellen verglichen. Es zeigt sich deutlich, dass diese Methode anwendbar ist und ein vielversprechender neuer Ansatz sein kann, um eine Synthese zwischen Proxy-Daten und Klimamodellen herzustellen.

Im Zuge der Vegetationsstudien wird im folgenden das dynamische Vegetationsmodell CARAIB benutzt und diagnostisch, in einer sehr hohen Auflösung, mit dem simulierten Klima des Planet Simulators angetrieben. Somit ergibt sich erstmals ein detailliertes Bild der Vegetationsentwicklung in Europa für das gesamte Holozän. Die Ergebnisse zeigen deutlich

die Auswirkungen des sich ändernden Klimas auf die Vegetation. In einigen Regionen, so zum Beispiel Spanien, erfolgt ein Wechsel von eher trockenen Vegetationstypen zu Beginn des Holozäns zu feuchteren während der späteren Phase. Deutlich zu erkennen ist ebenfalls die Verschiebung der Wachstumszone der Wälder, die sich im Zuge der erhöhten Einstrahlung zu Beginn des Holozäns nach Norden verschiebt und sich im weiteren Verlauf wieder nach Süden verlagert. Allerdings wird diese Verschiebung nach Norden bzw. die grundsätzliche Vegetationsverteilung in den hohen nördlichen Breiten möglicherweise vom Modell etwas überschätzt aufgrund des fehlenden Land-Eises. Als zusätzlichen Punkt im Zusammenhang mit den Vegetationsstudien werden weitere Simulationen durchgeführt, die der Untersuchung der Auswirkungen von extremen Änderungen der Landoberfläche auf das Klima dienen. Ausgehend von einem globalen Wald bzw. einer globalen Wüste werden der Einfluss sowohl auf die großskaligen Zirkulationsmuster als auch auf den Wasserhaushalt untersucht. Mittels zweier phänomenologischer Größen, der Koeppen Klima-Klassifizierung einerseits und des Budyko-Trockenheitsindexes andererseits, werden die Auswirkungen dieser veränderten klimatischen Bedingungen auf die globale Vegetationsverteilung sowie den globalen Wasser- und Energiehaushalt untersucht. Es zeigt sich hier im speziellen, daß zwei Regionen besonders sensitiv auf die extremen Vegetationsbedingungen zu reagieren scheinen. Das bedeutet gleichzeitig, daß sich aus den statischen, und eher wenig komplexen, Vegetations-Klassifizierungen bereits erste Rückschlüsse ziehen lassen auf mögliche Veränderungen der Vegetation. Dies ist von besonderer Wichtigkeit für den abschließenden Punkt, da über eine Einbeziehung der durch die Oberflächenänderungen modifizierten Parameter Albedo und Rauhigkeitslänge in das Klimamodell eine spätere Einbindung der anthropogenen Landnutzungsänderungen angestrebt wird.

Contents

1 Introduction

The climate period, which is investigated in this study, is called the Holocene and is the current interglacial period. It has started around 11.6 kiloyear (kyr) before present (BP, relative to 1950) after the last glacial period and lasts until present-day. In general, this period in the geological past can be potentially seen as one of the most interesting epochs in history and equally one of the most investigated. The special feature of the Holocene is illustrated in terms of three characteristics which is the **solar insolation** and the **continental ice sheets** in Sect. 1.1.1 as well as the **early human influence** in Sect. 1.1.2.

1.1 The Holocene

1.1.1 Solar insolation and ice sheet

In the geological history of the Earth, a succession of glacials and interglacials, linked with the expansion and retreats of land ice sheets, is appearing on an irregular basis. The expansions and retreats of the continental ice sheets induce a large impact on a variety of climatic factors, such as temperature, mean sea level, radiation or hydrology. Consequently, the large ice sheets persisting from the previous glacial at the high northern latitudes of e.g. North America (Laurentide ice sheet) and Eurasia dramatically changed the climatic conditions downstream in the North Atlantic and Europe. This has been assessed in several studies so far, such as, e.g. *Mitchell et al.* (1988) and *Renssen et al.* (2005a, 2009). Over the last several decades it could be proved that this glacial-interglacial succession is governed by orbital parameters, determining the amount of incoming solar radiation at the top of the atmosphere. On the typical time scales for glacials and interglacials, i.e. over thousands and millennia of years, the Earth's orbital configuration is changing regularly, influencing the total, spatial (latitudinal) and temporal distribution of incoming solar radiation and imposing an external orbital forcing on the climate system (*Milankovitch theory*, *Milankovitch* 1930). This configuration is mainly characterized by the parameters eccentricity, obliquity and precession of the vernal equinox. These orbital parameters vary on periods of approximately 100,000 years for the eccentricity, 40,000 years for the obliquity and 20,000 years for the precession (*Wanner et al.* 2008). The eccentricity modulates the amplitude of the precessional effect, which itself determines the orientation of the Earth relative to the Sun, i.e. perihelion (closest distance between Earth and Sun) and aphelion (largest distance). Over long time scales, a progress of the dates of perihelion and aphelion through the seasons occurs; thus, this parameter lately controls the seasonal

variations of insolation. Following Kepler's laws, this is also influencing the length of the season: The season closer to the perihelion is shorter. The third decisive parameter, the obliquity, determines the contrast between low and high latitudes.

These characteristics can also be identified in Figure 1.1; in Figure 1.1 a, the incoming solar radiation is longitudinally averaged, presented as the anomaly relative to 0 kyr BP (0k) as a function of months. The changing orbital configurations clearly lead to modifications of both the meridional and the seasonal distribution of the insolation. The seasonal deviation results in an enhanced magnitude of the seasonal cycle during the early and mid-Holocene, i.e. a positive (negative) anomaly occurs during summer (winter). At the same time the spring and summer seasons were shorter and the autumn and winter seasons were longer over the Northern Hemisphere, due to summer solstice being close to perihelion. Regarding the strength of the seasonal cycle, hemispheric differences are obvious. The strongly intensified (reduced) insolation during boreal summer (boreal winter) is inducing an increase in the amplitude of the seasonal insolation cycle in the Northern Hemisphere; on the contrary, over the Southern Hemisphere the effect is flipped and, more important, also dampened, which leads to a weaker seasonal cycle. Apart from this hemispheric asymmetric seasonal cycle, it is also latitudinally dissimilar, as the maxima of insolation are clearly restricted to the high latitudes in the respective seasons (i.e. obliquity). Both the seasonally and latitudinally different distribution in the solar radiation are, of course, inducing a strong impact on the climate (*Imbrie et al.* 1992). Figure 1.1 b shows the modifications in the seasonal cycle in more detail. Presented are the anomalies relative to 0 kyr BP in 60°N for selected months of each season, starting with the early Holocene at 9k. The June insolation is strongly increased by up to 40 W/m^2 at the early Holocene compared to the preindustrial, whereas during September, it is decreased by 20 W/m^2. March and December are showing a similar signal. Assigned to an annual signal, these changes in insolation are small and do not exceed 4 W/m^2. The importance of the seasonal insolation cycle on the mean climate has been shown in several studies on the Holocene (e.g. *Braconnot et al.* 2007b). This is lately based on the general consensus in the scientific community, founding on the pioneering study (*Crucifix et al.* 2002) by *Kutzbach and Otto-Bliesner* (1982), stating that this astronomical forcing is the driving mechanism for all climatic variations. It can thus be calculated precisely not only for the past but also for the future (*Berger* 1978b). The relationship between annual and seasonal signals, i.e. the latter are influencing the annual pattern (*Fischer and Jungclaus* 2010), and the inherent implications for this study are discussed in more detail in Section 5.3. The evolution of the greenhouse gas (GHG) CO_2 is equally shown in Figure 1.1 b. It shows the common trend in CO_2 with comparably low values at 9k and a strong increase over the last millennium. The values are taken from Taylor Dome (*Indermühle et al.* 1999), and are annually prescribed in all Holocene simulations with PlaSim. Thus, this acts as an additional forcing on the climate system.

Following the notation in *Wanner et al.* (2008), the Holocene can be roughly divided into three periods which themselves have specific characteristics:

–> 11.6 kyr BP to 9 kyr BP as the "first phase" or early Holocene.

–> 9 kyr BP to 5-6 kyr BP as the "second phase" or mid-Holocene, including the "climate optimum"

–> 5-6 kyr BP to the preindustrial as the "third phase" or late Holocene.

With regard to the remarks about the Holocene insolation, these three periods, i.e. the classification in the early, mid-and late Holocene, can also be understood in terms of the orbital forcing which was maximal in the early Holocene. Whereas the first melting stages of the large ice sheet over North America designate the starting point of the Holocene, its persistence posed a strong cooling on the climate of the

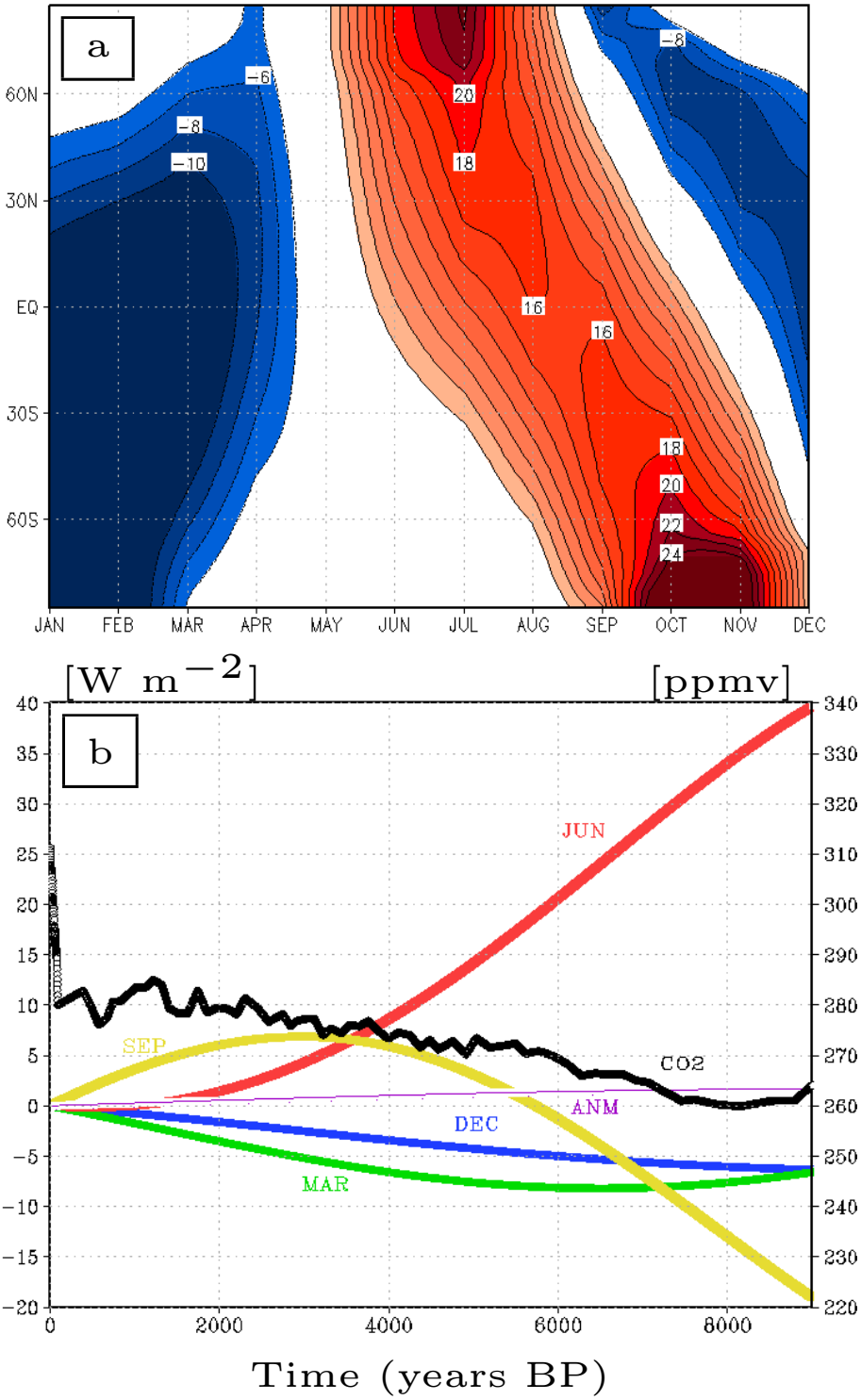

Figure 1.1: Applied orbital forcing during the Holocene, given by the incoming solar radiation at the top of the atmosphere [W/m^2], relative to 0 kyr BP; (a) longitudinally averaged and presented as a function of months, (b) at 60°N for selected months, and prescribed greenhouse gas forcing (given by the atmospheric concentration of CO_2).

North Atlantic and Eurasia, instead of a warming which could be expected due to the enhanced insolation. The second phase of the mid-Holocene corresponds still to a period of continuing high summer insolation in the Northern Hemisphere but the North American ice sheet was no longer large enough to influence the climate. This then led to the Holocene climatic optimum and the greening of the Sahara (e.g. *de Noblet et al.* 1996; *Claussen and Gayler* 1997; *Claussen et al.* 1999). In this period, the surface boundary conditions like the continental ice or the sea level were already comparable to modern times. Moreover, the CO_2 concentration was similar to the preindustrial times. The third phase of the late Holocene then shows a declining summer insolation in the Northern Hemisphere.

Calendar These remarks prove the enormous impact of this insolation forcing not only on the Holocene climate but also on the overall configuration of months and seasons. According to the aforementioned comments about the insolation cycle - the dates of maximum and minimum insolation are changing over the Holocene, including the length of the seasons - it is indeed worthwhile to shortly address these impacts which mark one of the essential issues in palaeoclimatology. Therefore, some concluding comments are made concerning the calendar. This must be defined for experiments on past climates to avoid misinterpretations. Following the altering insolation cycle during the Holocene, one consequently ought to adapt the calendar according to these changes. Although an adjustment of the months to account for the insolation changes is suggested by *Joussaume and Braconnot* (1997) of being more appropriate for the comparison of model outputs with palaeoreconstructions (*Crucifix et al.* 2002; *Marzin and Braconnot* 2009), it is confined to the modern calendar of 12 months and 30 days each in the PlaSim configuration for all simulations and thus to the common seasons DJF and JJA. This is additionally motivated by the new approach to reconstruct the Holocene climate on the basis of seasonal sensitivities (cf. Sect. 5.3) and also in line with other model studies (e.g. *Luterbacher et al.* 2004; *Renssen et al.* 2005a; *Wanner et al.* 2008).

1.1.2 Early human climate interaction

This subsection is now dedicated to the further motivation of this study and the larger framework it is embedded in. The Holocene is not only specific because of its aforementioned characteristics. Moreover, the current interglacial is also rather specific in terms of the onset and, in the following, increasing human influence on climate, which has culminated, for the time being, in the industrialization around the late 18th century. In general terms, the Holocene climate has been relatively stable compared to previous epochs (*Petit et al.* 1999; *Keigwin and Boyle* 2000; *Feynman and Ruzmaikin* 2007). This has slowly but continuously led to the first settlements of humans, which additionally implied a switch from hunting-gathering to farming. This switch had enormous impact on the composition of the landscapes as the humans started to burn forests for hunting, pastoralism and agriculture. The procedure of deforestation, also in terms of natural and human induced fires (*Olsson et al.* 2010), has imposed an important influence on the climate system through various aspects, modifying land surface properties like albedo, evapotranspiration, i.e. soil moisture, and surface roughness. These parameters have in common that they all affect the near surface energy balance as well as the radiation and hydrological budgets and also large-scale circulation patterns. In addition to these so called biogeophysical effects, deforestation is leading to emissions of greenhouse gases such as CO_2, i.e. biogeochemical effects, which also have a significant climatological impact. All these processes are climatically active on different temporal and spatial scales and may also be of opposite sign and thus counteracting. Because of these special features, they are subject of many studies so far. Without putting too much emphasis on individual studies, those of, for example, *Claussen et al.* (2001), *Bathiany et al.* (2010) or *Avila et al.* (2012) focus more on the

different aspects regarding the biogeophysical or biogeochemical effects of land cover change. Other authors in contrast are trying to quantify the human induced (historic) land cover change, such as, e.g. *Brovkin et al.* (1999, 2006), *Lynch et al.* (2003) or *Findell et al.* (2007) and the ones by *Pongratz et al.* (2008, 2009a,b, 2010); an approach, which also fits into the wider context of this study. *Matthews et al.* (2004) consider both natural and anthropogenic (human induced) land cover changes in their climate model studies. This onset of agriculture during the Holocene is also called the "Neolithic Revolution". Without going too much into detail here, this new development has started in the Near and Far East in the very early Holocene around 9 kyr BP. From there, it has spread over Europe over the subsequent centuries, determined by local and regional climatic and environmental properties. This has been verified by archaeological data (e.g. *Gronenborn* 2005; *Casely and Dugmore* 2007; *Lemmen et al.* 2011) and also by modelling studies (*Lemmen* 2009; *Lemmen et al.* 2011) on this topic. Recent analyses of early Holocene land use and climate impact (*Olofsson and Hickler* 2008; *Kaplan et al.* 2011) also identified Europe as one of the key regions for human-climate interactions, with a further validation from palaeobotany (e.g. *Gaillard et al.* 2010) of the feasibility of the simulated human-climate interaction for Europe. Thus, the main region of interest throughout this study is the European sector with a focus on European temperature and precipitation changes. In *Lemmen* (2009) and *Lemmen et al.* (2011), the authors are using a specific socio-technological model, the Global Land Use and Technological Evolution Simulator (GLUES, *Wirtz and Lemmen* 2003) to analyze this human movement, with regard to climatic and biogeographical boundary conditions, through the calculation of particular parameters like human population density, technological changes and agricultural activity which are given by dynamical hindcasts of the socio-economic development. In *Lemmen* (2009), the author quantifies the early Holocene, human induced land cover changes in terms of global carbon releases. It turns out that the model GLUES is indeed capable to provide a consistent and realistic hindcast of the early human cultures and that, despite some existing uncertainties, the land cover and technology modelling yields realistic estimates of land use changes and emissions on spatially varying scales (*Lemmen* 2009). The study by *Lemmen et al.* (2011) focusses more on the spatiotemporal pattern of the onset and expansion of agriculture across Eurasia and gives a wide overview about the development of the specific human-related properties. The settlement of humans also entailed a variety of aftereffects, as they started to organize themselves in more and more developed cultures. This implied further population growth and technological adaptation, which are both calculated by the model. Through this evolution, the humans consumed a growing amount of resources, which further affected climate. Thus, a distinct early human-climate interaction is not only hypothesized but rather becomes obvious with climate acting on the humans to that effect that they started to settle, and subsequently altered, at least the local, climatic conditions. Although the stable climate during the Holocene has initially helped humankind to settle and to create agropastoral societies (*Feynman and Ruzmaikin* 2007), climate has also had a limiting effect on the societies throughout the Holocene. Primarily strong and abrupt climate fluctuations may have been responsible for that, just as the so-called 8.2 kyr event (*Alley et al.* 1997; *Alley and Ágústsdóttir* 2005, cf. Sect. 5.1.2) or others around 4 kyr BP as addressed in *Cullen et al.* (2000), *Drysdale et al.* (2006) or *D'Andrea et al.* (2011). These unforeseen climate events dramatically influenced their prevailing subsistence way of life, e.g. regarding the water supply or the prevailing temperatures, and thus led, because of their less developed adaptation abilities, to a partial collapse of cultures or to migration waves (*Lemmen and Wirtz* 2010), recognizable for example in lake sediments (*deMenocal* 2001). Thus, an interplay of the increasing amount of resources the humans have disposed in their evolution together with exceptional climatic conditions may have potentially been, at least partly, responsible for the demise of whole cultures and societies (*Büntgen et al.* 2011). This two-sided approach of climatic as well as anthropogenic factors is, for example, hypothesized for the demise of the Maya culture by *deMenocal* (2001) and *Oglesby et al.* (2010), where their

increased deforestation may have led to less precipitation and thus stronger and longer-lasting droughts which themselves may have affected the Maya culture enormously. This topic is also addressed in a very elaborate manner by *Diamond* (1997, 2006) for several regions and cultures around the world. Especially with regard to the dominating impact in general, which climate had on the evolution of mankind, a knowledge of Holocene climate variability is of major importance, to also learn about the human's potential ability to adapt to climate or not. The pattern of natural climate variability, its amplitude and occurrence on different time-scales, being an important, if not the essential, source of uncertainty (*Hegerl et al.* 2007; *Jansen et al.* 2007), has been analyzed in many studies so far, such as by e.g. *Mayewski et al.* (2004), *Rimbu et al.* (2004) or *Wirtz et al.* (2010). The results of the latter study by *Wirtz et al.* (2010), regarding variability patterns using a variety of proxy time series, are essential for the further analyses in the forthcoming chapters.

1.2 Aim of this study-Thesis outline

In the following lines, the motivation of this study is shortly summarized and also contains the outline of this study. The larger framework, in which this study is embedded in, aims at finding answers to the question:

Which linkages exist between climate and preindustrial cultures?

This question can be seen in the context of an "early Climate Change Detection", thus the detection and attribution of climate change to human influences (*Jones et al.* 1998) - a notation which is normally used for modern climate change. In conjunction with this debate, the leading question is thus further motivated by the fact, that the early humans may have already been responsible for a non-negligible greenhouse effect. The historic land cover change is hypothesized to have led to the first greenhouse era (*Ruddiman* 2003). It is thus of special importance with regard to the discussions about climate change and the dictum that the key to understanding the future is to understand the past. A good overview of the complex structure of the (historic) human-climate interaction regarding different aspects is given by *Dearing* (2006), who is equally pointing at the specific challenges and thus the importance of an improved analysis of this interaction. The subsequent quantification of the human evolution with the model GLUES and their influence on climate goes beyond the scope of this study and is therefore not part of it. However, the combination of an Earth System Model, the Planet Simulator, with the socio-technological model GLUES, both forced by proxy time series, is a completely new approach in the scientific field, also with regard to the examination of the Holocene (climate), and significant improvements in the analysis of the early human-climate interaction can be expected.

Following these remarks and those of the previous introductory section, the outline of this thesis is rather straightforward. It consists of five chapters - including the introduction of the climate model Planet Simulator (PlaSim hereinafter) - to account for the major issues which have been addressed at the beginning of this chapter.

Each chapter begins with a short introduction to the specific problem and closes with a summary and discussion of the results and some concluding remarks.

Chapter 3 is dedicated to a present-day model evaluation of the Planet Simulator. This is a necessary prerequisite for the later studies of palaeoclimate and is part of an internal, scientific report[1]. The focus is set on individual parameters which are of further importance for the Holocene climate reconstruction

[1] Haberkorn, K., F. Sielmann, F. Lunkeit, E. Kirk, A. Schneidereit, and Klaus Fraedrich, 2009: Planet Simulator Climate, Meteorological Institute, University of Hamburg

as well as for the vegetation studies. Accordingly, both the global and the European perspective are considered. Thus, to learn about the linkages between climate and humans, the main objective of this study is a as realistic as possible simulation of the climatic conditions, including the vegetational boundary conditions, which are both leading to the settlement of early humans during the Holocene. The reliability of this aspired climate simulation shall be provided by global proxy time series which need to be assimilated into the climate model.

In Chapter 4, the Holocene climate is, at first, reconstructed using a transient simulation with the fully coupled, and thus optimal, version of PlaSim, i.e. atmosphere, ocean and biosphere. In this context, data of a transient Holocene simulation with PlaSim and the LSG ocean have been sent to the PANGAEA, a database for "Earth and Environmental Science". These results will serve as a first indication of the evolution of the European climate during the Holocene. In comparison to other existing model and proxy studies, at the same time the performance of this model setup is validated and potential discrepancies are discovered and discussed. Moreover, the results of this chapter are also used for a comparison to those of the subsequent chapter.

Chapter 5 addresses one of the leading issues of this study, which is the "Assimilation of proxy time series into the Planet Simulator". Assuming in either case an existing discrepancy between models and proxy data, the intention is to adjust the model to reliable proxy data to establish the prevailing climate conditions in Europe during the Holocene. The methodology for the assimilation is introduced, which is newly developed in this context. Afterwards, the results of various applications of this method for the reconstruction of Holocene climate are shown. The first part of this chapter with a description of the method and the first application on the reconstruction of selected time slices (Sections 5.3 and 5.4), has been published in Earth System Dynamics Discussion[2] and is included here with editorial adjustments. Confinements of the methodology and a comparison to SST-proxies are also included in this chapter. A discussion of the results is completing this chapter. The results are intercompared with each other as well as to those of the preceding chapter and the existing studies on the European palaeoclimate. Although this chapter is mainly dedicated to the implementation of this new methodology, the analysis of the results is essential for the discussion with regard to the general applicability of this approach as a potentially useful tool in combining models and palaeoobservations. It may thus be a beneficial new aspect in the palaeoclimate modelling community.

In Chapter 6, a set of vegetation models is used to study diverse vegetation-related aspects. In principle, it is distinguished between two parts here, which is the European vegetation evolution during the Holocene and the influence of vegetation extremes on the climate. The results of the latter are then related to the remarks in the previous section about early anthropogenic land cover changes and thus fit into the wider motivation for this study.

This will be the basis to stimulate further research on this topic, i.e. forcing a climate model with results from anthropogenic land cover changes, which will be discussed in the last chapter (Chapt. 7). This will conclude the thesis with a summary of the most important results of all chapters, and furthermore propose and discuss possible directions of future research.

[2]Haberkorn, K., C. Lemmen, R. Blender, and K. Fraedrich, 2012: Iterative land proxy based reconstruction of SST for the simulation of terrestrial Holocene climate. Earth System Dynamics Discussions, 3, 149-200

2 The climate model Planet Simulator

This chapter serves to introduce the climate model which is used throughout this study. All experiments in this work are carried out with the Planet Simulator, which is an Earth System model of intermediate complexity (EMIC). A comprehensive description of the model and its subcomponents is provided including the implemented parameterizations, and a short overview is given about the most recent applications of PlaSim. A model validation for present-day climate is then handled in the next chapter as the outcome is of special importance for the palaeoclimate studies in general and the vegetation studies in particular, which are introduced at a later stage.

2.1 Model Setup

2.1.1 Model description

PlaSim is a General Circulation Model (GCM), whose dynamical core (PUMA-2) for the atmosphere is adopted from PUMA (Portable University Model of the Atmosphere, *Fraedrich et al.* 2003, 2005c). Besides the atmospheric part, other climate subsystems are included with highly reduced, linear dynamics: a land surface with biosphere or, e.g. a mixed layer-ocean with sea ice. This is illustrated in Figure 2.1 and will be further described below. The atmosphere is modelled using the moist primitive equations for the vorticity, divergence, temperature and the logarithm of the surface pressure. The equations describe the momentum, energy and mass balance and are solved numerically in the spherical (λ, φ, σ) coordinate system, where λ represents the longitude, φ the latitude and σ the pressure. The vertical component is normalized with the surface pressure ($\sigma = p/p_s$) to obtain a terrain following σ-coordinate system. Here, the top of the atmosphere and the surface correspond to $\sigma = 0$ (p=0) and $\sigma = 1$ with $p = p_s$ respectively, thus σ is decreasing with height. In the σ-system, the four abovementioned equations are described in spherical harmonics and form up as:

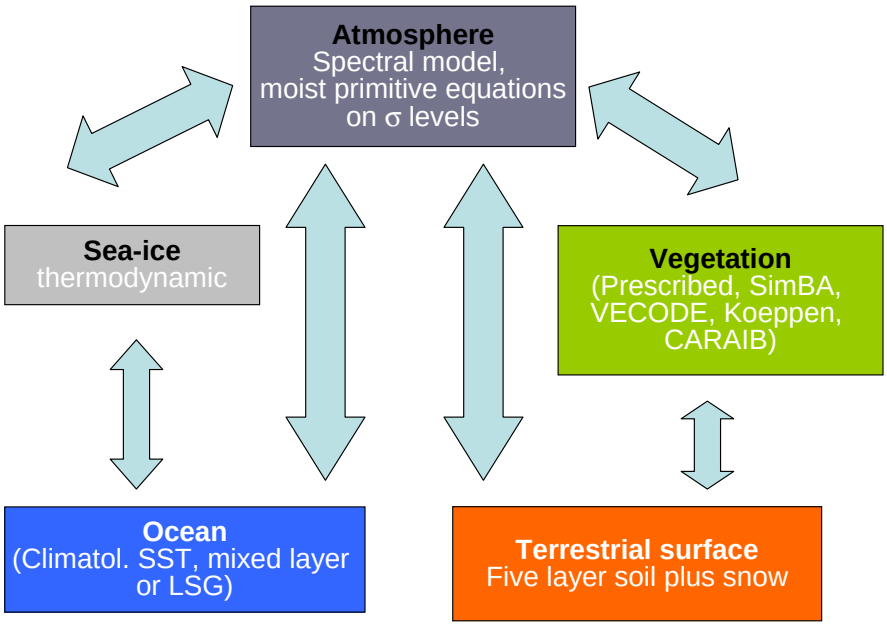

Figure 2.1: Available components (couplings) of the Planet Simulator.

Conservation of momentum

Vorticity

$$\frac{\partial(\zeta+f)}{\partial t} = \frac{1}{(1-\mu^2)}\frac{\partial F_v}{\partial \lambda} - \frac{\partial F_u}{\partial \mu} + P_\zeta \tag{2.1}$$

Divergence

$$\frac{\partial D}{\partial t} = \frac{1}{(1-\mu^2)}\frac{\partial F_u}{\partial \lambda} + \frac{F_v}{\partial \mu} - \nabla^2 E - \nabla^2(\phi + T_0 ln p_s) + P_D \tag{2.2}$$

Hydrostatic approximation

Hydrostatic equation

$$0 = \frac{\partial \phi}{\partial(ln\sigma)} + T \tag{2.3}$$

Conservation of mass

Continuity equation

$$\frac{\partial(ln p_s)}{\partial t} = -\int_0^1 A d\sigma \tag{2.4}$$

First Law of Thermodynamics

$$\frac{\partial T^{'}}{\partial t} = F_T - \dot{\sigma}\frac{\partial T}{\partial \sigma} + \kappa W T + \frac{J}{c_p} + P_T \tag{2.5}$$

The following relations have been used in the Equations (2.1)-(2.5):

$$F_u = (\zeta + f)V - \dot{\sigma}\frac{\partial U}{\partial \sigma} - T^{'}\frac{\partial ln p_s}{\partial \lambda} \tag{2.6}$$

$$F_v = -(\zeta + f)U - \dot{\sigma}\frac{\partial V}{\partial \sigma} - (1-\mu^2)T^{'}\frac{\partial ln p_s}{\partial \mu} \tag{2.7}$$

$$F_T = -\frac{1}{(1-\mu^2)}\frac{\partial (UT^{'})}{\partial \lambda} - \frac{\partial (VT^{'})}{\partial \mu} + DT^{'} \tag{2.8}$$

$$E = \frac{U^2 + V^2}{2(1-\mu^2)} \tag{2.9}$$

$$\dot{\sigma} = \sigma \int_0^1 A d\sigma - \int_0^\sigma A d\sigma \tag{2.10}$$

$$W = \frac{\omega}{p} = \vec{V} \cdot \nabla ln p_s - \frac{1}{\sigma}\int_0^\sigma A d\sigma \tag{2.11}$$

$$A = D + \vec{V} \cdot \nabla ln p_s = \frac{1}{p_s}\nabla \cdot p_s \vec{V} \tag{2.12}$$

The applied parameters are summarized in Table 2.1. In the horizontal, the equations are solved using the spectral transform method (*Eliasen et al.* 1970; *Orszag* 1970). In the vertical, finite differences are used with the vertical velocity being defined between the full levels, on which the prognostic variables temperature, moisture, vorticity and divergence are computed. The equations are integrated in time with a leap-frog semi-implicit time-stepping (*Hoskins and Simmons* 1975; *Simmons et al.* 1978) with Robert/Asselin time filter (*Robert* 1981; *Asselin* 1972). The horizontal resolution depends on the truncation used, i.e. either T21, T31 or T42. The first corresponds to a number of 64 longitudes and 32 latitudes on the corresponding Gaussian grid. In T31 and T42, the number of grid points increase up to 96 x 48 and 128 x 64 respectively. The model is available as an open source code (http://www.mi.uni-hamburg.de/plasim). For more details concerning the model description, it is referred to the Planet Simulator reference manual by *Lunkeit et al.* (2010), for on overview see *Fraedrich et al.* (2005a) or *Fraedrich* (2012).

2.1.2 Parameterizations

To finalize the description of PlaSim, a short overview of the parameterizations is given which are applied to consider the effects of unresolved processes in the model. Compared to other more comprehensive models, PlaSim uses simplified parameterizations.

ζ	relative vorticity	t	time
f	planetary vorticity	$\mu =$	$\sin(\varphi)$
D	divergence	φ	latitude
p	pressure	λ	longitude
p_s	surface pressure	$U =$	$u\cos\varphi$
$\sigma = p/p_s$	vertical coordinate in the $\sigma - system$	$V =$	$v\cos\varphi$
T	temperature	u	zonal velocity
T_0	reference temperature ($T_0 = 250K$)	v	meridional velocity
$T' = T - T_0$	temperature deviation of T_0	$\dot{\sigma} = d\sigma/dt$	vertical velocity in the $\sigma - system$
c_p	specific heat capacity for dry air at constant pressure	$\omega = dp/dt$	vertical velocity in the p-system
κ	adiabatic coefficient	ϕ	geopotential
J	diabatic heating	E	kinetic energy
P_λ, P_D, P_ζ	parameterizations of the divergence of the turbulent fluxes		

Table 2.1: List of symbols.

Land surface and soil

The terrestrial component in PlaSim contains the calculation of temperatures for the surface and the soil, a soil hydrology and a river transport scheme. In addition, surface properties such as the albedo, the roughness length or the evaporation efficiency are provided. As, up to the end of this work, a coupling to an external glacier module is not available, glaciers are treated like other land points with the appropriate surface and soil properties for ice, for example affecting the albedo.

The surface temperature is computed from the linearized energy balance of the uppermost 0.2 meters of the ground. Below this top layer, the soil column is discretized into five layers of thickness (0.4 m, 0.8 m, 1.6 m, 3.2 m and finally 6.4 m), where the temperatures are computed under consideration of the energy balance, which further takes into account the conductive heat flux between these layers.

The parameterizations for the soil hydrology imply the budgets for the snow and the soil water amount. The local runoff, which is induced by soil water exceeding the field capacity, is transported to the ocean by a river transport scheme with linear advection (*Sausen et al.* 1994). For each grid box (land and ocean points), the river amount is computed.

A further necessity is the setup of additional parameters characterizing the land surface of each grid box. These parameters are, for example, the land-sea mask and the orography, the global distribution of the surface roughness length, a background albedo, a glacier mask for permanent ice (as a surrogate for an ice model) and the bucket size for the soil water ($\equiv$ to the field capacity). For snow covered regions, the background albedo is modified to the actual albedo used in the radiation scheme.

Boundary layer and diffusion

Surface fluxes of zonal and meridional momentum (wind stress) as well as of sensible and latent heat are parameterized using the bulk aerodynamic formulas. The calculation of the drag and the transfer coefficients is based on the work done by *Roeckner et al.* (1992) for the ECHAM-3 model and taken from *Louis* (1979) and *Louis et al.* (1982).

Vertical diffusion, representing the non-resolved turbulent exchange is applied to the horizontal wind components, the potential temperature and the specific humidity. The parameterization for the horizontal diffusion instead is taken from *Laursen and Eliasen* (1989), as it is done in ECHAM-3 (*Roeckner et al.* 1992). The diffusion is computed in spectral space.

Radiation

The parameterization for the shortwave radiation is based on the work by *Lacis and Hansen* (1974) for the cloud free atmosphere with Rayleigh scattering, ozone and water vapor absorption. For the cloudy part, the parameterizations of the albedos and transmissivities for the high-, middle and low-level clouds are taken from *Stephens et al.* (1984). The long-wave radiation scheme for the clear sky uses a broad band emissivity method (*Sasamori* 1968), where the cloud flux emissivity is obtained from the cloud liquid water content (*Stephens* 1978; *Stephens et al.* 1984). The ozone concentration used in the radiation scheme is prescribed on the basis of an idealized annual cycle taken from *Green* (1964). The atmospheric carbon dioxide (CO_2) concentration can be freely prescribed and adjusted to the user-specific experiment which will be explained in detail in Chapter 4. Furthermore, no other greenhouse gases (GHG) are included in PlaSim.

Cumulus convection, clouds and precipitation

Cumulus convection is parameterized by the convection scheme taken from *Kuo* (1965, 1974). Large-scale condensation occurs if the air is supersaturated with the condensed water falling out instantaneously as precipitation. Hence, no storage of water in clouds is considered.

Cloud cover and its liquid water content are diagnostic quantities, with the fractional cloud cover of a grid-cell parameterized according to *Slingo and Slingo* (1991), where the relative humidity is taken for the stratiform cloud amount and the convective precipitation rate [mm/d] for the corresponding cloud amount. Other processes concerning cloud microphysics, e.g. phase changes, are not considered in the model. However, a distinction is made between rain and snow fall at the surface. If the temperature of the lowermost level falls below the freezing point, precipitation is assumed to be snow, otherwise all precipitation is considered to be rain.

Ocean and sea ice

PlaSim can be used with three ocean modules, which differ in their complexity and thus in the response they are able to impose on the atmosphere. In the very basic version of the model, sea surface temperatures (SST) are prescribed by a climatology and are thus the same each year. Due to the annual prescription of the ocean temperatures, the interaction with the atmosphere is suppressed. This leads to a strong dampening of the feedback between both systems. Alternatively, a coupling to a mixed layer ocean is established in PlaSim. This slab ocean model represents the oceanic mixed layer, which is kept fixed to a depth of 50 m. The depth of the mixed-layer also determines the band, up to which an oceanic interaction with the atmosphere can take place, i.e. in PlaSim, the atmosphere can interact with the first

50 m of the ocean. This is already a strong improvement compared to the fixed ocean with regard to the dampening of the feedbacks, but the interaction with the deep ocean, which would induce stronger or even initiate new responses, which do not emerge in the top oceanic layers, still cannot be reproduced. The latter is only possible with a dynamic ocean, which is, for PlaSim, the large-scale geostrophic ocean (LSG, *Maier-Reimer et al.* 1993). Included in PlaSim is also a thermodynamic sea ice model which is based on the zero layer model of *Semtner* (1976). It depends on the oceanic temperatures, i.e. sea ice is formed if the ocean temperature drops below the freezing point (set to 271.25 K) and is melted whenever the ocean temperature increases above this point. Comparable to the fixed ocean, sea ice can equally by prescribed by a climatology. The effects of using different oceans will be reported on at a later stage.

Vegetation

Comparable to the setup for the ocean, PlaSim can couple to in total four different vegetation representations, which are (i) a prescribed vegetation setting, or one of the vegetation modules SimBA (ii) or VECODE (*Brovkin et al.* 2002) (iii). As shown in Figure 2.1, other possibilities are the Koeppen climate classification (*Köppen* 1936) and the dynamic vegetation model CARAIB (*Warnant et al.* 1994). Whereas the first three settings are coupled interactively to PlaSim, the latter two can just be used asynchronously respectively diagnostically. The models are further described and handled in Section 6.3. The settings (i) - (iii) are shortly described in the following.

(i) Prescribed vegetation In the prescribed setup, global vegetation is accounted for by four parameters in the land surface scheme. These are the surface background albedo affecting the surface solar radiation, the surface roughness length with direct implication for the exchange of momentum and moisture and two parameters representing the effect of vegetation on the soil hydrology, i.e. the bucket size describing the maximum water storage of the soil, and a parameter controlling the fraction of actual and potential evapotranspiration, i.e. lately the fraction of available soil water. This is a standard and at the same time the easiest procedure to account for "vegetation" and is done similarly in other GCMs (*Brovkin et al.* 1998; *Claussen* 1998). As a remark it should be said, that these parameters can be easily adjusted, e.g. to carry out experiments to study the influence of extreme boundary on atmospheric processes. This procedure is further handled in Section 6.4 b.

(ii) SimBA Secondly, PlaSim can couple to the Simulator of Biospheric Aspects (SimBA), which is the original vegetation model being coupled to PlaSim. It provides a simplified, but dynamic and interactive representation of the terrestrial vegetation (*Kleidon* 2006). The model determines dynamically the aforementioned global land surface properties, that are affected by the presence of vegetation, e.g. background albedo, roughness length and the rooting depth (= bucket size), from the existing climatic conditions. The latter are given by the atmospheric part of PlaSim and are setting the constraints for the simulation of the vegetation productivity by SimBA, which is the gross carbon uptake or gross primary productivity (GPP). This then leads to the buildup of biomass. The change over time of the organic carbon stored in this biomass is equal to the net primary productivity (NPP) and can be related to GPP through

$$NPP \approx 0.5 \times GPP. \tag{2.13}$$

This ratio can deviate but, in any case, NPP is proportional to GPP, so that $NPP/GPP = const$. The change in biomass then translates again into the land surface properties such as surface albedo and so

forth. These in turn affect the interaction of the vegetation and climate model through surface energy and mass exchanges. SimBA is executed at every time step of the atmosphere (*Kleidon* 2006).

A more comprehensive description including the governing equations can be found in the PlaSim reference manual (*Lunkeit et al.* 2010) or in *Kleidon* (2006). So far, studies with SimBA have been made by *Kleidon* (2006) to investigate the impact of human-induced land cover changes on the water and energy budget at the surface, by *Kleidon et al.* (2007) to analyze the potential emergence of multiple steady states in the vegetation-atmosphere system as a direct consequence of discrete vegetation classes or by *Sujatta* (2011), who carried out Snowball Earth experiments investigating the influence of different PlaSim model setups.

(iii) VECODE As the third alternative, PlaSim can couple to the Vegetation Continuous Description model (VECODE, *Brovkin et al.* 2002). The coupling of PlaSim and VECODE has been implemented rather recently and is described in *Bathiany et al.* (2011). VECODE is a reduced-form dynamic global vegetation model, which has been originally designed, based on a previous work by *Brovkin et al.* (1997), as the vegetation module for an interactive coupling to a coarse resolution atmospheric model (CLIMBER-2, *Brovkin et al.* 2002) for performing long-term simulations. VECODE determines the potential cover fractions of two plant types (trees and grass) from annual mean temperature, precipitation and growing degree days above 0°C (GDD0) and simulates changes in the vegetation structure and the carbon pools on different time scales. The transformation from the climatic variables to a potential vegetation distribution and NPP is based on a fit of tolerance limits and performance curves to global observations. All vegetation variables are calculated as annual mean values. VECODE provides two different modes of coupling to the atmosphere: In equilibrium mode, the coupling is asynchronous. The cover fractions are set to their equilibrium values, which can be calculated from a mean over several atmosphere years. This mode is comparable to the coupling with the Koeppen climate classification which will be described later. In transient mode, the evolution of tree and grass cover is calculated with an annual time step. Each year, the potential vegetation cover is determined and the actual cover fractions approach their equilibrium on the basis of a linear relaxation law. The timescales for trees and grass are also updated each year and result from NPP, which itself depends on the annual mean temperature, precipitation and atmospheric CO_2 concentration.

So far, VECODE has been used for various studies by coupling it to different models. *Cramer et al.* (2001) compare it to five other global dynamic vegetation models with respect to their response on CO_2 and climate change. VECODE is also applied in palaeoclimatic studies to have the dynamics of grassland and forest included. In this context, special regional focus is set on the Holocene climate evolution in Northern Africa (*Renssen et al.* 2006a) or at the high latitudes of the Northern (*Renssen et al.* 2005a) and Southern Hemisphere (*Renssen et al.* 2005b). Other studies investigate the influence of changing external forcings, such as insolation or greenhouse gas concentration, on the Holocene climate variability in general (*Renssen et al.* 2006b) and, in particular, during the thermal maximum in the mid-Holocene (*Brovkin et al.* 2002; *Renssen et al.* 2009). When analyzing climate-vegetation interactions, the stability-problem has to be kept in mind, i.e. the question, whether the system is stable or maybe has different equilibria under the aspect of changing biogeophysical or biogeochemical conditions. The latter feedbacks and their influence on the atmosphere-biosphere interaction is shown by *Brovkin et al.* (2003) for present-day and doubled CO_2-climate. In contrast, *Renssen et al.* (2003) are evaluating the climate instability during the mid-Holocene in the Sahara/Sahel region. The study by *Lemmen* (2009) can be seen in a similar context as the author is quantifying the effects of land use change, i.e. biogeophysical changes, on the amount of released carbon in the atmosphere by coupling VECODE to the socio-technological evolution model GLUES instead of a climate model.

2.2 Applications

As indicated before, the coupling of the diverse subcomponents of PlaSim (cf. Fig. 2.1) to the atmosphere is very straightforward. Thus, this modular structure of the model is beneficial as it easily enables a problem-dependent configuration. This has led to different applications of PlaSim during the past several years, addressing a variety of scientific questions. To finalize this section, a short overview of these applications is presented in the following.

These are, for example, hysteresis experiments on a Snowball Earth (*Lucarini et al.* 2010) with regard to thermodynamic aspects and the identification of potential tipping points in the climate system. Another application of PlaSim is the work by *Kleidon et al.* (2006) or *Fraedrich and Lunkeit* (2008) who have investigated the entropy balance of the Earth system. Other studies - by *Fraedrich et al.* (2005c) or *Dekker et al.* (2010) - have analyzed the interactions between atmosphere and biosphere under extreme vegetation scenarios. As mentioned earlier, PlaSim can couple to three different ocean modules. In the study by *Schmittner et al.* (2011), this package is expanded through the usage of PlaSim together with the University of Victoria model (UVic), combining the atmospheric circulation of PlaSim with the ocean, sea ice, land surface and ocean biogeochemical components of UVic to form the new ocean-atmosphere Oregon State University-University of Victoria model (OSUVic) to investigate the impact of mountains and ice sheets on the large-scale circulation.

Compared to other EMICs in the scientific community, such as CLIMBER, ECBILT-CLIO, or others listed in the paper by *Claussen et al.* (2002), PlaSim can, from the atmospheric point of view, be regarded as a more complex, i.e. full, GCM: All atmospheric processes are included, but with the limitation of less sophisticated parameterizations. Whereas other EMICs may have a coarser atmosphere, they may be composed of, for example, a much more complex ocean model or include other subcomponents like a carbon cycle model. Besides their individual differences, all EMICs have in common that they are suitable for long-term and problem-specific experiments. This listing implies that PlaSim has been used in a wide range of fields yet; due to its medium complexity and associated less extensive computing requirements, it is further especially suitable for palaeoclimate research, which is of great importance for this study. So far, PlaSim has already been used for studies on geological time scales of several million years ago (*Romanova et al.* 2006; *Micheels and Montenari* 2008; *Micheels et al.* 2009b,a; *Henrot et al.* 2009, 2010). On the other hand, in the studies by *Micheels et al.* (2009a) and *Henrot et al.* (2009), PlaSim has already proven to provide realistic results in the comparison to either vegetation (pollen) and terrestrial proxies. Summing up, mainly the last two aspects are in line, and at the same time a feasible precondition, for the intention of this overall study of reconstructing the Holocene climate with (Chapt. 5) and without proxy data (Chapt. 4).

3 Validation of the Planet Simulator to present-day climate

As the aim is, at a later stage, to use PlaSim for the reconstruction of the Holocene climate, a profound knowledge of the model performance, as it is done by e.g. *Roeckner et al.* (1996), is required to avoid misinterpretations and to be aware of potential biases in the model. This can be achieved through a model validation for present-day conditions. Although the focus is set on studies about past climates, the reflection of present-day climate is not an additional aspect but an essential prerequisite. Before applying a climate model under conditions which strongly differ from the current state, a GCM must be validated to either direct observations or to reanalysis data (e.g. *Kållberg et al.* 2005); reanalysis data are treated as the best possible replication of the actual observations and are further explained in the next section. This implies that GCMs should be able to reproduce the climate indicated by observational or reanalysis data - despite inherent deficiencies of individual models.
To "validate" in this context means that a certain matter or issue is declared as "true"; so it can be understood as a kind of confirmation. With a validation, the reliability of climate models should be confirmed; whether the model is able to reproduce the climate mean state - given by observations or reanalysis data - in terms of different climate variables and/or important atmospheric processes. In principle, a model validation can be used for three essential purposes: The most important is the identification of the model performance mainly with regard to the deficiencies and systematic biases, to avoid scientific misinterpretations (i); to use the output and the systematic errors as a basis for a comparison with other climate models (ii); and finally to undertake model improvements if the results of the validation reveal strong model errors (iii). Nevertheless, besides the ability to simulate the present-day climate with a GCM, the model should at the same time be capable to represent a climate that is different from current conditions; this task is unequally more complicated. Driven by reconstructions of climate forcing factors to account for long-term changes of the atmospheric state, the GCM can potentially produce diverging simulation results because of its unknown internal variability or general model limitations (*Widmann et al.* 2010).

3.1 Planet Simulator data

A control run for a period of 50 years is performed with PlaSim for present-day climate (*Haberkorn et al.* 2009b) using prescribed SST and sea ice based on the climatological annual cycle taken from the

Atmospheric Model Intercomparison Project (AMIP II, years 1979 to 1996, *Gates* 1992 and *Taylor et al.* 2000). PlaSim is used in T21 horizontal resolution ($\approx 5.6^\circ \times 5.6^\circ$ on the corresponding Gaussian grid) with ten not equally spaced levels in σ-coordinates ($\sigma = p/p_s$) in the vertical. A fixed composition of the atmosphere is used, the annual cycle is included but not the diurnal. The default parameters used are the following: a year with 365 days (and 366 for leap years), a solar constant of 1365 W/m^2 and a CO_2-content of 348 ppmv. The control run is confined to the atmospheric part without interaction with the subcomponents. For the comparison to ERA-40, the last 30 years of the control experiment are selected to achieve a climatological basis. Besides annual means of the whole 30 yr period, the main seasons of boreal winter (DJF) and boreal summer (JJA) are presented.

3.2 ERA-40 reanalysis data

In this study, the reanalysis data ERA-40 (*Kållberg et al.* 2005; *Uppala et al.* 2005) from the European Center for Medium-Range Weather Forecasts (ECMWF) are chosen. As mentioned before, reanalysis data are treated as the best possible replication of the observed state of the atmosphere. They are obtained through a combination of actual observations (e.g. land stations, radiosondes or satellites) with analyses from a numerical weather prediction model (NWP). To account for the temporally and globally different observations, a data assimilation technique is used to interpolate the irregularly distributed observations on a global grid. Through this assimilation, a consistent data base in time and space is achieved which is then used for the numerical analysis. Nominally, observations are reprocessed, "reanalyzed", for a period of several years or even decades, using invariant techniques and models. The here used ERA-40 data are already the second generation of reanalysis data produced at the ECMWF, covering not only a longer period compared to the preceding generation ERA-15 (1979-1993), but, more important, also using improved methods in all aspects of the whole reanalysis procedure. ERA-40 spans the period of September 1957 to August 2002. Moreover, errors, which occurred during the first generation could thus be annihilated. But not only from the technical point of view but also in the presentation of the mean climate, improvements are achieved in ERA-40, as, for example, the global mean temperature was too low, mainly during winter, in ERA-15 (*Uppala et al.* 2005). The overall resolution of ERA-40 is the following:

Horizontally:

(a) Spectral resolution of T159 for the prognostic variables and,

(b) T106 for the diagnostic variables ($\sim 1.125^\circ$);

Vertically:

- 60 model levels for the atmospheric data, with a higher amount in the boundary layer following the orography and additional ones in the higher atmosphere (stratosphere and mesosphere) compared to ERA-15.

Temporally:

- Daily means of a six hourly data set

A comprehensive description on ERA-15 can be found in *Gibson et al.* (1997) and on ERA-40 in *Simmons and Gibson* (2000), *Kållberg et al.* (2005) and *Uppala et al.* (2005). In the last several

years, a third generation of ECMWF reanalysis data has been established, called ERA-Interim, again including new technical approaches, an extended set of variables, a higher resolution and several other improvements (*Dee et al.* 2011). Just for completeness it should be mentioned that another two sets of reanalyses are also widely used in climate research, which are the reanalysis data NCEP/NCAR (*Kalnay et al.* 1996) of the National Center for Environmental Prediction (NCEP) in cooperation with the National Center for Atmospheric Research (NCAR) on the one hand and, on the other hand, the reanalysis data JRA-25 (*Onogi et al.* 2007) from Japan, which have been established in a cooperation of the Japan Meteorological Agency (JMA) and the Central Research Institute of Electric Power Industry (CRIEPI).

3.3 Comparison

The climate of the PlaSim control run is analyzed and the results are compared to ERA-40 (ERA hereinafter). The climatology is presented in terms of global and Europe-wide means of the respective variables, using global (European) maps with meridional profiles of zonal means. The results of the validation are taken from *Haberkorn et al.* (2009b); this study has been the very first and comprehensive evaluation of the climate model Planet Simulator, accounting for first and second moments of the key atmospheric variables characterizing the thermal, dynamic and moisture processes, as well as eddy fluxes and other derived quantities (such as wavenumber spectra) of the dynamics of the atmosphere. However, at this stage, only a compendium of the validation results is presented for those variables which are of importance for further aspects of this thesis, i.e. surface air temperature and precipitation for the reconstruction of Holocene climate (cf. Chapt. 4 and 5) as well as evaporation and net surface radiation for the calculation of the vegetation-related quantities in Chapter 6. Of course, precipitation is essential for the vegetation studies as well. Due to the different resolutions in PlaSim and ERA, the latter data are interpolated on the PlaSim resolution of T21. Monthly means are further derived from daily means of the six hourly data set of ERA. The subsequent comparison will be dominated by the global view, which is more important for the vegetation studies. Only for the evaluation of the surface air temperature field, the European sector is presented separately in comparison to a high-resolution climatology to account for more local scale structures which cannot be identified on a global view.

3.3.1 Surface air temperature (T2m)

Global The first variable which is examined is the surface air temperature at 2 m (Fig. 3.1). This parameter is further needed for the Holocene experiments (cf. Chapt. 4), in particular for the adjustment of Holocene SST on the basis of the surface air temperature over land (cf. Chapt. 5). It is also further used for the calculation of the vegetation classifications in Chapter 6.

In general terms, PlaSim captures the major temperature pattern. In DJF (Fig. 3.1 a, d), temperatures rise up to 20-30°C in the tropics and to a maximum of > 30°C over Australia. At higher latitudes of the Northern Hemisphere, PlaSim shows colder temperatures compared to ERA, leading to a cold bias there and a lower global mean of 11.1°C compared to 12.6°C in ERA. The strongly reduced temperatures in the polar regions become especially evident in the meridional profile of the zonal means. The Southern Hemisphere instead shows a rather similar pattern - in both the global distribution and the meridional profile.

During boreal summer (JJA, Fig. 3.1 b, e), the maxima of 20-30°C occur over Northern Africa, North America and the Arabian regions, whereas the latter two regions are showing lower values in ERA. The southern polar regions are too cold during JJA as well; thus, a cold bias can be observed in the respective winter hemispheres. The Southern Hemisphere is represented very similarly in PlaSim compared to ERA - in the global distribution as well as in the meridional profile. In general, the temperature pattern in JJA is more analogical between PlaSim and ERA, which is most distinct in the meridional profile, despite the only minor differences south of 60°S. Accordingly, the global mean is only slightly lower in PlaSim (15.1°C compared to 16.0°C in ERA).

In the annual mean (ANM, Fig. 3.1 c, f), the 30°C-maxima is only reached in PlaSim and only in very few regions. The northern high latitudes are strongly influenced by the cold bias in DJF, causing again a larger difference in the global mean: 13.1°C compared to 14.3°C in ERA.

Europe For the reconstruction of the Holocene climate, the European sector is of main interest due to the beginning of the first human settlements in this region (cf. Sect. 1.1.2). Therefore, the European temperature pattern is investigated at this stage - at first on the basis of the global temperature distribution presented in Figure 3.1. The northeastern parts of Europe are a bit too cold in PlaSim in DJF, whereas the southwestern parts are a bit too warm. Central Europe instead is well represented in PlaSim. During JJA, the similarity between PlaSim and ERA is even stronger, with PlaSim showing only slightly lower values in the very northern and southern parts of Europe. In the annual mean, the northern and southern regions are also a bit colder in PlaSim, whereas the central parts are well represented. However, on a global scale, only a rather coarse overview of the temperature pattern can be achieved. Thus, due to the specific focus on Europe for reconstructing Holocene climate, the validation is extended to an additional data set, which is the observational data set of the Climate Research Unit (CRU TS2.1, *Mitchell and Jones* 2005). This data set is available for the period 1901-2009 in three different, very high resolutions (0.5°C, 1.0°C and 2.5°C), but does not include oceanic temperatures. Here, the 0.5°C-resolution is used. In Figure 3.2, European temperatures for PlaSim and CRU are shown for DJF, JJA and the annual mean. For CRU, only the period of 1961 to 1990 is selected instead of the full period of 109 years, as these 30 years are widely used as a reference period for present-day climate.

Despite the coarse resolution in PlaSim compared to CRU, the general pattern for the European winter (Fig. 3.2 a, d) is very similar between both with a spread from warmest surface air temperatures in the south and southwest of Europe to the coldest ones in the northeast. The latter regions of lowest temperatures are more pronounced in PlaSim which is closely related to the aforementioned cold bias

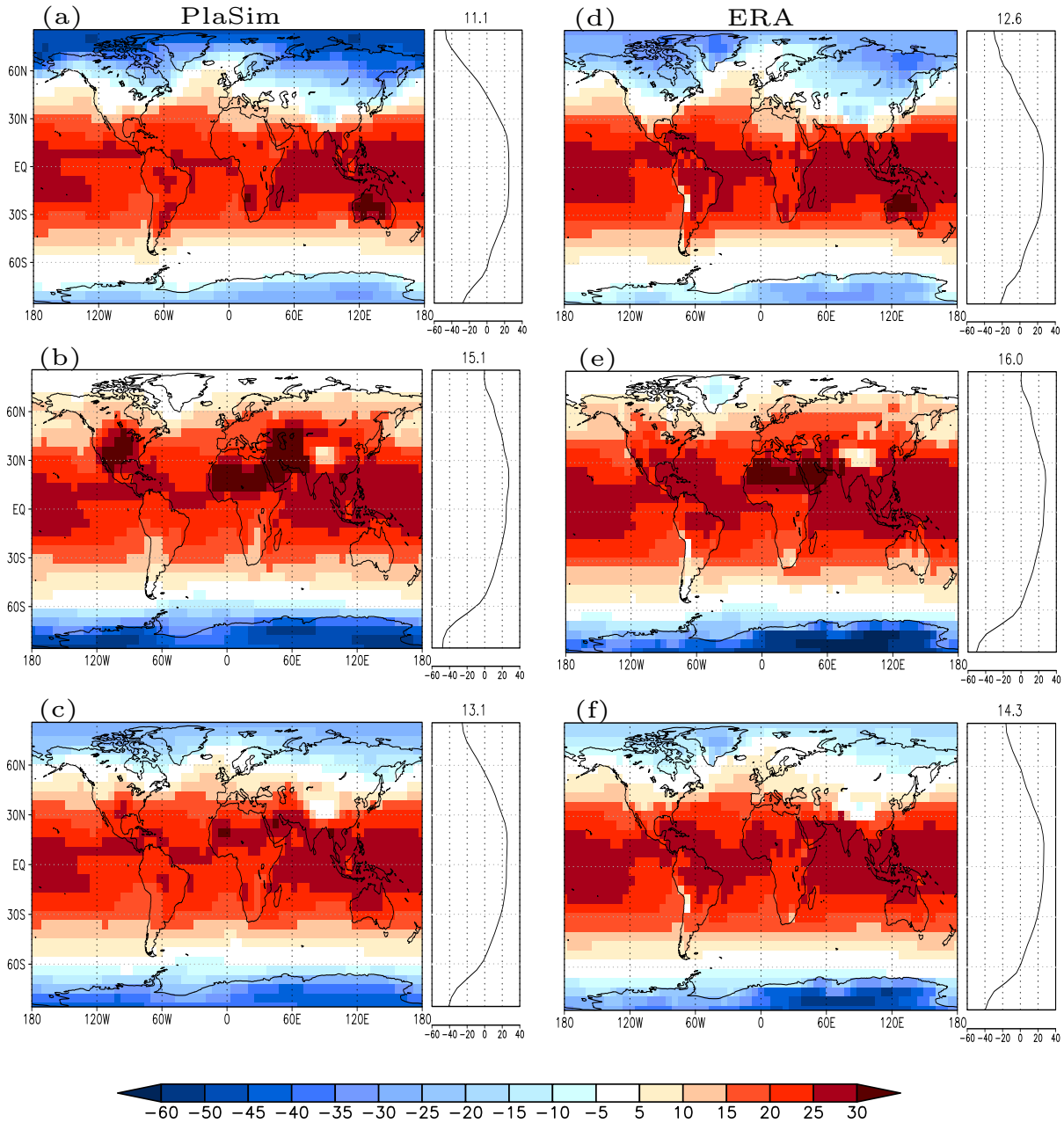

Figure 3.1: Surface air temperature (T2m) [°C] for PlaSim and ERA: (a), (d) DJF; (b), (e) JJA; (c), (f) ANM. Right panels: zonal mean with global mean on top.

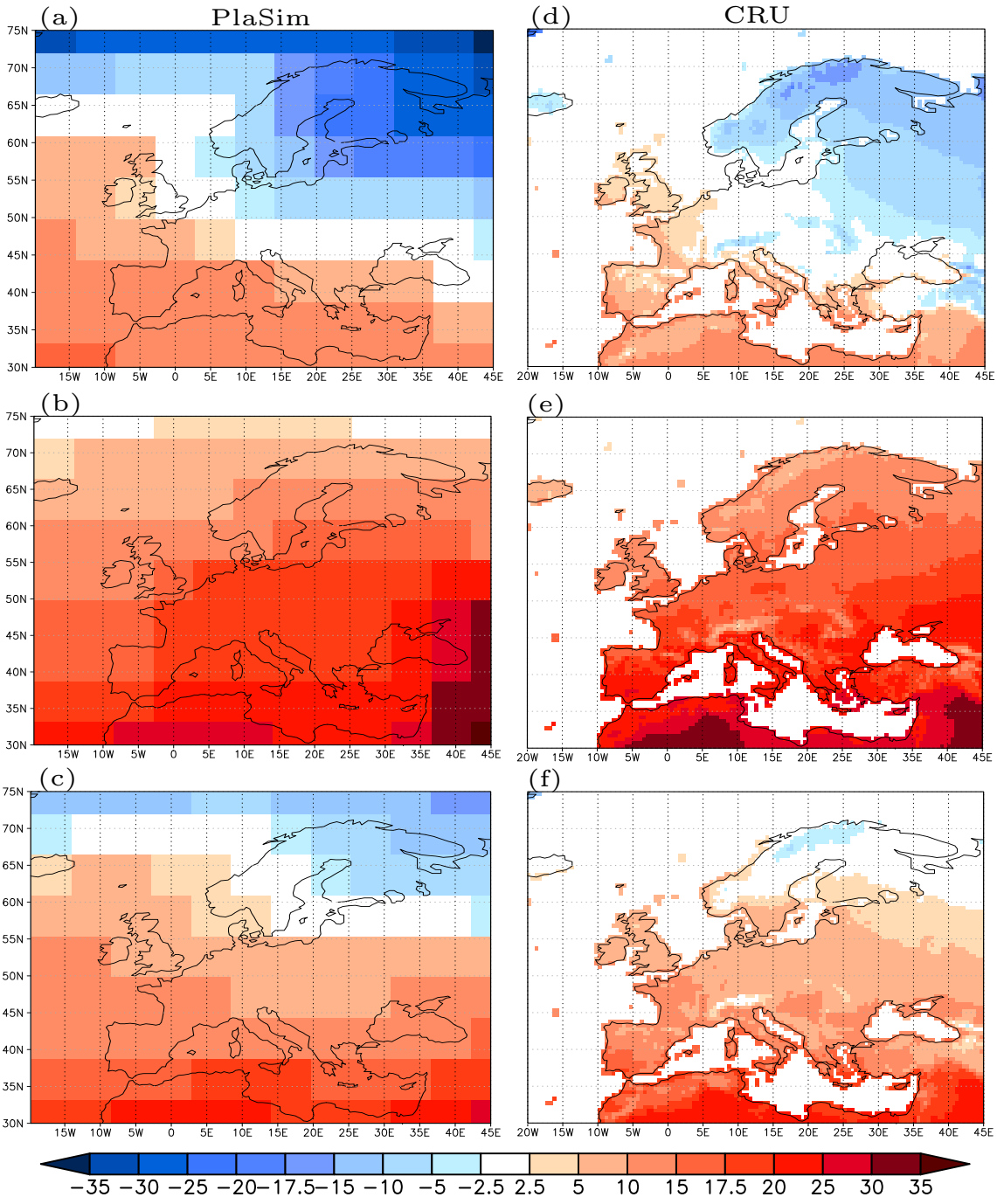

Figure 3.2: Surface air temperature (T2m) [°C] over Europe for PlaSim and the observational data set CRU TS2.1: (a), (d) DJF; (b), (e) JJA; (c), (f) ANM.

there. Therefore the northeastern parts of central Europe are too cold in PlaSim. Over southern Europe, slight differences occur over Spain and Turkey as well as over Northern Africa where PlaSim is warmer.

In boreal summer (Fig. 3.2 b, e), PlaSim is a bit warmer over central and southeastern Europe and slightly colder over Northern Europe and Northern Africa.

The PlaSim annual mean (Fig. 3.2 c) is again strongly influenced by the cold bias, leading to lower temperatures at the northern high latitudes compared to CRU (Fig. 3.2 f). These colder conditions prevail over most parts of northern Scandinavia and northern Russia; hence, the appearance of higher temperatures is slightly shifted southwards in PlaSim. Thus, central and southern Europe are very well represented in PlaSim, which is beneficial for the climate reconstruction of the Holocene, which is based upon the temperatures over Europe (cf. Chapt. 5).

3.3.2 Total precipitation

The validation of the total precipitation fields is confined to the global representation at this stage. The first step is again the direct comparison to ERA, however, in a second step, the evaluation is extended to another high-resolution climatology. The precipitation patterns for PlaSim and ERA are presented in Figure 3.3. To be more precise, it is the total precipitation, i.e. the sum of large-scale and convective precipitation. This variable is also further considered in the later studies of the palaeoclimate; moreover it is an essential part of the hydrological cycle and thus of major significance for the vegetation-related studies.

During winter (Fig. 3.3 a, d), large areas on the global scale show very little (up to 2 mm/day) precipitation in both PlaSim and ERA. South of 60°N, precipitation is enhanced mainly over North America and Asia; over the adjacent oceans it is increasing up to 8 mm/day. Precipitation is increasing more strongly in the tropics, which is mostly induced by the convective part (not shown here), whereas the stratiform ratio is decreasing. The latter is strongly dominating in the extratropical and polar regions. The maxima occur south of the equator over South America, the southern parts of Africa and over the Indian and Pacific Ocean. These features are found in PlaSim and ERA. In the equatorial region and southward, i.e. in the Atlantic and mainly in the Pacific and Indian Ocean, ERA shows higher maxima (ERA: about 16 mm/day, PlaSim: 12 mm/day). It must be mentioned in this context, that the precipitation is overestimated by ERA in the equatorial region of the tropics and especially over the oceans (*Hagemann et al.* 2005). This becomes even more obvious when looking at the zonal means which show a similar structure between PlaSim and ERA over the Northern Hemisphere but larger deviations over the Southern Hemisphere. Moreover, a stronger peak is given in ERA, indicating higher maxima in these regions compared to PlaSim.

The summer structure (Fig. 3.3 b, e) shows analogue features: weak precipitation over polar regions and mid-latitudes. Higher precipitation rates occur over the Pacific and Atlantic Ocean which are smaller in PlaSim compared to ERA (8 mm/day in PlaSim and up to 12 mm/day in ERA). In contrast, PlaSim shows higher rates over some parts of North America, Northern Asia and the eastern parts of India and China. The maxima in both data sets are located over the northern parts of South America/the Caribbean as well as the adjacent Atlantic Ocean and equatorial Africa. These are constantly more pronounced in ERA. Further to the east, there is the huge and extensive region influenced by the Asian Summer Monsoon showing maximum precipitation rates. These are mainly located over the Indian Ocean, India itself and parts of Eastern Asia and China respectively. This structure is similar between PlaSim and ERA but PlaSim is again continuously showing the lower maxima (PlaSim: 8 mm/day, ERA: about 16 mm/day), over the continents and over the oceans. This can again be explained by the remarks in *Hagemann et al.* (2005), referring to an overestimated precipitation in the tropics in ERA. In the zonal

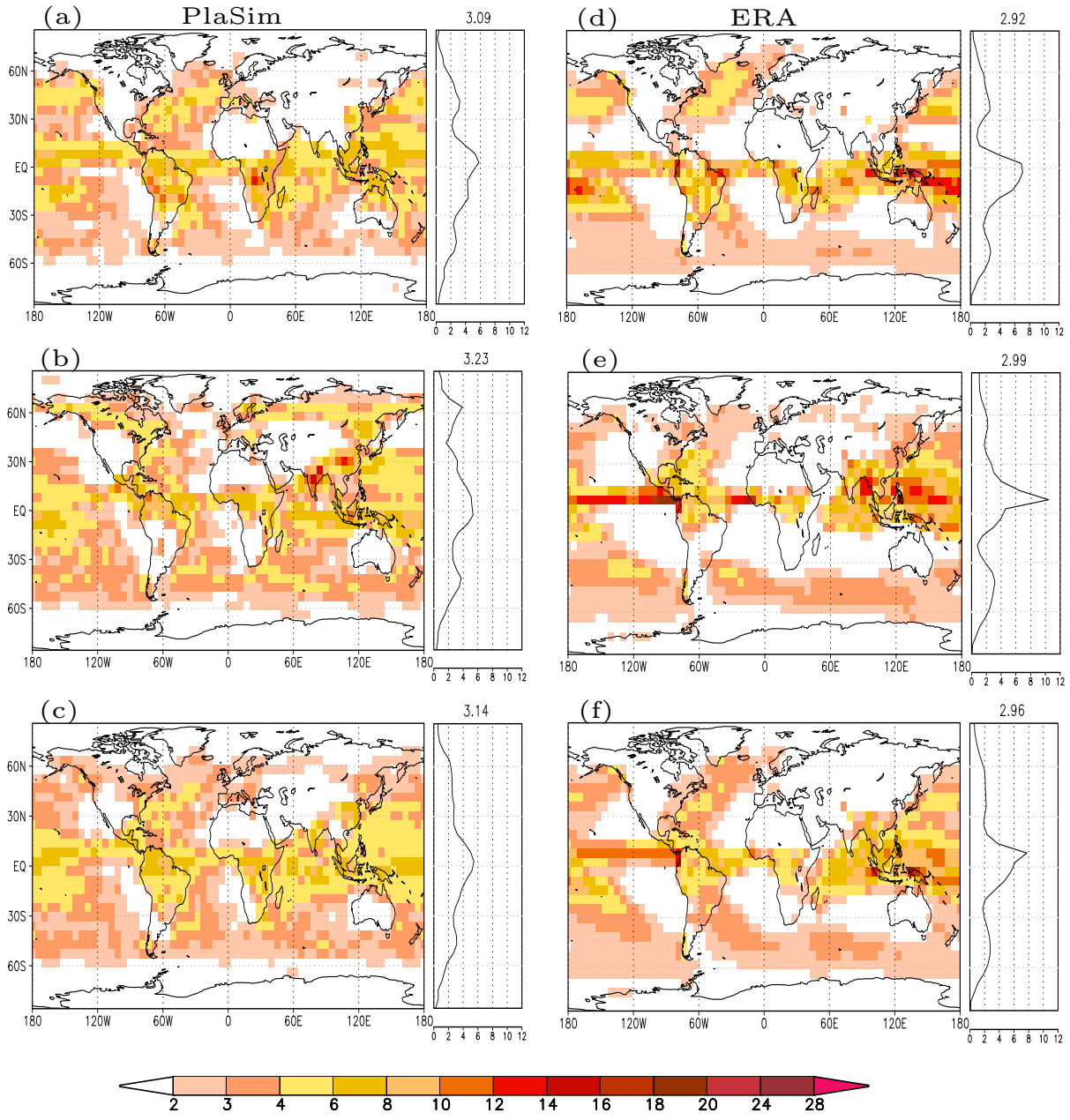

Figure 3.3: Total precipitation [mm/day] for PlaSim and ERA: (a), (d) DJF; (b), (e) JJA; (c), (f) ANM. Right panels: zonal mean with global mean on top.

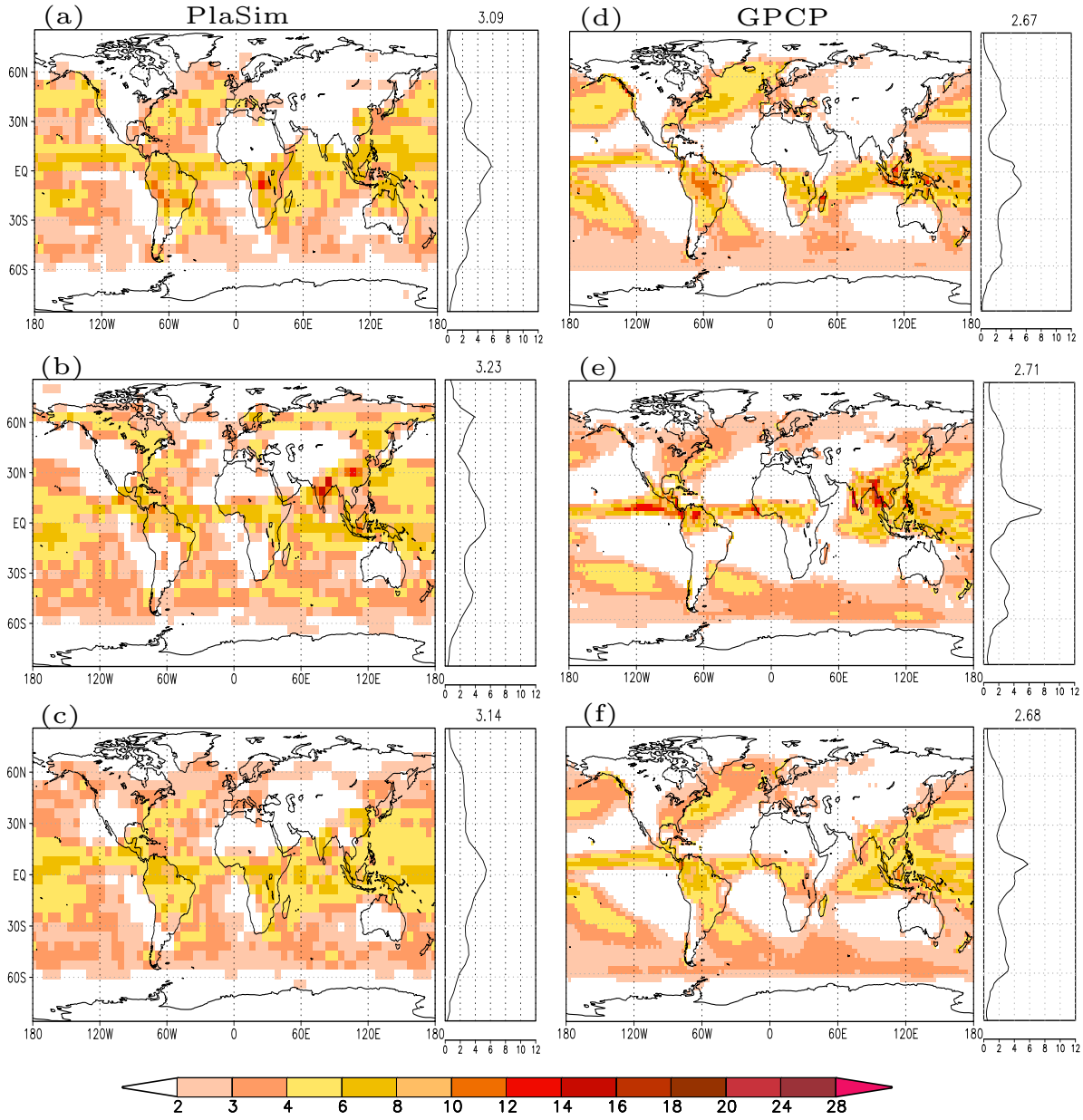

Figure 3.4: Total precipitation [mm/day] for PlaSim and the observed climatology GPCP: (a), (d) DJF; (b), (e) JJA; (c), (f) ANM. Right panels: zonal mean with global mean on top.

pattern for JJA, there are larger differences between PlaSim and ERA. However, the general pattern is shown by both. PlaSim simulates a larger maximum in about 70°N (PlaSim: about 4 mm/day, ERA: 2 mm/day). In contrast, ERA shows much larger precipitation rates in the Northern Hemisphere tropics with a strong peak at about 10°N (ERA: 10 mm/day, PlaSim: 5 mm/day) which is not simulated by PlaSim. South of the equator, ERA shows a distinct minimum at about 10°S which is weaker in PlaSim. The subtropical maximum at about 40°S is again more similar in PlaSim and ERA. Nevertheless, the global means are higher in both seasons in PlaSim, mostly generated by a more uniform precipitation pattern whereas in ERA, besides the strong maxima, also large rather dry areas occur.

In the annual mean (Fig. 3.3 c, f), the pattern is much more variable in PlaSim. Most parts on a global scale show precipitation rates of about 6 mm/day; in the tropics, the values increase up to 8 mm/day over larger areas as well as to about 10 mm/day in some local maxima. In ERA, the distribution is less variable. The precipitation rates also lie between 6 and 10 mm/day but the pattern is more uniform as in PlaSim, mainly over the Pacific and Atlantic Ocean. The ERA-maxima in general are much more pronounced in the annual mean as well, increasing up to 28 mm/day in the Pacific Ocean around the equator. The meridional profile is again more similar between PlaSim and ERA, despite the large peak around the equator in ERA, which is smaller in PlaSim.

Thus, stronger deviations exist in the precipitation patterns of both PlaSim and ERA. As these explanations do not give a clear estimate of whether the precipitation in PlaSim is simulated in an acceptable way, it is referred again to an observed climatology derived by the Global Precipitation Climatology Project (GPCP, *Adler et al.* 2003). This data set is available for the period 1979-2009 on a monthly basis and in a global resolution of 2.5°C. Again, not the full period of 30 years is chosen but the first ten years, i.e. 1979-1990, to have at least a partly identical time frame as in CRU. The latter indeed provides high-resolution precipitation data similar to temperature, but GPCP is chosen because of its profound analysis of rainfall data, based on a wide range of methods, such as rain gauge stations, sounding and satellite observations.

In Figure 3.4 a, d, the winter precipitation for PlaSim and GPCP is presented. The PlaSim pattern is in general slightly more variable but the precipitation rates are of similar magnitude compared to GPCP. Strongest differences occur over the tropical oceans of both hemispheres, where the precipitation is strongly overestimated in PlaSim. The meridional profile of the zonal means is much more similar between PlaSim and GPCP - only the maximum in the tropics is slightly shifted northwards in PlaSim but of the same magnitude as in GPCP.

During JJA (Fig. 3.4 b, e), the general pattern is more different between PlaSim and GPCP. Precipitation is overestimated in PlaSim over the continental high northern latitudes and again over most parts of the oceans. The distinct maxima in the equatorial region of the West Pacific and Atlantic Ocean, shown by the climatology, are not covered by PlaSim. These deviations also become obvious in the meridional profile. The overestimated high northern latitude precipitation leads to a stronger maximum in about 60°N whereas the peak around the equator is smaller as in GPCP.

The pattern of the annual mean precipitation (Fig. 3.4 c, f) shows again stronger similarity. The equatorial region is well represented with analogue rainfall rates in both PlaSim and GPCP. When looking at the zonal mean, the largest difference occurs in the tropics, despite the nearly equal maximum precipitation rate around the equator.

3.3.3 Total precipitation minus evaporation

As a second part of the hydrological cycle, the precipitation minus evaporation (P-E) patterns for PlaSim and ERA are presented in Figure 3.5. This parameter is equally important for the vegetation studies on

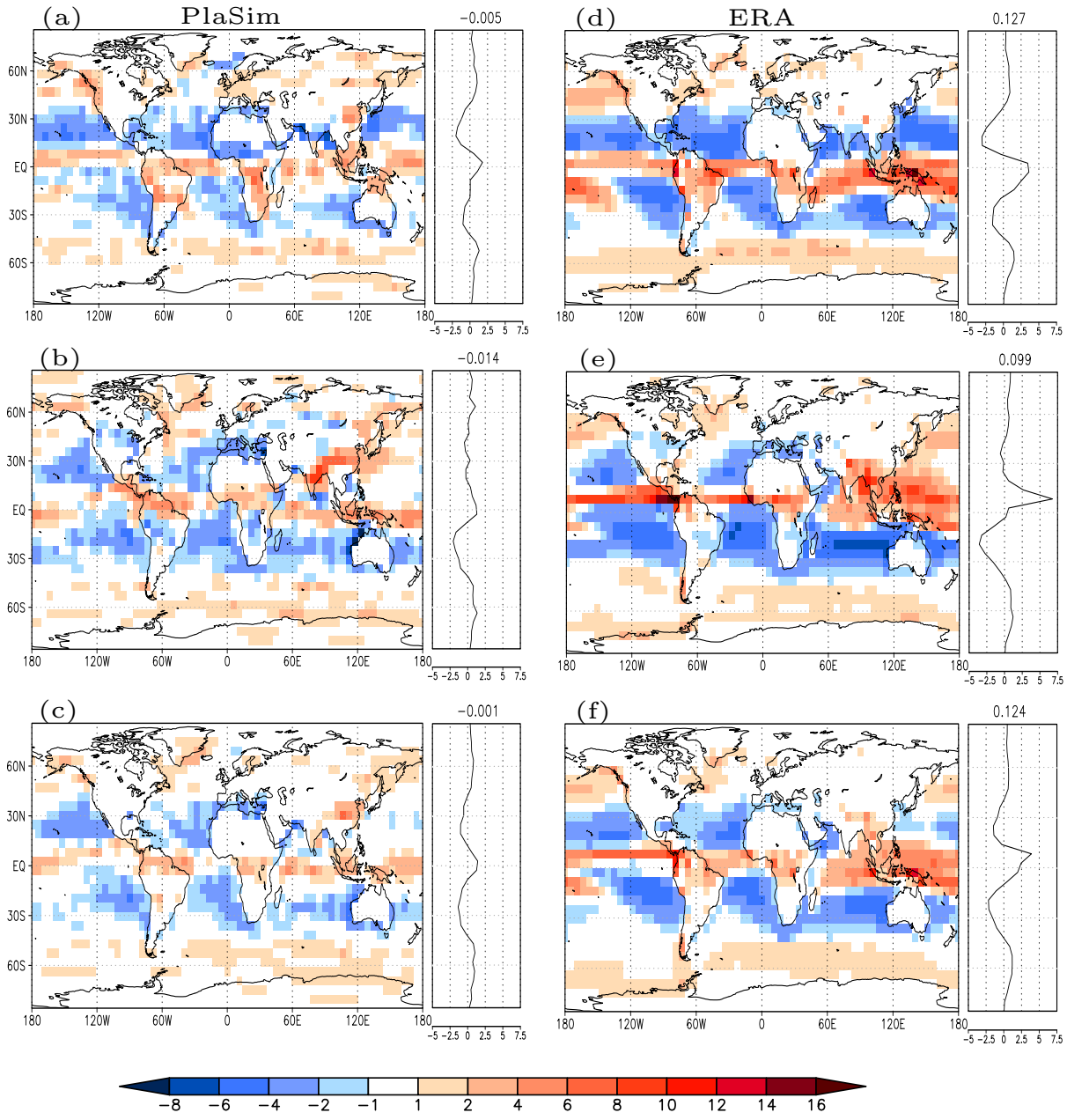

Figure 3.5: Precipitation minus evaporation (P-E) [mm/day] for PlaSim and ERA: (a), (d) DJF; (b), (e) JJA; (c), (f) ANM. Right panels: zonal mean with global mean on top.

the budgets of energy and water supply.

During winter (Fig. 3.5 a, d), similar spatial patterns can be observed for PlaSim and ERA with generally small values in the polar regions and mid-latitudes. In the tropics, the values are increasing. North of the equator, minima establish due to the low precipitation rates in those regions (cf. Fig. 3.3 a, d). While, in general terms, the spatial patterns in both PlaSim and ERA are similar, the minima are much more pronounced in ERA. In a small band to about 20°S, maxima in P-E can be observed due to the high precipitation values in those regions. This is again more distinct in ERA, which is thus caused by the overestimated tropical precipitation (*Hagemann et al.* 2005). In the Southern Hemisphere subtropics, minima can again form due to the dry conditions in those areas. The meridional profile consistently shows the largest differences (similarities) in the tropics (mid-latitudes and polar regions) with lower minima in the subtropics and a higher maximum around the equator.

In JJA (Fig. 3.5 b, e), low values occur again over the polar regions and mid-latitudes. Following the low precipitation rates over the tropical Pacific and Atlantic Ocean, minima in the P-E ratio form in both hemispheres, which are weaker in PlaSim. The higher precipitation rates and thus maxima in P-E occur again in the equatorial region, but now, following the shift due to the seasonal cycle, they appear in a small band ranging to about 20°N, which is again more distinct in ERA. In the region of the Asian monsoon, a strong maximum occurs in ERA which is smaller in size and magnitude in PlaSim. Regarding the meridional profile, again largest differences are obvious in the tropics. In ERA, there is a peak near 10°N (not simulated by PlaSim), which may possibly be due to the ERA bias (*Hagemann et al.* 2005), likewise the SH minimum at 10°S (PlaSim: about -2 mm/day, ERA: about -3.5 mm/day).

The annual mean pattern (Fig. 3.5 c, f) is characterized by strong tropical and subtropical minima and equatorial maxima which are constantly more pronounced in ERA, according to the seasonal deviations. Strongest differences between PlaSim and ERA occur in the tropics while there is good agreement in the mid-latitudes of both hemispheres. However, PlaSim simulates weaker maxima and minima and a much lower global mean. The latter is also higher in ERA during DJF and JJA.

3.3.4 Radiation

In this section, the energetics in terms of the net radiation at the surface are presented, thus the difference between the solar and the terrestrial radiation at the surface. This parameter is needed at a later stage for the interpretation of the global water and energy supply (cf. Sect. 6.5.2).

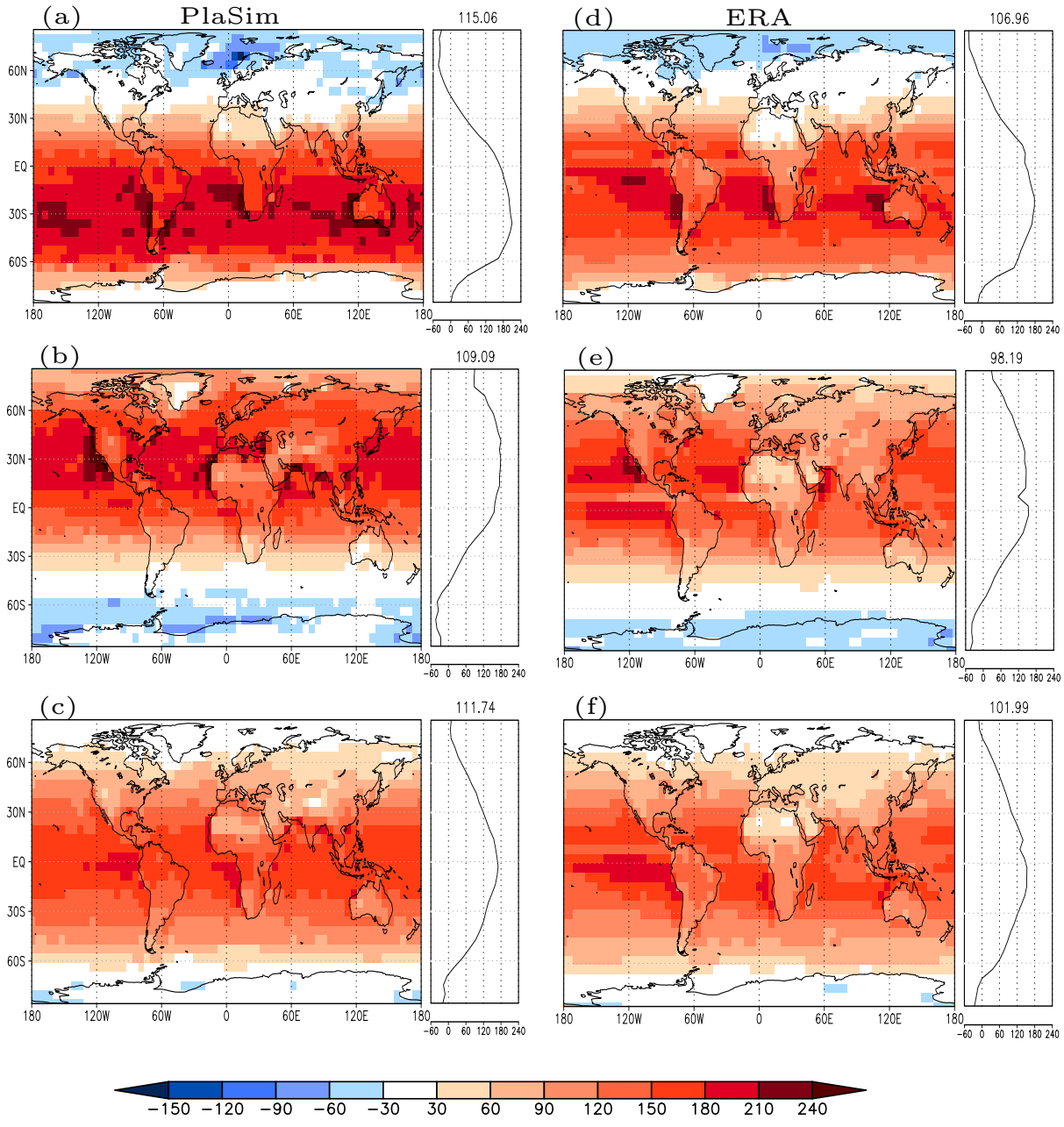

Figure 3.6: Net surface radiation [W/m^2] for PlaSim and ERA: (a), (d) DJF; (b), (e) JJA; (c), (f) ANM. Right panels: zonal mean with global mean on top.

During winter (Fig. 3.6 a, d), similar spatial patterns can be observed for PlaSim and ERA. The largest values occur between 15°N and 60°S with the maxima located to the west of South America, southern Africa and Australia. The largest difference between PlaSim and ERA can be found in the spatial extension of these maxima rather than in the magnitude. In PlaSim, these areas are more pronounced as in ERA. This leads to equally higher values in the meridional profile over the Southern Hemisphere and a slightly higher global mean.

During JJA (Fig. 3.6 b, e), the pattern has seasonally shifted, with the highest values located between 60°N and 15°S. The maxima are found to the west of North America and Africa and they are again more extended in PlaSim. The largest differences between both occur over Africa and Asia, where PlaSim is constantly simulating higher values (about 150 W/m^2 compared to 100 W/m^2). This also leads to deviations in the meridional profile over the Northern Hemisphere and a more increased global mean.

In the annual mean (Fig. 3.6 c, f), the patterns are most similar which is also evident in the meridional profile. The global mean is still higher in PlaSim, as, on average, the model simulates slightly higher values than ERA.

3.4 Summary and discussion

This chapter is dedicated to give an overview about the performance of the general circulation model Planet Simulator with respect to the simulation of the present-day climate. An evaluation of the model climate is undertaken for specific variables which are of major relevance for forthcoming parts of this study, i.e. surface air temperature, total precipitation, precipitation minus evaporation and net surface radiation. They are compared, on a global scale, to the reanalysis data set ERA-40 of the ECMWF and, for the surface air temperature on the European scale, to the high-resolution climatology CRU TS2.1. For the total precipitation, the PlaSim data are additionally referred to the climatology GPCP, which is assembled on a wide range of different rainfall analyses. The results are discussed and shortly interpreted with regard to their further use in this study.

The mean state of all four variables is captured by PlaSim reasonably well. The most apparent deviation in the temperature profile is the cold bias at the high latitudes of the respective winter hemisphere. This could be related to general model limitations with respect to the parameterizations of (low-level) clouds in PlaSim. A rather strong deviation in the total cloud cover occurs in the comparison of PlaSim and ERA (not shown) which is most pronounced at the high latitudes. The radiative effect of clouds on the temperature profile has been investigated by, e.g. *Hartmann et al.* (1992) and *Clement et al.* (2009), stating that especially low-level clouds impose a great impact on the climate system in terms of a net cooling effect, which marks exactly the outcome which is identified in PlaSim. Furthermore, changes in the cloud cover are closely linked with the local temperature structure and the large-scale circulation (*Clement et al.* 2009). Cloud feedbacks, due to its complexity, are still a primary cause of uncertainty in climate model simulations (*Clement et al.* 2009); this may become even more significant in models using less comprehensive parameterizations such as PlaSim. Another reason which may lead, together with the shortcomings in the cloud cover representation, to the strong temperature anomaly over the polar regions of the respective winter hemisphere, could be attributed to a deficient prescription of the sea-ice mask which may induce an additional cooling. Regarding the European temperature, a strong agreement in the simulated compared to the observed pattern can be constituted: Despite the low resolution, PlaSim captures the main characteristics given by CRU. This forms a good basis for the reconstruction of the Holocene climate on the basis of proxy time series (cf. Chapt. 5). As this reconstruction is built on the sensitivity between the SST and the land temperatures (cf. Sect. 5.3), a reliable and realistic temperature

distribution is essential to preclude biases there. Concerning the vegetation studies, the global instead of only the European temperatures is of importance. As the comparison shows, the general agreement is indicative of a realistic vegetation distribution. The discrepancies, mainly the lower temperatures over the polar regions of the respective winter hemisphere, may favor colder types. This is subject to prove in Chapter 6.

As a second parameter, the patterns of the total precipitation as the sum of large-scale and convective precipitation are analyzed. The latter is dominant in the tropics, where large, convection-triggered cloud clusters are forming, whereas in the extratropics and the polar regions, the stratiform (large-scale) rainfall is prevailing which itself is decreased in the tropics. The comparison to ERA has revealed at least a rather strong structural similarity, i.e. PlaSim reproduces the characteristic seasonal precipitation patterns, with maxima located in the equatorial region of the respective summer hemisphere and the minima over the desertic parts of North Africa and Australia as well as over the large continental regions of North America and Asia. However, PlaSim overestimates the precipitation over the (sub)tropical oceans, which should be very low, as shown by ERA. Due to this increased PlaSim rainfall over the oceans, the global mean is slightly too high in all seasons and in the annual mean. The equatorial maxima are of a lower magnitude in PlaSim, but they are not underestimated but overestimated in ERA (*Hagemann et al.* 2005). As a reliable estimate of the precipitation distribution in PlaSim is required for both the palaeoclimate and the vegetation studies, the model evaluation is extended to a second data set, which is the precipitation climatology GPCP. The comparison is coming to similar results as for ERA, i.e. at least during DJF and the annual mean, the precipitation is well represented in PlaSim, apart from the precipitation over the tropical oceans, which is indeed too strong in the model. In the opposite, the climatology shows much lower maxima in the respective regions which are much lower as in ERA and thus of similar magnitude as in PlaSim. For JJA, the differences are slightly more pronounced and appear again in an overestimated rainfall over the tropical oceans as well as over the continental high northern latitudes. In contrast, the distinct maxima in the equatorial region of the West Pacific and Atlantic Ocean are not covered by PlaSim. However, the maxima in GPCP are lower as in ERA and thus proving again the overestimated equatorial precipitation in ERA, which has been mentioned and shown before. In general terms, PlaSim is again wetter in the global mean. As can be discovered from the meridional pattern of the zonal means, this is mainly caused by the overestimated tropical ocean rainfall, as the extratropical pattern of the zonal means is quite similar for all seasons and both hemispheres, despite the aforementioned deviation over the high northern latitudes of the boreal summer hemisphere. Lately, the comparison to the climatology GPCP has opened new insights into the estimation of the model results with regard to a later usage for other studies. Discussing now the potential reasons for these differences in the precipitation patterns, especially over the tropical oceans, again relates to parameterization limitations. As mentioned earlier, the tropics and thus the tropical oceans are especially influenced by convective processes. Hence, convective precipitation is the dominating element in that region. The slightly deficient parameterization of convection is also apparent in the patterns of the outgoing long-wave radiation (OLR, not shown here). This parameter is a good criterion for the description and lately a measure of the strength of the convection in a model as it can be associated with the vertical depth of clouds and especially of large cloud clusters in the tropics. As mainly the latter are very deep, they are emitting less OLR. So higher (lower) OLR-values are indicative of a weaker (stronger) convection and less (more) extensive cloud clusters. As the OLR is overestimated by PlaSim in the tropics, which is equivalent to less extensive cloud systems, the convection is therefore too weak. As convection is acting on sub-grid scales, it needs to be parameterized (cf. Chapt. 2). The complex nature of the convection process also requires a complex parameterization. This cannot be achieved in models like PlaSim as it requires larger computing resources which contradicts the intention of EMICs. However, it must be mentioned, that an inappropriate representation of the

convective processes is an existing problem even of more comprehensive general circulation models.

As another important parameter of the hydrological cycle, the precipitation minus evaporation patterns are investigated for both PlaSim and ERA, which is equally important for the vegetation studies on the budgets of energy and water supply. The patterns of the P-E-difference are rather similar in PlaSim and ERA for both seasons and the annual mean. However, strongest deviations occur in the magnitude of the minima and maxima which are both more pronounced in ERA. This can also be identified in the meridional profile of the zonal means. The more distinct extremes in ERA are caused by the overestimated equatorial precipitation, which has already been mentioned before. Thus, the largest similarities in PlaSim and ERA occur over the mid-latitudes and polar regions. As shown above, the PlaSim maxima are of similar magnitude as those shown by the climatology GPCP. Therefore, a reliable representation of the P-E pattern in PlaSim is assumed.

The global energy supply has been presented in terms of the net radiation at the surface, i.e. the difference between the solar and the terrestrial radiation. This variable is further needed for the calculation of the global water and energy supply (cf. Chapt. 6). In general, PlaSim tends to slightly overestimate the net radiation compared to ERA. The maxima in all seasons and the minima are both more pronounced and the latter more expanded in the respective winter hemisphere. This leads to a slightly shifted pattern of the zonal means mainly in DJF and JJA, whereas the annual mean is very similar in both PlaSim and ERA. The stronger minima in the polar regions is closely related to the cold bias in those regions and lately to the aforementioned shortcomings with regard to the parameterization of (low-level) clouds. The higher net radiation can be seen as in line with the overestimated precipitation in PlaSim; which is important for the calculation of the ratio between water and energy supply in Section 6.5.2 and to make further estimates which are based on this ratio.

3.5 Conclusion

Overall, PlaSim is able to reproduce the climate mean state of the four considered variables for present-day conditions, forming a good basis for the forthcoming studies of palaeoclimate. The model provides a reliable estimate of those parameters for further analyses in this study. Nevertheless, details on rather small scale, i.e. over Europe, cannot be covered due to the coarse resolution of PlaSim. Shortcomings in the representation of these variables refer to general model limitations regarding the parameterization of clouds and convection.

4 Reconstruction of the Holocene climate

The following two chapters are dedicated to the main motivation of this study, using different approaches to reconstruct the Holocene climate. Besides the ability to simulate the present-day climate with a GCM, as has been shown in the preceding chapter, a model should at the same time be capable to represent a climate that is different from current conditions; this task is unequally more complicated. Driven by reconstructions of climate forcing factors to account for long-term changes of the atmospheric state, the GCM can potentially produce diverging simulation results because of its unknown internal variability or general model limitations (*Widmann et al.* 2010). In a first step, the climate is reconstructed using PlaSim in the fully coupled version, i.e. with a free ocean (LSG) and the dynamic vegetation module SimBA. For the reconstruction of the Holocene climate, the European sector is of special interest due to the beginning of the first human settlements in this region (cf. Sect. 1.1.2) and thus, consistent to the previous chapter for present-day, the focus is set on the European region throughout the next two chapters. To match the intention of a best possible realization of the European climate during the Holocene, the advanced, with regard to long-term simulations, model setup of PlaSim is used to establish an experiment which should be as realistic as possible and thus should match palaeoreconstructions obtained from diverse proxy data. Carrying out a completely transient Holocene simulation with a fully coupled GCM is only rarely done by the scientific community because of computational considerations. Mostly time slice simulations are chosen which are spun up to the respective atmospheric compositions. The dominating question is clearly whether such a fully coupled model is able to yield a realistic climate, i.e. a climate which is similar to palaeoclimate observations.

4.1 Types of palaeoreconstructions

The combined approach to compare model output with proxy data is also carried out in a variety of other studies, such as those of e.g. *Reichert et al.* (1999), *von Storch et al.* (2004), *Brewer et al.* (2007) or *Renssen et al.* (2005a, 2006b, 2009). Whereas the latter authors focus on the output from one GCM and several proxy time series for their comparison, such as e.g. terrestrial, marine or glacial types, *Brewer et al.* (2007) are using an ensemble of different models, taken from the Paleoclimate Modelling Intercomparison Project (PMIP I, e.g. *Joussaume et al.* 1999; *Masson et al.* 1999, or PMIP II, *Braconnot*

et al. 2007a), together with single-type proxy data (pollen), taken from the study by *Davis et al.* (2003). *Von Storch et al.* (2004) are presenting a very special approach to reconstruct surface temperatures over the Northern Hemisphere. The authors use climate model output to construct grid-point based empirical proxies, i.e. "pseudoproxies", as they could exist on the basis of climatic conditions. These are then related with statistical methods and again compared to climate model output. The study by *Reichert et al.* (1999) can be seen in a similar context of producing synthetic proxies, combining them with statistical downscaling methods and the subsequent comparison to in situ proxy data.

Another possibility of how one can approach the wide range of palaeoclimatology relies on proxy data alone. Several studies are dedicated to this aspect. One has to distinguish between diverse approaches here, which are shortly summed up in the following. In pure proxy reconstructions, it is mostly given attention to a profound analysis of the proxy data; this may imply an extension of the data with respect to the inclusion of a higher number of proxies as well as multiproxy types. For example, *Mann et al.* (2008) are using a greatly expanded set of proxy data in combination with instrumental data (taken from CRU) and statistical methods to reconstruct surface temperatures for the Northern Hemisphere. *Seppä et al.* (2009) are also combining different types of proxies to create Holocene temperature time series for the northern parts of Europe. *Moberg et al.* (2005) are combining proxies of higher resolution with an annual signal (e.g. tree rings) and those having a lower, multicentennial, resolution, such as lake or ocean sediments, with statistical methods to yield an improved understanding about natural climate variability. The studies by *Rutherford et al.* (2004) and *Mann et al.* (2005) are basically dealing with different statistical methods which can be used in this context. These are then further interpreted with regard to their advantages and deficiencies as well as the reliability of the reconstruction results. Going one step beyond, the studies by both *Davis et al.* (2003) and *Mann et al.* (2007) aim at introducing slight improvements in the (statistical) proxy analysis. Notably, the study by *Davis et al.* (2003) is of strong benefit in this overall context of reconstructing Holocene climate. The authors have introduced a gridding-procedure for the proxies so that area-averages can be calculated. As will be explained in more detail in Section 5.1.2, proxies are assimilated at single sites and they normally cannot easily be transferred to a larger area in the order of the size of a grid-point in climate models. Moreover, they have expanded this three-dimensional spatial gridding with a fourth dimension represented by time. Through this, it is possible to link irregular time series, which are very common in palaeoenvironmental data (cf. Sect. 5.1.2) with a regular time step. The strong benefit especially crops up in the aspired relation of climate models and proxy data with regard to the specific properties of models, where both a spatially and temporally reliable allocation of the data are essential elements. Due to this, the reconstruction results achieved in this and the subsequent chapter are compared to a very large part to the results of *Davis et al.* (2003); moreover, the authors investigated the Holocene temperatures over Europe, which perfectly matches the region of interest in this study. The third possibility which must be mentioned in this context of reconstructing past climates, is the combination of both climate model and proxy data to that effect, that the proxy data are incorporated in the GCM to adjust the climate model simulation. As this is the second and most important aspect of this study, this is further discussed in all details in the subsequent chapter.

This chapter is now organized as follows: At the very beginning, the model as well as the experimental design are described. This is followed by the presentation of the outcome of the full Holocene simulation, focussing on parameters which can be compared with proxy data, i.e. surface air temperature and total precipitation, as well as the simulated SST of the adjacent North Atlantic and vegetation related parameters. The latter two are investigated at a later stage, in Section 5.9 and Chapter 6 respectively. Parts of the results obtained in this chapter are also used in the subsequent chapter as the basis for further considerations and also for the investigation of the European vegetation evolution over the Holocene in

Chapter 6. A general remark is made at this stage concerning the availability of palaeoobservations on precipitation. These are even stronger limited and more uncertain compared to, for example, temperature proxies, so that they must be handled with caution in a comparative analysis (*Zhang et al.* 2010). Therefore, Holocene precipitation patterns reconstructed by models are also very rare; nevertheless the aim is to gain reasonable results here, providing some contribution to the scientific community. All results are intercompared with existing palaeoclimate reconstructions for Europe to emphasize similarities or potential differences. It is concluded with a discussion and final remarks.

4.2 Experimental design

For all further palaeoclimate applications, PlaSim is used in T21 horizontal resolution ($\approx 5.6^\circ \times 5.6^\circ$ on the corresponding Gaussian grid) with ten not equally spaced sigma levels in the vertical. A transient experiment is carried out, which is forced by long-term orbital (*Berger* 1978b) and greenhouse gas (GHG) forcing (from Taylor Dome, *Indermühle et al.* 1999); all forcings are shown in Figure 1.1. Instead, the solar constant is unaltered in all experiments as the corresponding changes in insolation are small compared to changes induced by variations of the orbital parameters (cf. Sect. 1.1.1). The constant is thus kept fixed to the value of 1365 W/m^2. Moreover, the model is used with a calendar of 360 days per year, i.e. 30 days per month. Despite the enormous computational resources which could have been saved using an acceleration technique (*Lorenz and Lohmann* 2004), transient experiments are preferred to obtain really complete Holocene time series - neglecting the time-demanding computational costs. The experiments started from a steady state at 11 kyr BP with the respective orbital forcing parameters and CO_2 ratio. The last simulated year is 0 BP in each case; it is thus simulated backwards. The following descriptions differ corresponding to the respective configuration: In the very basic version, PlaSim is used with prescribed SST and sea ice based on the present-day climatological annual cycle. The performance of this model setup, i.e. with the climatological cycle of SST and sea ice, has been investigated in the previous section for present-day conditions. This experiment is assigned to be the reference (control) simulation for the subsequent chapter, on which the analysis and the application of the new methodology are relying. Because of this, the presentation of the reference results is left out at this stage and is postponed to Chapter 5. In general terms, the choice of an oceanic setup with climatological SST may seem very basic and too unsophisticated in this context, when thinking of the state-of-the-art coupled versions existing in PlaSim and other GCMs; however, it is very straightforward in relation to the methodology to assimilate proxies into PlaSim, which will be introduced in the forthcoming chapter. As will be shown later, the pure response of the atmosphere to the SST is of interest for this, disregarding any further oceanic feedbacks. This approach is further in line with *Widmann et al.* (2010). In addition, vegetation and land surface changes are accounted for by the respective parameters in the land surface scheme of PlaSim (cf. Chapt. 2) for this experiment, i.e. no specific vegetation module is used in this simulation.

In the fully coupled version, of which the results are presented in this chapter, prescribed SST are substituted by the LSG ocean. This ocean module is used as described in Chapter 2. Moreover, the vegetation module SimBA replaces the basic land surface scheme to account for a complete climate-biosphere interaction.

4.3 Results

In the following section the results for a transient, full Holocene climate simulation with the fully coupled version of PlaSim are presented, i.e. using the LSG ocean and the vegetation module SimBA. The results

are mainly compared with those by *Davis et al.* (2003), as this study provides a profound overview of the European temperature changes during the Holocene. In this study, the authors have reconstructed European winter and summer temperatures from various pollen archives. For this aim, the authors have sub-divided the European continent into six zones for the northern, central and southern parts of Europe which are further divided into a western and eastern part. This sub-division is clearly motivated by the varying insolation distribution over the Holocene which induces a latitudinally different climate signal. Due to the coarse resolution of PlaSim, the European continent is divided in four regions to achieve a data base which is as consistent as possible to the one by *Davis et al.* (2003). Only the northern and southern parts of Europe are considered, respectively the western and eastern parts. 15°E and 50°N display the boundary between the West/East and North/South. Through this division, a further consistency with the model study by *Fischer and Jungclaus* (2011) is established so that the results can be intercompared. In this study, the authors analyze the mid-Holocene temperature cycle using a coupled atmosphere-ocean model.

4.3.1 T2m

In Figure 4.1, the anomalies of the Holocene surface air temperature with respect to the preindustrial period are presented. For preindustrial, a 200 yr mean around the preindustrial year 1860 (≙ 90 yr BP) is chosen. The time series are presented for the four selected regions: northwestern (NW), northeastern (NE), southwestern (SW), and southeastern (SE) Europe. The winter (DJF) temperatures are shown in blue, summer temperatures (JJA) in red and the annual mean (ANM) in black.

In general terms, a seasonally and regionally varying temperature evolution during the Holocene can be observed. Whereas during summer, a cooling trend can be observed in all four European regions, which only differs in amplitude, the general trends are different for DJF and the annual mean. Over the northwestern parts (Fig. 4.1 a), the winter temperature trend reveals first a slight cooling at the early Holocene, followed by a warming during the period from 8k to 5k. The last 4000 years until the preindustrial are more or less constant. Moreover, the annual mean temperature trend is rather constant over large parts of the Holocene, after a weak cooling at the early Holocene time slices. Over the northeastern parts (Fig. 4.1 c), the pattern is very similar to the northwestern parts and differs only in amplitude. Moreover, in the annual mean and DJF, there is no early Holocene cooling but a rather constant evolution. A slight warming occurs since 9k (8k) during winter (annual mean). Over southwestern Europe (Fig. 4.1 b), the pattern is close to the one of the northeastern parts, but the variability is slightly reduced in DJF, so the structure is rather smooth. In general, the variability over the winter season is stronger compared to JJA and the annual mean. The southeastern parts of Europe (Fig. 4.1 d) are showing the strongest signal with a pronounced summer warming at the early Holocene, i.e. a cooling trend until 3k. Consequently a slight cooling trend can also be observed in the annual mean. During DJF, the trend is comparable to northeastern and southwestern Europe. It can be said, that the temperature evolution, represented in the annual mean, is mainly dominated by the summer temperatures, which follows closely the decreasing insolation trend over the Holocene.

4.3.2 Total precipitation

Stronger differences between the four European regions, compared to the temperature evolution, are evident in the precipitation time series. In the northwestern parts (Fig. 4.2 a), the evolution is rather constant and no remarkable changes between the early and late Holocene occurs, i.e. there is no trend of an increase or decrease of Holocene precipitation in this part of Europe. In the northeastern parts

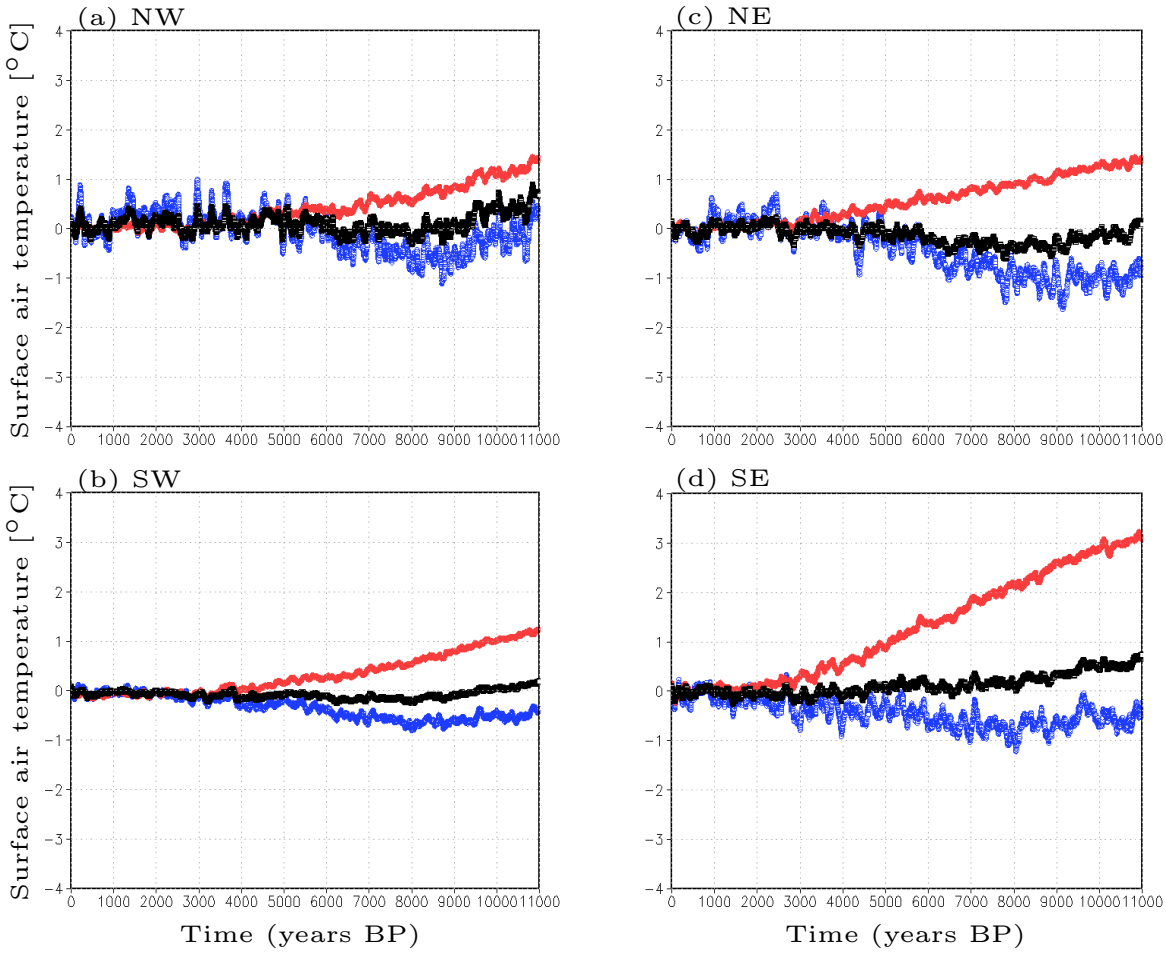

Figure 4.1: Holocene evolution of surface air temperature (T2m) anomalies (100 year running means) [°C] for (a) northwestern (NW), (c) northeastern (NE), (b) southwestern (SW) and (d) southeastern (SE) Europe - DJF (blue), JJA (red), ANM (black). Changes are with respect to the preindustrial (today).

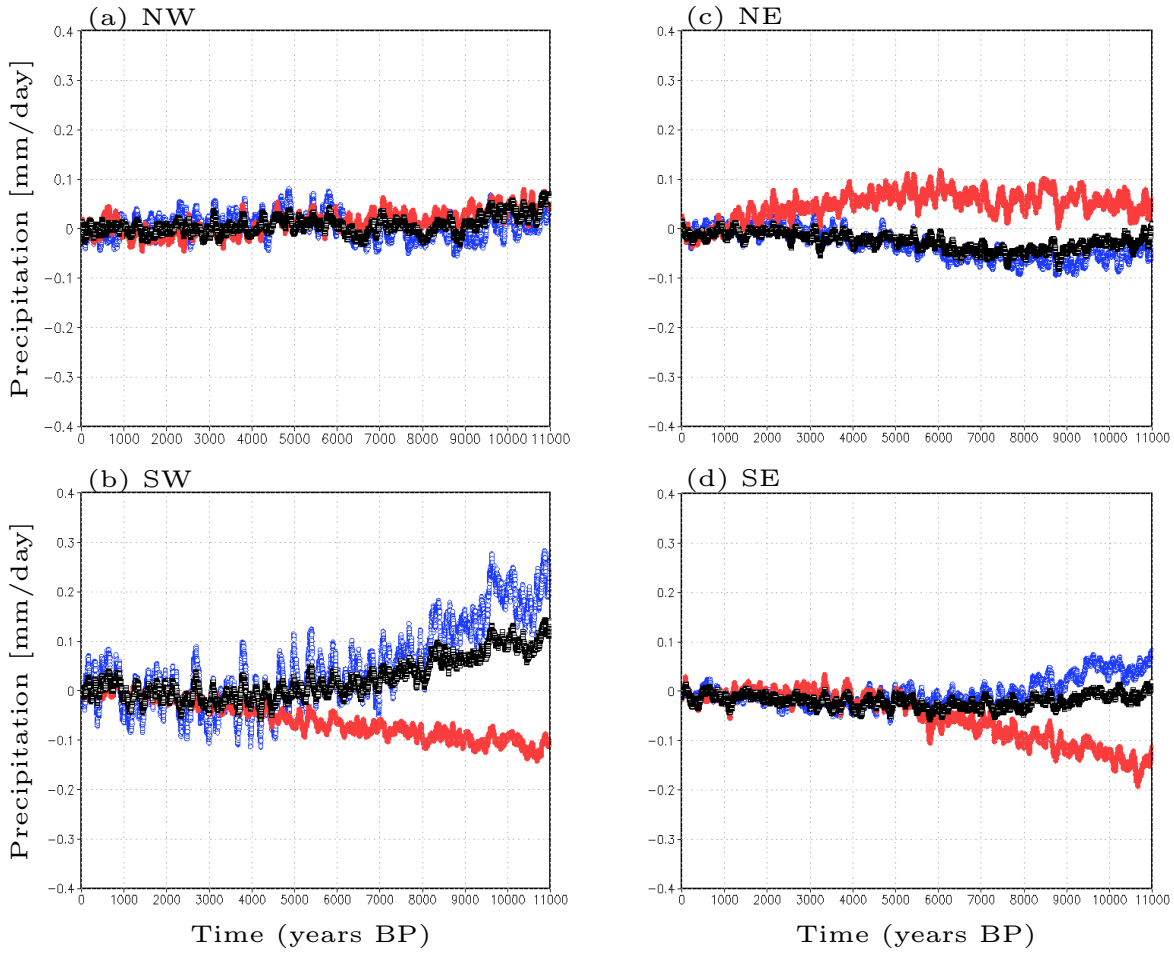

Figure 4.2: Holocene evolution of total precipitation anomalies (100 year running means) [mm/day] for (a) northwestern (NW), (c) northeastern (NE), (b) southwestern (SW) and (d) southeastern (SE) Europe - DJF (blue), JJA (red), ANM (black). Changes are with respect to the preindustrial (today).

(Fig. 4.2 c), a clear splitting in the seasons can be noticed. The trend is very similar between the annual mean and DJF and antipodal in JJA, i.e. in the first millennia of the early Holocene a drying occurs during DJF and the annual mean. This lasts until 6k and then the precipitation is slowly increasing again. The northeastern summer on the other hand is characterized by an early Holocene increase in precipitation and a decrease from the mid-Holocene until today. In the southwestern parts (Fig. 4.2 b), again an antipodal behavior occurs between the annual mean/DJF and JJA. Nevertheless, it is opposite to northeastern Europe, i.e. a drying until the mid-Holocene during DJF and ANM, followed by a slight increase in precipitation until today. During winter, this is even more pronounced. In summer, the early Holocene was drier as today and a moistening trend over the whole Holocene can be observed. The pattern over southeastern Europe (Fig. 4.2 d) is rather similar as over southwestern Europe. During summer, the region is getting wetter during the Holocene, whereas during DJF and partly also in the annual mean, a drying trend occurs whereas the amplitude is weaker in ANM.

4.3.3 Comparison

When now comparing, at first, the temperature results to other existing proxy reconstructions or model studies, certain similarities are obvious. For the summer temperatures in the northwestern region, the results show the same trend as the model results of *Fischer and Jungclaus* (2011) and the one reconstructed from pollen data by *Davis et al.* (2003). However, the amplitude is strongly weaker compared to the palaeoobservations but similar to the model results by *Fischer and Jungclaus* (2011), when considering the time period from 6k to today as done in the two other studies. During winter, a slight temperature increase starting in the mid-Holocene can be estimated in PlaSim, which would at least qualitatively agree with the pollen data but which show a much stronger warming. These remarks can also be transferred to the northeastern region, at least for JJA. The results show again a cooling trend from the mid-Holocene which is slightly weaker compared to the two other studies. During winter, the pattern is similar to the one over the northwestern region, i.e. showing a slight warming, and thus opposite to the clear cooling trend shown by *Fischer and Jungclaus* (2011). Indeed, the pollen data reveal no real trend during winter but cooler temperatures compared to the preindustrial for nearly the whole 6000 years. Thus, these colder temperatures match the ones shown by PlaSim at the mid-Holocene. The southern parts of Europe show the strongest deviations during summer, at least compared to the pollen data. Whereas trend and amplitude in PlaSim are very close to the results by *Fischer and Jungclaus* (2011) for DJF and JJA in both southern European regions, they are completely antipodal to the pollen data. These show a warming trend in both seasons over the Holocene over SW-Europe and also during summer in SE-Europe. During winter, no real trend occurs in the pollen data over SE-Europe but warmer conditions compared to today over nearly the complete 6000 years.

So far, only the period from the mid-Holocene until today is considered to be comparable to the results by *Davis et al.* (2003) and *Fischer and Jungclaus* (2011). When reconsidering now, in addition, the early Holocene time slices, an intensification of the signal can be observed during summer and for all four regions, i.e. the amplitude is increasing. Concerning the stronger summer signal in the early Holocene time slices, it must be commented that it may be overestimated by PlaSim because of the missing land ice, which would have a cooling effect. This is also shown by, for example, *Renssen et al.* (2005a). In this study, the authors present the results of a fully coupled Holocene climate simulation for the high northern latitudes. When intercomparing a control simulation with an experiment using a prescribed, static ice sheet which is instantaneously removed after 7 kyr BP, the authors rate the warming, caused by the missing ice, and thus the overestimated temperature response to $\approx 0.5^{\circ}$C. This overestimation may be even stronger when a dynamical ice sheet is included.

During winter, the responses are slightly different. In the northwestern, southwestern and -eastern parts, a cooling in the 10k and 11k-time slices is followed by a slight warming until the mid-Holocene. In the northwestern parts the trend from a cooler early Holocene to a warmer mid-Holocene is more pronounced as in the other three regions. In terms of the impact of the ice sheet during winter, *Renssen et al.* (2005a) find no effect of the ice on winter temperatures.

For precipitation, it is referred to the study by *Renssen et al.* (2005a). Although the considered regions in this study are not perfectly matching the chosen selection here, the results can at least quantitatively be compared to those of *Renssen et al.* (2005a) for Scandinavia. The authors detected an invariant summer precipitation evolution from the early Holocene at 9k to the preindustrial which is consistent to the pattern over NW-Europe (Fig. 4.2 a). However, the authors also identified local changes in precipitation in their spatial anomaly maps (*Renssen et al.* 2005a) for Scandinavia, i.e. a decrease in summer precipitation over the whole Holocene, thus wetter conditions at the early and mid-Holocene. These have also been found out by *Guiot et al.* (1993) for northeastern Europe in their study on Holocene precipitation patterns inferred from pollen and lake-level data. This indicates at least regionally different anomalies in the northern parts of Europe which are captured by PlaSim. The less pronounced changes mainly in the northern parts of Europe are also stated by *Crucifix et al.* (2002) in their analysis of the Holocene climate evolution over the high northern latitudes. For the southern European precipitation, *Guiot et al.* (1993) assume drier conditions from the palaeoobservations over the whole Holocene compared to today, thus a continuous increase in precipitation. This trend is also captured by PlaSim for both southerly regions (Fig. 4.2 b, d), at least for the summer precipitation. An exception is constituted by *Guiot et al.* (1993) over western France, showing wetter conditions at the early Holocene, despite the drier conditions in the rest of (southern) Europe. Although France cannot explicitly be recaptured in the time series here, at least a slight variation is obvious compared to SE-Europe. The precipitation increase over SW-Europe seems to be more slowly, i.e. the gradient is weaker, which may be caused by regional variations. Nevertheless, this moistening trend in the southern parts of Europe is opposed by the study by *Brewer et al.* (2009), where the authors intercompare a set of palaeoclimate (pollen) reconstructions to an ensemble of climate models. They indeed have identified more humid summers (together with the cooler conditions). Wetter conditions in these regions have also been detected by *Brewer et al.* (2007) and *Masson et al.* (1999). In general terms and at least for NE-Europe and the southern parts, the largest changes in precipitation occur during JJA and not during DJF, which is consistent to the remarks in the study by *Renssen et al.* (2005a). In contrast, the changes during DJF and ANM are rather low and are very similar to each other which is opposite to *Renssen et al.* (2005a) where the annual mean precipitation pattern is close to the summer picture. Thus, opposite to the temperature evolution, the summer precipitation is not dominating the annual mean precipitation evolution. Besides the northwestern regions, the summer precipitation is antipodal to the winter and annual mean precipitation trend, which are both very similar to each other.

4.4 Summary and discussion

This chapter has given an overview about the outcome of a fully coupled PlaSim-simulation with respect to the representation of the European climate over the Holocene. Temperature and precipitation anomalies to the preindustrial climate are investigated for four selected regions, into which Europe has been subdivided. This has thus been one approach of reconstructing palaeoclimate, i.e. with the use of climate models.

The results confirm that PlaSim is indeed able to simulate the general patterns for temperature and

precipitation which are also given by other model studies and palaeoclimate observations. A clear insolation induced and thus latitudinally varying temperature response can be detected in the four regions of Europe, i.e. decreasing trends during summer and slightly increasing during winter (cf. Fig. 1.1). The simulated results are in line with those of other model studies (*Brewer et al.* 2007) and those of *Fischer and Jungclaus* (2011) for nearly all four regions and both seasons, except the northeastern winter. Moreover, they agree with the reconstructed pollen data by *Davis et al.* (2003) at least qualitatively in trend and amplitude over the northern parts of Europe. Stronger deviations occur over the southern parts of Europe during summer, with antipodal trends in the model and pollen results. Nevertheless, as *Fischer and Jungclaus* (2011) state, these discrepancies have also been found out by *Davis and Brewer* (2009). Comparing data from a new pollen-based reconstruction and output from PMIP II with regard to an investigation of both the underlying mechanisms and responses of the orbital forcing (in terms of the latitudinal insolation gradient) on the climate system, *Davis and Brewer* (2009) found the same inconsistency in the southern European climate. Without going too much into detail in this context, the authors argue that this can be largely attributed to how the models simulate the temperature response to a changing latitudinal insolation gradient between the mid and high northern latitudes (*Raymo and Nisancioglu* 2003). Whereas the pollen data seem to be more sensitive to latitudinal insolation changes, models are more strongly influenced by the seasonal insolation. As *Fischer and Jungclaus* (2011) further discuss, the coarse resolution of the models may, besides this mismatch, also contribute to these shortcomings. It may be thus very likely that insolation induced changes in the atmospheric circulation are not resolved properly by the model. Moreover, this discrepancy can also result from internal feedbacks or mechanisms which are not captured by the model. However, as *Fischer and Jungclaus* (2011) point out, these deficient results, in terms of missing cooler summer temperatures in the mid-Holocene, are not specific for individual models. However, it seems to be a common feature of coupled climate models (*Braconnot et al.* 2007b) in all of which the mid-Holocene cooling is confined to the monsoon regions. Besides these low and mid-latitude differences in the temperature response, both *Davis and Brewer* (2009) and *Fischer and Jungclaus* (2011) have identified different responses at the high latitudes between models and data which can be attributed to the influence of the sea-ice evolution on the amplitude of the seasonal temperature cycle. This is not part of this study and is just mentioned as a short comment. To sum up for the Holocene temperature evolution, it must be said that for such a relatively restricted region, PlaSim and also other models are indeed able to partly capture the correct trends, with the strong limitation of a lower magnitude of the climate changes. Nevertheless, because of the small geographical area, the models have problems in capturing the correct trends everywhere.

For the precipitation, again larger similarities compared to reconstructions occur over the northern parts of Europe, where PlaSim is mostly in line with other models and reconstructed data cited above. Stronger changes again occur over southern Europe, where PlaSim does not cover the assumed wetter conditions during summer. However, as has been mentioned before, the precipitation evolution in PlaSim is not determined by the summer pattern; indeed, the annual mean is closer to the winter pattern. This is opposite to the remarks by *Renssen et al.* (2005a) where summer and annual mean are more similar to each other. However, when considering the today's conditions, the precipitation maxima in the southern European regions are clearly occurring during winter. This problem is slightly more discussed by *Masson et al.* (1999). Several considered models in this study simulate wetter conditions than today over southern Europe, caused by enhanced winter precipitation. This is associated with drier conditions in northern and northeastern Europe (similar to PlaSim during winter) and even more pronounced for the models which simulate colder conditions over the whole Europe in winter, which is thus more in line with the results shown by PlaSim. Summing up, the pattern of the Holocene precipitation changes over southern Europe seems to be more variable and potentially influenced by several parameters, such as the boundary

conditions or the resolution (*Masson et al.* 1999). Thus, the identification of the "correct" precipitation evolution mainly over southern Europe seems to be unequally more complicated as it is for the northern parts or the temperature. Therefore, more effort is surely needed on this topic, resulting from the model side as well as from the reconstructions.

4.5 Conclusion

This reconstruction method, using a fully coupled version of PlaSim, has marked one way of reconstructing palaeoclimate. Besides providing reasonable results, certain problems are obvious which have been discussed above. These results will further serve as a kind of verification for the outcome of the next chapter, i.e. the results of climate reconstructions for the Holocene using proxy data that are assimilated into PlaSim using a completely new methodology.

5 Assimilation of proxy time series into the Planet Simulator

In the previous chapter, the Holocene climate has been reconstructed using the fully coupled model version of PlaSim. The forthcoming chapter can still be regarded in the framework of the reconstruction of the Holocene climate, but it now goes one step beyond and is dedicated to one of the leading questions of this overall study, i.e. the "Assimilation of global proxy time series into a GCM like the Planet Simulator". With regard to the aforementioned approaches of reconstructing past climates, now both climate model and proxy data are combined to directly use the latter - as reliable and significant indicators of palaeoclimate - to improve the model simulation. The motivation for this new approach to assimilate global proxy time series into a GCM like PlaSim is embedded in an ongoing debate in the scientific community to link climate models and observations.

This chapter is structured as follows: At first, the data used in these studies are shortly presented. This includes the experimental design of PlaSim as well as an overview about the characteristics of palaeoenvironmental data and the inherent uncertainties. The specific problems when compared to climate model output are discussed together with the scientific background, the "state-of-the-art". After that, the novel method is introduced and the results of a variety of applications are presented, discussing similarities, differences and potential improvements to the reconstruction carried out in Chapter 4. The newly generated data are further compared to other existing proxy data; a discussion and conclusion will complete this chapter.

5.1 Data

5.1.1 Model data

As the reference experiment for all further analyses in this section, a transient Holocene climate simulation is carried out with prescribed SST. This simulation is based on an identical setup as in the preceding chapter but differs in the usage of climatological, present-day SST instead of the LSG ocean. This reference simulation yields a time series of (surface air) temperature for the Holocene which is characterized by the long-term changes in orbital and GHG forcing. The main deficiency of the ocean with climatological SST is the lack of internal variability which occurs at all time scales up to several millennia.

This low frequent variability cannot be recovered by this ocean representation because all oceanic responses and potential feedbacks are strongly dampened when the SST is predefined and not subject to change. Hence, the ocean is unable to vary which impedes the formation of any kind of internal (oceanic) variability. Proxy data may therefore stand in for providing information about the variability patterns.

5.1.2 Palaeoenvironmental data

As nearly the entire study is relying on proxy data, some remarks are made with regard to the reliability and uncertainty of this data. It can be easily comprehended that meteorological observations or measurements, as they exist today, haven't existed several hundred or thousand years ago. The establishment of an observational weather system has started in the 19th century, so, as a consequence, alternative tools have to be found to be able to make assumptions about the climatic conditions of the past. Already very early, in the first 1000 years before Christ (BC), the first attempts have been made by Greek philosophers to rely fossils to the climatic conditions of earlier times (*Lohmann* 2002). It hasn't been until several millennia later that these first attempts have received scientific justification. The hypothesis of "Uniformitarianism", formulated by the two geologists Karl von Hoff (1771-1837) and Charles Lyell (1797-1875, *Lyell* 1830), assuming that the natural laws and processes are valid over time and space, can be seen as the basis for palaeoclimate research (*Jones et al.* 1998), with the dictum that "the present is the key to the past". Hence, through a combination of taking data from natural climate-dependent archives of ancient times and the knowledge of the modern climatic conditions, it is possible to qualitatively interpret the palaeoenvironmental data in a climatic context. For the comparison of past climates simulated with climate models, records from these archives, i.e. "proxy" data, can be considered as observations. In contrast to those existing today, proxy data are indirect, or "proximate" (meaning substitute), measurements or even only estimates of climatic variables; where "indirect" refers to the fact that the climate signal cannot be extracted directly (*Ruddiman* 2000) from the data, but is derived from indirect relationships of a biological, physical or chemical quantity in the environmental archive (*Jones and Mann* 2004). Only rarely, and sometimes rather ambiguous, the relationship is sufficiently understood to really provide a quantitative measure of past temperature or precipitation from the proxy. To extract the climatic signal, the proxy data is reprocessed through a calibration - using e.g. statistical methods or so-called transfer functions (*Kohfeld and Harrison* 2000; *Jones and Mann* 2004) - against modern instrumental data. Following the aforementioned principle of uniformitarianism, it is assumed that the dominant modern relationships have also operated unaltered during the period of interest in the past (*Bradley* 1999). Moreover, the climatic signal, which may be inclosed in the records, may be weak and biased by extraneous noise caused by local, and potentially non-climatic processes (*Bradley* 1999). These local processes, whether of climatic nature or not, have an enormous impact on the proxy records. Precisely because of this dominating influence, proxies, which are located very close to each other, can show completely different (temperature) trends, involving at the same time an additional problem concerning the overall reliability of proxy data. In case of studies using multiproxy ensembles - a common approach which is used in many proxy reconstructions (e.g. *Rutherford et al.* 2004; *Renssen et al.* 2005a; *Mann et al.* 2008; *Sundqvist et al.* 2010; *Zhang et al.* 2010) and which is also aimed at in this context (cf. Sect. 5.8) - this has to be kept in mind and considered. These palaeoenvironmental (proxy) data can be:

- tree rings
- corals
- ice core records

- lake (varved) sediments
- pollen
- fossils
- marine sediments

The wide range of proxy data of different types does not necessarily include the possibility to make a significant analysis of past climates. These records all have their own characteristics and they vary considerably in their reliability as climatic indicators of long-term climate changes - they all differ according to their spatial coverage (i), the period which they are covering (ii) and their general accuracy related to the dating accuracy (iii). Studies as this should begin with a profound understanding of the specific proxy type. However, due to their complexity, these characteristics won't be discussed in detail here and it is referred to *Bradley* (1999) for a complete overview. Only those aspects are discussed having a direct impact on this study and on its aim to incorporate proxy time series into PlaSim.

(i) Spatial coverage The most hampering detail affecting all proxies is that they can be aggregated and analyzed, due to their specific properties (e.g. ice cores or tree rings), only in very limited regions of the world. This involves that proxy data can provide spatially only incomplete information, reflecting the climatic conditions on a very regional scale, which may indeed sometimes be representative for a larger region (see next section) ; however, this is not necessarily the case and must be carefully proven for each individual proxy.

Figure 5.1 illustrates the problem of the coarse spatial availability of proxy data in a direct comparison to the existing meteorological stations of the World Meteorological Organization (WMO). The later comparison is relying on palaeoclimate proxy time series from the long-term high-resolution time series compilation by *Wirtz et al.* (2010). They assembled a total of 124 climate proxies at 103 globally distributed sites from existing literature. There are, of course, existing more proxy data than those included in this study and shown in Figure 5.1 b; but even if all available data were included in one single chart, the quantity of proxy records would be several times lower than the amount of observations. The large discrepancy in the observational data of the Northern Hemisphere compared to the Southern Hemisphere is neglected and only the general picture is taken into account. Apart from the spatial limitation of the palaeoenvironmental data, they are also temporally strongly restricted. This can be divided in the overall temporal resolution (ii) and the uncertainty related to the chronology of the proxy records (iii), i.e. their general accuracy.

(ii) Overall resolution One could assume from Figure 5.1 that the proxy records are providing a temporally equally consistent and continuous data base compared to the observations. However, this is not the case. In fact, the data do not even span identical time periods - instead, they all have their respective time axis. In general, it can be said, that the more the data are extending back in the geological past, the fewer data exist and the more their quality and reliability is deteriorating (*Jones et al.* 1998; *Wanner et al.* 2008). All time series of *Wirtz et al.* (2010) span at least 4000 years, and most have a sampling resolution of 200 years or better. Thus, the proxy records are intermittent and mostly do not provide an instantaneous and periodic signal of the climate state. Only very rarely, depending on the specific proxy type, the data are on an annual or seasonal basis - e.g. temperature of the warmest or coldest month. This high resolution can be received from tree rings, varved sediments, corals and ice cores. For all other records listed above, only longer-term means (up to several decades) are available (*Jones et al.* 1998;

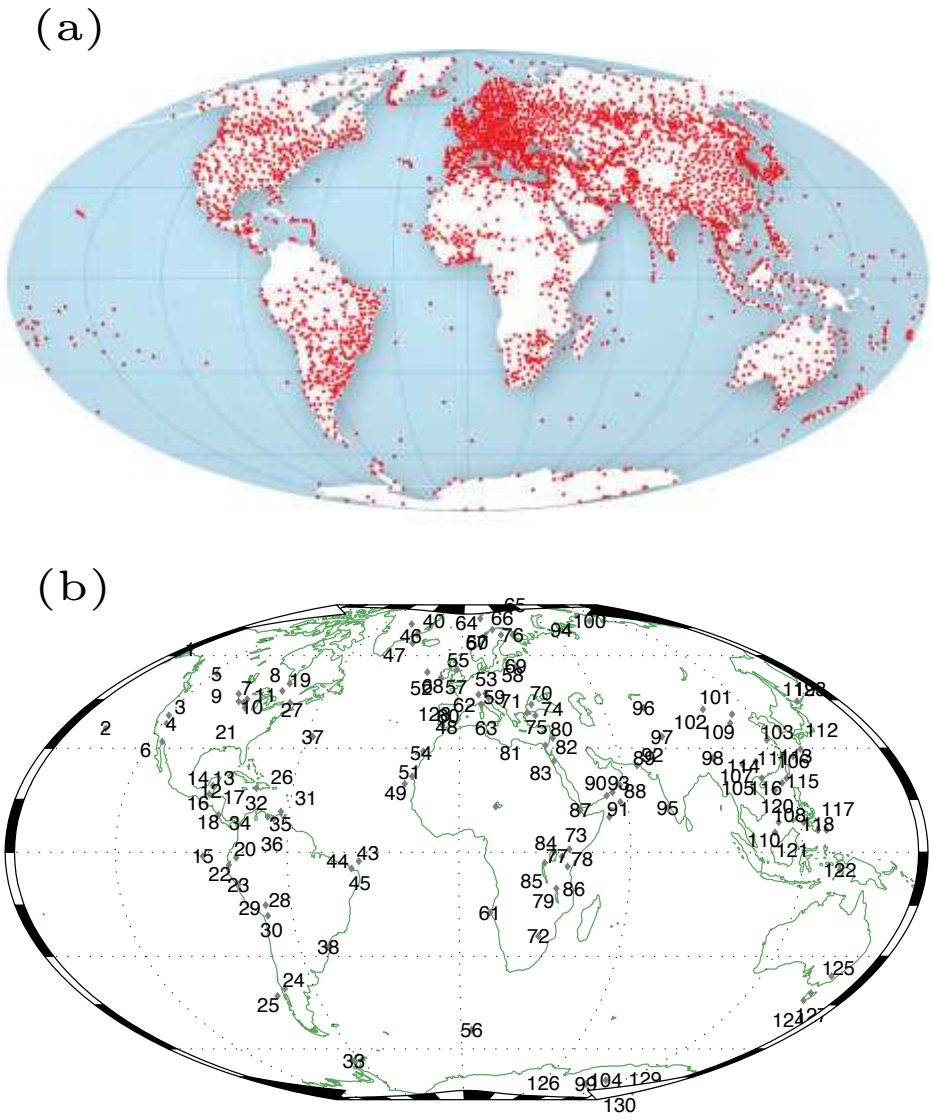

Figure 5.1: Overview of globally distributed (a) meteorological stations, taken from the WMO, and (b) proxy data, taken from the study by *Wirtz et al.* (2010). Each number in (b) represents an individual proxy time series, explanations and details are given in *Wirtz et al.* (2010).

Bradley 1999; *Rutherford et al.* 2004). Temperatures of the warmest and coldest months are sometimes used in palaeoclimate reconstructions (e.g. *Davis et al.* 2003; *Rutherford et al.* 2004) as seasonal means. This nomenclature, called bioclimatic parameter (*Kohfeld and Harrison* 2000), may sound weird, as not the winter (December-January-February, DJF) and summer (June-July-August, JJA) temperatures are considered; it is indeed comprehensible and motivated by the insolation induced slight shifts of the seasons during the Holocene, which may have led to a different composition of the warmest summer/coldest winter months (cf. Fig. 1.1 in Sect. 1.1.1). As mentioned before, monthly and seasonal means are used according to the modern calendar, which is in line with other model studies (e.g. *Luterbacher et al.* 2004; *Renssen et al.* 2005a; *Wanner et al.* 2008).

(iii) Dating accuracy Another aspect impeding the complete and impeccable reliability on proxy data is the dating accuracy, which is of substantial importance for palaeoclimatology in general (*Bradley* 1999). When the proxy records are assembled, they initially don't have a respective time axis. Therefore, the data must be assigned temporally to enable an interpretation in a geological and climatological context. Depending on the proxy type (trees, corals, ice, sediments), different dating methods have to be used. These are derived indirectly and can be, for example, of radioisotopic, biological or chemical nature - according to the specific characteristics of the records. Each method has its own accuracy and contains its own source of error and uncertainty. In general, when interpreting proxy data, a profound knowledge of the dating procedure and the inherent limitations is essential, as it allows an estimate of the degree of detail which is available from the proxy record (*Bradley* 1999). To know about the latter may be even more worthwhile than the knowledge of the correct date itself (*Bradley* 1999).

Summing up, the proxy data are accompanied by a large range of uncertainties or even deficiencies which are important and non-negligible caveats in this field. These limitations, regarding the interpretation of the raw data, the dating accuracy and the restriction to single sites, are at the same time the governing requirements if the proxy data are used for further analyses, e.g. in a comparison with climate model output, where, for example, a reliable information on the time axis is indispensable - at least, one should be aware of the inherent uncertainties. These remarks further underpin the difficulty of relating proxy data and climate models and, even more, of incorporating them in GCMs, which is the aim of this study. For further and more detailed aspects concerning the uncertainties and peculiarities of proxy data, it is referred to *Jones et al.* (1998); *Jones and Mann* (2004) or *Bradley* (1999).

Ammersee proxy

After the more general remarks concerning the palaeoenvironmental data and its limits, now one specific proxy is introduced, which is used primarily in the further analysis of this chapter. As mentioned in the preceding section, the comparison relies on palaeoclimate proxy time series from the long-term high-resolution time series compilation by *Wirtz et al.* (2010). In this study, palaeoclimate records are analyzed with regard to their statistical behavior, i.e. mainly the variability on different time scales. Besides an evidence for a variability change in the mid-Holocene, around 5000 years BP, geographically organized clusters of each six to ten proxies are found which exhibit identical variability trends. This is remarkable because diverse climatological variables are forming these clusters so one would have expected a different spectral behavior. These clusters are composed on a subcontinental scale with a diameter of roughly 3000 km. The statistical similarity is significant over a relatively large area and not only for one single proxy (*Wirtz et al.* 2010). This result is relevant for the choice of the proxy with regard to its representativeness as a valuable indicator of European climate change over the Holocene and can be seen as further in line with the improvements in *Davis et al.* (2003) regarding the spatial

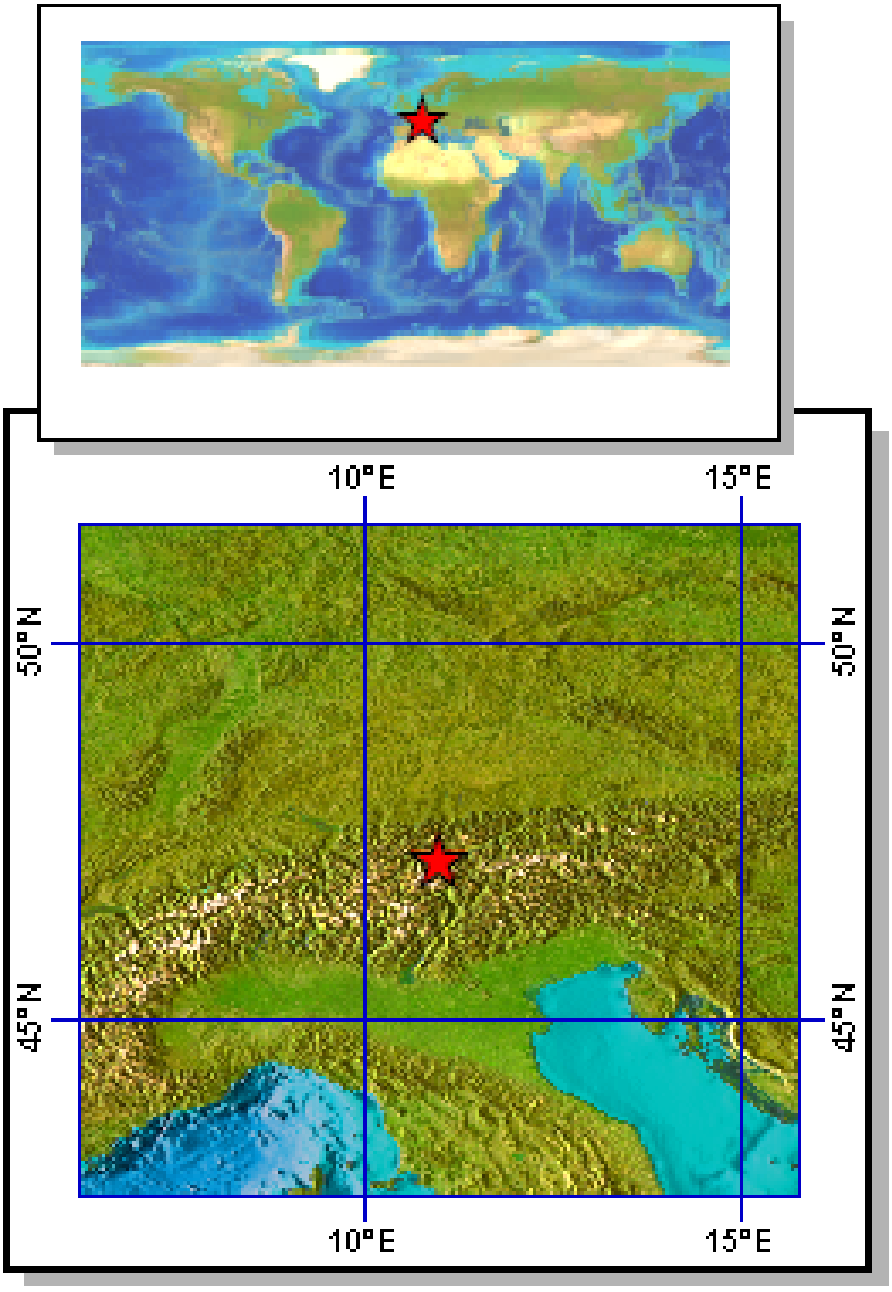

Figure 5.2: Location of the Lake Ammersee proxy to the southwest of Munich, taken from the National Oceanic and Atmospheric Administration (NOAA).

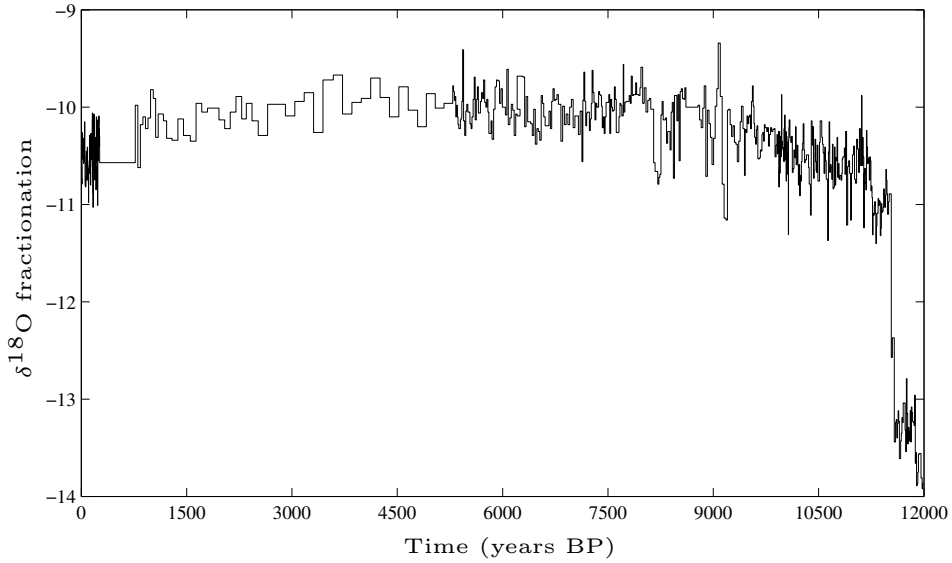

Figure 5.3: Raw data (ostracod δ^{18}O-record) from the Lake Ammersee proxy (*von Grafenstein et al.* 1998) from 0 to 12 kyr BP. The resolution between individual data points is 20-years on average.

gridding procedure with respect to an enhanced spatial reliability of proxy data. Due to the specific aim to reconstruct the European climate, the proxies are selected accordingly. As the climate model should be related to climate proxy data, only those data are chosen which give quantitative information on climatological variables, i.e. surface temperature or annual precipitation, such as mid- and high-latitude palaeothermometer proxies based on δ^{18}O.

The exemplary record, for which the method is introduced at a later stage, is obtained from Lake Ammersee in southern Germany at 48°N and 11°E, to the southwest of Munich (Fig. 5.2). Only one specific proxy time series is chosen here to avoid the problem of potentially inconsistent and opposing proxy signals (cf. Sect. 5.1.2). From 80 m water depth, *von Grafenstein et al.* (1998) analyzed the oxygen isotope ratio (δ^{18}O) of ostracod shells in a sediment core. The oxygen isotope fractionation (δ^{18}O) as the difference of the sample ratio of ^{18}O to ^{16}O relative to the Pee Dee Belemnite (PDB) standard (*von Grafenstein et al.* 1998) is a well-established indicator of climate changes. This is due to a close interplay between temperature and hydrologic parameters (precipitation, evaporation and runoff) - thus very local environmental settings depending on the geographic location - which is acting as the regulatory mechanism of the isotopic composition of water. An analysis with regard to the hydrological cycle has been carried out by *Czymzik et al.* (2010) using a varved sediment record in the Ammersee. Here, a flood time series is reconstructed from this sediment for the last half millennium taking into account that the detrital layers in those varved lake sediments are caused by flood-triggered fluxes from the nearby Ammer River (*Alefs* 1997; *Czymzik et al.* 2010). *Czymzik et al.* (2010) identified a clear seasonal, thus temperature-dependent, signal of flood-induced detrital material in the annual sedimentation rates.

The temporal evolution of the δ^{18}O ratio thus allows conclusions to be drawn about the corresponding evolution of the prevailing local climatic conditions, as, for example, evaporation is affecting the lighter (heavier) ^{16}O (^{18}O) differently depending on the temperature. δ^{18}O will be higher (≙ less neg-

ative values as deviations form the standard mean) in case of higher temperatures and lower (≙ more negative values) during colder conditions (Fig. 5.3). For Lake Ammersee, *von Grafenstein et al.* (1996) reveal that, due to the specific isotopic composition of the lake water, the proxy reflects the temporal variation in local precipitation. In addition, the proxy strongly correlates with the time series of annual mean air temperatures from an observational station in the catchment area of the lake during a period of 200 years of the last millennium. This correlation to an instrumental record may additionally serve as a validation for Lake Ammersee as a very sensitive archive for high-resolution palaeotemperature reconstructions (*von Grafenstein et al.* 1998, 1999), being a reliable climate indicator also for temperature ranges occurring during the whole Holocene (*von Grafenstein et al.* 1996). The seeming discrepancy between a proxy reflecting precipitation variations and its interpretation with regard to temperature changes has been rectified by, for example, *Dansgaard* (1964), *Siegenthaler and Oeschger* (1980) or *Rozanski et al.* (1992), who demonstrated a strong relationship between annual mean precipitation and annual mean surface air temperature. *Rozanski et al.* (1992) found a close correlation between both climatic variables for different regions around the globe, which indicates the suitability of these isotopes as a palaeoclimatic indicator. As the adjustment relies on the Ammersee proxy as an indicator of European climate change during the Holocene, it is necessary to know about the representativeness of the proxy for the European climate during the Holocene. Using a newly derived core in Lake Ammersee, *von Grafenstein et al.* (1998) identified, for the first time in a European proxy time series, a similar signal as it is so far only been found in Greenland ice (*Grootes et al.* 1993) and which is pointing to the 8.2 kyr event (*Alley et al.* 1997; *Alley and Ágústsdóttir* 2005). This event is characterized by strong freshwater pulses - triggered by the final melting stages of the Laurentide ice shield - which strongly influenced the North Atlantic thermohaline circulation by affecting the North Atlantic deep water formation. These freshwater pulses impeded the northward heat transport (*Rohling et al.* 2002) and initiated cooler and drier conditions lasting about 300 years. Moreover, they had an influence on the δ^{18}O-ratio. Although the causal relation between the proxy signal in the Ammersee and the freshwater discharge is not fully resolved (*von Grafenstein et al.* 1998), a close relationship is strongly hypothesized. Due to the very complex structure of this cooling event, it is neither easily identified by models (*Ágústsdóttir* 1998; *Renssen et al.* 2001, 2002; *Bauer and Ganopolski* 2004) nor proxy data in the affected regions. Whereas for the models the problem is mostly due to simulating the forcing correctly, the difficulty of the chronology uncertainty (*Alley et al.* 1997; *Wiersma and Renssen* 2006) may be, amongst the others described in the previous section, such as temporal and spatial resolution, the most relevant obstacle for the proxies. This becomes even more significant when an event of short duration, like the 8.2 kyr event, is of interest: The brevity of the event (≈300 years) further complicates the selection of proxies as many sites do not have a sufficient temporal resolution to find a signal of this temporal span (*Alley and Ágústsdóttir* 2005). For the Ammersee proxy, the chronology of the core has been tested using two independent age models where both show a strong similarity and thus reliability (*von Grafenstein et al.* 1998). Despite the Lake Ammersee proxy, the 8.2 kyr signal is registered in several high-resolution proxy data around the North Atlantic (*Renssen et al.* 2001), such as in ice cores from Greenland (*Grootes et al.* 1993; *Blunier et al.* 1995; *Alley et al.* 1997), ocean or lake sediments of the North Atlantic (*Bond et al.* 1997) or the ones cited in the study by *Wiersma and Renssen* (2006) as well as tree ring records from northern and southern Germany (*Klitgaard-Kristensen et al.* 1998). In the context of the 8.2 kyr event, the studies by *Klitgaard-Kristensen et al.* (1998) and *von Grafenstein et al.* (1998) have also been cited by *Jansen et al.* (2007), which additionally fosters a conclusive reliability on this proxy.

Summing up, because of the consistency and the contemporaneous signal also in studies on other proxy types and regions across Europe - even on temporally very small scales as for the 8.2 kyr event - the δ^{18}O-record of the Ammersee proxy seems to be a reliable and significant European climate indicator

(*von Grafenstein et al.* 1998), providing quantitative material for palaeoclimatic analyses but also for the upcoming reconstruction of the Holocene climate.

The original data curve of the Ammersee proxy, presented in Figure 5.3, is built on the raw data (*von Grafenstein et al.* 2003) of the δ^{18}O-values for the period from 0 to 12 kyr BP, thus covering the whole Holocene which is of strong benefit for the further analysis. Moreover, the sample resolution between individual data points is 20 years on average for the whole Holocene, which is very high for a proxy in general. However, as can be discerned from Figure 5.3, this sample resolution varies rather strongly for different parts of the Holocene. It is below or close to the average for eight millennia in total (mostly at the early and late Holocene) and more distinctly above the average between 1 to 4 kyr BP.

5.2 Models and proxy synthesis: State-of-the-art

After having learnt about the different data which will be used in this chapter including their specific features, it is further proceeded with the particular challenge of relating climate models and the "real" world - derived from observations. For the comparison of simulated palaeoclimate, palaeoenvironmental data can be considered as observations.

Over the last several years, efforts have been made to find a way to combine climate models and proxy data to that effect that proxies are incorporated into the models to improve the model simulations. Referring to the remarks in Section 5.1.2, the specific difficulty of relating a GCM with observational (proxy) data, respectively their climates, is discussed which is unequally more complicated compared to present-day conditions, and includes a wider range of obstacles which have to be overcome. It thus represents one of the largest challenges to the modelling community. Here, the coarse spatial and temporal resolution, the influence of very local processes, which may be decisive for the proxies but either be completely unknown or not resolvable by climate models, as well as their limited representativeness as a climate indicator for a wider region presumably contribute most to this difficulty. Concerning the climate modelling part, an additional source of uncertainty is added through the essential inclusion of climate forcing factors - for example orbital or GHG forcing - to account for long-term changes of the atmospheric state. However, this reconstructed forcing can potentially produce diverging simulation results because of its unknown internal variability or general model limitations (*Widmann et al.* 2010). These uncertainties in model and proxy data make it difficult to find out whether the differences between both are caused by model biases or by the diverse realizations of internal variability in both model and data (*Goosse et al.* 2010). It is an important and ongoing challenge to solve this problem of the inconsistency between models and proxy data and has opened so far a variety of either statistical or dynamical approaches. However, the direct implementation of proxy data in a GCM is still at the very beginning. First attempts have been made by e.g. *Werner et al.* (2011) who incorporated stable water isotopes into the hydrological cycle of the European Center Hamburg Atmosphere Model (ECHAM5). This implementation has been successful with regard to a close agreement to newly available measurements of atmospheric water vapor.

One common way to overcome the model-data inconsistency and to establish a synthesis between both are data assimilation techniques (DA hereinafter), where a combination between model and data takes place, such that an additional (observational) data set is included in the model. Following the very basic definition of DA, brought up by e.g. *Ghent et al.* (2010), the inclusion is acting to constrain the model simulation to the observations so that the inherent uncertainty of models can be reduced.

DA have been utilized for a long time in weather forecasting with the aim that the atmospheric states as given by the climate model - or more specifically the numerical weather prediction models

(NWP) - agree with observations; in recent years, DA have been applied to model-proxy relationships in palaeoclimate simulations, with the proxies serving as the observations. However, DA developed for the weather forecast cannot be transferred to palaeoclimate studies due to the strong differences between observations and proxy data (*Widmann et al.* 2010, cf. Sect. 5.1.2). The most relevant and hampering shortcoming results from the fact, that many proxies do not provide an instantaneous and periodic signal of the climate state but seasonal, annual, or longer-term means which is not adequate for DA methods used in weather forecasts. In their study, *Widmann et al.* (2010) present three DA which were developed for palaeoclimatic analyses and to overcome the inherent difficulties of the proxy data. These DA have been used to predict the extratropical Northern Hemisphere climate over the last millennium through the use of a climate model and several proxy records. Although all three methods succeeded in closing the gap between the simulations and the reconstructions, there still remained uncertainties which were caused by the inconsistency of the different proxies, which showed partly opposing signals, and by the methodological difficulties of each DA and its inherent limitations. In this context, *Goosse et al.* (2010) point out that it is very unlikely that it will ever be technically possible to bring the two components model climate and proxy data together, i.e. to find a system state that is compatible with the model physics and at the same time consistent with the observational data: The more complex structure in the data cannot be represented by the simplified physics of the model (*Goosse et al.* 2010). Besides for the weather forecast, DA is a widely used tool in various scientific fields, such as for the implementation of satellite data in climate or land surface models (*Reichle et al.* 2004; *Xia et al.* 2012b,a). In the framework of DA, the inverse procedure can be equally used to combine models and data. Both DA and inverse modelling are closely related and arise from a similar theoretical background. They both employ the basic principle of estimating the input from the knowledge of the output or target state (*Wu et al.* 2007; *Widmann et al.* 2010; *Guiot et al.* 2000, 2009). Different, mainly statistical, approaches to the inversion problem have been used in diverse applications, such as palaeovegetation modelling (*Guiot et al.* 2000, 2009; *Wu et al.* 2007; *Garreta et al.* 2010), where modelled and reconstructed vegetation (through pollen assemblages) are compared to deduce the climatic conditions which correspond best to the reconstructed vegetation. Other examples for applications of inverse methods are the identification and reconstruction of atmospheric CO_2-patterns (e.g. *Bousquet et al.* 1999a,b; *Göckede et al.* 2010a,b; *van de Wal et al.* 2011), or the analysis of the past deep ocean circulation, based on the ^{231}Pa/^{230}Th-ratio in ocean sediments (*Burke et al.* 2011); this ratio can serve as a proxy for the overturning circulation. In their study, *Burke et al.* (2011) investigate the spatially only limited occurrence of ^{231}Pa/^{230}Th using an inverse approach to test potential consistencies with the estimated ocean circulation of modern times. *Goosse et al.* (2006) have also provided a useful contribution to the model-data synthesis through the combination of statistical methods with an ensemble of climate model simulations as well as a wide range of proxy time series. This study is tackled in more detail in the forthcoming section on the introduction of the new methodology.

Model-proxy differences

After the general remarks it is now analyzed how PlaSim compares with the proxy data, i.e. the Ammersee proxy in particular. This confrontation is of major importance, as all further analyses will base on this comparison.

Proxy conversion Before it can be analyzed how PlaSim compares with the proxy data, a short paragraph needs to be included to explain how a climate signal can be obtained from the indirect, chemical δ^{18}O-record of Lake Ammersee. Although this ratio is indeed affected by local climate conditions, it is not instantaneously providing any precise climatic information. For the conversion of environmental

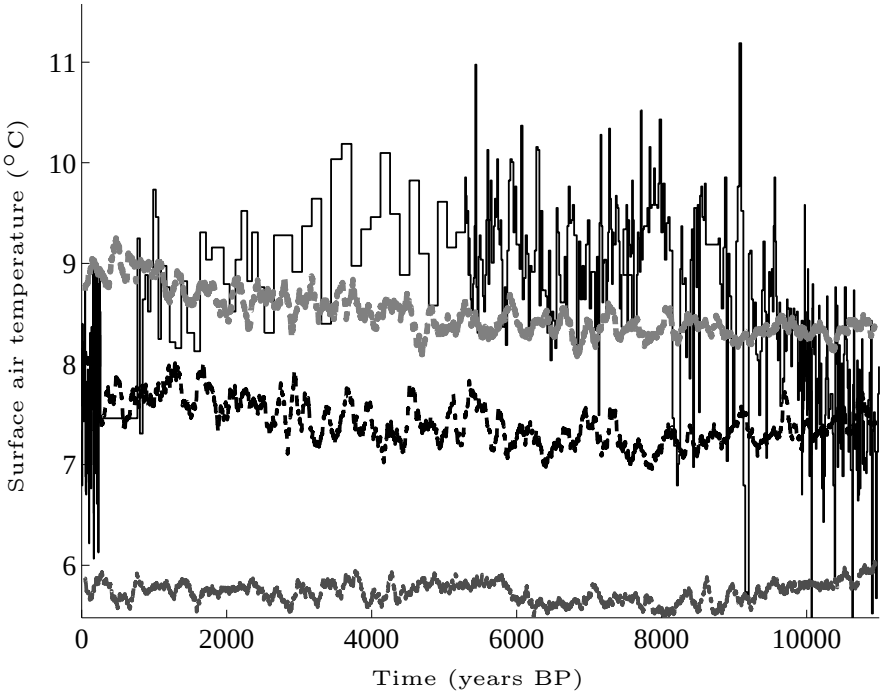

Figure 5.4: Surface air temperature [°C] reconstructed for the Lake Ammersee proxy (solid black stairs) and simulated with PlaSim (100 year running means); driven by fixed climatological SST (light gray dashed), coupled to a mixed layer (black dashed) and the LSG ocean (medium gray dashed) for 0 to 11 kyr BP.

quantities into a specific kind of climate variable, the already mentioned transfer functions or calibration equations (*Leduc et al.* 2010) are necessary. These are determined for various environmental conditions and are by no means fixed or explicitly defined but still subject of ongoing research. As listed in *Leduc et al.* (2010), various approaches are, exemplarily, existing for the calculation of SST from the alkenone unsaturation index or the Mg/Ca ratio. For the δ^{18}O-ratio, the studies by *Dansgaard* (1964), *Yurtsever* (1975) or *Rozanski et al.* (1992) may serve as a reference. Here, a slightly modified version is used, given as

$$\delta^{18}O = 0.33 \cdot T_{ann} - b, \tag{5.1}$$

where T_{ann} is defined as the annual mean temperature, i.e. the quantity which should be determined, and b can be interpreted as the reference temperature, thus the calibration to today's climate instead of using a constant as in *Dansgaard* (1964) or *Yurtsever* (1975). Through this, a slightly smoother structure in the proxy trend is achieved. One comment should be made at this stage: The other transfer functions existing for the δ^{18}O-ratio may certainly lead to slightly different results in terms of the absolute temperature values. However, as will be shown later, this does not affect the intention of the reconstruction of the European climate through, more important, the adjustment to an observational data set. Moreover and as shown by *Leduc et al.* (2010), different calibrations can indeed be feasible for an analysis of global SST trends.

The reconstructed temperature time series of the Lake Ammersee proxy (solid black stairs) for the period 0 to 11 kyr BP on the basis of the aforementioned transfer function is presented in Figure 5.4 together with the time series taken from an ensemble of transient Holocene simulations with PlaSim (100 year running means), using different ocean modules: (i) fixed, climatological SST (light gray dashed), (ii) mixed layer ocean (ML, black dashed) and (iii) LSG ocean (medium gray dashed, analyzed in Chapter 4). To obtain the PlaSim time series, the region as close as possible to the grid points of the Lake Ammersee proxy (48°N and 11°E) is selected, i.e. eight grid points surrounding the proxy. The time series then represent area-averages over these grid points.

The proxy shows the commonly observed temperature trend (*Wanner et al.* 2008) for the Holocene with an early Holocene cooling, followed by a mid-Holocene warming (climate optimum) and again a cooling from around 3000 years BP until the preindustrial period. All PlaSim time series show similar and weak warming trends during the Holocene without a climate optimum during the mid-Holocene. Furthermore, the variability of the simulated time series is clearly below the proxy based variability. Neither the mixed layer nor the dynamic (LSG) ocean, as the more sophisticated ocean configurations of a climate model, reveal any impact on the central European temperature, or, more precisely, on selected grid points in central Europe, although the LSG ocean indeed has shown a realistic climate evolution over Europe, as has been elaborated in Chapter 4. The seasonally split results have shown a clear insolation induced signal which is strongly reduced and rather negligible on an annual basis (cf. Fig. 1.1 b) and thus hardly detectable in the complete annual PlaSim time series of Europe and also of the Lake Ammersee region. Since CO_2 is the single forcing with a continuous increase, this is most likely the cause for the temperature trend in PlaSim. In principle, a perfect climate model (including atmosphere, ocean, land and sea ice, biosphere, etc.) and subject to realistic external forcings should suffice to simulate the observed climate reflected in the proxy data. However, a severe problem in a climate reconstruction by dynamic models is posed by the ocean. Due to the internal variability of the ocean it is impossible to capture the observed time evolution by a dynamic model (*Goosse et al.* 2010; *Widmann et al.* 2010). The inconsistency demonstrates the inability of the present coupled model configurations to reconstruct the local Holocene climate and its variability. Thus, among all drivers in the coupled system, the SST is of particular relevance and pivotal for the simulations of global climate models (*Rind et al.* 1986; *Lehman and Keigwin* 1992). Therefore, in order to combine model and proxy data, one is forced to resort to the simplest ocean configurations, i.e. climatological SST (with an unknown although important abyssal ocean). This is to avoid oceanic feedbacks which would have to be considered using a dynamic ocean. In order to retrieve a local climate consistent with the Lake Ammersee proxy data, an indirect nudging method is developed in the subsequent section.

Considering now only the simulation with fixed SST, it becomes obvious that the mean differences over the whole period are very small; for several longer periods during the mid-Holocene, PlaSim is slightly colder. During the early and late Holocene there is a tendency of a warmer model climate compared to the proxy.

5.3 Methodology

After the short abridgement of model proxy synthesis methods in Section 5.2, the approach is introduced in the forthcoming section.
In general terms, an assimilation technique is employed to incorporate a proxy time series into a GCM to initialize new palaeoclimate simulations. As *Ghent et al.* (2010) illustrates, DA involves a model adjustment to observations at time steps where the latter are available with the aim to minimize model

induced errors, if one can assume the observations to be less uncertain compared to the models. The application with the proxy data instead of observations indeed matches the original definition of DA, as it is presumed that the proxies provide a sufficient climatic signal, despite the inherent deficiencies. However, this assumption, in retrospect, further explains why the Ammersee proxy has been contemplated in so much detail before. As the proxy data serve as the reference climate indicator, a careful analysis of both the resolution and its representativeness is an essential requirement in advance. If the proxy data are thus assumed to be the more reliable climate indicator than the climate model, the latter is then adjusted to correspond more closely to the palaeoenvironmental data (*Ghent et al.* 2010). The approach follows the inverse modelling idea, respectively DA, but unlike other studies, it is not based on an analytical inversion but on a dynamical procedure where it is gradually proceeded to converge the proxy climate with the GCM. That means that PlaSim is adjusted to a specific set of proxies, respectively the Lake Ammersee proxy, which is the key point of this approach. As a basis, simple maps of both model and proxy are compared, as done in the previous section, considering that, in any case, there will be a more or less strong difference between them. As this approach to assimilate the proxy time series is not based on the common statistical methods, it is referred to the respective studies of e.g. *Goosse et al.* (2006), *Ghent et al.* (2010) or *Widmann et al.* (2010) or the ones by *Evensen* (1994, 1997, 2003) for more detailed information on this topic. The forthcoming sections are now dedicated to the stepwise declaration of this new algorithm.

What is the relation between SST and land temperatures?

Regarding the existing difference between the two time series, it has thus to be found a way how this can be overcome, i.e. how the model and data time series can converge. The approach follows the assumption of a distinct dependency between an imposed forcing on the climate system and its response with the result that any kind of external perturbation to the climate system will lead to a change in climate. This can be related to the so-called climate sensitivity, which is, in its original sense, defined as a change in global and annual mean equilibrium surface air temperature resulting from changes in the radiative flux (*Roe and Baker* 2007). The response in terms of the temperature changes is thus related to the global mean radiative forcing (*Boer and Yu* 2003), which can be expressed as

$$\Delta T = \lambda \times \Delta R, \tag{5.2}$$

where ΔT and ΔR are the changes in global and annual mean air temperature and in the radiative flux. The constant of proportionality which relates the forcing to the changes in climate, is called the climate sensitivity parameter λ. It is equivalent to a measure of the strength of the feedback processes and thus to the sensitivity of the climate system (*Boer and Yu* 2003; *Gregory et al.* 2004; *Pachauri and Reisinger* 2007). It can be determined in climate change simulations with a GCM and, as *Boer and Yu* (2003) point out, it is approximately constant and hence independent of both climate state and forcing (*Boer and Yu* 2003; *Gregory et al.* 2004). Consequently, each GCM and the real climate system have different response parameters (sensitivities). Therefore, this concept is commonly used in analyses of climate change when different models and/or forcings are intercompared (*Gregory et al.* 2004). In a more generalized form, ΔR is consistent with a forcing triggered by changing boundary conditions. Thus, assuming the climate sensitivity to be nearly constant, it can be used to reconstruct the response to any kind of forcing - and not only radiative - in a straightforward way, which is shown by *Good et al.* (2011) who used this theory to reproduce climate model projections. Moreover, as *Wirtz et al.* (2010) point out in their proxy analysis, variations in one variable like SST may have a strong influence on another variable in close vicinity, for example, surface air temperature. This statistically determined spatial relationship is also

shown by *Wilson et al.* (2010) who identified a strong correlation between tree ring series in the western parts of South America and SST in the tropical Pacific, which they used for reconstructing the El Niño-Southern Oscillation (ENSO) during the past century. These studies support the idea of directly linking SST anomalies to modifications of adjacent land temperatures. So far, also other studies (*Reason and Mulenga* 1999; *Perlwitz et al.* 2009), based on model results as well as statistical analyses, indicate a close relation between regional climate response and SST anomaly patterns (*Li et al.* 2012).

After these theoretical considerations, the essential points for the approach are now shortly summarized:

- The principle is based on the close relationship between an imposed forcing on the climate system (through changes in the boundary conditions) and the resulting response in terms of a temperature change, adjusted by the sensitivity parameter λ.
- As λ is supposed to be constant, it can be used to reconstruct the response to any kind of forcing.
- The statistical findings of *Wirtz et al.* (2010) on the close relationship of neighbouring climatic parameters, strongly assuming that a variable like SST has a strong influence on, for example, nearby surface air temperature, underpin the application to the relation between SST and land temperatures.

At this stage, some further comments should be made regarding the climate sensitivity λ. Compared to the aforementioned selection of studies on this topic, the feedback parameter λ has to be interpreted in a slightly different way. In its original sense, the equilibrium climate sensitivity is defined as the response of the global mean surface air temperature to a doubling of the atmospheric CO_2 concentration. It is thus an important parameter of model intercomparisons. In a wider sense, λ can be interpreted as a parameter giving the strength in global surface air temperature change to a particular forcing, affecting the radiation budget of the Earth. It is thus given in units of a temperature change K per W/m^2 forcing. Examples may be changing boundary conditions or processes having an radiative impact, such as volcanoes.

Studies concerning the different processes having an influence on the overall climate sensitivity have been carried out, for example, by *Klocke et al.* (2011) and *Klocke* (2011). The climate sensitivity of PlaSim related to doubling the CO_2 has been determined by *Fraedrich et al.* (2005b) and *Henrot* (2010) for present-day and palaeoclimate setups respectively.

Emanating from the theoretical considerations in the preceding itemization, the practical applicability emerges as follows:

(i) The focus is the close relationship between the SST and the adjacent surface air temperature over land. The SST is the main driver of simulated climate in GCMs and thus an important boundary condition in climate models.

(ii) The land temperatures are given by the terrestrial proxy data (e.g. Lake Ammersee) and are representing the reference climate which shall be resimulated.

(iii) After determining λ, it is used to adjust the SST forcing on the basis of the terrestrial proxy data.

Following substep (iii), a linear sensitivity relationship between the SST and the adjacent land climate is approved. This assumed linearity is also emphasized by *Ljungqvist et al.* (2012) analyzing the Northern Hemisphere temperature variability over the last century. A similar strategy has been pursued by *Jones and Widmann* (2003), who apply a nudging technique for the modification of the atmospheric circulation.

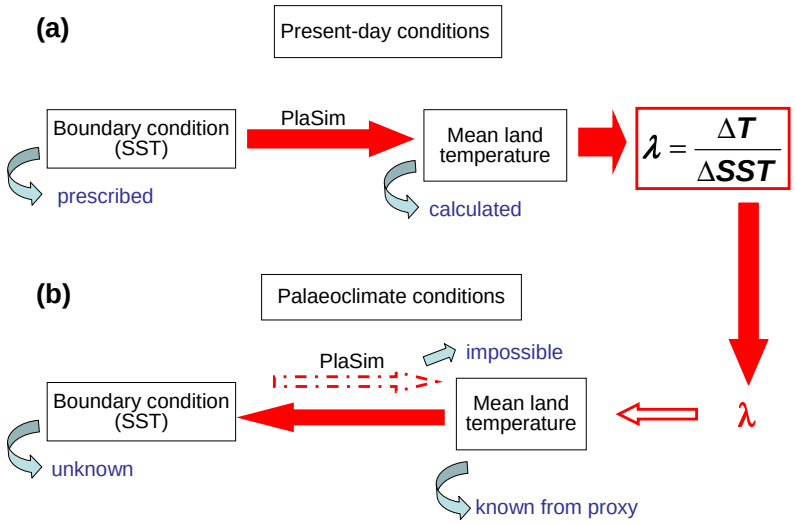

Figure 5.5: Procedure of forward modelling for present-day conditions (a) and the inverse modelling part for palaeoclimate conditions (b).

The study by *Li et al.* (2012) can also be cited in this context, where the authors also assume this linearity to estimate the sensitivity at both regional and seasonal scales to SST perturbations in the tropics using ensemble simulations. As a short comment, it is worthwhile to allude, that, through this SST-adjustment, both methods are covered of how, following the remarks by *Kohfeld and Harrison* (2000), palaeoenvironmental data can be used in climate models: They can either serve as data sets for model evaluation, as it was done in the previous chapter (cf. Chapt. 4) and will be done also at a later stage in this chapter, or they can be used as boundary conditions (≙ input data sets), as it is done in this chapter, at least comparably, as they serve as the reference climate. Modifying Equation (5.2) according to the linear approach yields:

$$\overline{T} = \lambda \times \overline{SST}, \tag{5.3}$$

where λ is the sensitivity and $\overline{T}$ and $\overline{SST}$ are the global and annual mean temperature and SST respectively.

However, this simple theoretical relationship in Equation (5.3) is currently not completely adequate to achieve a synthesis between the climate model and the proxy. If $\overline{T}$ is assumed to be given by the proxy data, λ **and** $\overline{SST}$ **are still unknown parameters!**

To fill this gap, one clearly has to distinguish between present-day climate (a) and palaeoclimate (b), which is explained in the following lines and illustrated in Figure 5.5: As already mentioned, the SST serves as an essential boundary condition in a model independent of the ocean configuration. They are either prescribed on a climatological basis throughout the simulation period (fixed ocean), or initially for the spin-up phase at the beginning of a simulation with a subsequent free interaction (in the mixed layer and LSG oceans, cf. Chapt. 2). Setting up a simulation yields a specific mean climate, e.g. mean surface (air) temperature, which can be regarded as the more or less direct (linear) response of the prescribed SST (forcing). Please note that the focus is only on the SST in this case; all other boundary conditions (e.g. glacier mask or vegetation-related parameters like albedo or roughness length) or external forcings (e.g. orbital and GHG) are not considered in this context (*Rind et al.* 1986). This standard procedure of climate modelling is limited to present-day conditions (Fig. 5.5 a) or at least to those circumstances where the boundary conditions are completely known - apart from their general uncertainty. The coeffi-

cient λ is then calculated from Equation (5.3) and serves as the correcting (sensitivity) term, determining the strength of the response between the global mean (land) climate and the global mean SST. If not stated otherwise, in the following all parameters such as $\overline{T}$, λ and $\overline{SST}$ are specified to their annual values. However, this approach cannot be easily transferred to palaeoclimatic studies (Fig. 5.5 b), where, in its original sense, both quantities are unknown: Neither the mean climate nor, or even less, the oceanic conditions are known for a specific time period in the past. Thus, a direct simulation as for present-day conditions is not possible. At this stage, the proxy data become important by serving as an indicator of the past mean climate in the influence region of the proxy. This implies a switch from the global to the regional perspective - Europe in this case. Together with the sensitivity λ, which has been determined in part (a), the corresponding SST conditions can be calculated on the basis of the reference proxy data.
As a remark it should be mentioned, that the various SST-proxies existing in the literature are not taken into account in this study, because of several reasons. The main reason is the inherent uncertainty of the SST-proxies. According to *Berner et al.* (2008), *Leduc et al.* (2010) or *Lohmann et al.* (2012), the existing SST-proxies show different (even opposing) patterns and trends, depending on the kind of proxies used, i.e. alkenone unsaturation or Mg/Ca ratio. This complicates an intercomparison of different proxy types (*Kim et al.* 2004; *Weldeab et al.* 2007; *Wirtz et al.* 2010) and, even more, an implementation into climate models. Studies which have analyzed specific features like the climate (*Rimbu et al.* 2004; *Lorenz et al.* 2006) or SST variability (*Kim et al.* 2004) during the Holocene, have also only used a single SST-proxy type. In this approach of the linear sensitivity relationship with the combination of an external (SST) forcing, the sensitivity and the land climate, a climate state can be maintained which is consistent with the model physics. Despite the inclusion of proxy data as the reference land climate, it is ensured to still obtain a climate state which is consistent with model physics. This approach is in line with the study presented by (*Goosse et al.* 2006). Moreover, due to the fact of the SST being an important boundary condition, the SST-proxies signify an artificial forcing in the model. Newly generated SST are indeed included in this adjustment process but they are constructed on the basis of the reference proxy data and the model's sensitivity and are thus simply deduced by the model; in contrast, the SST-proxies are completely independent of the climate model and may thus very likely lead to an inconsistency with the model physics. Another limiting factor for the inclusion of SST-proxies is that they are assembled at single grid points which are mostly located in the vicinity of the coasts. They are thus unable to yield any information about the SST in the inner oceans. However, for a usage as a boundary condition, they must exist on a complete grid, specifying the oceanic conditions continuously (*Kohfeld and Harrison* 2000) - a feature which cannot be provided by proxies in general (cf. Sect. 5.1.2) and especially not by SST-proxies. This would require an interpolation to the model grid and may assumably lead to further model inconsistencies. The incorporation of SST-proxies may thus further enhance the general uncertainty due to the inherent limitations encompassing the oceanic proxies.
This methodology, described above and illustrated in Figure 5.5, will help to overcome the apparent discrepancy between the still unknown oceanic conditions and the known mean climate given by the proxies. The model's boundary conditions (SST) will be adjusted to a given climate instead of setting up a climate simulation where known boundary conditions are leading to a specific mean climate. The adjustment of the SST is made possible by using the sensitivity which was calculated in Equation (5.3) on the basis of the prescribed SST and the calculated mean land temperatures for Europe. This is equivalent to a switch from forward to inverse modelling, i.e. to estimate the input from the known output or target state (*Kohfeld and Harrison* 2000; *Wu et al.* 2007; *Widmann et al.* 2010; *Guiot et al.* 2000, 2009). Through this, the SST is derived which is appropriate to simulate a predefined climate. For this purpose, Equation (5.3) needs to be slightly modified, to include the deviations between the simulated and the

land proxy climate. This is expressed as

$$\Delta T = \lambda \times \Delta SST, \tag{5.4}$$

where ΔT is defined as the difference between the annual mean model climate $\overline{T}$ for Europe and the proxy climate T_P, i.e. $\overline{T} - T_P$, and ΔSST as the corresponding annual mean SST anomalies. Based on the assumed linearity, the SST has to be increased if ΔT is < 0, i.e. if PlaSim is colder than the proxy, or vice versa - this either results in positive or negative SST (forcing) anomalies. Consequently, anomalies in land temperature are converted into SST anomalies and, accordingly, each resimulation on the basis of the proxy climate instantaneously leads to a new SST-field. Although they are deduced on the basis of the proxy climate, thus "the reality", one could consequently assume the newly created SST to be the real SST during the Holocene. Nevertheless, they are simply assessed using the proxy climate and the PlaSim-specific sensitivity and, for this reason, they may rather be regarded as a first order approximation of Holocene SST (*Rind et al.* 1986) and not necessarily as the realistic SST of this period in the past. However, this is subject to prove at a later stage of this study (cf. Sect. 5.9) in a direct comparison of the newly constructed SST to those of the fully coupled simulation as well as to SST-proxies. The SST anomalies thus emerge from model simulations at two different model states: the undisturbed state (SST_0) and the adapted (modified) state (SST_1) respectively.

This general methodology can also be seen in line with the study by *Goosse et al.* (2006), who also try to find a useful way to combine model results and proxy data. In more detail, they are aiming at a simulation which is closest to proxy time series, but are choosing, among an ensemble of simulations, the one which minimizes a cost function, i.e. which fits best to the proxy. Although, lately, the studies are differing, they are similar with respect to the intention of approaching the proxy time series through calculating the deviations between model and proxy. Consequently, similarities are apparent between the cost function relation cited in *Goosse et al.* (2006) and the basic equation, Equation (5.4). Model-data differences are calculated in this context as well (cf. Sect. 5.2), but, in contrast to *Goosse et al.* (2006), the simulation is adjusted to the proxy pattern in regular time steps.

Sensitivity studies

After having explained the underlying assumptions of this approach and the theoretical procedure, the practical application of determining the necessary parameters for the reconstruction of past climate is now revealed step by step. This includes the performance of a wide range of sensitivity studies, whose most important results are summarized at the beginning. In the further course of this section, the method will be illustrated in more detail, as direct consequences of the results of the sensitivity studies. These studies are a commonly applied tool in model studies to investigate the behavior of a system, mainly with regard to changes in the most important variables (*Carter et al.* 2007). The response (≙sensitivity) of the climate system is then analyzed with regard to the unperturbed system to reveal potential or dominant feedbacks. Common examples are global warming experiments or studies about land use changes. Referring to the remarks in the preceding section, the following steps have to be fulfilled:

(1.) Establish the sensitivity λ;

- (1.1) Define a proxy (target) region where proxies are available and represent the climate during the period of interest;
- (1.2) Detect the source region in the ocean which is most relevant for the target region;

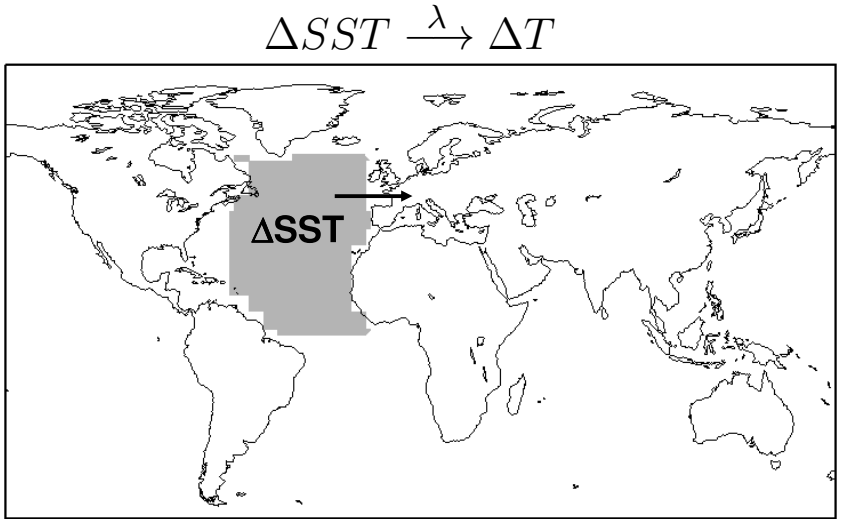

Figure 5.6: Relationship between SST anomalies and land climate, corrected by the sensitivity λ, as determined in Equation (5.4). The forcing (source) region is the North Atlantic (between 0° and 60°N), which has the strongest influence on the European land (target) climate, given by terrestrial proxy data.

(1.3) Define λ as the sensitivity of the model climate ΔT in the target region to a change of SST (ΔSST) in the source region (Eq. (5.4));

(2.) Determine the source SST conditions necessary for the adjustment to the target climate by using the inverse of this sensitivity, or feedback parameter (λ^{-1}, *Boer and Yu* 2003) and reapply the climate model with the adapted source SST.

These are essential prestudies for a reliable reconstruction of the Holocene climate at a later stage, mainly regarding the items (1.2) and (1.3), which include a wide range of tests. Once λ has been ultimately defined, it will remain constant for all subsequent experiments, which is consistent with the aforementioned remarks.

(1.) Calculation of sensitivity

Through the focus on the European sector, substep (1.1) is already achieved. Indeed, this could also be any other region of interest. Europe is here confined to 20°W - 50°E and 30° - 75°N. All sensitivity studies are carried out under present-day conditions (100 years simulations each), and assuming that the interaction between the climate subsystems remains the same through time. This is consistent with assumptions made in other studies (*Wu et al.* 2007; *Guiot et al.* 2009; *Sundqvist et al.* 2010; *Laepple and Lohmann* 2009; *Wilson et al.* 2010; *Ljungqvist et al.* 2012) on palaeoclimatic reconstructions and an essential prerequisite for the overall possibility of reconstructing past climates (i.e. principle of uniformitarianism, cf. Sect. 5.1.2). For substep (1.2), different oceanic regions are forced with arbitrary but known SST anomalies and subsequently calculated the responses of the land temperatures in the adjacent regions - relative to a control simulation without SST forcing. As the results reveal, for a proxy in central Europe, the source region in the ocean with the strongest influence on the European land climate is the North Atlantic between 0° - 60°N. This is also illustrated in Figure 5.6. These results could have been

expected and the findings are in line with the study by *Rodwell et al.* (1999), where the authors quantified the oceanic role in the forcing of the climate of the North Atlantic and Europe. They revealed that SST anomalies and the strength of the North Atlantic Oscillation (NAO) are strongly related and that the oceanic information is exchanged with the atmosphere in terms of hydrological processes having a direct influence on the climatic conditions in Europe. Other studies, for example by *Sutton and Hodson* (2003, 2005), by *Löptien and Ruprecht* (2005), or by *Grosfeld et al.* (2008), also emphasize the special role of the North Atlantic and the NAO for European weather and climate. Therefore, the results of the sensitivity studies concerning the identification of the oceanic source region are left out at this stage. After its identification of the source region (substep (1.2)), the sensitivity λ needs to be determined (substep (1.3)). For this, Equation (5.4) is applied to a simulation where the SST is modified in the North Atlantic (ΔSST) and, subsequently, the responding temperature change over Europe is calculated (ΔT, cf. Fig. 5.5 a). The resulting sensitivity value is λ **= 0.5532**.

(2.) Determination of the source SST conditions and reapplication of the climate model

Sensitivity	ΔT_{ann}	ΔSST	$\Delta T_{sim,ann}$
constant, annual	+ 1.5°C	+2.71°C	+ 1.79°C
seasonally	+ 1.5°C	MAM: +2.71°C	+ 1.51°C
		SON: +2.71°C	
		DJF: +2.0°C	
dependent		JJA: +3.4°C	
	$\lambda_{\mathbf{DJF}}$ **= 0.75**		
Final seasonal sensitivities		$\lambda_{\mathbf{MAM}}$ **= 0.5532**	
		$\lambda_{\mathbf{SON}}$ **= 0.5532**	
			$\lambda_{\mathbf{JJA}}$ **= 0.4411**

Table 5.1: Overview of the essential results from the sensitivity studies using annual and seasonal sensitivities (left column). The two columns in the middle give a description of the experiments in terms of the assigned parameter values ΔT_{ann} and ΔSST. In the right column, the results, i.e. the simulated temperature changes $\Delta T_{sim,ann}$, are shown.

Now, the intention is to determine the SST conditions which are appropriate to simulate a predefined climate; this implies the switch to the inverse modelling procedure and is, in the end, assignable to the palaeoclimatic studies.
The most important results of these prestudies are presented in the following. For the test studies, an arbitrary annual temperature change ΔT of 1.5°C is assumed over Europe (this will be given by the proxy climate in a later stage) and Equation (5.4) is adapted using the inverse of the previously calculated sensitivity λ to determine the corresponding annual SST anomalies (ΔSST) for the Northern Hemisphere Atlantic. As the SST is prescribed on a monthly basis, the SST has to be adjusted on a monthly basis as well. The resulting values of SST on the basis of λ and ΔT are shown in the first line of Table 5.1, which gives an overview of selected experiments, providing the most important results. The three columns show the assumed temperature change ΔT_{ann} of +1.5°C, the corresponding (annual and seasonal) SST anomalies ΔSST and the simulated annual temperature change $\Delta T_{sim,ann}$.

As the results in the first line of Table 5.1 show, the SST forcing based on the annual sensitivity is not appropriate to resimulate the assumed mean climate change: The constant annual SST anomaly of +2.71°C, prescribed every month, leads to a higher than expected simulated temperature change $\Delta T_{sim,ann}$ of 1.79°C. These results indicate the necessity to consider further aspects to achieve a reliable reconstruction.

A potential solution to the monthly invariant modification, which has not worked properly, may be a seasonal variation. Taking into account the seasonal signal for the sensitivities in contrast to the annual mean temperature changes, which build the basis for the comparison of model and proxy data, may be inconsistent but becomes more comprehensible when recalling the remarks in Section 1.1.1. Moreover, it is also strongly recommended by *Davis et al.* (2003) as an essential result of their study. In general, the factor of seasonality is an essential point in the Holocene. Mainly with regard to the Holocene insolation distribution, the procedure with the seasonal splitting is rather consistent. As mentioned in Section 1.1.1, this distribution changes on geological time scales (i.e. for glacials and interglacials) due to variations in the Earth's orbit around the sun. This led to more (less) incoming solar radiation during summer (winter) in the mid-Holocene (cf. Fig. 1.1), which then caused an intensification of the seasonal cycle. Assigned to an annual signal, these changes in insolation (and the respective changes in e.g. temperature) are small but the annual temperature change is indeed influenced by the seasonal variations (*Fischer and Jungclaus* 2010). This is also verified by the results of the fully coupled PlaSim simulation presented in the preceding chapter. Apart from these modelling studies, this approach is further underpinned by proxy analyses, such as the work of *Davis et al.* (2003), who clearly identified seasonal differences in Holocene temperature trends in their pollen climate reconstruction, which has also been discussed in the preceding chapter. In their investigations of SST-proxy records, both *Leduc et al.* (2010) and *Schneider et al.* (2010) revealed a seasonal signal which is induced by the changing orbital forcing throughout the Holocene. As already mentioned in Section 5.1.2, proxies are generally influenced by the climatic conditions during particular periods of the year. It is rather comprehensible that winter and summer, respectively the coldest or warmest month, are providing the strongest climatic signal on the environmental data (*Goosse et al.* 2006). The seasonal signal, also in the SST-proxies is thus especially important for the SST-adjustment in the model. Moreover, the study by *Laepple and Lohmann* (2009), who presented a statistical model to simulate the palaeoclimatic temperature evolution, further corroborate this modification. Their idea is based on the modern relationship between temperature and insolation which is governed by the seasonally varying insolation. Assuming an identical temperature response, this relation can be applied to palaeoclimate timescales. Another two more aspects also support this seasonal splitting, which are the zonal wind structure and the different thermal inertia of the ocean influencing the land temperature, with the latter being strongest in winter and summer. Although a free ocean is not used in these studies, the annual cycle is included in the climatological SST, already accounting for seasonally different SST. Differences between winter and summer can also be noticed in the zonal wind pattern. This is weaker during summer, causing a reduced temperature response over the European continent (*Rind et al.* 1986). This seasonally different impact has also been found out by *Masson et al.* (1999), who carried out sensitivity experiments to analyze the influence of various components on the European climate. The authors discovered that the Atlantic Ocean strongly influences the European climate due to the heat and moisture transport and that, mainly during winter, (insolation induced) SST changes are a key factor for the European temperature patterns (*Masson et al.* 1999). It is thus indeed reasonable to adapt the seasons differently. The seasonal consideration requires a modification of Equation (5.4):

$$\Delta T_{ann} = \overline{\lambda_s \times \Delta SST_s}, \tag{5.5}$$

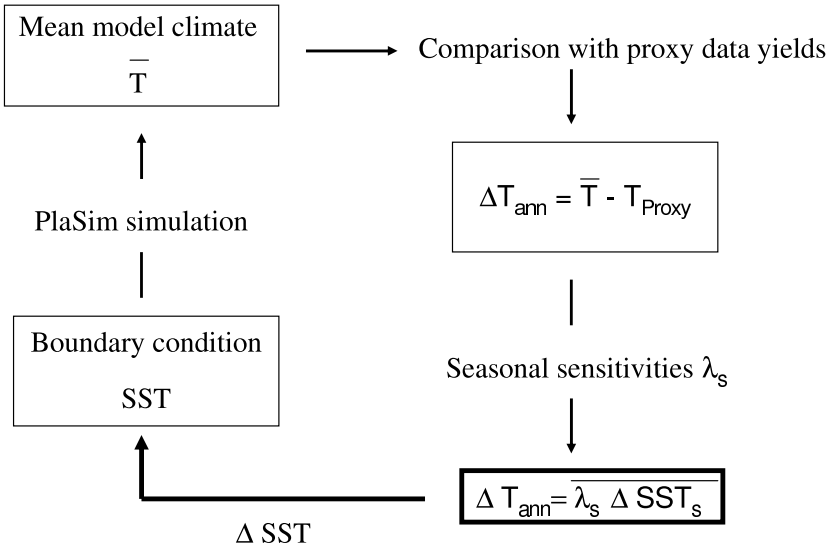

Figure 5.7: Schematic of the adjustment of the SST to the land proxy climate through the inverse modelling procedure. The application of the inverse method is highlighted in bold lettering.

where the increment s denotes the consideration of the seasonal signal, i.e. the respective seasonal sensitivity and SST, and

$$\lambda_{ann} \times \Delta SST_{ann} = \overline{\lambda_s \times \Delta SST_s}. \tag{5.6}$$

The linearity assumption on λ_{ann} implies that the annual sensitivity is the mean over the four seasons, i.e.

$$\lambda_{ann} = \frac{1}{4} \cdot \overline{\lambda_s} = \frac{1}{4} \cdot (\lambda_{DJF} + \lambda_{MAM} + \lambda_{JJA} + \lambda_{SON}). \tag{5.7}$$

Based on the aforementioned remarks on the seasonal characteristics, the sensitivities of MAM and SON are therefore defined to their annual values, i.e. $\lambda_{MAM} = \lambda_{SON} = \lambda_{ann}$ (Table 5.1). Thus, only λ_{DJF} and λ_{JJA} must be adjusted so that Equation (5.7) is fulfilled. This yields $\lambda_{DJF} > \lambda_{MAM} = \lambda_{SON} > \lambda_{JJA}$ and thus $\Delta SST_{DJF} < \Delta SST_{MAM} = \Delta SST_{SON} < \Delta SST_{JJA}$. Thereby, the necessity is considered to modify the summer more strongly compared to winter. Through this, the annual cycle of SST is indeed modified, i.e. intensified, but the original characteristics are maintained.

The detection of the best-fitting seasonal sensitivities - in terms of the simulation of the assumed annual temperature change over Europe (ΔT_{ann}) of +1.5°C - has been achieved over a wide range of test-studies for present-day conditions, which, in theory, follows the procedure in Figure 5.5 a and Figure 5.7, whereas the latter already shows the later application to the proxy data: Starting with the default (standard) set of SST from the AMIP climatology, which is used for a first simulation, a mean model climate, i.e. the mean land temperature for a specific region - Europe in this case, is obtained. This simulated mean is then compared to the assumed climate mean. This comparison leads to the ΔT_{ann}, defined as the anomaly between model simulations at two different model states: the undisturbed state (T_0) and the adapted (modified) state (T_1) respectively (comment: At a later stage, after the complete definition of the sensitivities, the ΔT_{ann} is replaced by the anomaly between the annual mean model climate $\overline{T}$ and the proxy climate T_P, also at two different model states t_{old} and t_{new} respectively.). At this stage, the splitting

to the seasonal sensitivities must take place, as the annual sensitivity is not appropriate. This has led to a stepwise variation of the seasonal sensitivities for DJF and JJA in a variety of sensitivity studies, as those of MAM and SON remain fixed (see remarks above), considering the warming (cooling) impact on the land during winter (summer). Hence, the sensitivities for winter and summer must be modified to that effect, that the winter (summer) temperatures are not getting too warm (cold). The seasonal SST anomalies, resulting from the respective seasonal sensitivities through Equation (5.5), are then used to modulate the initial set of SST and to start a subsequent test-simulation ($\hat{=}$ substep (2.)) which will then give a new mean model climate which is then again compared to the assumed mean; respectively the proxy mean at a later stage. Accordingly, substep (2.) implies a gradual procedure, until mean model and the assumed mean (proxy mean) converge best possibly. This is thus again comparable to the approach of *Goosse et al.* (2006) with the minimization of a cost function (*Zhang et al.* 2010) between model and proxy climate and the choice of a best-fitting simulation. However, this gradual procedure is only used to determine the definite seasonal sensitivities. During the later process of reconstructing the proxy climate over the whole Holocene, the resimulation is carried out only once.

The most important and recurrent part of this procedure is highlighted in bold in Figure 5.7. Moreover, *Wu et al.* (2007) and *Guiot et al.* (2000) use a similar schematic representation of their inverse vegetation modelling approach. The included transfer matrix accounts for the use of the vegetation proxies to be converted into the appropriate model output for the different biomes and is comparable to other transfer functions for the conversion of metadata from proxies into climatic data.

The results of the studies using a seasonal modification are given in the second line of Table 5.1. As the simulated temperature anomaly fits well to the assumed temperature change of +1.5°C, it clearly turns out that a consideration of the seasonal cycle of the SST indeed leads to a strongly improved result (*Haberkorn et al.* 2009a). The ultimate seasonal sensitivities are given in the last line. As mentioned earlier, they remain constant for all subsequent experiments. The different λ_s are now applied to the Holocene climate simulation with prescribed SST (reference simulation, cf. Fig. 5.4 in light gray). In the following sections, three different attempts are made to reconstruct the Holocene proxy climate in a best possible way, i.e. closest to the Lake Ammersee time series:

–> Section 5.4 is the very basic and first step of reconstructing the Holocene climate. It is based on selected time slices at the early, mid- and late Holocene. For a later identification, the simulation is called *TS*-experiment (time slices);

–> Section 5.5 is the first improvement as the climate of the whole Holocene is reconstructed in terms of millennial time slice means (*TTS*-experiment - transient time slices);

–> The last and most sophisticated alternative, presented in Section 5.6, is the interactive (fully transient) reconstruction of the proxy climate in terms of climatological means of 40 years (*ITS*-experiment - interactive time slices).

An intercomparison of all three approaches will highlight potential limitations of this method in general and potential improvements or disadvantages of each individual alternative. Two final comments are made at this stage: In Section 5.2, the matter of different transfer functions for the δ^{18}O-ratio has been addressed. After introducing the methodology of how to adjust the climate model to the proxy data set, it is now justified why the choice of the transfer function does not counteract the intention of the reconstruction of the Holocene climate. Through the ΔT and thus the ΔSST, the climate model is readjusted continuously to the proxy. Moreover, the transfer functions differ only very slightly, so that neither a completely different trend nor strongly differing absolute temperature values are expected. The

second comment on this adjustment of SST according to land temperatures should be made concerning the oceanic influence. Although the strong impact of the Northern Hemisphere Atlantic on the European region could be shown, it may be argued that also other oceanic regions may be of importance, maybe even the global perspective through teleconnections. This would have substantially complicated the approach and the linear relationship might be not valid any more due to large-scale feedbacks resulting from other global variability modes. Additionally, these may only be represented insufficiently by PlaSim mainly with regard to the ocean used in these studies. These shortcomings would initially have induced additional uncertainties. Therefore, the SST in the other regions are all kept at their undisturbed, present-day values; thus, the potential climatic impact of these regions on the European climate is muted (*Rind et al.* 1986).

5.4 Time slice reconstructions

In this section, the first application of the adjustment method on the basis of the linearity relationship between SST and land temperatures is presented for selected time slices during the Holocene. It will give a first estimate on the overall practicability of the method and will reveal potential improvements of the climate simulation as well as limitations of the newly developed methodology. This chapter has been published in Earth System Dynamics Discussions[1] (*Haberkorn et al.* 2012) and is included here with editorial adjustments.

5.4.1 Results

The results are presented for three independent time slices of the Holocene: the late Holocene or present-day (0 kyr BP: years 0-999 BP), the mid-Holocene (6 kyr BP: years 6000-6999 BP) and the early Holocene (9 kyr BP: years 9000-9999 BP). These time slices are extracted from the transient Holocene (reference) simulation (Fig. 5.4 in light gray) by taking the respective periods as references for the reconstruction. For the application of the method and Equation (5.5), the temporal means over the whole time slices, i.e. 1000 years, are used. To yield two temporally consistent time series for both PlaSim and the proxy, the latter is interpolated to achieve an annually resolved signal. ΔT is calculated as the difference between the mean over the reference time slice and the temporally corresponding mean of the proxy time series. Based on the seasonal sensitivities determined in Section 5.3 (Table 5.1), the ΔSST are deduced in a straightforward way. In this case, the SST anomalies emerge from the climatic state of the reference simulation (i.e. SST_0) and the adapted one (SST_1) based on the anomaly to the proxy climate during the individual time slices. With these new sets of SST, the respective time slices are resimulated once (no iteration) and compared to the corresponding time series of both the proxy and the PlaSim reference simulation. Consistent with Figure 5.4, the comparison is first confined to area-averages of the region, i.e. the grid points of the Ammersee proxy. After that, quantile-quantile (qq) plots of the reference and the *TS*-experiment are presented, before showing the anomalies between both and with respect to the preindustrial climate.

Before the results are presented, one comment is made concerning the dating uncertainty of the Lake Ammersee proxy, which is of course important, when comparing specific time slices. However, following the remarks by *Sundqvist et al.* (2010), this uncertainty, coming along with nearly every proxy time series, is of only minor importance, when the considered time scale is larger than the dating uncertainty.

[1] Haberkorn, K., C. Lemmen, R. Blender, and K. Fraedrich, 2012: Iterative land proxy based reconstruction of SST for the simulation of terrestrial Holocene climate. Earth System Dynamics Discussions, 3, 149-200

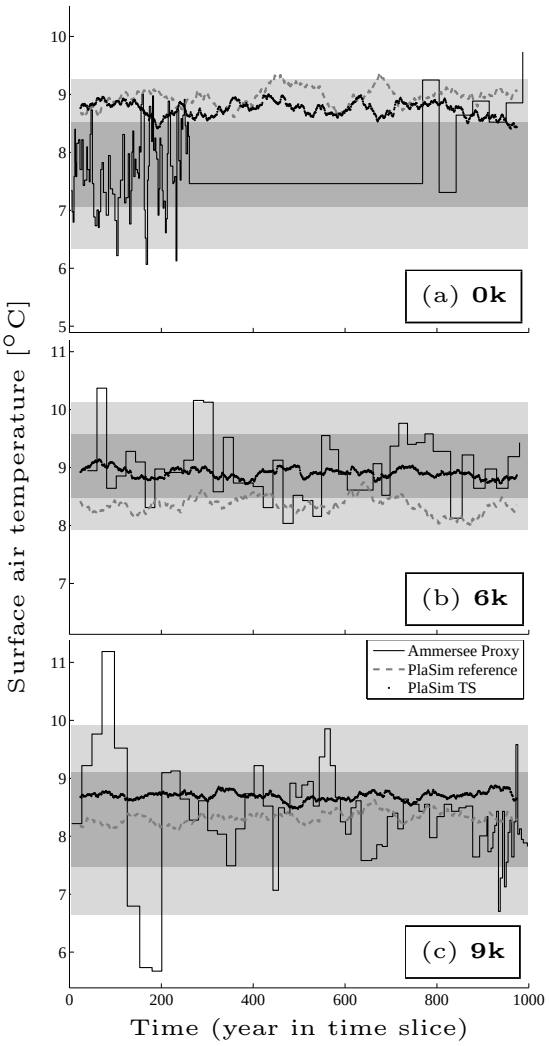

Figure 5.8: Surface air temperature [°C] of the selected time slices 0k, 6k and 9k, reconstructed for the Lake Ammersee proxy (solid black stairs) and simulated with PlaSim (50 year running means); taken from the reference simulation with climatological SST (light gray dashed) and the *TS*-experiment (black dotted) with adapted SST obtained by inverse modelling. Gray shading indicates 1σ- and 2σ-ranges in the proxy data set during each millennium.

Although this is not totally clear (cf. Sect. 5.1.2), it is definitely smaller compared to the 1000 yr means which are considered in this very first step; thus the problem of the age control can be disregarded.

Ammersee time series

The outcome in terms of surface air temperature for the three time slices is shown in Figures 5.8 a-c. The time series of the proxy is always shown in solid black (stairs), those of the transient reference simulation with prescribed SST in dashed light gray and those with the adapted SST in black dotted. The light and dark gray bands are indicating the 1σ- and 2σ-ranges of the proxy, with σ being the standard

deviation. At 0k (Fig. 5.8 a), PlaSim is warmer than the proxy in the reference experiment, despite some colder periods at the beginning of the time slice. Although the reconstruction leads to a decreasing mean temperature, PlaSim is still warmer over large parts of the 0k-time slice. At 6k (Fig. 5.8 b), the PlaSim reference simulation is colder than the Ammersee proxy in the long-term mean despite some periods where PlaSim is warmer. After the reconstruction, the mean temperature is increasing, leading to a convergence of both time series. In the early Holocene (9k, Fig. 5.8 c), PlaSim is also colder in the long-term mean of the reference experiment, although longer periods exist, where PlaSim is warmer than the proxy. In the resimulation of the time slice with the adjusted SST, PlaSim becomes warmer in general, apart from only some years where PlaSim is colder. Apparent in all PlaSim time series is the much lower variability compared to the proxy, leading to a comparably smooth structure.

	Proxy $\pm 2\sigma$	PlaSim reference $\pm 2\sigma$	PlaSim reconstructed $\pm 2\sigma$	$\Delta T_1 \pm 2\sigma$	$\Delta T_2 \pm 2\sigma$
0k	8.26 $\pm$ 1.34°C	8.95 $\pm$ 1.44°C	8.74 $\pm$ 1.44°C	0.69 $\pm$ 1.94°C	0.48 $\pm$ 2.04°C
6k	9.09 $\pm$ 1.0 °C	8.36 $\pm$ 1.27°C	8.90 $\pm$ 1.04°C	-0.73 $\pm$ 1.48°C	-0.18 $\pm$ 1.41°C
9k	8.66 $\pm$ 1.95°C	8.32 $\pm$ 1.20°C	8.69 $\pm$ 1.04°C	-0.34 $\pm$ 2.35°C	0.03 $\pm$ 2.21°C

Table 5.2: Time slice means (*TS*) and 2σ-significance for the Lake Ammersee proxy (left column), PlaSim reference (second left column), PlaSim reconstructed (middle column) and anomalies between PlaSim reference and the proxy ΔT_1 (second right column) and between PlaSim reconstructed and the proxy ΔT_2 (right column).

An overview about the results of the reconstruction is presented in Table 5.2, where the time slice means of both the proxy and the PlaSim experiments including the 2σ-variability range as well as the anomalies between the PlaSim simulations and the proxy are listed. In general terms, the means are converging in all time slices, leading to a strong improvement of the reconstruction compared to the reference experiment at 6k and especially at 9k. However, regarding the statistical significance of the reconstructed time series (given by the shaded σ-ranges), the reconstruction of the mid-Holocene climate seems to show the best results, whereas it is less significant in the other two time slices, especially at 0k (cf. Fig.5.8 a).

These results of limited statistical significance for the region of the Ammersee proxy are further interpreted with qq plots to provide a graphical comparison between the reference (proxy) data and the simulated data through relating the percentiles of the empirical cumulative distribution function of both data sets (*Wilks* 2006). In case of a perfect match between both, all points will fall on a straight line, leading to the assumption of identically distributed data points. For the three time slices, the temperature time series of the Ammersee proxy are compared with those of the reference experiment (Fig. 5.9, left columns) as well as of the reconstruction (right columns in Fig. 5.9). For the 0k-time slice, PlaSim simulates higher temperature values compared to the proxy at the tails of the distribution, whereas the main distribution fits well to that of the proxy (Fig. 5.9, first row). The deviations in the lower (higher) range are indicative of a narrower (wider) distribution there. The overall differences between the reference and the reconstruction are only minor at 0k, which is in line with the aforementioned results of only hardly converging time slice means. In the mid-Holocene (Fig. 5.9, second row), the distribution of the PlaSim data is a bit wider in the lower range (indicated by the simulated data points below the proxy) which is even more pronounced in the reconstruction. Equally, the points are more similarly distributed in the mid range compared to the proxy, which is slightly improved in the reconstruction. The higher range is very

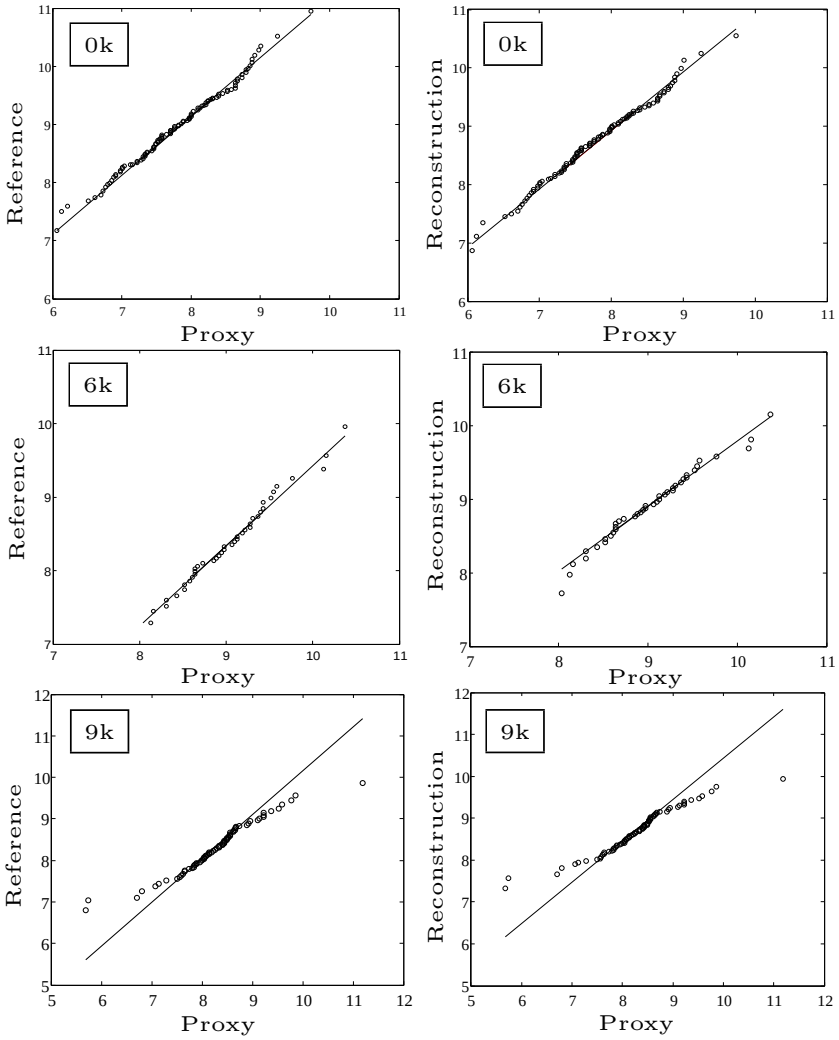

Figure 5.9: Quantile-quantile (qq) plots of annual mean surface air temperature for the Lake Ammersee proxy and the reference simulation time slices (left columns) as well as the reconstructed time slices (right columns).

similarly distributed in both PlaSim simulations. The results for the early Holocene (Fig. 5.9, third row) show the strongest deviations from the distribution of the proxy. In both the reference and the reconstructed time slice, the data points lie above the proxy in the lower range and below in the higher range, whereas the mid range is represented similarly. Consequently, the distribution of the PlaSim points is much narrower, i.e. the variability is lower and less extreme values occur. This is also clearly visible in Figure 5.4 and in more detail in Figure 5.8 c and is further discussed below. Although the reconstruction does not lead to a distinctive improvement of the distribution at 9k, the convergence of the time means is strongest (Table 5.2) when compared to the other two time slices.

Spatial pattern of European climate change

The reconstruction of the land temperature for the region of the Ammersee proxy has led to ambiguous results: Converging time slice means, thus improving the representation of the PlaSim mean climate with respect to the proxy mean, are accompanied by statistically non-significant modifications after the SST-adjustment (except for 6k). It is now tested whether a statistical significant improvement is achieved when a wider region is considered, i.e. a higher number of grid points. In addition, as mentioned earlier in this study, the focus is not only the mere response to the SST forcing in the region of the Ammersee proxy, but rather the climate changes for the whole region of Europe. The outcome of the reconstruction is now evaluated in terms of the spatial patterns of surface air temperature changes over Europe, presented as anomalies for all three time slices between the reconstructed time slices and the corresponding ones of the reference simulation (Fig. 5.10 a-c). Shown are only anomalies exceeding the 95%-significance level of a two-tailed standard t-test. By doing so, the significant climate changes for Europe (non-significant areas are indicated in white), induced by the adjusted SST, can immediately be identified. In accordance with the negative (positive) anomaly (Fig. 5.4 and Table 5.2) between the reference simulation and the proxy at 9k and 6k (0k), the reconstruction leads to a warming (cooling) in the respective time slices, and exhibits antipodal patterns in all three time slices. The adjustment of the SST leads to a spatially inconsistent picture, with the warming at 6k and 9k (Fig. 5.10 b and c) more pronounced in the western and eastern parts of Europe, i.e. the reference experiment is too cold there. Over central and northern Europe, the warming is less distinctive. It is strongest and more pronounced in both regions at 6k. This may be indicative of a better representation of the mid-Holocene climatic optimum with the adjusted SST based on the Ammersee proxy where the climate optimum is clearly visible (cf. Fig. 5.4). This hypothesis needs more investigation and can be verified in a future transient simulation with adjusted SST (presented in the next two sections). The cooling at 0k (Fig. 5.10 a), resulting from the positive anomaly between the reference simulation and the proxy, is also more pronounced in the western and eastern parts of Europe.

These time slice means only show the changes over the whole period of 1000 years and suppress the submillennial - especially interannual - variability which may show a different picture for individual years. However, the statistical significance of the results is strongly increased when considering the European region and not only the grid points around the Ammersee proxy.

Summing up, a very variable temperature distribution occurs over Europe during the Holocene. This can be clearly attributed to the incoming solar radiation as well as to the influence of the Laurentide ice shield, which persisted over North America during the early Holocene (*Renssen et al.* 2009). Both forcings affected the European climate differently: As Figure 1.1 shows, the insolation signal was strongest in the early and mid-Holocene, inducing a warming mainly at the high northern latitudes. The impact of the Laurentide ice shield was also most pronounced in the early time slices of the Holocene, however, it exerted a strong cooling at the high northern latitudes, i.e. latitudinally different (cf. Sect. 1.1.1), and thus

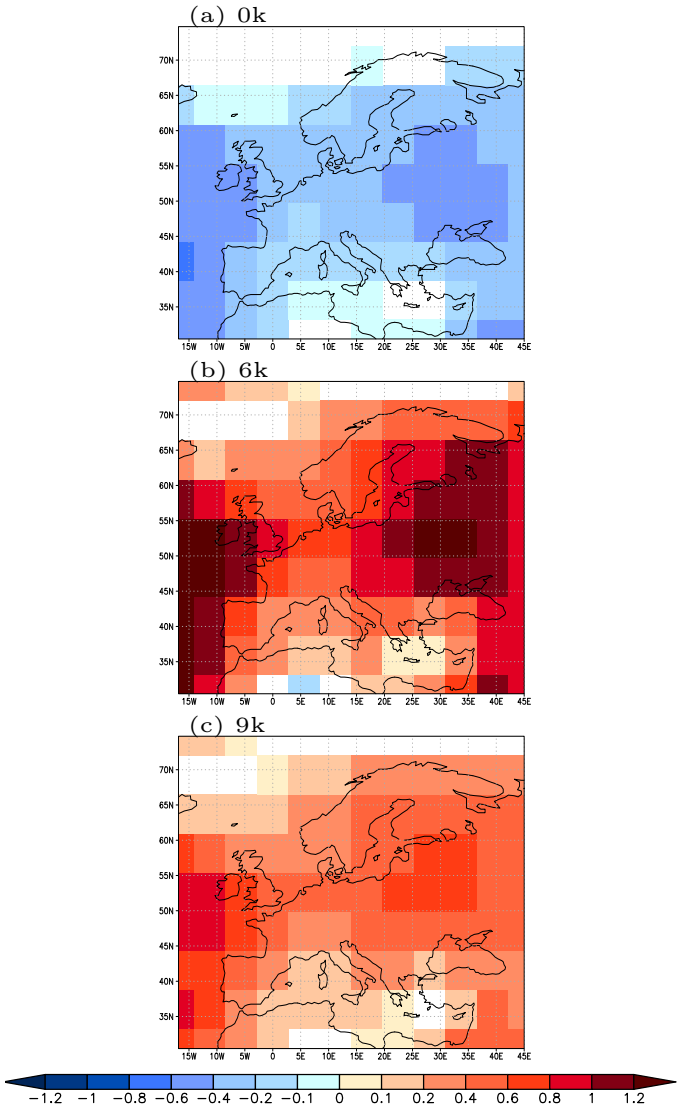

Figure 5.10: Surface air temperature anomalies [°C] over Europe between reconstructed time slices and the PlaSim reference simulation at a significance level of 95% (two-sided t-test, sample size $N = 1000$). Non-significant regions are indicated in white.

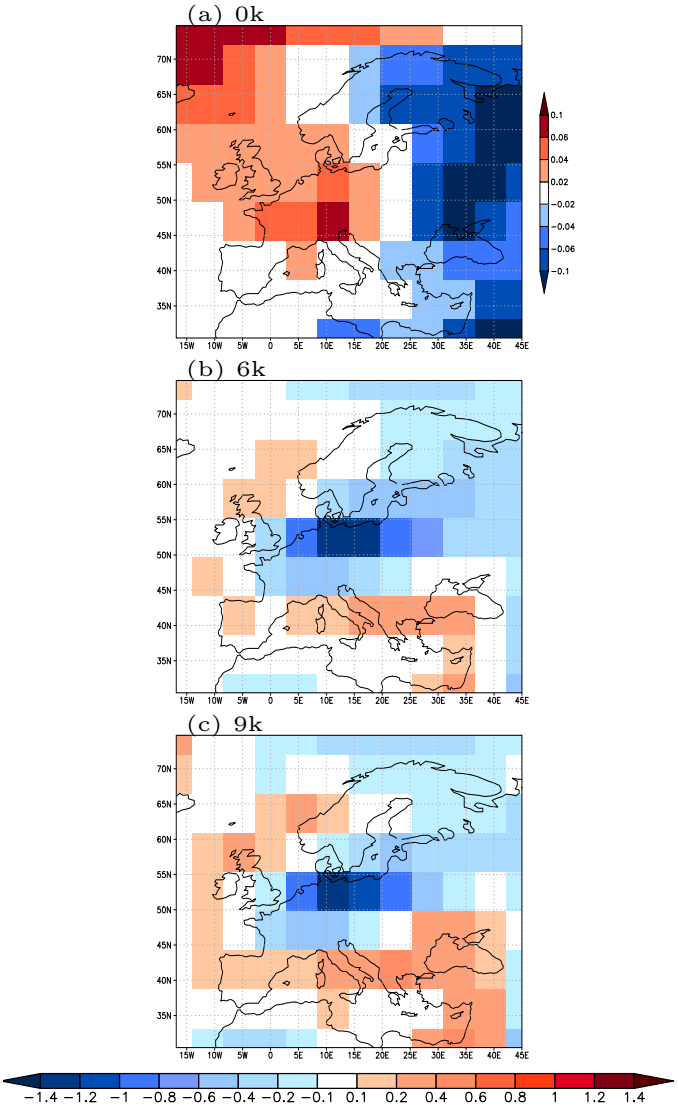

Figure 5.11: Surface air temperature anomalies [°C] over Europe between the reference simulation time slices and preindustrial climate. Please note the different color bar for 0k due to the very small anomalies to the preindustrial period.

counteracted the insolation induced warming. As *Renssen et al.* (2009) show, the ice shield determined to a large extent the timing and magnitude of the Holocene thermal maximum over the northern high latitudes. The inherent difficulties of the ice sheet are further discussed in the following section.

Anomalies to preindustrial climate

Anomalies to preindustrial climate are presented to enable a further concluding comparison to other climate reconstructions for Europe existing in the literature, and hence a reflection of these results in a wider context. For preindustrial, a 200 yr mean around the preindustrial year 1860 (≙ 90 yr BP) is

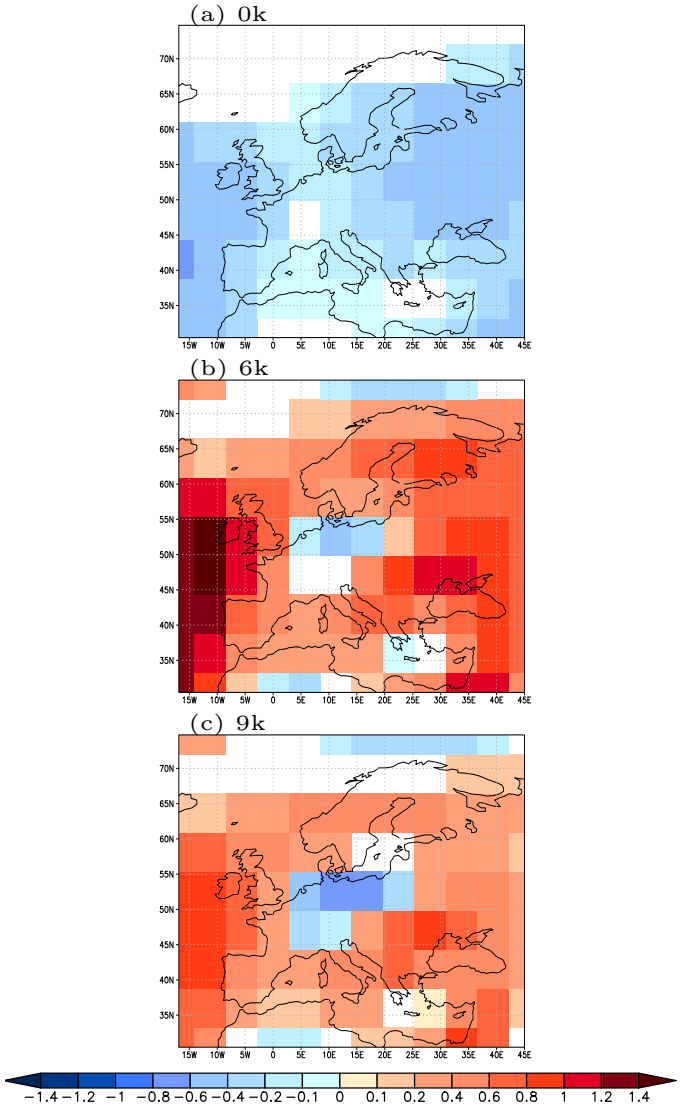

Figure 5.12: Surface air temperature anomalies [°C] over Europe between the reconstructed time slices and preindustrial climate at a significance level of 95% (two-sided t-test, $N_1 = 1000$, $N_2 = 200$). Non-significant regions are indicated in white.

chosen throughout these studies, taken from the PlaSim reference simulation. The anomalies between the reference experiment time slices and preindustrial climate are presented in Fig. 5.11. At 9k (Fig. 5.11 c), the climate is colder than at preindustrial times, mainly in the northern and central parts of Europe where a cold anomaly can be observed. In the western and southern parts of Europe, a slight warming occurs. When these findings are compared to the anomaly between the reconstructed 9k-time slice and the preindustrial, in this case at a significance level of 95% (Fig. 5.12 c), the pattern is more variable. At the northern high latitudes, a cooling can still be observed, but it is weaker than before. Large parts of Europe, except central Europe, which also shows a cooling, are warmer than the preindustrial period. The reconstruction has even led to a warmer climate in regions which showed colder conditions in the reference simulation. For the time slice of the mid-Holocene (6k, Fig. 5.11 b), the pattern is nearly identical compared to 9k. A general cooling trend occurs in the anomaly of the reference simulation, which is a bit weaker at the northern high latitudes compared to 9k, but stronger in the eastern parts of Europe. The warmer regions in the western and southern parts are less pronounced compared to 9k. In the anomaly of the reconstructed 6k-time slice (Fig. 5.12 b), colder conditions only persist in central Europe and at the high northern latitudes, but they are much weaker. On the contrary, the warming in the eastern and western parts of Europe is significantly more pronounced than at 9k. In general it can be said, that nearly the whole region of Europe is characterized by warmer conditions compared to the preindustrial, which can be attributed by the mid-Holocene climate optimum. Its representation in PlaSim is now much better than before. For the 0k-time slice (Fig. 5.11 a), the trend is antipodal. The differences between the reference PlaSim simulation and preindustrial climate are very small with a slightly more pronounced cooling in the eastern parts of Europe. Due to the reconstruction (Fig. 5.12 a), the cooling intensifies, most strongly in the western and eastern parts of Europe, so the mean over the whole time slice is lower than the preindustrial mean.

5.4.2 Summary and discussion

Discussing these first results in the context of other reconstructions and Holocene simulations for the European region will highlight potential benefits as well as deficiencies of this reconstruction method. Although the reconstruction is based only on the few grid points around the Lake Ammersee, Germany, the comparison of the extrapolated reconstructed climate to the whole region of Europe shows trends which are similar to those shown by other studies.

The results for the 6k-time slice are consistent with *Davis et al.*'s (2003) temperature reconstruction. The authors have identified warmer conditions over the northwestern, western and eastern central Europe during the mid-Holocene. Only the reconstructed PlaSim simulation and not the reference experiment agree with this pollen-based reconstruction: The reconstruction (Fig. 5.12 b) clearly performs better than the reference simulation (Fig. 5.11 b) for this time slice. Further to the south, however, where the reconstruction indicates a warming, *Davis et al.* (2003) identified a cooling.

The cold anomaly of the late Holocene (0k) as a result of the colder proxy climate can be expected from the slightly stronger CO_2-forcing during the preindustrial period. The anomaly may still be underestimated, as can be seen from the lower time slice mean in the proxy compared to PlaSim. Nevertheless, a gap of several decades in the time series of the Ammersee proxy for 0k impedes a reliable temperature reconstruction. This may also be the reason for the remaining deviations in the distribution of the PlaSim data (cf. Fig. 5.9 first row, right column). Besides this gap in the proxy time series, the results for this time slice show the feasibility of the method to not only adjust the model to a warmer but also to a colder climate (i.e. the symmetry of Eq. (5.4)), as well as the inherent complexity of the adjustment being strongly dependent on the proxy data.

A closer look at the 9k-time slice, of which the reconstruction shows weaker but similar warming and cooling trends as the 6k-time slice, shows less agreement with *Davis et al.* (2003). Although the results of the reconstruction for the Ammersee proxy showed the best approximation to the mean proxy climate for 9k (Table 5.2), the warming, in particular in the southern regions of Europe, contrasts the cooling identified by *Davis et al.* (2003) - or others (*Renssen et al.* 2005a, 2006b). As indicated before, comparing model results with proxy data always includes a range of obstacles which have to be considered. Although proxies may sometimes be representative for a larger region, as it is the case with the Ammersee proxy (cf. Sect. 5.1.2), they mostly reflect the climatic conditions on a very regional scale as they are mainly influenced by local processes. These small scales cannot be resolved by the models as their resolution is too coarse which precludes the incorporation of local processes potentially important for the proxies. Furthermore, these local influences may either be not fully understood or even completely unknown. Together with the coarse resolution, they contribute to the discrepancies in the results over southern Europe during 6k and also during 9k, where comparably large spatial differences occur, whereas the model's time slice mean converges best to the proxy mean. As already discussed in Chapter 4, the study by *Davis and Brewer* (2009) sheds more light on this regional deviation. In their model-data intercomparison, the authors have revealed the same inconsistency in the southern European climate and attribute this mainly to a model-specific feature of simulating the temperature response to a changing latitudinal insolation gradient between the mid and high northern latitudes (*Raymo and Nisancioglu* 2003). Together with the coarse model resolution, this may thus contribute to the discrepancy over southern Europe. Although both *Davis and Brewer* (2009) and *Fischer and Jungclaus* (2011) make assumptions about seasonal temperature changes, whereas annual changes are investigated in this context, these findings can be seen in line with the results, as the seasonal insolation cycle is not only visible on seasonal time scales but also affects the annual mean climate response; thus, the annual temperature changes are caused by seasonally different temperature changes (*Braconnot et al.* 2007b; *Wanner et al.* 2008; *Fischer and Jungclaus* 2011). This again supports the approach of a seasonal adjustment of SST (cf. Sect. 5.3). However, rather than to the reconstruction method itself, the deficiencies in the spatial reconstruction of the early Holocene time slice (9k) should also be attributed to northern high-latitude climatic peculiarities of this time period, which is characterized by a strong variability as well as the influence of the Laurentide ice sheet. The enhanced variability (cf. Fig. 5.9, third row) can also be detected in the proxy time series at the early Holocene (Fig. 5.4). The anomalies between PlaSim and the proxy alternate in sign on very short time scales. Whereas PlaSim is mostly warmer as the proxy at 10 kyr BP, it is much more variable at 9 kyr BP, which leads to the negative anomaly (Table 5.2). This complicates a reconstruction of this time slice, because the strong variability changes cannot be resimulated instantaneously. Secondly, and although the insolation was very strong, which would normally have induced a strong warming, the persisting Laurentide ice sheet strongly influenced the high northern latitudes and produced a no-analogue climate with both a weaker warming and a stronger cooling (e.g. *Mitchell et al.* 1988; *Renssen et al.* 2005a). The perturbing influence of the ice sheet further complicates the simulation of a realistic early Holocene climate. In contrast, the warmer mid- and late Holocene can be reconstructed by climate models more simply as a more or less direct response to the orbital forcing. To account for the ice sheet-induced cooling, models either need to include a dynamic ice model or a reconstruction of the ice sheet (e.g. *Peltier* 2004). The most frequent approach is, however, to circumvent the ice sheet complication by leaving out the early Holocene time slices, thus, by starting the simulations after the retreat of the ice sheet (*Lorenz et al.* 2006; *Renssen et al.* 2009; *Mann et al.* 2009). By not considering the land ice despite palaeoclimatic evidence, climate model simulations will always show a substantial bias. Indeed, the missing land ice in the PlaSim simulation very likely contributes to the opposing warming trends in the model reconstruction versus the pollen reconstruction. Even when an

ice sheet was considered, however, basing the reconstruction on only the 9k-time slice would be inappropriate. Instead, the full early Holocene climate should be considered, i.e. the 10k- and 11k-time slices in addition. As the results of especially the 0k-time slice reveal, the dependency of the reconstruction method on the proxy data can also be interpreted critically because it strongly relies on the quality of the proxy data which therefore must be carefully chosen. Apart from these limitations related to the proxy data, other indeed become apparent due to the misleading results of the 9k-time slice, pointing to a general limitation of this first reconstruction application, because the adjustment can only take into account the prevailing conditions, i.e. the current climatic state (in terms of temperature) and not any variations on longer time scales, especially of the preceding time slice. Moreover, no improvement in the representation of the variability pattern could be discovered after the reconstruction. Nevertheless, the presentation of these first results including a critical assessment of this new reconstruction method illustrates its general usefulness and benefits but also its limitations.

5.5 Transient reconstruction

Based on the preceding results for selected time slices and the occurrent shortcomings, two refinements of this reconstruction method are conceived, whose results will be presented in the following two sections. Shortcomings in the overall pattern as well as the lacking variability have been revealed as limitations of the very first reconstruction alternative. It will now be investigated whether an improvement with regard to these deficiencies can be achieved by the other two alternatives already mentioned at the end of Section 5.3, i.e. a transient run in terms of millennial time slice means as well as an interactive reconstruction of the proxy climate in terms of climatological means of 40 years (Sect. 5.6). The basic methodology is identical as before, but the adaptation procedure is slightly different, which is explained in the following listing:

–> The reconstruction is not carried out independently for the time slices as before but continuously.

–> The reconstruction starts with the 10k-time slice to consider the cooler early Holocene climate which is also shown by the proxy (Fig. 5.4), thus to decrease the mean temperature of PlaSim.

–> Consequently, this newly derived SST emerges from the climatic state of the reference simulation and the adapted one only at the very beginning and in the further progress from the already reconstructed preceding time slice on the basis of the anomaly to the proxy climate.

Thus, the approach is different compared to the time slice reconstructions and will thus yield differing climatic states and SST. But again, each time slice is only resimulated once and it is not iterated to converge the proxy climate best. Mainly with regard to the overall (temperature) pattern and the converging time slice means, the fact that only the actual time slice is considered for the reconstruction and not the preceding time slice, to account for potential long-term changes, has been debated as a potential source for the inconsistencies in the previous section. Thus, an improvement is anticipated at this stage, as constantly the preceding time slice with all its climatic information is taken into account. The dating uncertainty of the Ammersee proxy is again not decisive in this context, as once again time slice means of 1000 years are considered.

5.5.1 Results

The results are presented nearly in the same manner as in the preceding section. At first, the reconstructions of the surface air temperatures for now each time slice of the Holocene are shown as area-averages

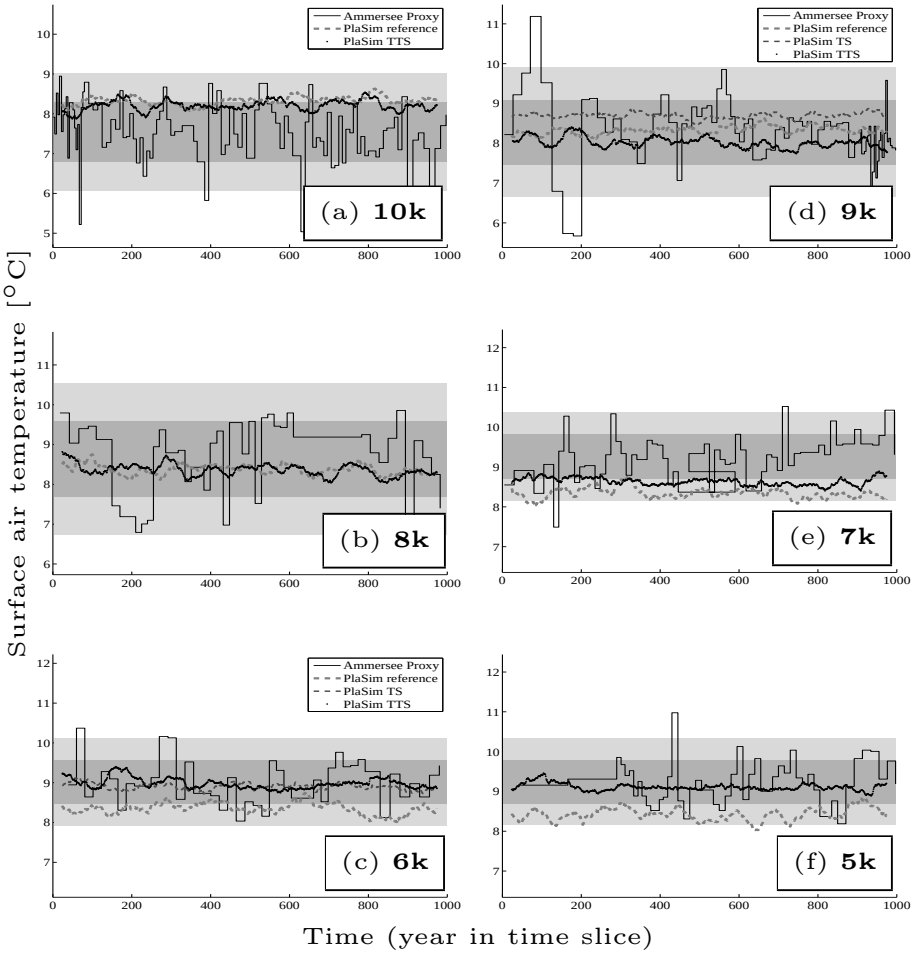

Figure 5.13: Reconstructed surface air temperature (°C) for the Lake Ammersee proxy (solid black stairs) and simulated with PlaSim (50 year running means) for the time slices 10 to 5 kyr BP; PlaSim reference (with climatological SST) in light gray dashed and the *TTS*-experiment in black dotted. For the time slices 0k, 6k and 9k, the *TS*-time series are shown in medium gray. Gray shading indicates 1σ- and 2σ-ranges in the proxy data set during each millennium.

for the region of the Ammersee proxy. After that, the complete Holocene time series for the Ammersee region is presented comparable to Figure 5.4, due to the fact that the temperature is reconstructed for the whole Holocene. A similar plot has been left out for the *TS*-experiment because of the mere reconstruction of selected time slices while leaving the other eight time slices unchanged. This section is closing with a short summary and a discussion of the results. A more profound analysis, e.g. in terms of the anomalies to the preindustrial climate, as done in the preceding section, is performed in the subsequent section to achieve a combined overview and intercomparison between all results.

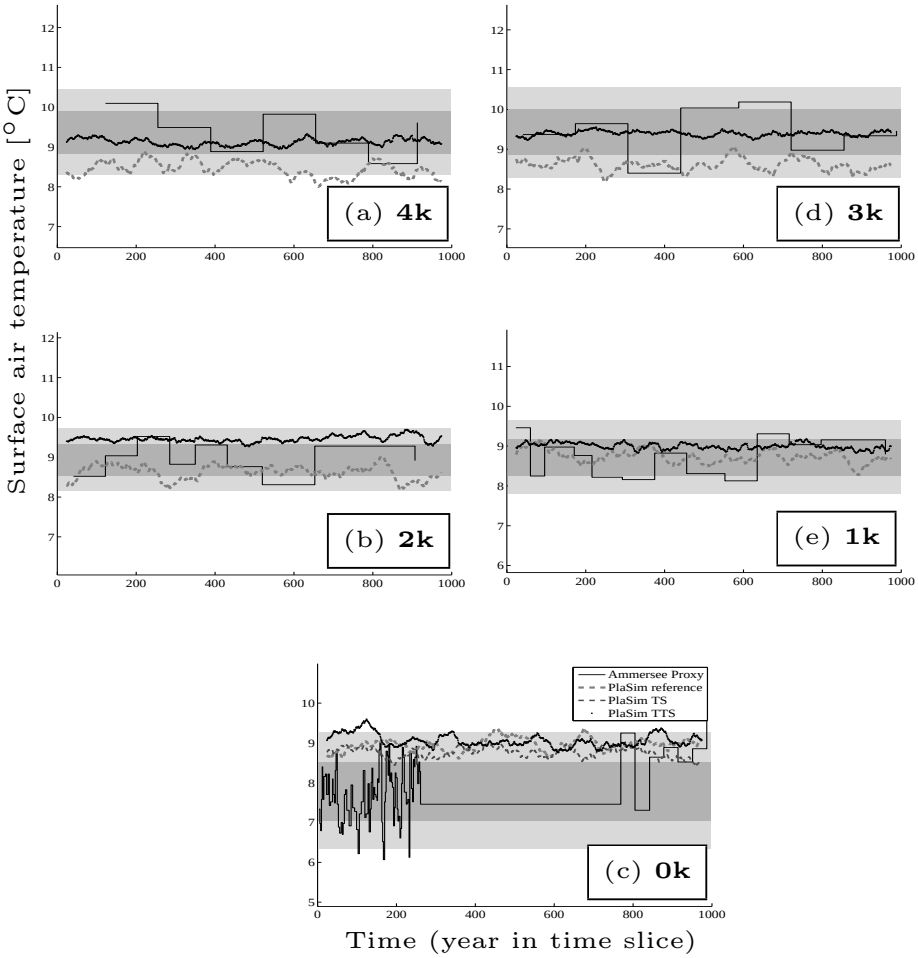

Figure 5.14: Figure 5.13 continued for the time slices 4 to 0 kyr BP.

Ammersee time series

The outcome in terms of surface air temperature for all time slices is shown in Figures 5.13 and 5.14. The time series of the proxy is again always shown in solid black (stairs), those of the transient reference simulation with prescribed SST in dashed light gray and those with the adapted SST of the *TTS*-experiment in black dotted. The light and dark gray bands are indicating the 1σ- and 2σ-ranges of the proxy. For the time slices 0k, 6k, and 9k, the reconstructed time series of the preceding section (cf. Sect. 5.4, *TS*) are also included in medium gray to give a first estimate about the potential improvements. Opposite to the presentation of the preceding section, the time slices are ordered conversely as this is consistent with the simulation which is also backwards starting at year 11 kyr BP. Moreover, the reconstruction of each time slice depends on the previous one. As the time slices in the preceding section are resimulated individually, the presentation was in chronological order. The outcome of the individual time slices is discussed in terms of a comparison of the time series, as well as of the time slice means presented in Table 5.3. Consistent to the preceding section, the time slice means of both the proxy and the PlaSim

	Proxy $\pm 2\sigma$	PlaSim reference $\pm 2\sigma$	PlaSim reconstructed $\pm 2\sigma$	$\Delta T_1 \pm 2\sigma$	$\Delta T_2 \pm 2\sigma$
10k	7.95 ± 1.26°C	8.33 ± 1.16°C	8.21 ± 1.28°C	0.38 ± 1.74°C	0.26 ± 1.82°C
9k	8.66 ± 1.95°C	8.32 ± 1.20°C	8.01 ± 1.24°C	-0.34 ± 2.35°C	-0.65 ± 2.28°C
8k	8.94 ± 1.62°C	8.38 ± 1.21°C	8.37 ± 1.27°C	-0.56 ± 1.98°C	-0.57 ± 1.97°C
7k	8.99 ± 0.88°C	8.34 ± 1.25°C	8.64 ± 1.13°C	-0.65 ± 1.52°C	-0.35 ± 1.43°C
6k	9.09 ± 1.0 °C	8.36 ± 1.27°C	8.98 ± 1.08°C	-0.73 ± 1.48°C	-0.11 ± 1.53°C
5k	9.19 ± 0.76°C	8.43 ± 1.29°C	9.11 ± 1.09°C	-0.76 ± 1.49°C	-0.08 ± 1.36°C
4k	9.38 ± 0.63°C	8.44 ± 1.36°C	9.12 ± 1.04°C	-0.94 ± 1.46°C	-0.26 ± 1.21°C
3k	9.43 ± 0.84°C	8.62 ± 1.37°C	9.40 ± 0.96°C	-0.81 ± 1.59°C	-0.03 ± 1.30°C
2k	8.97 ± 0.54°C	8.61 ± 1.43°C	9.47 ± 0.98°C	-0.36 ± 1.51°C	0.50 ± 1.10°C
1k	8.73 ± 0.73°C	8.73 ± 1.38°C	8.99 ± 1.09°C	0.007 ± 1.54°C	0.26 ± 1.32°C
0k	8.26 ± 1.34°C	8.95 ± 1.44°C	9.06 ± 1.31°C	0.69 ± 1.94°C	0.80 ± 1.92°C

Table 5.3: Time slice means (*TTS*) and 2σ-significance for the Lake Ammersee proxy (left column), PlaSim reference (second left column), PlaSim reconstructed (middle column) and anomalies between PlaSim reference and the proxy ΔT_1 (second right column) and between PlaSim reconstructed and the proxy ΔT_2 (right column).

experiments including the 2σ-variability ranges are summed up as well as the anomalies between the PlaSim simulations and the proxy. The evaluation of the results is then done in the next section, where the results are discussed.

In the first reconstructed time slice, 10k, in general a high amount of proxy data points can be observed. The reconstruction is slightly better than the reference experiment in terms of the time slice mean. Moreover, the new time series are lying nearly completely in the σ-range of the proxy. The time slice mean of the reference, 8.33°C, is indeed slightly reduced (8.21°C) due to a lower proxy mean of 7.95°C.

At the beginning of the 9k-time slice (Fig. 5.13 d), PlaSim seems to be very similar compared to the proxy in terms of the mean temperature. Moreover, PlaSim is in phase with the proxy over several parts of the time slice but the amplitude is always lower, i.e. the strong warming or cooling peaks cannot be recovered. Moreover, PlaSim simulates lower temperatures compared to the proxy over large parts of the time slice and is also considerably colder as the reference time series and also as in the *TS*-experiment. Consequently, the time slice mean is strongly reduced compared to the proxy.

At 8k, the variability pattern of the proxy is slightly stronger which can be detected in the 2σ-ranges. The reconstructed time series is located in the lower parts of the σ-range of the proxy, thus a stronger deviation to the proxy occurs which can also be detected from the respective time slice mean in Table 5.3, which is very close to the reference (8.37°C compared to 8.38°C) and thus distinctly different from the proxy mean of 8.94°C.

At 7k (Fig. 5.13 e), the reconstruction has led to an improvement in terms of the time slice mean (8.64°C compared to 8.34°C) and is thus more close to the proxy mean of 8.99°C. Nevertheless, the time series is only very roughly reaching the σ-range of the proxy.

The mid-Holocene is strongly improved compared to the reference and, similar to the *TS*-experiment, is located in the middle of the σ-range of the proxy. Also in terms of the time slice means, this resimulation is improved, also to the preceding time slice experiment which was already close to the proxy mean

(8.98°C compared to 8.90°C in the *TS*-experiment and 9.09°C of the proxy).

In the following 5k-time slice, the improvements are also more considerable - the resimulation is strongly improved and again located directly in the variability range of Lake Ammersee. The mean is also very close to the proxy, making this time slice result the second best of the whole Holocene.

During 4k, the representation is better with respect to the σ-range of the proxy as the reference is nearly lying below this range. The time slice mean is closer to the proxy (9.12°C compared to 8.44°C and 9.38°C of the proxy) but still slightly too cold.

At 3k (Fig. 5.14 d), the resimulation is again improving the reference and is located close to the proxy with regard to the σ-range. This resimulation shows the best results as also the time slice mean is very close or rather equal to the proxy mean (9.40°C compared to 9.43°C of the proxy).

During the 2k-time slice, there is a stronger difference to the reference simulation. Whereas the latter is located below the σ-range of the proxy, the resimulated time slice is located above the σ-range. This is indicative of a strongly increased time slice mean which is moreover distinctly too high compared to the proxy (9.47°C compared to 8.97°C of the proxy and 8.61°C of the reference).

In the late Holocene, i.e. the 1k-time slice, the time series is slightly shifted to higher temperature values compared to the reference and thus the representation is worse with regard to the variability range of the proxy. Consequently, the time slice mean is too warm compared to the proxy.

The last resimulated time slice, 0k, is showing a distinctly too warm trend over nearly the whole time slice. The *TTS*-time series is rather close to the reference and to the *TS*-experiment over larger parts but also shows pronounced warming peaks which are partly out of phase, i.e. a warming in PlaSim but a cooling in the proxy, or at least overestimated by PlaSim. Consequently, the mean is much too high and even higher than the reference although the proxy mean is lower.

In Figure 5.15, the individual *TTS*-time slices are merged to give a complete overview about the Holocene temperature trend (cf. Fig. 5.4). When comparing the time series, strong differences are obvious between the reconstructed and the reference experiment. At the early Holocene, a slight improvement in terms of colder temperatures is achieved. They further decrease in *TTS* around 9k, followed by a slight but distinct warming trend until 2k, when a more or less abrupt cooling occurs. This warming trend is clearly pronounced after the reconstruction, whereas the reference run shows a rather smooth trend. So, already at a first glance, a considerable improvement is achieved after the modified simulation, mainly with respect to a more distinctive mid-Holocene climate optimum. Despite these positive aspects, it is also obvious that, on the one hand, the amplitude of the warming is much lower in PlaSim so that neither the maximum temperature of around 11°C nor the strong minima are reached. On the other hand, the timing of the maximum warming in PlaSim between ≈2k and 4k is slightly out of phase to the proxy, i.e. the adjustment shows a temporal lag which has already been indicated in the individual time slices. Moreover, the variability pattern is again not covered with the reconstructed PlaSim simulation.

The corresponding qq plots for the *TTS*-experiments are left out at this stage, as the results are close to those of the preceding section, so that no decisive new insights can be expected.

5.5.2 Summary and discussion

In this section, the results of the transient reconstruction of the Holocene climate over Europe are presented. They are based on a millennial-scale adjustment of the SST. The results are now further discussed in general terms and also with respect to the previously mentioned, anticipated improvements compared to the *TS*-experiment. When summing up the remarks of the individual time slices, an overall tendency of a distinct improvement of this second alternative for the SST-adjustment can be diagnosed in most of the time slices from the direct comparison between the reference and the *TTS*-time series. Refinements with

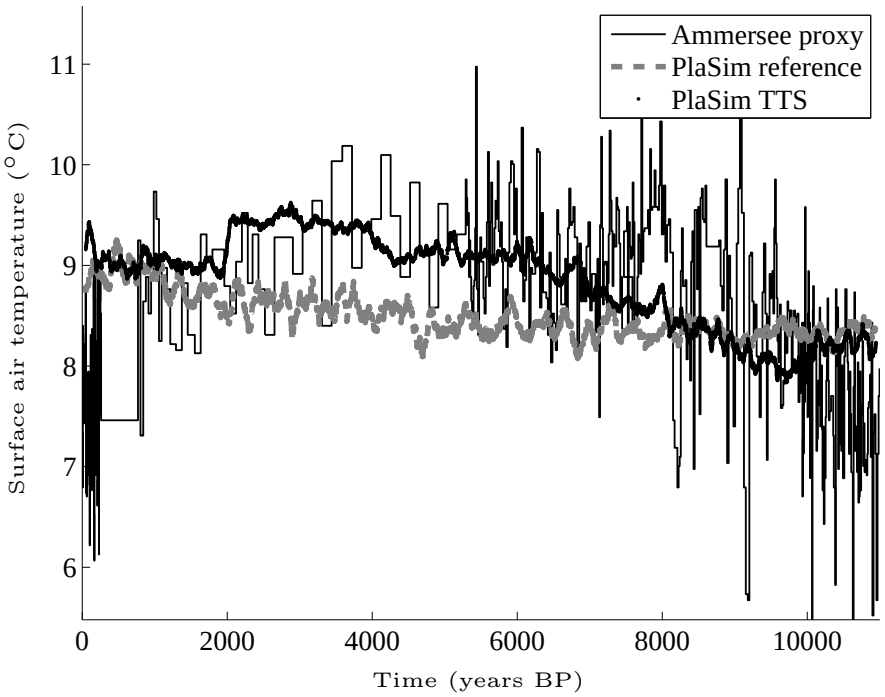

Figure 5.15: Reconstructed annual mean surface air temperature (°C) for the Lake Ammersee proxy (solid black stairs) and the respective PlaSim time series (100 year running means) from 0 to 11 kyr BP; light gray: reference, black: PlaSim *TTS*.

regard to the proxy mean are achieved in the time slices 10k, 7k, 6k, 5k, 4k, 3k and 2k. In contrast, in the time slices 9k, 8k, and 0k, the reconstruction has led to a deterioration as the adaptation is misdirecting, i.e. the anomaly between both time series is larger. The 1k-time slice is very specific, as the reference simulation is already very close to the proxy mean, so that the reconstruction is misleading. The wrong reconstruction of the 9k, 8k, and 0k-time slices clearly results from the preceding time slices, respectively from a change in sign. For example at 10k: The PlaSim reference simulation yields a too warm climate compared to the proxy at the beginning of the Holocene (8.33°C compared to 7.95°C, cf. Table 5.3). The SST has therefore been decreased accordingly, leading to a mean of 8.21°C. As this yields again a positive anomaly, the SST has been reduced again to simulate the 9k-time slice. Consequently, this then yielded a time slice mean of 8.01°C. However, the proxy mean of the 9k-time slice is 8.66°C and the reference value is 8.32°C. Thus at 9k, a negative anomaly actually occurs which would have normally caused an increase in SST. This is now counteracting the positive anomaly from the preceding time slice; the adaptation is consequently reinforcing the signal instead of dampening it. The result for the 8k-time slice is equally not improved with respect to the reference, which is also caused by the previous time slice. For the 0k-time slice, the adjustment is misdirecting despite the positive anomaly (ΔT) after the 1k-reconstruction. The improvements are thus slightly dominating the deteriorations. When comparing the results of this reconstruction method to the one of the *TS*-experiment, the mid-Holocene time slice is now slightly better represented, both in terms of the overall structure with regard to the variability pattern and the time slice mean, although the pure time slice reconstruction has already led to a converging

time slice mean. In the early Holocene, i.e. the 9k-time slice, the time series is slightly shifted to cooler temperatures and thus to the 2σ-range of the proxy although this is not reached. The time slice mean, which is very close to the proxy mean in the *TS*-experiment (cf. Sect. 5.4), is strongly reduced in the *TTS*-experiment. This context has already been mentioned above: The actual increase of SST due to the lower time slice mean of the reference compared to the proxy at 9k is confronted by the negative temperature and thus SST anomaly induced by the 10k-time slice. In the late Holocene (0k), the *TS*-experiment also yields slightly better results. The differences in the overall structure are only minor, as both the *TS*- and the *TTS*-time series are lying in the extended 2σ-range of the proxy or even out of this range. The time slice mean is slightly decreased in the pure time slice reconstruction (8.74°C compared to 8.95°C in the reference and 8.26°C in the proxy) but increased after the readjustment of this section (9.06°C). This misleading adjustment is also induced by the 1k-time slice as in the early Holocene.

A reconsideration of the representation of the full Holocene, i.e. the mere sequence of the individual time slices, enables some general but important concluding remarks of this section. Figure 5.15 can be seen as a better proof for the feasibility of this new methodology. Through this adjustment, PlaSim is indeed able to reproduce the major variations of the proxy, for example at 9k or 7k. As expected - as the adjustment of the SST is always taking place at the beginning of each time slice - the similarity to the proxy is most pronounced in the first decades of each millennium. Moreover, it is only maintained when no abrupt changes in the proxy are occurring, as Plasim, respectively the SST-adjustment, cannot instantaneously react on these short scale variations. Also, as for example between 10k and 9k, when an alternation of the sign is occurring, i.e. a change between positive and negative ΔT, this cannot be accounted for by this method. In general, PlaSim again also yields a smooth structure (similar to the *TS*-experiment) over all time slices - thus, the variability pattern and the maxima and minima are not reached. The strong fluctuation of the proxy time series further amplifies this problem, so that the PlaSim time series is consequently out of phase over larger parts. This is a distinct shortcoming of this millennial-scale adjustment. The adaptations between the individual time slices indeed succeeded but were not completely feasible with regard to an overall improvement between the reference and the resimulated time slices. Besides the achieved improvements regarding the overall pattern and the converging time slice means, the two aspects of the "memory" respectively the influence of the preceding time slice together with the adjustment of the SST only at the beginning of each time slice clearly point to the necessity for a further modification of the methodology. Consequently, it is heading to an adjustment of SST on much shorter time scales than millennial, which is done in the following section. Furthermore, a better representation of the variability pattern is anticipated. The discussion of the *TS*-results in the context of other reconstructions and Holocene simulations for the European region, as has been done in the preceding section, will be carried out in the subsequent section as a general overview. A wider discussion, also of the limitations of the methodology is also postponed to the next section.

5.6 Interactive reconstruction

Whereas distinct improvements with regard to the overall pattern and the convergence of the time slice means could have been constituted in the preceding section on the basis of the millennial adaptation of SST, i.e. transient time slices means, at this stage the very last modification of this linear sensitivity relationship is analyzed which is an interactive reconstruction of the proxy climate. Instead of a reconstruction in terms of millennial time slice means, the time scale of the SST-adjustment is reduced to 40 years, i.e. to a common climatological time frame. A period of 40 years is assigned to be a feasible time span to enable the model to adjust to the new boundary conditions over a reasonable time step on

the one hand, and, on the other hand, to account for the common climatological time period. Moreover, this is rather close to the average resolution of the proxy without going below it. Thus, a shorter time scale would make no sense and would be defective due to the proxy resolution and its dating uncertainty. Moreover, stronger statistical analogues (correlations) can rather be found on decadal time scales as on interannual (*Jones et al.* 1997; *Jones and Mann* 2004; *Goosse et al.* 2006).

Improved results are anticipated with regard to the reproduction of the variability pattern of the proxy. The basic methodology is identical as before, but of course the process of reconstructing the proxy climate is slightly different. At first, the setup of such an interactive adaptation requires a modification of the main equation, Equation (5.4):

$$\Delta SST(\tau) = \frac{1}{\lambda} \times (\overline{T}(\tau) - T_P(\tau)), \tag{5.8}$$

where $\overline{T}$, T_P and $1/\lambda$ have the same meaning as before. τ is a slower time scale and complies with the period of adjusting the SST, i.e. in intervals of 40 years. Starting with the identical model configuration and the same initial steady state of the reference run at 11 kyr BP, which has also been used for the *TTS*-experiment, the full Holocene climate is reconstructed, following the modified relation of Equation (5.4). For the later continuous application of Equation (5.8), the temporal means over the preceding time period, i.e. 40 years, are used. ΔT is calculated as the difference between the mean over the 40 years time slice and the temporally corresponding mean of the proxy time series. Based on the seasonal sensitivities determined in Section 5.3 (Table 5.1), the ΔSST are deduced in a straightforward way. The SST anomalies emerge only at the very beginning, i.e. the first 40 years of the Holocene, from the climatic states of the reference simulation and the adapted one on the basis of the anomaly to the proxy climate. In the further progress of the simulation, the oceanic anomalies then always originate from the current and the already reconstructed preceding 40 years time slice with respect to the proxy climate. Each set of newly derived SST is then used for the simulation of the next 40 years time slice. Thus, the approach is different compared to the transient time slice reconstructions of the preceding section and will thus yield differing climatic states and SST. Nevertheless, the 40 years are resimulated only once and it is not iterated. The SST anomalies thus evolve from model simulations at two different model states SST_0 and the adapted (modified) SST_1 respectively, coming from the current simulation and the one of the previous 40 years. As a consequence of this reduced adaptation time scale of 40 years, improvements are anticipated in the reconstructed time series, mainly with regard to the variability pattern but potentially also with regard to the overall pattern. Although the adaptation time scale is strongly decreased, the dating uncertainty of the Ammersee proxy is again not decisive in this context, as the time scale of 40 years is still above the dating uncertainty of the proxy. With this continuous adaptation of the model climate to the proxy, for the first time an interactive reconstruction of the full Holocene climate, based on land proxy data, is achieved.

5.6.1 Results

The results are presented nearly in the same manner as in the preceding sections. Although the adjustment takes place on the 40 years time scale, it is refrained from showing the results for each 40 years time slice to accomplish a consistency and comparability to the results of the two preceding sections. Thus, at first, reconstructions of the surface air temperatures for each 1000 yr time slice of the Holocene are shown as area-averages for the region of the Ammersee proxy. Moreover, at this stage, the very last climate reconstruction alternative of this overall study is carried out. Therefore, a profound and concluding analysis of the outcome is aspired, including a comparison with the results from other proxy

reconstructions (*Davis et al.* 2003) as well as with those of the previous fully coupled model simulation. After all, the latter simulation has revealed some shortcomings, mainly with regard to the representation of the Lake Ammersee region (cf. Fig. 5.4). These have eventually been the motivation for the climate reconstruction on the basis of the Lake Ammersee proxy. Therefore, the same representation of the European climate evolution over the Holocene is chosen as in Chapter 4, i.e. in terms of anomaly-time series for the four selected regions in Europe, and refrain from showing the spatially distributed anomalies over Europe as done in Section 5.4. Moreover, these spatial patterns do not differ so much from the ones in the *TS*-section, i.e. the general pattern is very similar, only the strength of the response varies.

Again, the corresponding qq plots for the *ITS*-experiments are left out here as the results are close to those of the preceding section so that no decisive new insights can be expected. The spatial anomalies between the reconstructed and reference time slices (cf. Fig. 5.10) are also only minor and are thus left out. The presentation is confined to the anomalies to preindustrial climate for the *TTS*- and *ITS*-experiments as well as for the reference simulation, as the results are compared to those of the fully coupled simulation. Therefore, the evolution over the full Holocene is required. In the *TS*-simulation only three time slices have been resimulated, i.e. a representation of the anomalies to the preindustrial would be meaningless at this stage. To achieve also a wider overview about the European climate change, induced by the SST-adjustment, also the changes in the precipitation patterns over Europe are investigated. This section is closing with a summary and a concluding discussion of the results which will highlight the improvements or disadvantages of each individual alternative and thus reveal potential general limitations of this methodology and its applicability.

Ammersee time series

The outcome in terms of surface air temperature for all time slices is shown in Figures 5.16 and 5.17. The time series of the proxy is again always shown in solid black (stairs), those of the transient reference simulation with prescribed SST in dashed light gray and those with the adapted SST in black dotted (*ITS*). The light and dark gray bands are indicating the 1σ- and 2σ-ranges of the proxy. In addition, the reconstructed time slices of the preceding sections (*TTS*, Sect. 5.5) are included in dark gray and those of the three time slices 0k, 6k and 9k (*TS*, Sect. 5.4) in medium gray to give again an immediate estimate about the potential improvements. Equal to the presentation of the preceding section, the time slices are again ordered conversely.

The outcome of the individual time slices is discussed in terms of a comparison of the time series as well as of the time slice means presented in Table 5.4. Consistent to the preceding section, the time slice means of both the proxy and the PlaSim experiments including the 2σ-variability ranges are summed up there as well as the anomalies between the PlaSim simulations and the proxy. The evaluation of the results is then done in the next section, where the results are discussed.

The 10k-time slice, which shows a very variable pattern in the Lake Ammersee proxy time series, is improved by this reconstruction. The PlaSim time series is located in the σ-range of the proxy over nearly the whole time slice. Moreover, the time slice mean is reduced compared to the reference and the *TTS*-experiment and thus more closely to the proxy mean (8.06°C compared to 8.33°C (reference), 8.21°C (*TTS*) and 7.95°C (proxy)).

In the 9k-time slice (Fig. 5.16 d), the time slice mean is increasing again, following the trend given by the proxy. This is thus improved in this interactive reconstruction, as the mean has been decreasing in the *TTS*-experiment. Nevertheless, the mean is still lower compared to the *TS*-experiment. However, the time series are in the σ-range of the proxy and, over larger parts, PlaSim is at least roughly in phase with the proxy, despite a temporal lag and a lower amplitude.

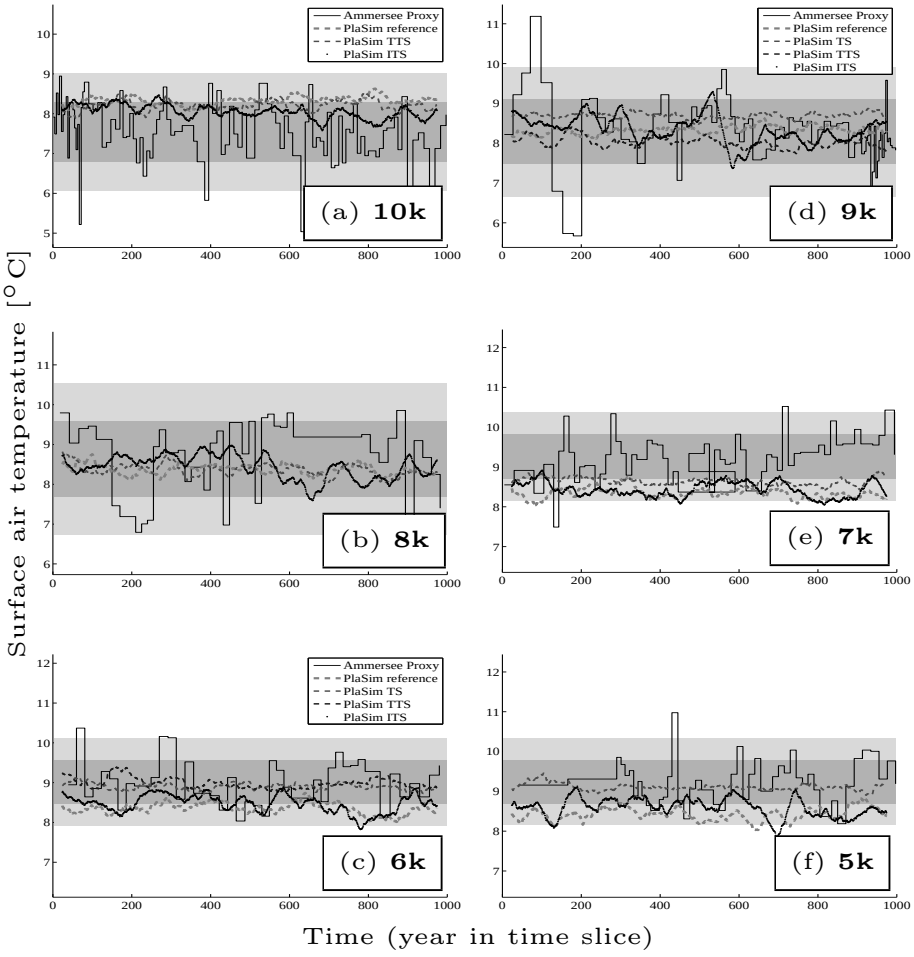

Figure 5.16: Reconstructed surface air temperature [°C] for the Lake Ammersee proxy (solid black stairs) and simulated with PlaSim (50 year running means) for the time slices 10 to 5 kyr BP; PlaSim reference (with climatological SST) in light gray dashed, the *TTS*-experiment in dark gray dashed, *ITS*-experiment in black dotted. For the time slices 0k, 6k and 9k, the *TS*-time series are shown in medium gray. Gray shading indicates 1σ- and 2σ-ranges in the proxy data set during each millennium.

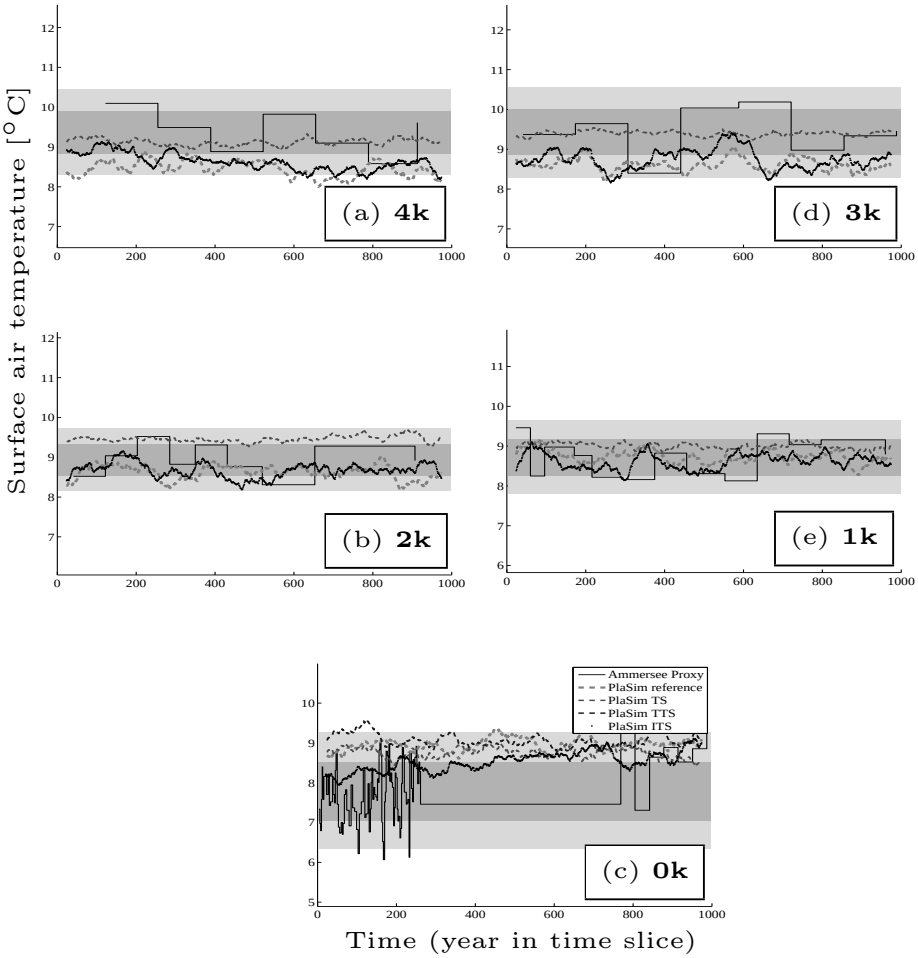

Figure 5.17: Figure 5.16 continued for the time slices 4 to 0 kyr BP.

In the following 8k-time slice, the time slice mean is slightly closer to the proxy compared to the results of the previous section. Moreover, the general pattern seems to improve during this time slice, as, for the last 500 years, the time series are located directly in the middle of the variability range of the proxy, whereas, over the first 500 years, it is slightly shifted to the lower bounds of the σ-range.

At 7k (Fig. 5.16 e), the reconstruction has again led to an improvement in terms of the time slice mean (8.43°C compared to 8.34°C) and is thus more close to the proxy mean of 8.99°C. Nevertheless, the adjustment is weaker as in the *TTS*-experiment and no improvement could be achieved with regard to the σ-range of the proxy; in contrast the representation even is a bit worse with respect to the variability pattern of the proxy.

In the mid-Holocene, there is again a slight improvement in terms of the time slice mean with regard to the reference but this adjustment is much lower compared to both previous experiments. Moreover, the time series are shifted to the lower bounds of the σ-range, which is similar to the reference simulation.

For the next three slices, 5k, 4k and 3k (Fig. 5.16 f and Fig. 5.17 a, d), similar remarks can be made: A slight improvement in terms of the time slice means can be assessed, nevertheless it is much weaker

	Proxy $\pm 2\sigma$	PlaSim reference $\pm 2\sigma$	PlaSim reconstructed $\pm 2\sigma$	$\Delta T_1 \pm 2\sigma$	$\Delta T_2 \pm 2\sigma$
10k	7.95 $\pm$ 1.26°C	8.33 $\pm$ 1.16°C	8.06 $\pm$ 1.31°C	0.38 $\pm$ 1.74°C	0.11 $\pm$ 1.73°C
9k	8.66 $\pm$ 1.95°C	8.32 $\pm$ 1.20°C	8.36 $\pm$ 1.54°C	-0.34 $\pm$ 2.35°C	-0.30 $\pm$ 2.20°C
8k	8.94 $\pm$ 1.62°C	8.38 $\pm$ 1.21°C	8.45 $\pm$ 1.39°C	-0.56 $\pm$ 1.98°C	-0.49 $\pm$ 1.85°C
7k	8.99 $\pm$ 0.88°C	8.34 $\pm$ 1.25°C	8.43 $\pm$ 1.34°C	-0.65 $\pm$ 1.52°C	-0.56 $\pm$ 1.52°C
6k	9.09 $\pm$ 1.0°C	8.36 $\pm$ 1.27°C	8.48 $\pm$ 1.33°C	-0.73 $\pm$ 1.48°C	-0.61 $\pm$ 1.50°C
5k	9.19 $\pm$ 0.76°C	8.43 $\pm$ 1.29°C	8.59 $\pm$ 1.42°C	-0.76 $\pm$ 1.49°C	-0.60 $\pm$ 1.59°C
4k	9.38 $\pm$ 0.63°C	8.44 $\pm$ 1.36°C	8.62 $\pm$ 1.32°C	-0.94 $\pm$ 1.46°C	-0.76 $\pm$ 1.30°C
3k	9.43 $\pm$ 0.84°C	8.62 $\pm$ 1.37°C	8.75 $\pm$ 1.50°C	-0.81 $\pm$ 1.59°C	-0.68 $\pm$ 1.52°C
2k	8.97 $\pm$ 0.54°C	8.61 $\pm$ 1.43°C	8.66 $\pm$ 1.47°C	-0.36 $\pm$ 1.51°C	-0.31 $\pm$ 1.47°C
1k	8.73 $\pm$ 0.73°C	8.73 $\pm$ 1.38°C	8.60 $\pm$ 1.45°C	0.007 $\pm$ 1.54°C	-0.13 $\pm$ 1.56°C
0k	8.26 $\pm$ 1.34°C	8.95 $\pm$ 1.44°C	8.53 $\pm$ 1.48°C	0.69 $\pm$ 1.94°C	0.27 $\pm$ 1.75°C

Table 5.4: Interactive time slice means (*ITS*) and 2σ-significance for the Lake Ammersee proxy (left column), PlaSim reference (second left column), PlaSim reconstructed (middle column) and anomalies between PlaSim reference and the proxy ΔT_1 (second right column) and between PlaSim reconstructed and the proxy ΔT_2 (right column).

as in the *TTS*-experiment. Moreover, the variability pattern is distinctly not covered, as both PlaSim time series are shifted to the lower bounds or even out of the 2σ-range of the proxy. Nevertheless, a slight increase in the variability pattern of PlaSim can be observed at 5k and 3k, i.e. the time series is less smooth as in the preceding experiment or the reference.

During the 2k-time slice, PlaSim is again in the lower bound of the proxy's σ-range and its time series is again roughly in phase with the proxy but again with a temporal lag. Moreover, there is an improvement with regard to the time slice mean which has increased compared to the reference (8.66°C compared to 8.61°C). Although this increase is very weak, the outcome is better in comparison to the *TTS*-experiment, as this has been misdirected and thus too high.

During 1k, the variability pattern of PlaSim is again slightly improved, covering now the complete σ-range of the Lake Ammersee proxy. In terms of the time slice mean, no distinct improvements could be achieved as the reference is already the same as the proxy, which has already been remarked. Thus the mean is as worse as in the *TTS*-experiment.

The last reconstructed time slice, 0k, seems to be best resimulated in this interactive reconstruction compared to both the *TS*- and *TTS*-experiments. The time slice mean is closest to the proxy and the time series is at least partly located in the σ-range of the proxy.

At this stage, it is refrained from showing the merged individual *ITS*-time slices to give a complete overview about the Holocene temperature trend (cf. Fig. 5.4 and Fig. 5.15) and it is referred to the appendix. As the result of each time slice indicated, the adjustment is too weak so that the reconstructed temperature time series is very close to the reference simulation, yielding thus a very poor result.

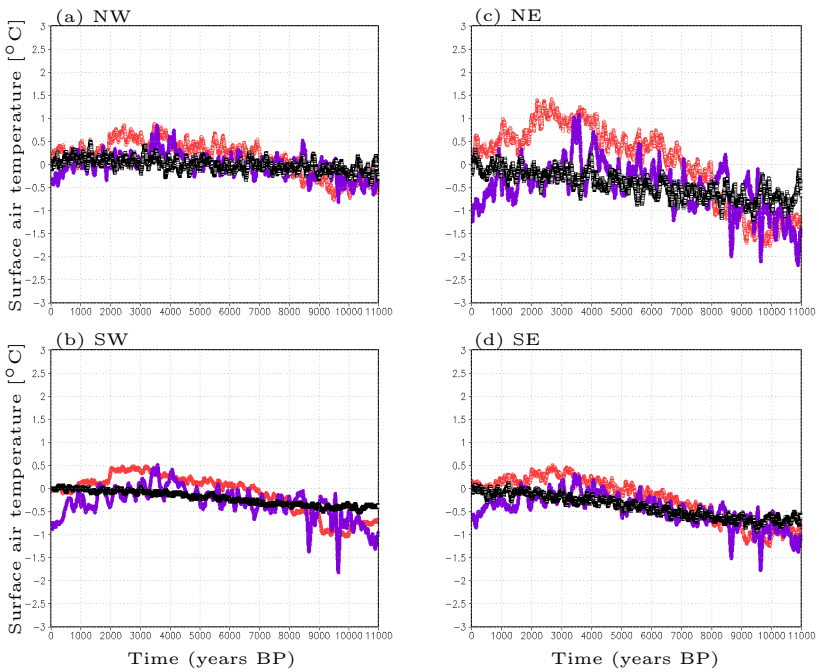

Figure 5.18: Holocene evolution of surface air temperature (T2m) anomalies [°C] for DJF (100 year running means) for (a) northwestern (NW), (c) northeastern (NE), (b) southwestern (SW) and (d) southeastern (SE) Europe; red: *TTS*, dark purple: *ITS*, black: reference. Changes are with respect to the preindustrial (today).

European climate change patterns

Similar to Chapter 4, a corresponding overview of the climate evolution over the Holocene is now given, i.e. in terms of time series for the four selected regions in Europe, to show the outcome of these adjustment approaches as well as potential improvements in comparison to the fully coupled version. These are hypothesized due to the adaptation to the proxy climate. In the Figures 5.18, 5.19 and 5.20, the anomalies of Holocene surface air temperatures with respect to the preindustrial period are presented for boreal winter, boreal summer and the annual mean respectively. The time series are presented for the four selected regions: northwestern (NW), northeastern (NE), southwestern (SW), and southeastern (SE) Europe. The reference experiment with climatological SST is always shown in black, the millennial-scale adaptation (*TTS*) in red and the interactive reconstruction (*ITS*) in dark purple.

In general, differences between the three time series can be detected. When first comparing the reference simulation for DJF (Fig. 5.18), it shows a rather smooth and constant (mainly in NW-Europe) structure for all four regions except the northeastern part, where it is slightly more variable. For this region and the southern parts of Europe, a slight warming trend can be observed which is consistent to the insolation trend during Holocene winter (Fig. 1.1 b). Compared to the fully coupled simulation (Fig. 4.1), the slight warming trend is similar, but reduced in amplitude in the simulation with climatological SST, as their annual prescription is dampening the response of the atmosphere. When now contemplating the time series of the adaptation approaches, the amplitudes are clearly more pronounced,

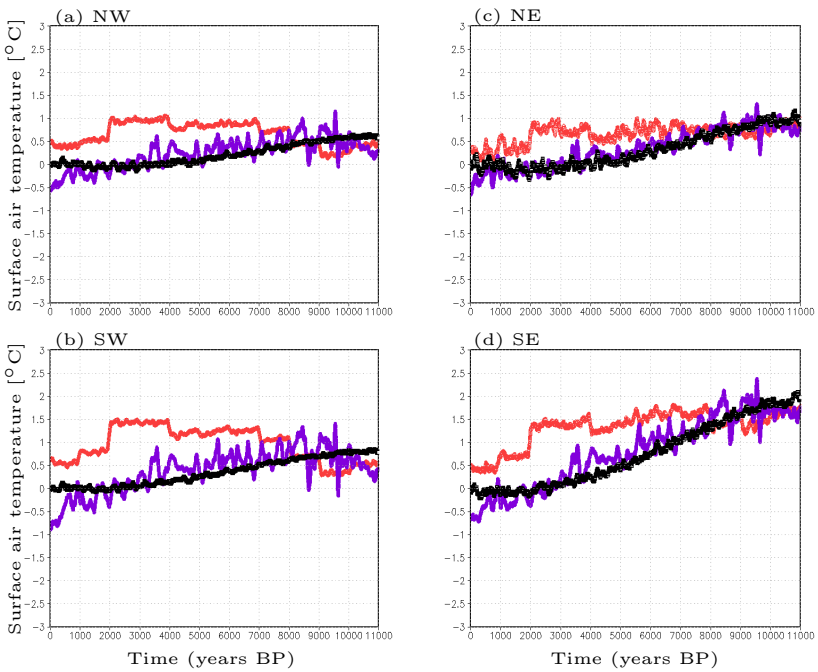

Figure 5.19: Holocene evolution of surface air temperature (T2m) anomalies [°C] for JJA (100 year running means) for (a) northwestern (NW), (c) northeastern (NE), (b) southwestern (SW) and (d) southeastern (SE) Europe; red: *TTS*, dark purple: *ITS*, black: reference. Changes are with respect to the preindustrial (today).

most decisive in the northeastern and southern European regions. However, over NW-Europe, the time series are very similar to the reference and hence the fully coupled simulation. Although the slightly increased warming trend in the *TTS*-experiment is approximating the pronounced warming trend shown by *Davis et al.* (2003), the weak positive anomaly which occurs over several millennia (also partly in the *ITS*-simulation) may be overestimated compared to the pollen reconstruction where the temperatures are below the preindustrial mean over the whole Holocene. Over the northeastern parts, this positive anomaly is also strongly overestimated as it is not captured by the palaeoobservations, which show no real trend from the mid-Holocene to the preindustrial but constantly colder temperatures compared to today. However, the pronounced early Holocene warming is similar to the pollen data, albeit strongly reduced in amplitude. In contrast, in the southwestern parts of Europe the adjusted time series are much closer to the observed ones in terms of a distinct (early Holocene) warming trend. This is a clear improvement, as the fully coupled version and the results by *Fischer and Jungclaus* (2011) both show only a very weak or rather no warming trend in the southwestern European region. Again, both the positive anomaly in the *TTS*-experiment around 3k and the negative anomaly in the *ITS* at 1k are overestimated and not shown by the data (*Davis et al.* 2003). Consistent to the southwestern parts, the *TTS*-experiment is also very similar to the pollen data over SE-Europe, due to the positive anomaly, whereas the interactive simulation is again closer to the fully coupled simulation and the results by *Fischer and Jungclaus* (2011).

During summer (Fig. 5.19), distinct cooling trends can be observed for nearly all three time series

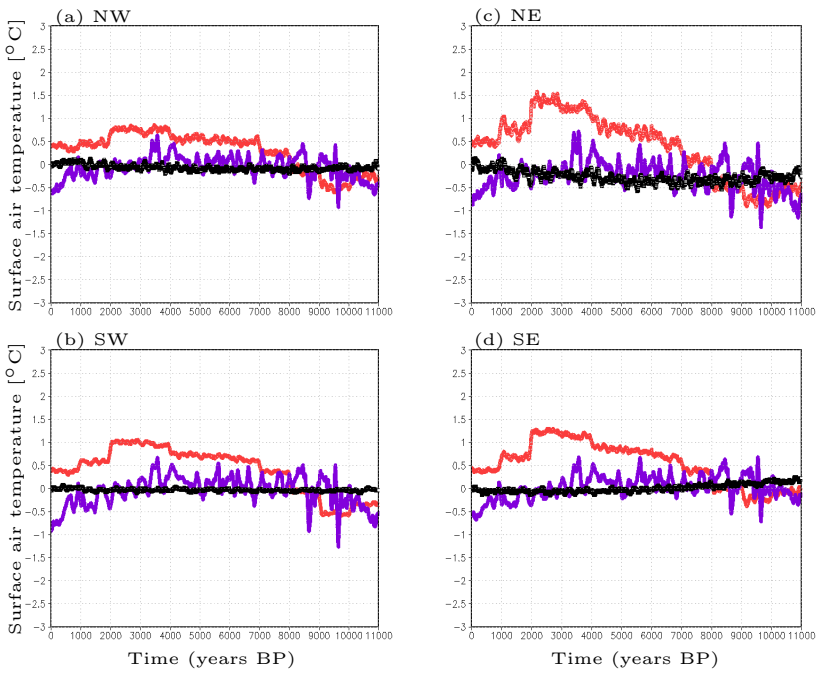

Figure 5.20: Holocene evolution of surface air temperature (T2m) anomalies [°C] for ANM (100 year running means) for (a) northwestern (NW), (c) northeastern (NE), (b) southwestern (SW) and (d) southeastern (SE) Europe; red: *TTS*, dark purple: *ITS*, black: reference. Changes are with respect to the preindustrial (today).

and all four regions, following the decreasing insolation during the Holocene. Again, the reference simulation yields the smoothest and least variable structure. In general, stronger deviations between the two reconstruction experiments can be observed. The *ITS*-simulation is rather close to the reference and thus mainly confirming the outcome of the fully coupled simulation and the one by *Fischer and Jungclaus* (2011). In the millennial-scale reconstruction, the more or less distinct cooling trend is strongly dampened over eastern Europe due to the positive anomaly mainly around 2k-3k and thus underestimated compared to the fully coupled simulation as well as the pollen data. Nevertheless, for NE-Europe, the *TTS*-reconstruction yields a similar structure of the Holocene temperature evolution compared to the pollen data because of the pronounced positive anomaly between ≈2k and 8k, comparable to the Holocene climate optimum. Exceptions are the early Holocene time slices, which are warmer in PlaSim, but rather constant in the palaeoobservations. Over SE-Europe, where the cooling trend is even stronger dampened in the *TTS*-reconstruction, it is still opposing the trend of the pollen data. Emerging from colder conditions at the early Holocene, which are also shown by PlaSim, the data show a slight warming trend until the preindustrial. Moreover, over the western regions, the cooling trend is reversed: Although a slight cooling can still be observed in the early Holocene time slices between 9k and 10k, this is converted into a pronounced warming until 2k and a cooling afterwards. This general pattern is even slightly enhanced over SW-Europe. Thus, the structures over the western parts are again resembling the mid-Holocene climate optimum, with the NW-European pattern being close to the one obtained with the pollen data. A distinct and continuous warming trend over SW-Europe, besides a stronger cooling

between 8k and 10k, is also shown by *Davis et al.* (2003). Considering the results of Chapter 4, this has been the region showing the strongest discrepancies between models and data, as this increase is neither shown by the fully coupled nor by the simulation carried out by *Fischer and Jungclaus* (2011). The result of the *TTS*-reconstruction with the warming until 2k is therefore a strong improvement, although this positive anomaly may be overestimated compared to the pollen reconstruction where the temperatures are below the preindustrial mean over the whole Holocene.

For the annual mean (Fig. 5.20), the reference simulation is showing no trend for the western European regions and a very weak warming (cooling) trend in the northeastern (southeastern) parts of Europe. This is thus consistent to the nearly constant insolation evolution. The structure of the two reconstruction experiments is again similar to the outcome of the summer time series. The interactive experiment is slightly modifying the reference simulation, showing an increase in amplitude, which is also partly changing the overall trend (e.g. over SW-Europe). Similar to the fully coupled experiment, the annual mean temperature evolution is again dominated by the summer temperatures. As the results for DJF and JJA already indicate, the *TTS*-experiment leads to stronger improvements. When now comparing the annual mean results to the pollen time series by *Davis et al.* (2003), strong similarities in terms of the general trends can be observed for all four regions. However, the amplitudes are partly underestimated, e.g. the early Holocene cooling over NW-Europe. Again, the warming trends in the southern parts are also shown in the pollen reconstruction, but, at least over SW-Europe, the temperatures are below the preindustrial mean and not above as in PlaSim. Over the eastern parts, a strong maximum is also indicated by the pollen data, but already for the period of 6 to 7 kyr BP. In PlaSim, this is slightly shifted, i.e. has a temporal lag of one to two millennia. This problem results from the shifted adjustment to the proxy climate and has already been discussed in Section 5.5 and earlier in this section.

It is now analyzed, whether the rather convincing results for the temperature evolution are also leading to an improvement in the corresponding precipitation evolution. Consistent to the temperature time series, in the Figures 5.21, 5.22 and 5.23 - for DJF, JJA and ANM respectively - the anomalies of the Holocene precipitation with respect to the preindustrial period are presented for the four regions in Europe. As expected, the reference simulation reveals the lowest variability in the precipitation during both seasons and in the annual mean. During winter, (Fig. 5.21), the reference simulation reveals no trend in precipitation in northern Europe and a slight drying trend in the southern parts. Both are confirmed by the reconstruction experiments over the eastern parts of Europe, which are very close to the control and also similar to the fully coupled simulation (Fig. 4.2 c, d). This similarity between the reference and the interactive simulation has already been assessed before, in the context of the results for the region of the Lake Ammersee (Fig. A.1). Over the western parts of Europe, the trend is much more pronounced and even modified during the early and late Holocene time slices in the *ITS*-reconstruction. Moreover, the trend is reversed in the millennial scale experiment, where a moistening trend can be observed. In a less pronounced manner, this is also shown by the fully coupled simulation over NW-Europe, whereas the strong warming trend over SW-Europe is antipodal to the fully coupled simulation but more in line with the results by *Brewer et al.* (2007, 2009), which reveal wetter conditions in the mid-Holocene.

During boreal summer (Fig. 5.22), the precipitation trends clearly differentiate between the northern and southern European regions. Over NE-Europe, all three simulations show a conversion from drier conditions during the early Holocene time slices to wetter conditions from the mid-Holocene to the preindustrial. This drying trend is dampened in the *TTS*-experiment but nevertheless the trend is very close to the one of the fully coupled simulation, albeit the amplitude is stronger here. Over the other three regions, the three simulations differ again more strongly; whereas the reference and the *ITS*-experiment are close to each other, both showing the same trends (drying in NW-Europe, no trend in SW-Europe and a weak moistening over SE-Europe), these trends are differing more strongly in the *TTS*-experiment.

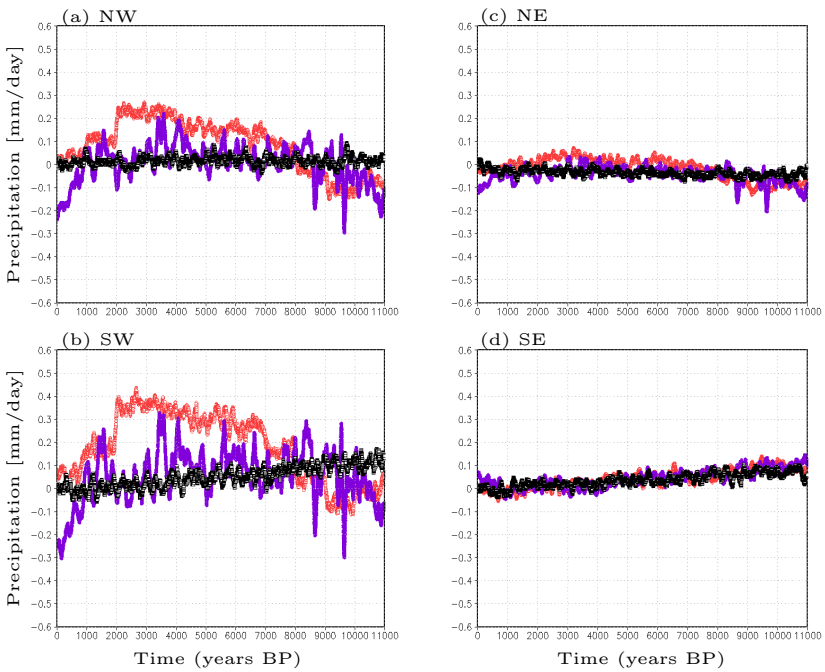

Figure 5.21: Holocene evolution of total precipitation anomalies [mm/day] for DJF (100 year running means) for (a) northwestern (NW), (c) northeastern (NE), (b) southwestern (SW) and (d) southeastern (SE) Europe; red: *TTS*, dark purple: *ITS*, black: reference. Changes are with respect to the preindustrial (today).

The pronounced positive anomaly between 2 to 4 kyr BP over NW-Europe seems to be overestimated compared to the fully coupled simulation and the results by *Crucifix et al.* (2002) and *Renssen et al.* (2005a), both identifying a rather invariant respectively a slight drying pattern over the Holocene, which is also shown by the other two experiments. In SW-Europe, the millennial-scale leads to an increase of precipitation during the Holocene, which is consistent to the fully coupled simulation. Opposite to the latter, this increase is leading to a positive anomaly from the mid- to the late Holocene which is close to the remarks by *Brewer et al.* (2007, 2009). The *TTS*-trend over SE-Europe, showing a precipitation decrease, deviates again from the other two simulations and also from the fully coupled experiment, so stronger discrepancies are occurring in this region.
In the annual mean, (Fig. 5.23), all four regions are very similar to the remarks for JJA, with the trends solely weakened by the influence of DJF. This is thus in contrast to the results for the fully coupled simulation where the annual mean trend is dominated by the winter precipitation (cf. Sect. 4.3.3). Here, it is rather the summer precipitation which is showing the general characteristics; these results are thus more consistent to those of *Renssen et al.* (2005a) and, in general, more similar to the proxy reconstructions, at least over the southern parts of Europe. But, reflecting the results of Chapter 4, this has been the region showing the strongest discrepancies in several climate model simulations.

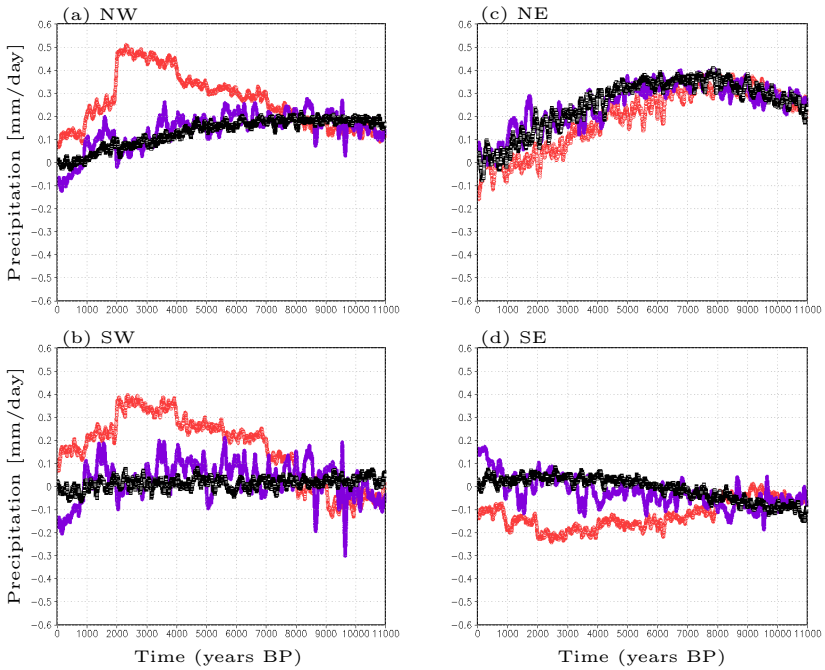

Figure 5.22: Holocene evolution of total precipitation anomalies [mm/day] for JJA (100 year running means) for (a) northwestern (NW), (c) northeastern (NE), (b) southwestern (SW) and (d) southeastern (SE) Europe; red: *TTS*, dark purple: *ITS*, black: reference. Changes are with respect to the preindustrial (today).

5.6.2 Summary and discussion

In this section, the results of the interactive reconstruction of the Holocene climate over Europe are presented. They are based on a short-scale adjustment of the SST in terms of a climatological time frame of 40 years. Again, the results are discussed in general terms and also with respect to the previously mentioned, anticipated improvements compared to the other two reconstruction alternatives.

When summing up the remarks of the individual time slices, the results of this last alternative are rather conflicting. On the one hand, there is an overall tendency of an improvement, as refinements with regard to the proxy mean can be diagnosed in every time slice, thus, no misdirected adjustments as in the *TTS*-experiment are occurring here. Moreover, the variability structure of the reconstructed temperature is increased; however, the amplitude is still lower and sometimes out of phase to the proxy time series. With respect to the anticipated improvements compared to the *TS*- and *TTS*-experiments, at least the variability pattern is displayed more exactly. On the other hand, it is very apparent that these adjustments are constantly too small and much lower as in the *TTS*-simulation. Thus, when regarding the full Holocene time series (Fig. A.1), a strong similarity to the reference simulation is striking, which is equivalent to a very reduced adjustment. Thus, one must conclude that there is no tendency of an improvement with regard to the overall pattern of the time series, despite the achieved correct adjustments in each time slice. The overall pattern is clearly better in the *TTS*-simulation, although some time slice means are antipodal. Hence, for the correct (in terms of convergence to the proxy mean) time slice

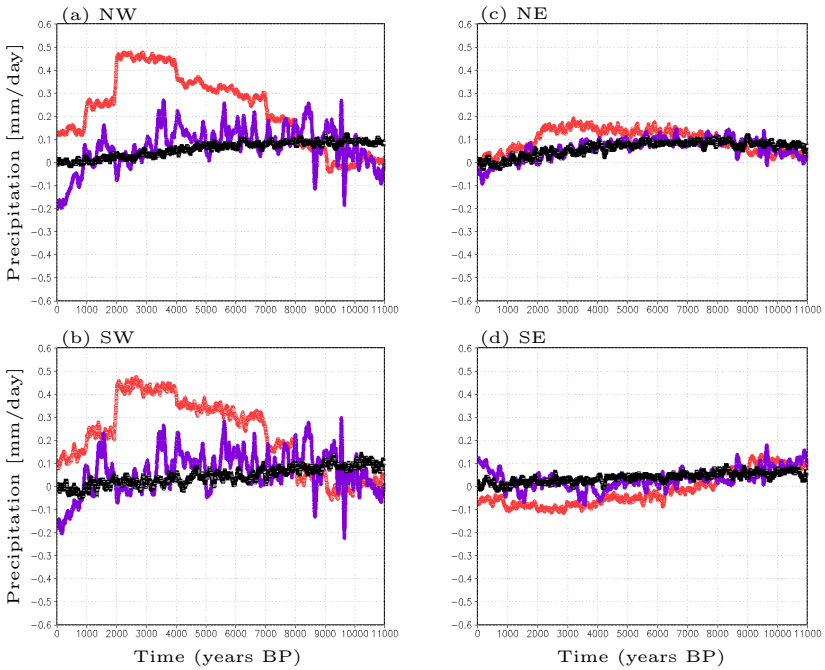

Figure 5.23: Holocene evolution of total precipitation anomalies [mm/day] for ANM (100 year running means) for (a) northwestern (NW), (c) northeastern (NE), (b) southwestern (SW) and (d) southeastern (SE) Europe; red: *TTS*, dark purple: *ITS*, black: reference. Changes are with respect to the preindustrial (today).

means and the display of the variability, the shorter time scale indeed seems to be more feasible and advantageous compared to the millennial-scale adjustment, as PlaSim can instantaneously react on the short scale variations of the proxy. Therefore, no misdirected adjustments are taking place, when a shift in sign between positive and negative anomalies occurs. Nevertheless, the short time scale seems to be disadvantageous for the adjustment itself, as maybe part of the response is immediately dampened so that the time slice mean cannot converge the proxy mean as required. Thus, a slightly longer adjustment period should be favored. The "memory" problem, i.e. the influence of the preceding time slice, which has also led to the misdirected adjustment as well as the temporal lag, indicates the requirement of further modifications of the methodology and is discussed below.

After having investigated whether the adjustment to the proxy has led to a better picture of the proxy region, it is now discussed whether the adaptation also reveals improvements in the European region. Therefore, in a second step besides the region of Lake Ammersee, the surface air temperature and the precipitation are calculated as anomalies to the preindustrial climate for the four regions in Europe. This representation is chosen to be consistent with other model/proxy reconstructions and finally with that of the fully coupled experiment in Chapter 4. The discovery of some deficiencies in the latter - with regard to the representation of the European climate and mainly of the region of the Lake Ammersee - has finally been a decisive point for the motivation of the reconstruction method, as not even the fully coupled model version has been able to simulate the correct proxy trend. Thus, potential refinements of the adaptation experiments would even imply improved results compared to the fully coupled simulation. Using now an

ocean with climatological SST, the trend is completely different compared to the fully coupled simulation and the pollen reconstruction by *Davis et al.* (2003) (Fig. 5.18 and so forth). The atmospheric response is strongly dampened by the use of fixed SST, therefore the trends during the Holocene are not captured at all in the four regions. Although both reconstructions methods still reveal some problems which require further modifications, clear improvements can be constituted. The results reveal similarities to the patterns which are shown by the pollen reconstructions. Comparable to the pure representation of the Lake Ammersee region, the *ITS*-simulation is very close to the reference simulation. Instead, the *TTS*-experiment is strongly modifying the trend. Although the response is sometimes overestimated (e.g. in terms of a positive anomaly in Fig. 5.19 or Fig. 5.22), the overall trend is partially much closer to the observed one as in the fully coupled simulation. Also over the southern parts of Europe, where it seems to be especially complicated for models to simulate the observed trend (cf. Chapt. 4), a correction of the trend after the adjustment can be assessed. This can be clearly seen as a belated corroboration for the choice of the easiest oceanic setup to apply this reconstruction method.

5.7 Iterative reconstruction

Although the three different approaches of the preceding sections, which have been introduced to resimulate a climate, which is given by proxy data, have indeed been successful, at least partly, to combine the climate modelling and the palaeoobservations, certain problems are indisputable. Even when being completely aware of the fact that it will be impossible to achieve identical results of both model and proxy, i.e. the exact temperature means, due to model uncertainties and its internal variability. In general, models are only rarely able to simulate the magnitude of climate change correctly which is given by the proxy reconstructions, as this, in part, is related to noise in the proxy data (*Brewer et al.* 2007). Moreover, the variability in models is mostly much lower as the natural variability. Nevertheless, the shortcomings in the results of the previous reconstructions, and especially in the *ITS*-experiment, which was anticipated to be the best approach, now require a separate investigation and short discussion. From this concluding discussion, further ideas are considered for potential new improvements which could be done in this context.

One definitely has to pose the question, why parts of the reconstruction did not lead to satisfying results? Although an improvement could be achieved in terms of converging time slice means, several critical aspects emerge, especially:

–> Why does the methodology, i.e. the linear reconstruction relationship, sometimes seem not to work properly? Why is the adjustment not “strong” enough? That means, why is the resimulated time slice mean too low (high) related to a negative (positive) anomaly although it should be clearly determined through the linear relationship?

–> May the methodology or parts of it be deficient? Is the region in the North Atlantic not properly defined?

–> Does the proxy resolution play an important role?

–> Where may the problems come from?

–> What kind of improvement can be made?

To clarify these questions, additional tests have been carried out. These points are discussed as a whole and not separately, as they are connected with each other. Regarding the first point, the general

methodology indeed seems to be right. The sensitivity could be proved and also the seasonal splitting could be verified by a variety of other studies which have already been mentioned in the respective section. The region in the Northern Hemisphere Atlantic, which has been determined by a set of sensitivity studies, has been verified additionally by a correlation pattern calculated with the fully coupled version of PlaSim. It has revealed a very variable pattern where the values differ only slightly from the deduced seasonal sensitivities but are still in line, thus confirming the very specific role of the North Atlantic for the climate of Europe. Due to the sometimes very high variability in the proxies and the general limitation of the models to capture the amplitude of climate changes correctly, it may potentially be impossible to generate an identical trend in models and data. The internal variability of the climate model as well as the impact of the changing external forcings, which could not have been considered in the sensitivity studies, may also contribute to the reduced response in the adjustment process.
Moreover, the resolution in the proxy data also plays a role. It is surely of dominating importance how well the proxies are resolved. One can assume that it is even more essential for the dynamic reconstruction approach and would be of less significance in a more statistical procedure. Certainly, the interpolation to an annual resolution could be a problem and may also be subject of discussion but is in line with other studies. Referring to the original years of the proxy data, despite their dating uncertainty, would have potentially caused more uncertainties.

The problems in general, i.e. in both the *TTS*- and the *ITS*-experiment, may thus result from the direct practical application process of this new methodology. Mainly for the latter experiment it has been stated, that the PlaSim time series were sometimes indeed in phase with the proxy but mostly show a temporal lag. Moreover, this lag could also be identified in the millennial-scale reconstruction, partly leading to delayed maxima. It has been concluded from Section 5.4, that the adjustment must take into account the climatic variations which occur on longer time scales, i.e. the information of the preceding time slice and not only the prevailing climatic conditions. Although this can still be approved with regard to long-term climate changes, this has, in the end, proven to cause the partly misleading results in the *TTS*-experiment, i.e. a misdirected adjustment, which was even more pronounced, when a shift in sign occurs in the temperature anomaly between the model and the proxy. This deficiency must be related to the fact, that each new set of SST which has been used for the next time slice, has been calculated on the basis of the temperature anomaly of the preceding time slice; however, because of the strong variability in the proxy, this may differ enormously from the temperature evolution of the subsequent time slice. Thus the influence of the preceding time slice is somehow overestimated, with the discussed consequences addressed for both the *TTS*- and *ITS*-experiment. This kind of "memory-effect" of the preceding time slice can thus only be avoided if the subsequent time slice is somehow accounted for, which is further discussed in the following lines.
The results of the 0k-time slice in the *ITS*-experiment indicate a gradual approximation to the proxy climate in the last years of the time slice, which is mainly enabled by the large gap of missing data in the original proxy data set and therefore the constant annual means resulting from the interpolation to an annual signal. This progressive convergence can be compared to an iteration procedure to approach the proxy climate. The general idea would then be to make several ($\approx$three to five) iterations of the selected time slices to best converge the proxy climate. After each iteration, the SST anomalies are recalculated to start a new iteration (cf. Fig. 5.7). After the last iteration, a statistical quantity, the so-called cost function is calculated. This principle is used to select, among an ensemble of climate model simulations, the one that is closest to the observed climate (*Zhang et al.* 2010). Adopted to these purposes, this would mean to identify the iteration, and thus the optimal set of SST, that shows the best fit with the Lake Ammersee proxy for the specific time slice. This best fit, i.e. the optimal simulation, is selected as the one that yields the minimum of the cost function CF:

$$CF_k(t) = \sqrt{\frac{1}{n}\sum_{i=1}^{n} \omega_i (F_{obs}(t) - F^k_{mod,i}(t))^2}, \tag{5.9}$$

where CF_k is the value of the cost function for each simulation (iteration) k and for a particular period t. n is the number of reconstructions used in the comparison between the model and the proxy. $F_{obs}(t)$ is the reconstruction of a variable F based on observations, i.e. in this case it is the temperature value of the Lake Ammersee proxy. $F^k_{mod,i}$ is the value of the corresponding variable F simulated in iteration k in the model grid box containing the location of the proxy-record i. In general terms, F can be any kind of physical variable, such as temperature, precipitation or pressure (*Goosse et al.* 2006). Thus, both observed and modelled variables F are consistent to the quantities T_P and $\overline{T}$ for the proxy climate and the value of the corresponding temperature change of PlaSim in the region of the Lake Ammersee proxy respectively, which have been used throughout this study. ω is a weight factor, characterizing the statistics and reliability of the proxy data. It could be chosen as constant for all i or it could also be related to the spatial distribution of the proxies or the correlation of a proxy with observations during the instrumental records (*Goosse et al.* 2006). In general, CF_k can be calculated for each season individually as well as for the annual mean; according to the climatic information recorded in the proxy. The value is performed for each simulation consistently and is thus similar to the previously mentioned data assimilation approaches. As mentioned in Section 5.3, this cost function is also used by *Goosse et al.* (2006) and *Zhang et al.* (2010) for the selection of the best-fit simulation. The usage of the cost function here would then be similar to the one by *Goosse et al.* (2006) where the authors select the optimal simulation out of an ensemble of different experiments with one single model whereas *Zhang et al.* (2010) apply this approach to an ensemble of model simulations with different models.

Adopted to the specific problem of the SST-adjustment, a slightly modified application of the cost function is used here, which is described in the following and illustrated in Figure 5.24 for one exemplary time slice. This adaptation is due to the specific nature of the adjustment process as with each single iteration, the model climate is already approaching the proxy climate as the anomalies are based on the preceding iteration. This is thus different from the application in *Goosse et al.* (2006) where the ensemble of simulations is based on different initial conditions.

The iteration procedure is applied here to the easiest of the previous reconstruction alternatives, i.e. the *TS*-experiment with the resimulation of the 0k-, 6k- and 9k-time slices, to verify whether it yields improved results. These experiments are thus repeated using the iterative adaptation. Consequently, the initial conditions of each time slice are identical, but the subsequent procedure differs. At first, each time slice is first split into periods of 100 years to account for smaller scale variations in the proxy and thus its variability pattern. This time frame is further consistent to the simulation period of the sensitivity studies (cf. Sect. 5.3) where λ has been determined. In addition, the dating uncertainty of the proxy even plays a less important role as in the 40 years period. After each iteration, the cost function $CF_k(t)$ is evaluated, and ΔT and ΔSST are recalculated, so that a second iteration of the same 100 years can be started with the identical atmospheric composition as the previous one. When the cost function is at its minimum, respectively after three to five iterations at the most, the minimum $CF_k(t)$ is chosen to be the best one for each specific time period. Moreover, the corresponding SST is then finally determined for this specific time frame and a new set of iterations is started for the subsequent 100 years, using the SST of the reference simulation. It is important to mention here that each first iteration should be made with the SST of the reference run to avoid the problem of the "memory effect". However, as the atmospheric composition has to be kept fixed, i.e. taken from the preceding time slice, this first iteration resembles the creation of a new reference simulation. Thus, even when only iterating once more after each "new"

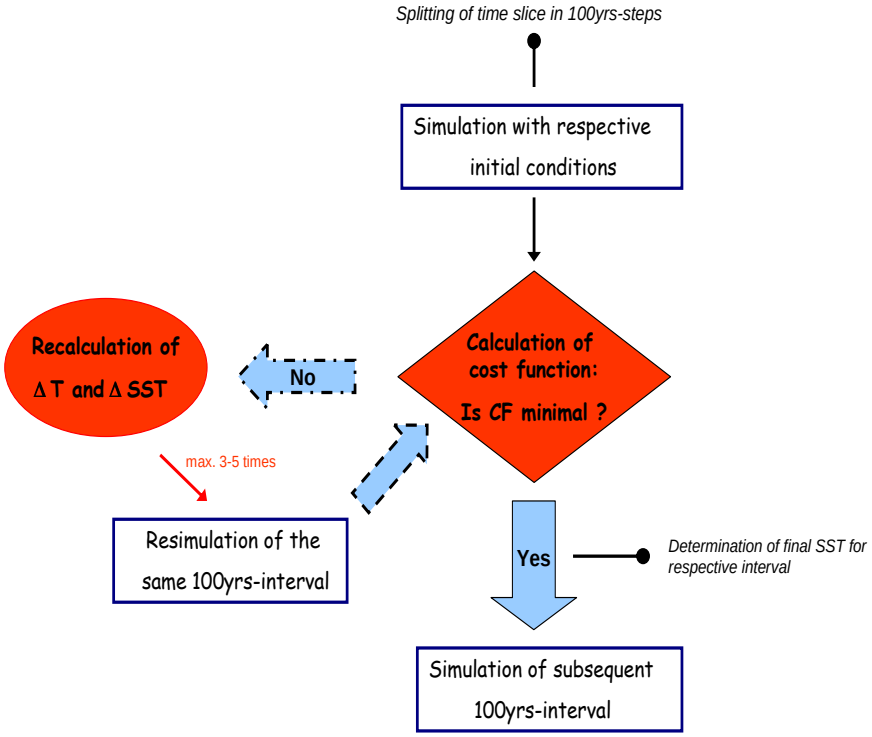

Figure 5.24: Schematic of the iteration procedure.

reference simulation, instead of ≈three to five times, this would definitely eliminate the problem of misleading time slice means as in the *TTS*-experiment. However, the slightly higher number of iterations is recommended because of the strong variability in the proxy.

Another possibility to avoid misleadings resulting from the mismatch between calculated temperatures and derived SST anomalies would be to somehow consider the subsequent time slice. However, this seems to be more prone to further uncertainties.

5.7.1 Results

The results are presented in a slightly different manner as in the preceding sections, as we confine the presentation of the results to the region of the Lake Ammersee proxy to provide a direct overview and intercomparison between all results. The representation of the anomalies over Europe with respect to the preindustrial climate, as it is done in Figure 5.12, is left out at this stage. Please note that a representation of the European climate evolution, as it is done in Chapter 4 and at the end of the preceding section, i.e. in terms of anomaly-time series for the four selected regions in Europe, is again not possible here as the evolution over the full Holocene is required. Comparable to Section 5.4, only three selected time slices are resimulated here. A short summary and some concluding remarks on the outcome of this iterative procedure are postponed to the final summary and discussion of this chapter in Section 5.10 to provide an overall context of all findings.

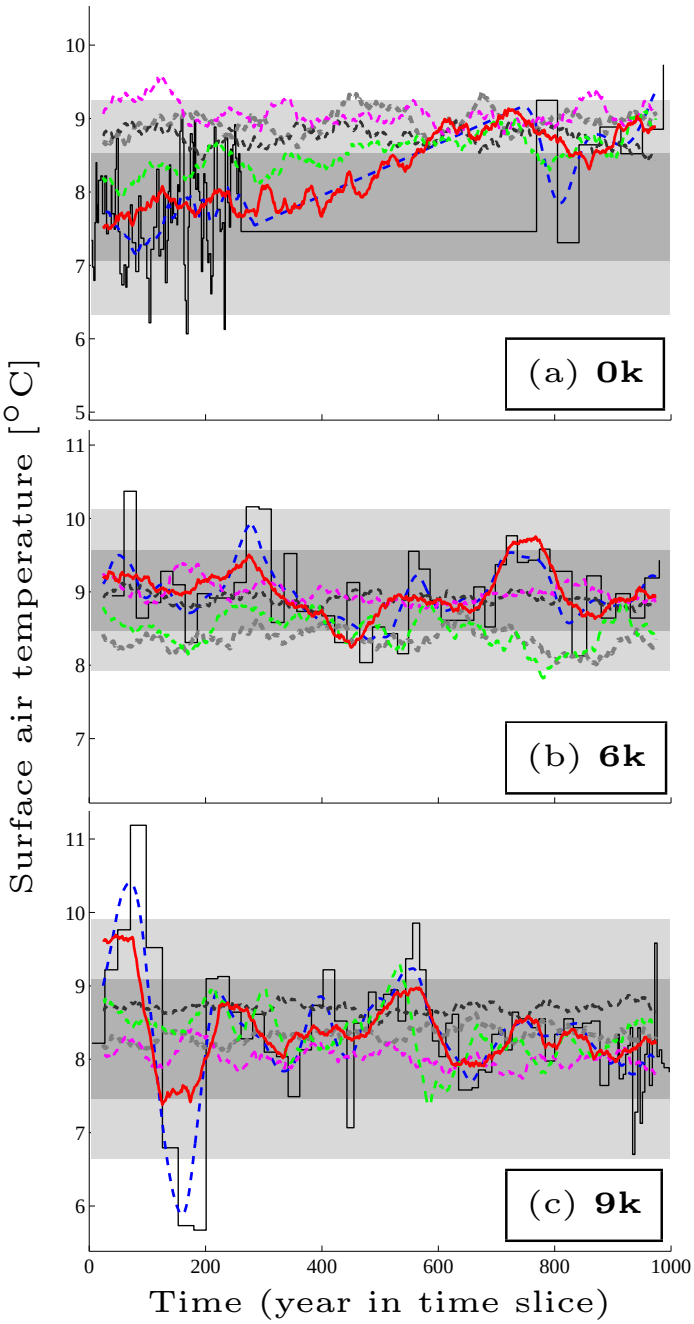

Figure 5.25: Surface air temperature [°C] of the selected time slices 0k, 6k and 9k , reconstructed for the Lake Ammersee proxy and simulated with PlaSim (50 year running means). The proxy is given in solid black (stairs, original data) and in blue (interpolated and smoothed time series), PlaSim reference in light gray, the *TS*-experiment in medium gray, the *TTS*-experiment in purple, the *ITS*-experiment in green and the iterative *TS*-experiment in red. Gray shading indicates 1σ and 2σ ranges in the proxy data set during each millennium.

The results of the iteration for the three time slices are given in Figure 5.25 for the region of the Lake Ammersee proxy, compared to the results (50 year running means) of all the preceding sections: the *TS*-experiment in medium gray, the *TTS*-experiment in purple and the *ITS*-experiment in green, PlaSim reference in light gray and the final iterated *TS*-experiment in red. This is composed of the best iteration for each 100 years. The proxy is given in black (stairs). Included here are also the interpolated time series of the proxy in blue, which are used in the reconstruction. These are also given as 50 year running means here.

The iterative results show a strong improvement compared to all other reconstructions. The agreement between these new temperature time series and the proxy is encouraging as each best PlaSim simulation is very close to the proxy in all time slices, over some parts even completely covering the proxy trend. Thus, the major variations of the proxy are now captured and resimulated by PlaSim over all three time slices. Consistently, the anomalies to the proxy time slice means have decreased enormously (as this is the main requirement of the cost function) and are now below 0.05°C for all three time slices, which is considerably better compared to nearly all time slice results of the preceding reconstructions (cf. Tables 5.2, 5.3 and 5.4). This strong similarity in the PlaSim and proxy time series has exactly not been the case in the other experiments, especially in the *TS*- and *TTS*-experiment (medium gray and purple respectively), both yielding a smooth structure with the variations being mostly out of phase. The time series coming closest to the interpolated proxy time series and therefore being at least similar to the iteration results are those of the *ITS*-experiment in green. It is the only time series which approximately shows the proxy given trend and the major variations, albeit the discussed problems of a weaker adjustment and the temporal lag. As mentioned earlier, it has lately been the result of the 0k-time slice in the *ITS*-experiment, indicating a gradual approximation to the proxy climate in the last years of the time slice (cf. Fig. 5.25 a) and thus a progressive convergence to the climate mean state of the proxy, which has led to the iteration approach. Misdirected as well as distinctly too low adjustments, i.e. the problems of the *TTS*- and *ITS*-simulations, are now avoided due to the iteration procedure. Moreover, more or less abrupt adjustments, which, for example, occurred around 4 kyr BP in the *TTS*-experiment, and which could already be dampened in the *ITS*-experiment due to the shorter adjustment period, are also completely eliminated due to the iteration procedure. However, besides the achieved improvements after the iteration, it must be remarked that the amplitudes cannot be completely captured by PlaSim, such as in the early centennials of the 0k- or 9k-time slices. Moreover, a slight temporal lag still occurs in the PlaSim time series which partly show a phase shift. Nevertheless, both features are only less distinct and in line with the iteration results for the last millennium by *Goosse et al.* (2006). In this study, the best simulation also captures the major temperature changes but not their full magnitude. This is supposed to be solvable only through stronger modifications in the representation of the physical processes in the model (*Goosse et al.* 2006).

5.8 Application to several proxies

So far, the methodology has been introduced with respect to one exemplary proxy record. This was mainly to present this new approach and to discuss advantages and limitations with regard to the overall applicability; the latter mainly with regard to the question whether this approach is a helpful tool in the wide category of studies which aim at combining climate models and palaeoclimate observations. Although the reliability of the Lake Ammersee record has been pointed out, the fact that the resimulation of the Holocene climate is only based on one single proxy record imposes a strong constraint on the overall procedure. Therefore, a real necessity is evident to consider several proxies. This will then be

consistent with other studies, relying on a wide range of different proxies (*Renssen et al.* 2009). Although the authors show similar trends as *Davis et al.* (2003) when comparing climate model output and proxy data from lake sediments, they also identify a comparably large discrepancy between models and proxy data in their intercomparison, which may be partly due to the fact that only one single proxy is used as a reference (*Renssen et al.* 2009). Although in general, a certain bias must be accounted for when only considering one single proxy, the results by *Renssen et al.* (2009) are consistent and can thus be seen as an additional corroboration of the approach of relying the reconstruction on only one proxy before extending it to several proxies. For Europe, these multiple proxies can be expected to be in close vicinity to each other. It is assumed that a close proximity of these proxies is of advantage for a successful climate reconstruction; *Wirtz et al.* (2010), for example, showed that on a spatial scale of a few 1000 km, the variability changes found in palaeoclimate time series are spatially coherent.
For the setup of a simulation incorporating several different proxies, a modification of the basic equation, Equation (5.4), yields:

$$\Delta SST = \frac{1}{\lambda} \times \sum_{n=1}^{N} (\overline{T}_n - \overline{T}_{P,n}). \tag{5.10}$$

Equation (5.4) is thus simply adjusted to n number of proxies used for the comparison, where $\overline{T}_{P,n}$ is the mean over all the proxies which are taken into consideration.
Nevertheless, a multiproxy approach involves a variety of problems, which have to be considered. As mentioned in earlier stages of this study, several requirements are encompassing the proxies. They all must or should have the same or at least a very similar temporal overall resolution. For the intention to resimulate the full Holocene climate, this resembles a rather high obstacle, as this means that the proxy records must cover a time range of $\approx$11,000 years. Moreover, as it is also the case for the Lake Ammersee proxy, large and varying temporal gaps between individual data points are not exceptional but a common problem of all proxies. Especially when thinking about statistical methods, further problems may arise when there is a temporal gap between sample sizes. Furthermore, it must be kept in mind that proxies, even those which are located very close to each other, can show completely different (temperature) trends, caused by local phenomena affecting the proxies. This has already been shortly addressed in the context of the non-consideration of existing SST-proxies in Section 5.3 because of the same reasons. As mentioned in this section, the opposing trend is indeed at least partly caused by the different type of SST-proxy used, i.e. alkenone unsaturation or Mg/Ca ratio. However, this may also be the case for different land proxy types. Such an antipodal behavior in the proxy time series may thus lead to an annihilation of the signal for the reconstruction (positive versus negative ΔT); this has mainly been the reason, why the method has been introduced only on one proxy, i.e. to avoid the problem of inconsistent and opposing proxy signals, which would have posed an additional uncertainty to the whole methodology. At this first stage, the intention was mainly to test whether the method works.
When using several proxies at the same time (in terms of the overall number as well as different types of proxies), they must be carefully chosen in advance or it should maybe constrained on less proxies or only on those showing similar trends (*Leduc et al.* 2010). However, statistical methods of course also help to overcome these diverse obstacles. Approaches are given in the studies by *Li et al.* (2010) and *Tingley et al.* (2012) or the ones which have been discussed before in the context of the various ways to reconstruct the Holocene climate (cf. Chapt. 4).

Region	Notation	Location	Time range	Classification	Reference
North Atlantic	GIK23258-2	75°N, 13.97°E	995-9094 years BP	Alkenone	*Marchal et al.* (2002)
					Sarnthein et al. (2003)
	JR51-GC35	67°N, 17.96°W	62-10171 years BP	Alkenone	*Bendle and Rosell-Melé* (2007)
	MD95-2011	67°N, 7.64°E	514-8494 years BP	Alkenone	*Calvo et al.* (2002)
	MD95-2015	58.76°N, 25.96°W	693-10469 years BP	Alkenone	*Marchal et al.* (2002)
	IOW225517	57.67°N, 7.09°E	1820-10383 years BP	Alkenone	*Emeis et al.* (2003)
	IOW225514	57.84°N, 8.70°E	449-6432 years BP	Alkenone	*Emeis et al.* (2003)
West Atlantic	OCE326-GGC30	43.88°N, 62.80°W	0-10440 years BP	Alkenone	*Sachs* (2007)
	OCE326-GGC26	43.48°N, 54.87°W	100-10470 years BP	Alkenone	*Sachs* (2007)
				Mg/Ca	*Keigwin et al.* (2005)
	CH07-98-GGC19	36.87°N, 74.57°W	520-10500 years BP	Alkenone	*Sachs* (2007)
	M35003-4	12.09°N, 61.24°W	0-10402 years BP	Alkenone	*Rühlemann et al.* (1999)
	ODP-1002C	10.70°N, 65.17°W	690-10070 years BP	Alkenone	*Herbert and Schuffert* (2000)
	PL07-39PC	10.03°N, 63.30°W	305-13992 years BP	Mg/Ca	*Lea et al.* (2003)
East Atlantic	D13882	38.63°N, 9.45°W	442-10471 years BP	Alkenone	*Rodrigues et al.* (2009)
	MD01-2443	37.88°N, 10.17°W	60-10450 years BP	Alkenone	*Martrat et al.* (2007)
	MD95-2042	37.80°N, 10.10°W	400-10500 years BP	Alkenone	*Pailler and Bard* (2002)
	M39-008	36.38°N, 7.07°W	1458-10453 years BP	Alkenone	*Cacho et al.* (2001)
	GeoB5901-2	36.38°N, 7.07°W	1134-9921 years BP	Alkenone	*Kim et al.* (2004)
	M40-4-SL78	37.04°N, 13.19°E	20-11380 years BP	Alkenone	*Emeis and Dawson* (2003)
	GeoB6007-2	30.85°N, 10.27°W	254-10502 years BP	Alkenone	*Kim et al.* (2007)
	GeoB5546-2	27.54°N, 13.74°W	3310-10421 years BP	Alkenone	*Leduc et al.* (2010)
	ODP-658C	20.75°N, 18.58°W	71-10406 years BP	Alkenone	*Zhao et al.* (1995)
					deMenocal et al. (2000a,b)
	GeoB7926-2	20.21°N, 18.45°W	0-10407 years BP	Alkenone	*Romero et al.* (2008)
	BOFS31B	18.99°N, 20.16°W	0-10360 years BP	Alkenone	*Zhao et al.* (1995)

Table 5.5: Overview of selected SST-proxies.

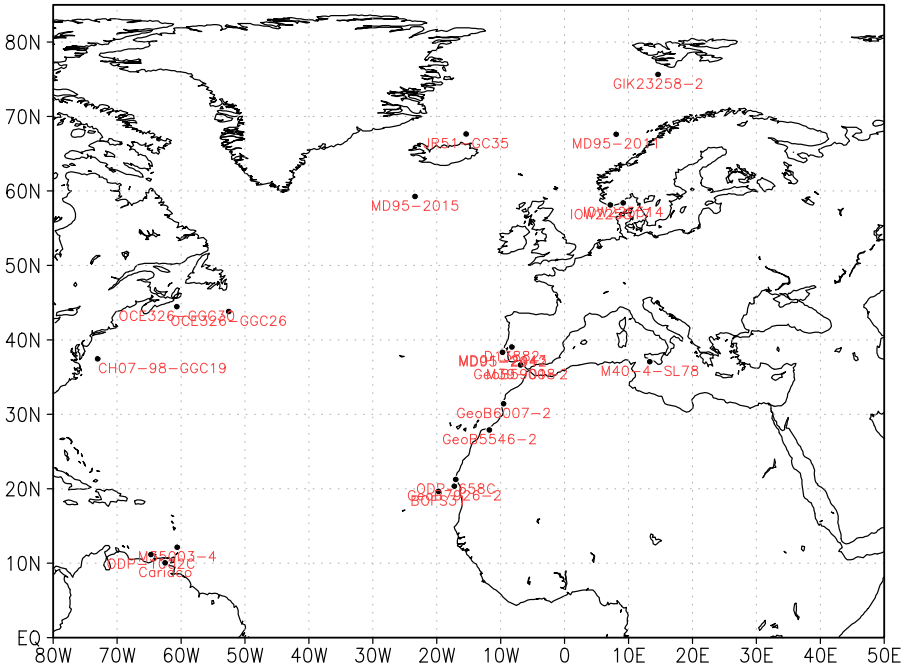

Figure 5.26: Overview of the selected SST-proxies in the North Atlantic basin summarized in Table 5.5.

5.9 Comparison to SST-proxies

After reconstructing the Holocene climate over Europe, a comparison to SST-proxies, which are existing in the literature, will be the completion of this chapter. Although it is refrained from directly using SST-proxies to force the model (cf. Sect. 5.3), they are now compared with the model SST. This is further in line with the remarks in the study by *Kohfeld and Harrison* (2000) on the global CLIMAP SST reconstruction which has been used to test the output of a GCM as well as to provide the boundary conditions for a specific period in the past. In fact, the latter has been left out in these studies for the already discussed reasons (cf. Sect. 5.3). The PlaSim-SST are taken from both the fully coupled model version (cf. Chapt. 4) and from the *ITS*-experiment in Section 5.6. Although the latter are not the result of a simulation with a dynamic ocean and thus of the corresponding climate conditions as it is the case for the fully coupled simulation, they are adjusted on the basis of the proxy climate, i.e. to the actual climate. Therefore, as has been mentioned already in Section 5.3, they can be regarded as a first order approximation of Holocene SST (*Rind et al.* 1986). This comparison to SST-proxies will thus serve as a verification of the model results of both experiments and the aim is clearly to get an estimate whether or not the PlaSim-SST and the SST-proxies are showing similar trends.

It may further highlight potential benefits as well as deficiencies of the climate reconstruction method. This comparison thus enables a more qualitative interpretation and may provide a framework for future scientific discussions of a synthesis between palaeoclimate observations and climate models. To establish a broad basis for the comparison, a set of SST-proxies in the North Atlantic is chosen to yield a good overview about the SST conditions during the Holocene. These are taken from the study by *Leduc et al.* (2010), where the authors have recalculated globally aggregated SST-proxy time series - based on the two common types alkenone and foraminiferal Mg/Ca - with regard to an identification and analysis of

sometimes diverging SST trends, depending on which proxy type is used. The alkenone proxies belong to an actualized version of the GHOST database (*Kim et al.* 2004; *Kim and Schneider* 2004), including new oceanic regions, whereas the calculation of the Mg/Ca-derived SST is completely new (*Leduc et al.* 2010).

An overview about the selected proxies and their locations can be gained from Figure 5.26. These proxies are then further subdivided into three different regions, corresponding to the North, West and East Atlantic respectively. Thereby, an adequate coverage of the Atlantic basin is achieved. It can be clearly seen from Figure 5.26 that nearly all proxies are located directly at the coasts or very close nearby - a feature, which has been already mentioned earlier in this study. All the necessary information, i.e. about the notations of the proxies, their exact location, their spatial resolution and the references, is summarized in Table 5.5 The respective conversions to SST temperature values used in the studies on the individual proxy time series are mentioned in *Leduc et al.* (2010).

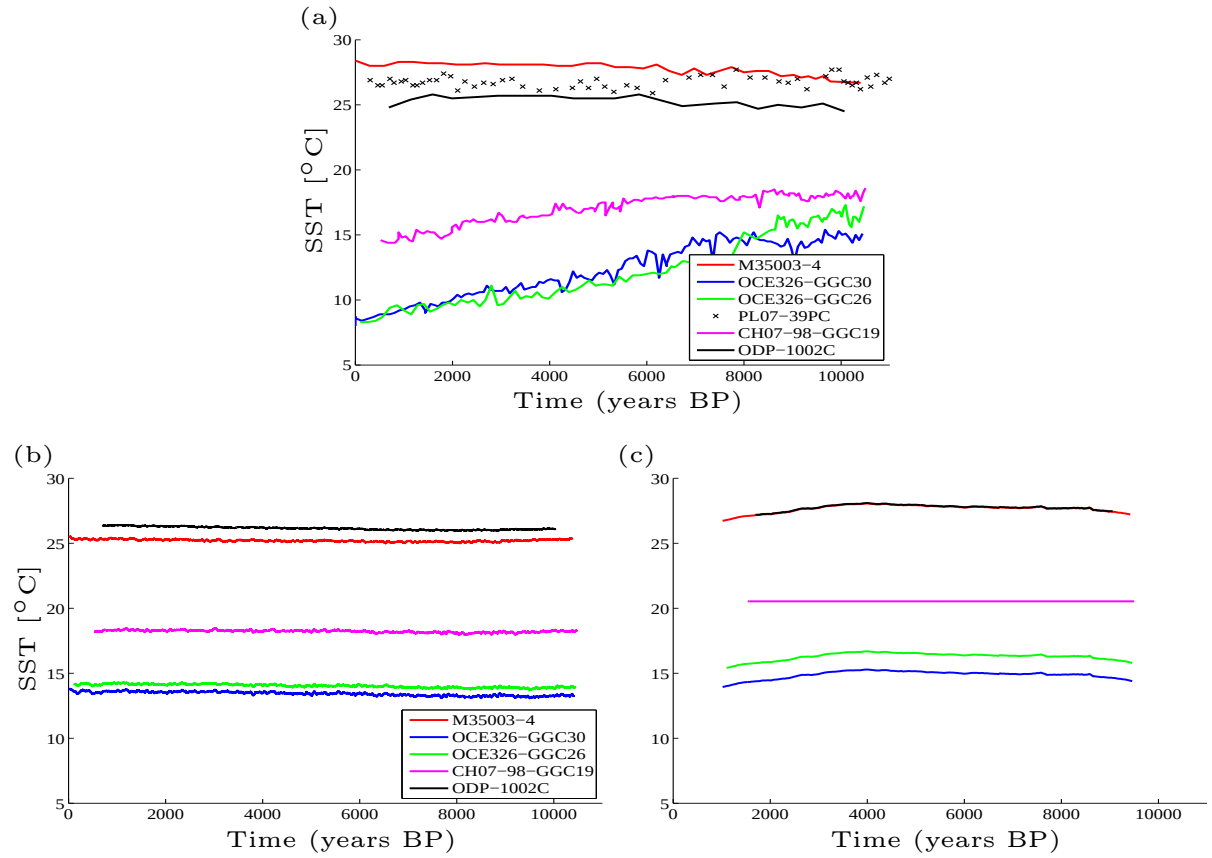

Figure 5.27: SST time series in the West Atlantic basin taken from (a) SST-proxies, (b) simulated with PlaSim-LSG, (c) resulting from the readjustment to the Lake Ammersee proxy (*ITS*-experiment). Both (b) and (c) are shown as 50 year running means. The colored time series in (b) and (c) match those in (a).

In Figures 5.27 and 5.28, the SST-proxies are now compared to those of the fully coupled simulation as well as the *ITS*-experiment. It is confined to the region in which the SST has been adjusted before,

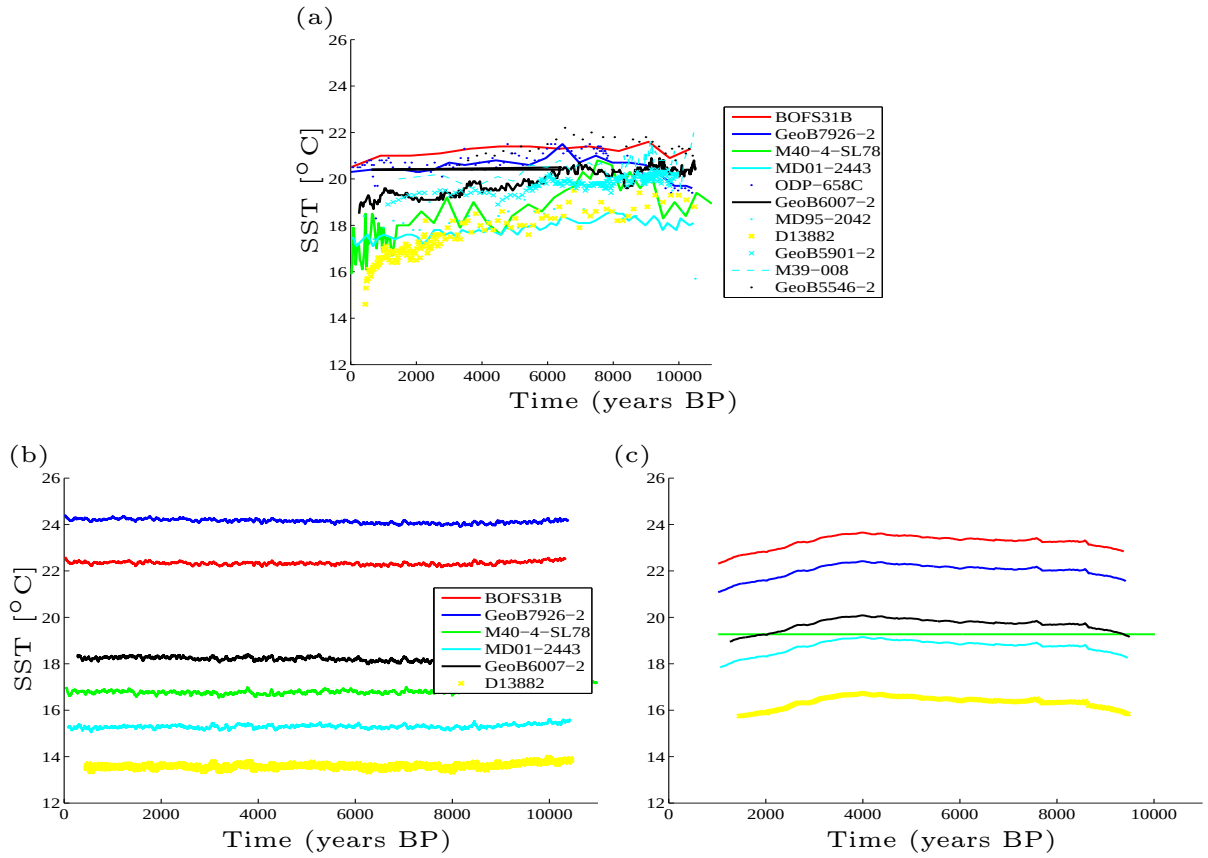

Figure 5.28: SST time series in the East Atlantic basin taken from (a) SST-proxies, (b) simulated with PlaSim-LSG, (c) resulting from the readjustment to the Lake Ammersee proxy (*ITS*-experiment). Both (b) and (c) are shown as 50 year running means. The colored time series in (b) and (c) match those in (a).

i.e. between 0° and 60°N. Thus, only the SST-proxies of the West and East Atlantic are considered here. To enable the comparison, the grid points closest to the individual proxies are selected in PlaSim, as has been done before for the region of the Lake Ammersee proxy. For the PlaSim-SST, the same time frame is selected as it is given by each individual proxy (cf. Table 5.5). Nevertheless, the model SST is given in an annual resolution whereas the SST-proxies are given in their original resolution (cf. the representation of the Lake Ammersee proxy in Figures, e.g. , 5.8 or 5.13). The colors are identical in all plots. A different style, e.g. dots, is chosen for proxies which are located very close to each other. In the latter case, they cannot be represented by PlaSim due to its coarse resolution; therefore, the total number of PlaSim time series is reduced, especially for the proxies in the eastern Atlantic.

When now comparing proxies and simulated SST, certain similarities are obvious. The strongest difference between both is the rather smooth structure in PlaSim for both Atlantic regions, i.e. no trend over the Holocene can be observed. For the interactive reconstruction (Fig. 5.27 c and 5.28 c), at least a slight trend according to the Lake Ammersee time series can be guessed. These results are in line with the study of *Lohmann et al.* (2012), in which simulated SST from an ensemble of climate models are

compared with marine temperature proxies, finding a strong mismatch between modelled and observed SST. In terms of its absolute values, the simulated SST and the proxies are rather close to each other in both Atlantic basins. In the western Atlantic, i.e. to the east of North and South America (Fig. 5.27), the early Holocene SST is nearly the same for both the blue and green time series with ≈14°C. The decreasing trend in those proxies is thus not captured by PlaSim. The black time series, which is very close to the red one in the fully coupled version respectively identical in the *ITS*-experiment is lying around ≈26°C in both PlaSim and the proxies, whereas the red time series is deviating from the SST-proxy with ≈2°C. The magenta time series is too warm over large parts of the Holocene but similar during the early millennia.

In the eastern Atlantic, i.e. to the west of Europe and North Africa (Fig. 5.28), where the number of proxies captured by PlaSim is strongly reduced, a decreasing trend over the Holocene can be observed in almost all proxy time series. In terms of the absolute values, stronger differences exist. The blue and red time series are both distinctly warmer compared to the proxy. In contrast, the black time series is represented very well in PlaSim. The light blue proxy is less well captured in both PlaSim simulations; it is too cold (warm) over the whole Holocene in the fully coupled (*ITS*)-experiment. The green time series, which shows a constant value over the whole Holocene in the reconstructed experiment, comes close to the proxy for some parts of the early Holocene but, in general, the PlaSim-SST is too warm here. In contrast, in the fully coupled version, the values are more similar compared to the proxy. The yellow time series are underestimating the SST-values given by the proxy. This is even more pronounced in the fully coupled PlaSim, whereas it is slightly closer in the *ITS*-experiment.

To sum up, a rather strong similarity between the aggregated SST-proxies and PlaSim can be observed, and, more decisively, for both PlaSim simulations, which could not necessarily have been expected, mainly when reconsidering the rather deficient results of Section 5.6. This comparison to the SST-proxies can thus be regarded as an additional approval for the applicability of this methodology.

5.10 Summary and discussion

In the current chapter, a methodology is presented to assimilate global proxy time series into a climate model. However, in the original terms of the word, it is refrained from really assimilating the proxy time series into the model. Instead, the intention is to resimulate the mean climate which is given by one specific proxy data. For this, a new methodology is developed using a linear sensitivity relationship between the SST and the adjacent land temperatures. The latter is then represented by the proxy data - Lake Ammersee in this case - and via this relationship, the model SST is adjusted to the proxy climate. The proxy has been carefully chosen in terms of the temporal resolution and reliability of being a qualitative indicator of the European climate evolution during the Holocene. In detail, the relationship between the SST and the land climate is discussed, as well as the characteristics of the proxy data in general and the Lake Ammersee in particular. After that, the new methodology is gradually introduced, explaining all decisive steps. In total, three different applications of the methodology are presented in the main part of this chapter. The first reconstruction alternative, the *TS*-experiment, has shown the general applicability of this approach through the reconstruction of three individual time slices at the early, mid- and late Holocene. The results have been promising with regard to an achieved approximation to the proxy time slice means. Nevertheless, shortcomings of this approach are obvious, as the variability pattern of the proxy still cannot be displayed by PlaSim. Moreover, variations on larger time scales are not captured by the time slice reconstruction as the time slices are arbitrarily chosen and thus independent from each other. In addition, for the evolution of the full Holocene climate, a reconstruction of the complete time

series of 10 to 0 kyr BP is required.

Thus, two refinements of the methodology are considered to achieve improvements with regard to the overall structure and the variability pattern. The first modification is the millennial-scale adjustment of the model climate to the proxy, i.e. at the beginning of each time slice, the SST is adjusted on the basis of the temperature anomaly of the preceding time slice. Although the strong variability of the proxy, including its amplitudes, is still not captured after the adjustment, a stronger convergence to the proxy means can be achieved in nearly every time slice. Exceptional cases are those time slices, where positive (PlaSim warmer) and negative anomalies are alternating, such as in, for example, 8k and 9k. As a consequence, the adjustment is misdirecting, leading to diverging time slice means compared to the proxy. Nevertheless, regarding the overall evolution of the temperature in the region of the Lake Ammersee proxy, it is more in line with the latter and distinctly better compared to the reference simulation.

As the final procedure, the PlaSim climate is adjusted interactively to the proxy, i.e. during a transient, full Holocene simulation, the model's temperature is compared and adjusted to the proxy in a constant climatological time frame of 40 years. Thereby, an instantaneous modification of the model climate is taking place, immediately correcting the deviations with regard to the proxy-representation of the Holocene climate. Thus, instead of an adjustment period of 1000 years as before, this is now carried out every 40 years. Even with this shorter time scale, it is assured to be above the average temporal resolution of the proxy and, more important, its dating uncertainty. In contrast to the *TTS*-experiment, each time slice is converging correctly to the proxy mean, thus no misdirected adjustments are occurring. This short-scale adaptation also induces a change in the variability patterns, i.e. it is slightly enhanced compared to the reference or the previous experiments; however, it is still lower as in the proxy. Besides these improvements, it is obvious that the adjustments, albeit not antipodal, are constantly too weak, resulting in relatively strong anomalies compared to the proxy. However, the magnitude of climate change shown by the proxy can only rarely be simulated by models as the proxies are themselves influenced by noise. Contemplating the full Holocene representation, the proxy trend isn't captured at all; moreover, the differences to the reference are only minor.

When switching from the perspective of the Ammersee region to the wider region of Europe (in terms of anomalies to the preindustrial), i.e. the region of interest in this study, one can indeed observe strong improvements compared to the reference run. The shown trends are similar to those of the fully coupled simulation and of other model studies as well as of palaeodata reconstructions. Specifically, a better representation of the Holocene climate is obtained over SW-Europe, where the fully coupled PlaSim and also other models apparently have deficiencies in simulating the warming trend which is indicated by the palaeodata. The reconstruction, and here mainly the *TTS*-experiment, provides more qualitative results. One must thus conclude that the *TTS*-experiment provides the best results, in terms of the complete Holocene time series as well as the European temperature and precipitation patterns.

However, when now reconsidering the results of the iterative modification it can be concluded, that this can indeed be regarded as the key to an optimal approximation and thus resimulation of the proxy given climate and thus the European temperature evolution over the Holocene. The - besides all shortcomings - existing similarity of the results of the *ITS*-simulation to those of the iterative reconstruction can be seen, on the one hand, as a proof of the general feasibility of the methodology including all its assumptions. On the other hand, it confirms the hypothesis made in Section 5.7 that the deficient results of the *ITS*-simulation are mainly caused by the practical application of the methodology meaning that only one resimulation is clearly insufficient. Instead, through the iteration procedure, the problem of the overestimated influence of the preceding time slice, which has led to the shortcomings, only exists in the very first iteration and is dampened over the further resimulations so that the climatic influence of the prevailing time slice is growing. Albeit a distinct improvement is achieved performing this iterative procedure

for the selected time slices, it must be alluded that its application strongly increases the computational resources, on average a triplication of the simulation years. This should not be disregarded, especially when considering the anticipated time frame of 11,000 years, which requires enormous computing time. Already the interactive reconstruction (*ITS*-simulation) has consumed large amounts of resources. Due to this, the iterative procedure could not have been applied to the full Holocene within this overall study.

In an additional section, an extension is shown how to apply the methodology if one wishes to include several proxies at the same time. The special requirements of the proxies and the caveats one has to be aware of are discussed. Additionally, another section gives an overview of the newly generated SST compared to selected SST-proxies from the Atlantic basin. Besides the slightly disappointing results of the reconstruction alternatives, this comparison is helpful to reclassify the results. As it is shown, both the SST of the fully coupled simulation and, more important, those of the reconstructed climate simulations show a rather strong similarity which could not necessarily be expected - especially for the latter, where the ocean temperatures are merely deduced using the (model dependent) sensitivity between the SST and the contiguous land climate as well as the climate model's difference in land temperatures compared to the proxy. The model's variability in the SST time series is again lower, mostly showing no trend, nevertheless, the PlaSim-SST shows the same range of temperature values which can be observed for the various regions of the SST-proxies. These summarizing remarks and the designated limitations now directly lead over to the conclusion of this chapter which is done in the subsequent section.

Conclusion

In the following lines, some concluding remarks are made. Regarding the overall purpose of this reconstruction methodology as a whole, several aspects are important to mention. Through the application of this straightforward linear sensitivity approach, promising results are achieved - besides all shortcomings - in the adjustment of a climate model to a given data set, which does not necessarily need to be a proxy data set but could also be any other. The results are feasible with regard to a successful resimulation of the proxy climate: It seems to be possible to adjust a GCM to a climate which is given by proxy data. Moreover, this methodology can be transferred to any other climate model; of course, the model's sensitivity has to be determined in advance. Moreover, the choice of valuable proxy data must also be carried out at the very early stages. Thereby, the temporal and spatial resolution as well as its reliability as a climate indicator and the dating uncertainty are essential features one has to consider.

In addition, the general usefulness of this model-proxy-adjustment can also be argued for with regard to the problem of the missing land ice in climate models. By using this reconstruction method, one achieves the setup of realistic initial conditions for the beginning of the Holocene, where the climate model is tuned not only to colder temperatures but to existing palaeodata. In this context, this approach can be used to initialize a realistic simulation of the early Holocene climate, even in case of a missing dynamic ice sheet model and instead of other land ice prescriptions. Indeed, the missing land ice in the PlaSim simulation very likely contributes to the opposing warming trends in the model simulation versus the pollen reconstruction (comment: This overestimated warming also has an impact on the vegetation distribution over the Holocene which is discussed in the next chapter). The intention for setting up a Holocene experiment at the early Holocene without considering the land ice and therefore accepting this bias may be inconsistent but can be substantiated in several ways. The main intention of this study yields at the resimulation of the realistic Holocene climate over Europe. To achieve this, the study intended mainly to introduce this new method on the basis of the actual model climate, which is not modified - and thus perturbed - by the inclusion of an ice sheet reconstruction, affecting not only the mean climate state but also climate feedbacks. This land proxy-based adjustment of sea surface temperature is envis-

aged to become part of an ongoing process relating proxies and GCMs in an easy and straightforward way. Although not based on statistical analyses, the dynamical approach can by all means be seen in the framework of data assimilation. As it is explicitly not based on statistical properties but on a dynamical adjustment, it may open new insights in this field. This simple technique may seem too unsophisticated when thinking of the state-of-the-art coupled versions of existing GCMs - it is, however, very straightforward when keeping the actual intentions in mind of reconstructing a climate which shows the optimal fit to a specific proxy climate. The main interest is the response of the atmosphere to the adjustment of the SST, thus, a disregard of oceanic feedbacks is permissible and in line with *Widmann et al.* (2010).

6 Vegetation studies

The forthcoming chapter is dedicated to study two different aspects related to vegetation. A set of less and more comprehensive vegetation modules and models is used here together with PlaSim: the vegetation models SimBA and CARAIB as well as two more phenomenological quantities, the Koeppen climate classification and the Budyko dryness index. The first main part of this chapter can be seen in the context of the European climate change during the Holocene, and the vegetation evolution over Europe (a) is investigated from the early to the late Holocene, using the models SimBA and CARAIB. The second part is made up by studying the interaction between climate and vegetation (b), i.e. by analyzing the influence of vegetation extremes on the climate. As mentioned at the very beginning (cf. Sect. 1.1.2), these studies are carried out to estimate the feedbacks of (anthropogenic) land cover changes on climate, using two climate classifications.

The forthcoming section is divided as follows: At first, the two different parts of this chapter are shortly discussed before introducing the different vegetation modules which are used in this context, ranging from two phenomenological quantities, the Koeppen climate classification and the Budyko-Lettau dryness index, to the more complex dynamic vegetation models CARAIB and SimBA, whereas the description of the latter has already been done in Chapter 2. In this context, peculiarities of each individual model are pointed out as well as the differences between them, also with regard to the coupling procedure. After that, the experiments are explained which are carried out for the respective studies before presenting the results of both sections (a) and (b). This chapter is closing with a summary and a conclusion.

6.1 European vegetation evolution during the Holocene (a)

This part aims at the investigation of the European vegetation evolution during the Holocene. To achieve reliable information about this is as important for the overall motivation as the reconstruction of the climate and is therefore comparable to Chapter 4 on the analysis of the European climate during the Holocene with the fully coupled PlaSim. The focus is set on the presentation of the vegetation-related parameter GDD as well as of European vegetation maps. The parameter GDD, also called bioclimatic variable, is a measure of the length of the growing season and thus a decisive parameter for plants. It yields the annual sum of the continental surface air temperature for days exceeding a certain temperature threshold, which can be 0°C and 5°C. GDD is also of further importance for the model GLUES (cf.

Sect. 1.1.2). Moreover, the vegetation maps are presented in a very high resolution for Europe with results obtained from CARAIB to provide a detailed insight into the European vegetation distribution and evolution over the whole Holocene. As will be addressed in more detail in the context of the description of the Koeppen climatology (cf. Sect. 6.3.1), the climatic conditions can be regarded as natural boundaries for vegetation. Thus, changing climatic conditions, as in the Holocene, will potentially cause shifts in vegetation types or the emergence or disappearance of types.

6.2 Climate-vegetation interaction (b)

In the second main part of this chapter, the focus is the interaction between climate and vegetation. The motivation for these analyses is related to the remarks in Section 1.1.2 and the aim is to quantify the **influence of extreme land cover changes on the climate**, assuming a global "green world" as well as a "desert world". This question is decisive for the overall motivation regarding the linkages between climate and (preindustrial) cultures. The interaction of vegetation and climate has been a widely studied aspect in climate research for the past several decades. Less and more complex approaches (see next section) have contributed so far to the ongoing discussion of how climate and vegetation influence each other and how this can be quantified. In general, biosphere and climate are closely related with each other - thus, variations in the climatic parameters are not stand-alone but must be regarded in a larger context, considering their influence on the environment, mainly the vegetation. This interaction is thus designated by the dominating influence climate has on the global distribution of vegetation and, on the other hand, by the strong climatic impact of terrestrial plants through, for example, the modification of the water and energy budget in the atmosphere.

6.3 Vegetation Models

In the following sections, an overview is given on the set of vegetation modules and models which are used together with PlaSim.

6.3.1 Koeppen climate classification

Based on the assumption of a close dependency between climate and vegetation, the first qualitative descriptions accounting for them have already been made at the beginning of the 20th century by defining specific climate factors as classification indices. Since then, climate classifications have been emphasized to be a useful tool in scientific research. They have been originally constructed to designate the various existing local climates to a more convenient number of climate types by determining the spatial distributions of these types on the basis of the climatic data for a selected, but arbitrary period of time. As the climatic circumstances are variable, e.g. under global warming conditions, the classification is also subject to change. Therefore, it is useful not only for determining the mean state of the climate but also for an analysis of the modifications on a regional or global scale as a direct result of a different climatic reference period (*Beck et al.* 2006). One such classification, the Koeppen climate classification (*Köppen* 1936) expresses climate in terms of natural vegetation, assigning different vegetation types on the basis of the respective climatic boundaries. This is explained in more detail in the next sections.

Previous applications

The Koeppen climate classification can be used with a variety of data sets or model outputs. Due to this, numerous studies using the Koeppen climate classification can be identified. *Lohmann et al.* (1993) show the possibility of the Koeppen classification to be used as a diagnostic tool for general circulation models (GCM). A similar investigation is done by *Kalvová et al.* (2003), applying the classification to observed data and model output from different GCMs, with the latter also under possible future climate changes. Global warming scenarios are also part of the studies of *Fraedrich et al.* (2001), defining the regions with the most significant climate shifts, or of *Gnanadesikan and Stouffer* (2006), who use the Koeppen classification to find out model errors relevant for the land biosphere. Regarding palaeoclimatic conditions, *Guetter and Kutzbach* (1990) examine the change in the classifications by considering a completely different climate than it is today, i.e. the glacial and interglacial period of 18 kyr and 126 kyr BP. Other studies focus more on the aspect of detecting changes on a regional scale, such as *Wang and Overland* (2004) who use the Koeppen classification together with satellite and reanalysis data for detecting climate and vegetation changes in the Arctic domain, or the one of *Diaz and Eischeid* (2007) looking for an alteration in the climate classes in the mountainous region of the western United States. Comparable studies with regard to the use of vegetation modules are those of *Henderson-Sellers* (1993) and *Claussen* (1994) who are using the Holdridge scheme and the more detailed BIOME model of *Prentice et al.* (1992) respectively. The latter gives a more qualitative overview about the global biome or vegetation distribution. This model is based on physiological considerations of the plants rather than on the correlations between climate and biomes. In total 14 plant functional types (PFT), which are assigned specific climatic conditions and tolerances, are included in the model. It predicts which biome types can occur in the respective region due to the climate, and selects the potentially dominant plant types according to a dominance hierarchy (*Claussen* 1994), which is an artificial device enabling comparisons with vegetation classifications such as that of *Olson et al.* (1983). It is important to mention that this exclusion of plants is not based on climate but on the presence of other, more dominant plants. Biomes are then defined as combinations of the dominant types. Nevertheless, the BIOME model is a static model, i.e. the calculation of biome changes due to internal vegetation dynamics is not possible. In contrast to this, the less complex Holdridge scheme is, like the Koeppen classification, relating vegetation to climate and gives an estimate of the potential natural vegetation by using annual values of precipitation and the growing season length.

Allocation of classes

As mentioned earlier, the distribution of the major vegetation or biome types is clearly constrained by climatic boundaries, so that natural vegetation can be seen as an expression of climate (*Wang and Overland* 2004). The classification itself is based on this assumption of vegetation being a good indicator of climate in the respective region and associates climatic with biogeographical boundaries (*Kleidon et al.* 2000). It combines near surface air temperature and precipitation and the annual cycle (i.e. seasonality) of both variables. It thus classifies the world climates by climate state variables combining the thermal energy and water cycle aspects at the surface. Originally, five main climates are distinguished, with four thermal climate types and one hydrological type: equatorial (A), arid (B), warm-temperate (C), snow (D) and polar (E), where B is described by the moisture budget and the other ones are defined by their temperature limits. Each of these five types is further subdivided into two or three subtypes. Here, a modified version is used, which has been developed in this context and which is based on *Trewartha* (1980), *Rudloff* (1981) and *Hendl* (1991), and also applied in *Fraedrich et al.* (2001), but with slightly different algorithms. The most important are summed up in the following, a more detailed overview is given in

Climate zone	Climate type	Vegetation type
A Tropical	Ar Permanent wet	Tropical rain forest
	Am Monsoonal	Tropical seasonal forest
	Aw Winter dry	Savanna
	As Summer dry	Savanna
B Dry	BS Steppe	Warm grass/shrub
	BW Desert	Hot desert
C Subtropical	Cr Permanent wet	Warm mixed forest
	Cw Winter dry	Warm mixed forest and xerophytic woods/shrub
	Cs Summer dry	Warm mixed forest and xerophytic woods/shrub
D Temperate	Do Maritime	Cool mixed forest and temperate deciduous forest
	Dc Continental	Cool conifer forest
E Boreal	Eo Maritime	Cold mixed forest
	Ec Continental	Taiga
F Ice	FT Polar	Tundra
	FI Ice	Polar desert

Table 6.1: Zones and types of the modified Koeppen climate classification.

the appendix. Compared to the five main climates, the regional representation is improved by using six main climates: tropical (A), dry (B), subtropical (C), temperate (D), boreal (E), and snow climates (F). The A- and C-zones are further subdivided into permanent wet, summer-dry and winter-dry (r, s, w) and an additional monsoonal type (m, only in A). The B-zone consists of the two subtypes steppe (BS) and desert (BW), the D- and E-zones are both split depending on maritime (o) or continental (c) aspects. The F-zone is either Tundra (FT) or ice climate (FT). This then yields 15 classes in total. Starting from the monthly mean values, several factors are defined (Table 6.3). Here, the period from April to September is regarded as Northern Hemisphere summer (Southern Hemisphere winter) and from October to March as the Northern Hemisphere winter (Southern Hemisphere summer). When defining the Koeppen classes, temperature is taken in °C and precipitation in cm per month. Together with a dryness threshold, such as

$$P_t = 2 \times (30 \times \frac{P_s}{P_y} + T_{mean} - 10) \tag{6.1}$$

and a monsoon threshold

$$P_m = 2.5 \times (100 - 10 \times P_{min}) \tag{6.2}$$

the climate classes and their respective thresholds are obtained. The original version of the Koeppen climate classification by *Köppen* (1936) has been used with various modifications or different interpretations so far. As there is no general agreement on the classes themselves, the classification is explained in detail in the Tables 6.1, 6.2 and 6.3. The biomes, which can be allocated to these classes, can be also found in Table 6.1.

Climate	Criteria
Ar	(not B) & ($T_{min} \geq 18°C$) & ($2 \geq N_{dry}$)
As	(not B) & ($T_{min} \geq 18°C$) & ($2 < N_{dry}$) & ($P_y < P_m$) & ($N_{dry,w} < N_{dry,s}$) or [($N_{dry,w} = N_{dry,s}$) & $P_w > P_s$]
Aw	(not B) & ($T_{min} \geq 18°C$) & ($2 < N_{dry}$) & ($P_y < P_m$) & ($N_{dry,w} > N_{dry,s}$) or [($N_{dry,w} = N_{dry,s}$) & $P_w < P_s$]
Am	(not B) & ($T_{min} \geq 18°C$) & ($2 < N_{dry}$) & ($P_y \geq P_m$)
BS	($P_t/2 \leq P_y \leq P_t$)
BW	($P_t/2 > P_y$)
Cr	(not B) & ($8 \leq N_{T10}$) & ($P_{s,max} < 10 \times P_{w,min}$) & [($P_{w,max} < 3 \times P_{s,min}$) or ($P_{s,min} > 3cm$) or ($P_y \geq 89cm$)]
Cs	(not B) & ($8 \leq N_{T10}$) & ($P_{s,max} < 10 \times P_{w,min}$) & [($P_{w,max} \geq 3 \times P_{s,min}$) & ($P_{s,min} \leq 3cm$) & ($P_y < 89cm$)]
Cw	(not B) & ($8 \leq N_{T10}$) & ($P_{s,max} \geq 10 \times P_{w,min}$)
Do	(not B) & ($4 \leq N_{T10} \leq 7$) & $T_{min} \geq 0°C$)
Dc	(not B) & ($4 \leq N_{T10} \leq 7$) & $T_{min} < 0°C$)
Eo	(not B) & ($1 \leq N_{T10} \leq 3$) & $T_{min} \geq -10°C$)
Ec	(not B) & ($4 \leq N_{T10} \leq 7$) & $T_{min} < -10°C$)
FT	(not B) & ($0°C < T_{max} \leq 10°C$)
FI	(not B) & ($0°C \geq T_{max}$)

Table 6.2: Koeppen classes and its boundaries.

Variable	Unit	Meaning
P_y	cm	Total annual precipitation
P_s (P_w)	cm	Total summer (winter) precipitation
P_{max} (P_{min})	cm	Maximum (minimum) precipitation
$P_{s,max}$, $P_{s,min}$	cm	Maximum summer Minimum summer precipitation
$P_{w,max}$, $P_{w,min}$	cm	Maximum winter Minimum winter precipitation
T_{mean}	°C	Mean temperature
T_{max} (T_{min})	°C	Maximum (minimum) temperature
N_{dry}		Number of months with less than 6 cm precipitation
$N_{dry,s}$		Number of summer months with less than 6 cm precipitation
$N_{dry,w}$		Number of winter months with less than 6 cm precipitation
N_{T10}		Number of months with at least 10°C temperature
P_t (P_m)	cm	Dryness (monsoon) threshold

Table 6.3: Meaning of the Koeppen variables.

6.3.2 Budyko-Lettau dryness index

The second classification which is used is the Budyko-Lettau dryness ratio (*Budyko* 1958, 1974; *Lettau* 1969). As *Budyko* (1974) reveals, the most important meteorological factors affecting the development of plants are the thermal and the radiation regime as well as the conditions of moisture. The dryness ratio (D = net radiation/precipitation) thus characterizes the continental surface climates combining long-term mean surface energy fluxes to a dimensionless parameter (precipitation enters in terms of its latent energy equivalent). According to this, different zones can be identified on the basis of their hydrological conditions, and energy limited ($D < 1$) can be discerned from water limited ($D > 1$) regimes (*Budyko* 1958, 1974; *Lettau* 1969), with D = 1 serving as a threshold separating both regimes on a global scale. At the same time, the dryness ratio can be applied to the climate-vegetation relation, defining biome types with respect to the dryness ratio, so that five main climate classes are distinguished: Tundra ($0 < D < 0.3$), humid savanna to forest ($0.3 < D < 1$), savanna and steppe ($1 < D < 2$), semi-desert ($2 < D < 3$), desert ($D > 3$). Interpreting these classes with regard to the limits mentioned before, it turns out that tundra and forests are energy limited due to the lower available energy compared to the water supply. In contrast, the other three classes, savanna and steppe, semi-desert and desert, are water-limited climates, as the available energy clearly exceeds the water supply.

Previous applications

Several studies are existing using the Budyko ratio. In a similar way as it will be done further below, *Monserud et al.* (1993) used the Budyko ratio to identify global vegetation patterns, mainly with regard to a global warming scenario. In a slightly different version, the Budyko hypothesis is used by, for example, *Donohue et al.* (2007), *Hanasaki et al.* (2008) or *Istanbulluoglu et al.* (2012) to analyze local/global water and energy balances through the respective patterns of evaporation and run-off.

6.3.3 CARAIB

In this section, the vegetation model CARAIB (CARbon Assimilation In the Biosphere) is described, including its different modules, as well as the climatic inputs required to perform simulations. CARAIB is a dynamic global vegetation model which has been developed at the Laboratory for Planetary and Atmospheric Physics (LPAP) and Unité de Modélisation du Climat et des Cycles Biogéochimiques (UMCCB) of the University of Liège. In its very original version it was designed to study the carbon cycle in the terrestrial biosphere and the role of land ecosystems for the atmospheric CO_2 sequestration. Since the first version of *Warnant et al.* (1994), the model has undergone various adaptations, mainly with regard to improved parameterizations or the implementation of new modules, and has been used in a variety of applications. These are, for example, aiming at analyzing the role of vegetation in the global carbon cycle or at the reconstruction of the vegetation distribution for present-day conditions (*Warnant et al.* 1994; *Nemry et al.* 1996; *Laurent et al.* 2008). The model has also been used for the investigation of the palaeovegetation during the Miocene (*François et al.* 2006; *Henrot et al.* 2010) or the Last Glacial Maximum (*François et al.* 1998, 1999; *Otto et al.* 2002; *Galy et al.* 2008; *Henrot et al.* 2009).

Model description, input data and coupling procedure

In its current version, CARAIB composes of five modules for (i) the hydrological budget, (ii) the canopy photosynthesis and the stomatal regulation, (iii) the carbon allocation and the plant growth, (iv) the heterotrophic respiration and litter/soil dynamics , and (v) the plant competition and biogeography. This

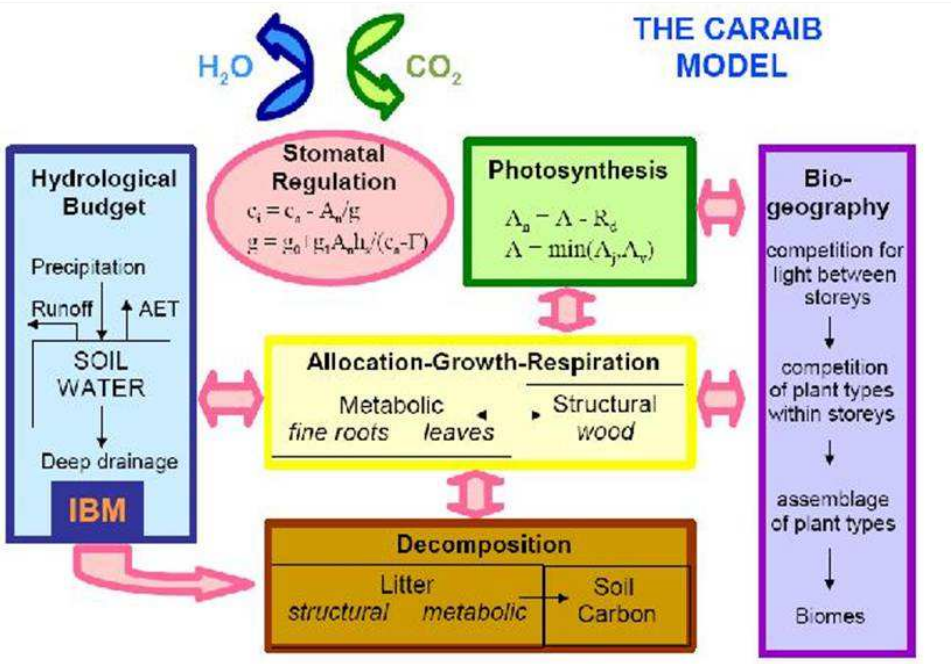

Figure 6.1: Components of the CARAIB model; schematic provided by A.-J. Henrot.

is illustrated in Figure 6.1. In general, the model makes use of a set of herbaceous and tree PFTs which can coexist on the same grid cell. Plants are classified to PFTs according to specific properties, such as their individual plant physiology (e.g. plant size as well as the size and shape of the leaves) or taxonomic features. Different time steps are used in the model for the diverse components corresponding to their respective time scales: The contents of the slower water and carbon reservoirs are updated once per day, whereas the processes of photosynthesis and plant respiration are calculated every two hours to consider nonlinear effects of their fluxes associated with the diurnal cycle (*Henrot* 2010). Finally, the vegetation cover for grasses is updated once per month, whereas for trees, it is recalculated only once per year, as trees are growing much more slowly. Spatially, CARAIB is a grid-point model and can be used at different spatial resolutions (global or regional scale), as will be shown later. Especially for the regional-scale setups, special PFTs and Bioclimatic Affinity Groups (BAG) can be implemented in the model (*Otto et al.* 2002; *Laurent et al.* 2004). In the following, the most important aspects of the five modules are shortly described. A more detailed overview can be found in *Henrot* (2010).

(i) Hydrological module The hydrological module, called Improved Bucket Model (IBM), calculates the hydrological quantities in the soil, such as the water content, the snow amount and the associated fluxes (*Hubert et al.* 1998). The soil water budget is derived from the balance between precipitation and snow melt as the input quantities, and evapotranspiration, drainage and surface runoff as the output fluxes.

(ii) Canopy photosynthesis and stomatal regulation The calculation of photosynthesis is performed separately for all model PFTs, using two different parameterizations for C_3- (*Farquhar et al.* 1980) and C_4-plants (*Collatz et al.* 1992). C_3-plants are the globally dominating type of plant species. They flourish in cool, wet and cloudy climates, whereas the C_4-plants are better adapted to hot and dry environments. This classification in C_3- and C_4-plants mainly reflects different photosynthesis pathways. The stomatal conductance is parameterized according to *Ball et al.* (1987), with a modification by *van Wijk et al.* (2000) to account for soil water dependence. Both the photosynthetic rates and the stomatal conductance are evaluated in a series of 16 layers in total throughout the canopy.

(iii) Carbon allocation and plant growth The photosynthetic products are allocated to two carbon reservoirs, which correspond to metabolic and structural tissues, i.e. leaves/fine roots and wood/coarse roots respectively. The partitioning between these two pools is specific for each PFT and depends on the environmental conditions (*Otto et al.* 2002). The output fluxes are autotrophic respiration and litter production. Whereas respiration can be further subdivided into maintenance and growth respiration, depending on the carbon content in the pool, litter is produced by the mortality of metabolic and structural tissues - thus leaf fall or the death of plants as a consequence of both natural regeneration of the canopy or of unfavorable climatic conditions (*Otto et al.* 2002).

(iv) Heterotrophic respiration and plant growth This module calculates the budget of three carbon reservoirs of dead organic matter: the previously mentioned metabolic and structural litter as well as soil carbon. Heterotrophic respiration is the output of these reservoirs. As a function of temperature and soil moisture, it is proportional to the carbon content of the reservoir (*Nemry et al.* 1996; *Warnant* 1999; *François et al.* 2006).

(v) Plant competition and biogeography As mentioned earlier, plant species are classified into PFTs. A PFT comprises botanical species sharing mutual morphological and phenological characteristics and thus playing a similar role in the ecosystem (*Utescher et al.* 2007; *Henrot* 2010). A classification with 15 PFT is most often used in CARAIB (*Utescher et al.* 2007; *Galy et al.* 2008; *François et al.* 2011), which has been extended from an 8-class type (*François et al.* 2006). This 15-type classification comprises two types of herbs (C_3- and C_4-herbs) and 13 types for trees, mainly divided into needleleaved evergreen, needleleaved summergreen, broadleaved deciduous, broadleaved raingreen and broadleaved evergreen trees. All tree types are differentiated with regard to climatic thresholds. A list of the 15 PFTs is given in the upper panel of Table 6.4. For an overview of the respective species of each individual PFT, it is referred to *Henrot* (2010). For this study, a very recently developed classification with 26 PFTs (*Favre et al.* 2010) is used. This 26-type classification includes three types of herbs, eight types of shrubs and 15 types of trees. For this expansion, new types were included (numbers 4 to 11) and several existing PFTs were split (for C_3-herbs, needle- and broadleaved evergreen mediterranean trees) - details are summarized in Table 6.5. Recent studies using this expanded classification (*Jimenez-Moreno* 2006; *Jimenez-Moreno et al.* 2008; *Henrot* 2010) have yielded improved results for Europe in comparison to pollen analysis; therefore, the usage of this classification for the studies on Europe is indeed reasonable.

The biogeography in CARAIB is described in a fully interactive way with the carbon cycle part. Both photosynthesis and the carbon fluxes are calculated for each PFT. This module thus evaluates the steady state distribution of all tree and herbal-type PFTs on each grid cell. The share of the area in a storey between different PFTs, i.e. the cover fraction, is determined according to the respective NPPs of the relevant PFTs. In general, the model canopy is divided into an over- and an understorey corresponding to

Number$_{PFT}$	PFT
1.	C_3-herbs
2.	C_4-herbs
3.	Needleleaved evergreen boreal/temperate cold
4.	Needleleaved evergreen temperate cool
5.	Needleleaved evergreen temperate dry warm (mediterranean)
6.	Needleleaved evergreen temperate perhumid warm (subtropical)
7.	Needleleaved summergreen boreal/temperate cold
8.	Needleleaved summergreen temperate warm (subtropical swamp)
9.	Needleleaved evergreen temperate dry warm (mediterranean)
10.	Broadleaved evergreen temperate perhumid warm (subtropical)
11.	Broadleaved summergreen boreal/temperate cold
12.	Broadleaved summergreen temperate cool
13.	Broadleaved summergreen temperate warm
14.	Broadleaved raingreen tropical
15.	Broadleaved evergreen tropical

Number$_{Biome}$	Biomes
1.	Ice/Polar Desert
2.	Desert
3.	Semi-desert
4.	Tundra
5.	Tropical grassland
6.	Temperate grassland
7.	Tropical savanna
8.	Warm temperate open woodland
9.	Cold temperate/boreal open woodland
10.	Tropical rainforest
11.	Tropical seasonal forest
12.	Subtropical forest
13.	Warm temperate broadleaved evergreen forest
14.	Warm temperate conifer forest
15.	Warm temperate mixed forest
16.	Temperate broadleaved deciduous forest
17.	Cool temperate conifer forest
18.	Cool temperate mixed forest
19.	Boreal/montane forest

Table 6.4: Overview of the CARAIB PFTs for the 15 PFT-classification (upper panel) and for the assignment to 19 biomes (lower panel).

Number$_{15PFT}$	15 PFT-classification	Number$_{26PFT}$	26 PFT-classification
1.	C_3-herbs	1.	C_3-herbs (humid)
		2.	C_3-herbs (dry)
		4.	Broadleaved summergreen arctic shrubs
		5.	Broadleaved summergreen boreal/ temperate cold shrubs
		6.	Broadleaved summergreen temperate warm shrubs
		7.	Broadleaved evergreen boreal/ temperate cold shrubs
		8.	Broadleaved evergreen temperate warm shrubs
		9.	Broadleaved evergreen xeric shrubs
		10.	Subdesertic shrubs
		11.	Tropical shrubs
5.	Needleleaved evergreen mediterranean	14.	Needleleaved evergreen supra-mediterranean
		15.	Needleleaved evergreen meso-mediterranean
9.	Broadleaved evergreen mediterranean	19.	Broadleaved evergreen meso-mediterranean
		20.	Broadleaved evergreen thermo-mediterranean

Table 6.5: Modifications for the 26 PFT-classification.

trees and grasses respectively. The module thus predicts PFT assemblages for each pixel. In an off-line scheme, the PFT assemblages are then converted into biomes (19 in total) to visualize the simulation results (see Table 6.4 lower panel and Figure 6.2 as an example). This conversion depends on several (mostly vegetation-related) criteria, which are calculated by the model, such as, for example, the dominant PFT and its cover fraction, the NPP and the leaf area index (LAI). For a more detailed description of this simplified biome description scheme, it is referred to *Henrot* (2010) and *François et al.* (2011). Warm deserts evolve from areas where the NPP of all PFTs is equal to zero. The ice/polar desert is not related to vegetation parameters but to the climatological quantity GDD5, i.e. a temperature threshold of 5°C. In general, the classification into biomes is based on plant physiology rather than on empirical climate-vegetation relationships (*Henrot* 2010). This is very similar to the remarks in Section 6.3.1 on the BIOME model by *Prentice et al.* (1992). The advantage is that the assemblages for both PFT and the biomes can be calculated even for climatic and environmental conditions which do not have present-day analogues. However, the PFT-classification is based on present-day vegetation and its characteristics. To reconstruct past vegetation, it is assumed that plants were close to modern plants in terms of physiology and metabolism, following the approach by *Mosbrugger and Utescher* (1997). This is thus in line with the remarks in Section 5.3 as essential prerequisites for the diverse kinds of palaeoclimatic

reconstructions.

CARAIB inputs: climatic forcings To determine vegetation distributions, CARAIB needs climatic input fields, which can either be taken from a meteorological database, i.e. observations or reanalysis data, or can be the output from a climate model. The required variables are: daily mean surface air temperature, diurnal amplitude of air temperature variation (difference between maximum and minimum daily air temperature), precipitation, sunshine hours per day (fraction), relative humidity and wind speed. These climatic inputs must be provided at a daily frequency. However, climatic data can also be provided as climatological monthly means, as it is sometimes the case for GCMs or other climatologies (*New et al.* 2002). CARAIB then uses a stochastic generator (*Hubert et al.* 1998) to transform the monthly means into the required daily values. As a further input variable, CARAIB needs the soil texture (percentages of silt, sand and clay) which is used in the hydrological module. Concerning the input fields, a special feature has to be mentioned. For using CARAIB, the results from the GCMs are not used directly. Instead, the anomaly method is used, which is described in detail in *François et al.* (1999) or *Otto et al.* (2002). In this context, only the most important points are mentioned. The anomalies, which are used as direct input fields, are calculated between the respective period of interest in the past and present-day and are then added to a reference climatology (*Leemans and Cramer* 1991; *New et al.* 2002), which can be expressed as

$$D = \Delta D + D_{obs}, \tag{6.3}$$

where D denotes any climatic input field, ΔD is the anomaly between the respective simulation and a present-day control run and D_{obs} denotes the present-day climatological fields. These climatologies can also be used to derive the inputs for present-day climate (*Henrot* 2010). The use of anomalies is preferred to avoid systematic errors in the vegetation distribution linked to climate model errors. This implies that the relative changes calculated by the climate model are assumed to be more reliable than the absolute results (*François et al.* 2006). Moreover, further assumptions are made related to the calculation of the anomalies and it is referred to the previously mentioned studies for further details.

For all studies with CARAIB, the climatology by *New et al.* (2002) has been used. It provides global monthly mean climate data for the period 1961-1990 in a spatial resolution of 10'; this climatology also belongs to the observational data set CRU which has been used in Chapter 3. These climatic fields have been interpolated from station means. The climatology has already been used in previous studies with CARAIB (*Otto et al.* 2002; *François et al.* 2006; *Henrot et al.* 2010) and is also used in this context together with the PlaSim data.

In Figure 6.2 a, the present-day biome distribution at a 0.5° by 0.5° resolution is presented, obtained from an equilibrium simulation with CARAIB forced with the reference climatology by *New et al.* (2002) and a preindustrial CO_2 concentration of 280 ppmv. It is important to mention that this vegetation distribution, as well as all others which will be shown below, represent the potential vegetation in equilibrium with climate. Urban zones or human land-use are not considered. Moreover, Antarctica is not included in the climatologies.

In general (*Henrot* 2010), the CARAIB biome distributions are in good agreement with published potential vegetation maps from, for example, *Melillo et al.* (1993) and *Crowley and Baum* (1997). Moreover, the distribution is consistent with other distributions derived from satellite observations (*Woodward et al.* 2004) and from pollen samples of the Palaeovegetation Mapping Project (*Prentice et al.* 1996). Comparable to the classification in Koeppen, the allocation to the respective biome types is neither unique nor generally defined. Thus, differences in the biome distributions may be attributed to differ-

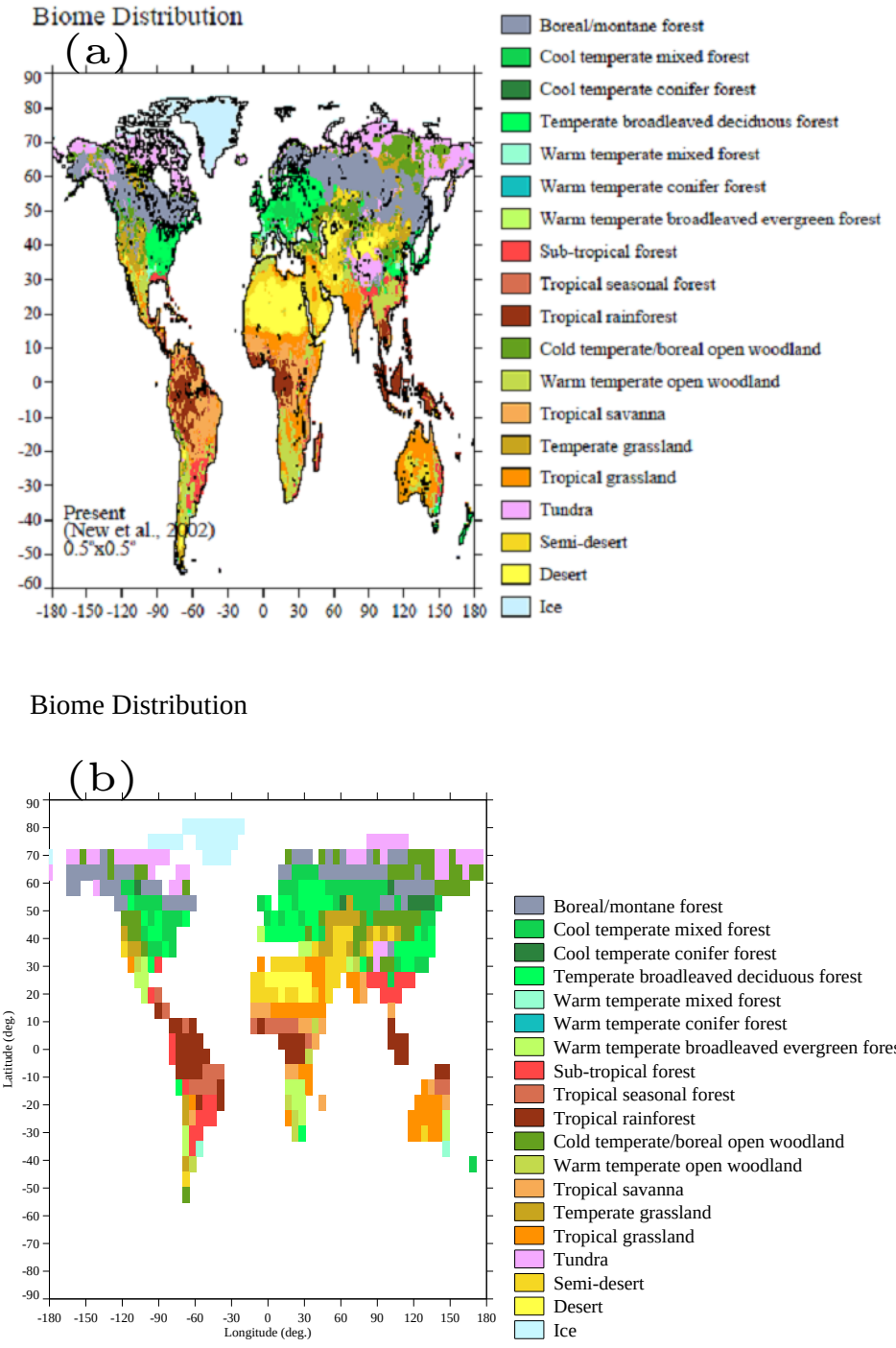

Figure 6.2: CARAIB global biome distributions for present-day using 15 PFT, obtained from: (a) a simulation with the reference climatology by *New et al.* (2002), taken from (*Henrot* 2010), (b) a simulation with PlaSim input data which has been modified in advance with the reference climatology according to the anomaly method.

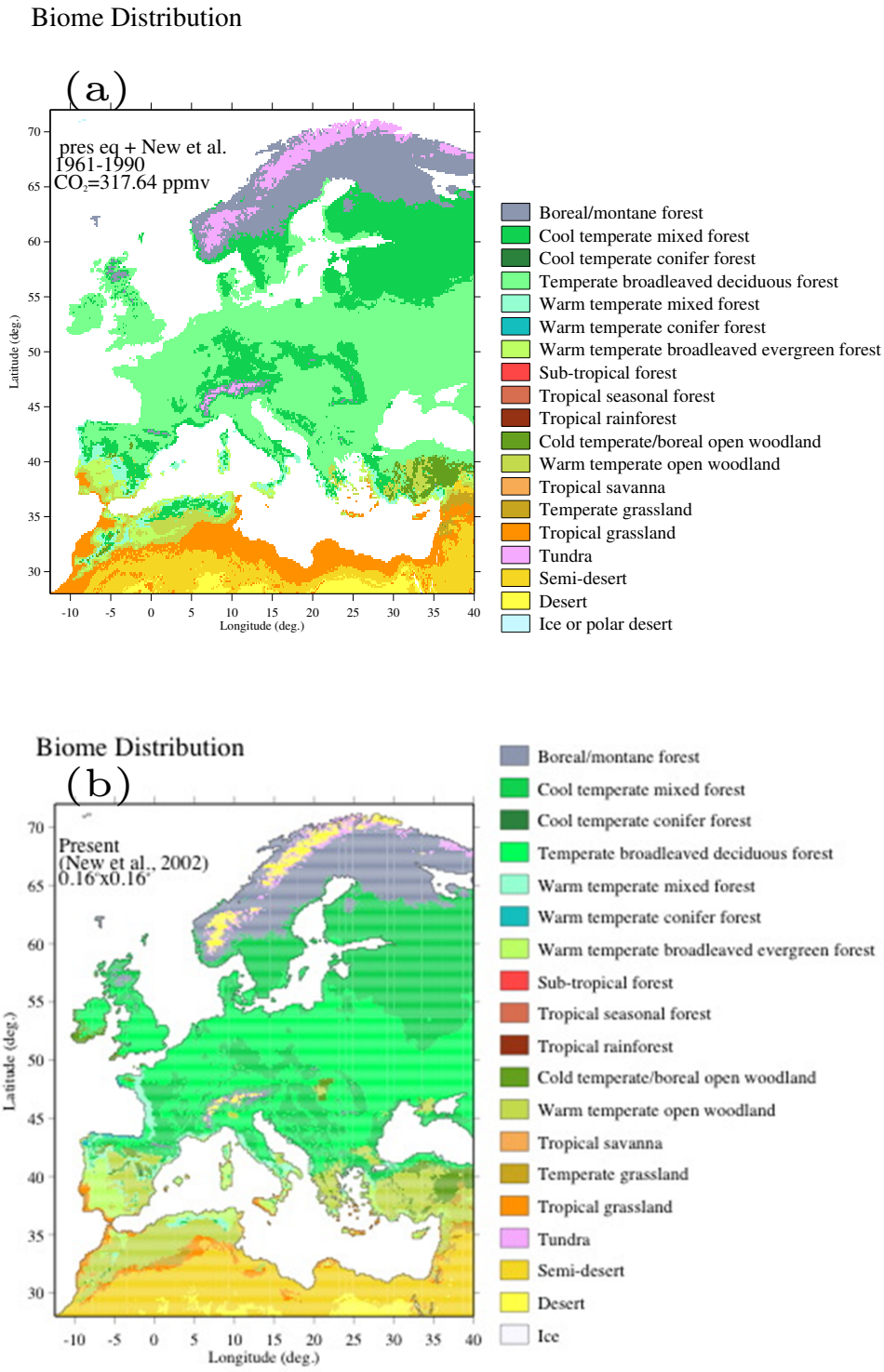

Figure 6.3: CARAIB European biome distributions for present-day using 26 BAG, obtained from: (a) a simulation with the modified PlaSim input data, (b) a simulation with the reference climatology by *New et al.* (2002), provided by L. M. François.

ent biome classifications and different resolutions used in the studies mentioned before (*Henrot* 2010). Nevertheless, the general patterns for tundra and boreal forests at high northern latitudes, as well as the deserts and semi-deserts and the tropical rainforests are correctly predicted by CARAIB.

In Figure 6.2 b, the corresponding vegetation distribution, now obtained from an equilibrium simulation with CARAIB forced with PlaSim input data is presented. Although the very fine structure of the climatology cannot be resolved by the model, the different biome types can be clearly constituted and the general pattern is captured by PlaSim. Similar to the climatology, the high northern latitudes are covered by tundra types, sometimes pervaded by woodland types. Over large parts of North America and mainly Asia, the boreal/montane forest is less pronounced in PlaSim - instead the more temperate types are more extended. The same is the case with the warmer types in the tropics, mainly desert but also the tropical rainforest and subtropical forest. Whereas the latter are both more extended in PlaSim over the northern parts of South America and Asia respectively, the desert and semi-desert types are less extended over North Africa, Arabia and also Australia. Part of the differences can be clearly attributed to the lower resolution of the model compared to the climatology. To gain a more specific insight into the region of interest, i.e. Europe, these global biome distributions are of limited suitability, even that of the reference climatology. However, with CARAIB, it is possible to use a setup for a very high-resolution simulation for certain regions of the world, i.e. Europe, China or Eurasia. The climatic anomalies derived from the PlaSim input data are thereby interpolated to this high spatial resolution, which is 10' $\times$ 10' or $\approx 0.16^\circ \times 0.16^\circ$ for Europe. Moreover, for each of these setups, the plant classification is adapted for an optimal representation of the regional vegetation. Compared to global plant classifications, the adapted one is more refined and specifically developed for the prevailing regional vegetation types (*François et al.* 2011). For Europe, a classification of 26 BAGs is used which has been developed by *Laurent et al.* (2004) and applied in *Laurent et al.* (2008) and *François et al.* (2011).

In Figure 6.3, the high-resolution European vegetation distribution is presented for present-day conditions. Again, the modified PlaSim input is used for the simulation with CARAIB (Fig. 6.3 a) and the reference climatology alone in Figure 6.3 b. Although slightly different colors are used in both distributions, certain differences are evident. Forest types are less pronounced in northeastern Europe in PlaSim. Over large parts of western and eastern Europe the pattern is rather uniform in PlaSim with dominating temperate deciduous forest types, except over central Europe and north of the Alps, where colder types occur. Mainly in France the pattern is much more variable in the reference climatology, where also warm temperate types occur (western parts of France). The more southern parts of Europe (Spain) and the northern parts of Africa and Turkey yield wetter types and also forest with the PlaSim climate data, whereas grassland, woodland or semi-desert types prevail with the reference climatology.

Coupling procedure So far, CARAIB is used in a simple diagnostic manner with PlaSim output, calculating the equilibrium biome distribution. Rather recently, in the work by *Henrot* (2010), an asynchronous coupling procedure (*Foley et al.* 1998) has been developed for PlaSim and CARAIB. As CARAIB is not used in this way in this study, only the main points are quickly summarized to provide a complete overview about the available applications of CARAIB. Asynchronous coupling is characterized as an iterative procedure where the (long-term mean) output from an equilibrium climate simulation is used to force the vegetation model to an equilibrium distribution of vegetation types. These in turn are then fed back into the climate model in terms of their respective parameters such as e.g. albedo and roughness length. This iterating cycle of equilibrium simulations with both the climate and the vegetation model is repeated until the results of both models converge to a steady state, where no significant trend between successive simulations can be observed in the climatic variables as well as in the global and local land surface parameters (*Foley et al.* 1998; *Henrot* 2010). This procedure is very well illustrated in both stud-

ies. So far, this coupling procedure has been applied in several studies on different geological periods and also with various climate and vegetation models (*Claussen* 1994, 1998; *de Noblet et al.* 1996; *Betts et al.* 1997; *de Noblet-Ducoudré et al.* 2000). In these studies the asynchronous coupling procedure has proven its usefulness to study climate-vegetation interaction and to emphasize the impact of a changing vegetation cover on climate and thus its necessity to be considered in climate models. However, as *Foley et al.* (2000) point out, this coupling also has some limitations. As mentioned above, during the coupling one iterates between subsequent states of equilibrium, both in climate and vegetation. Thus, neither transient changes in climate and vegetation can be analyzed nor any response of the vegetation to climate variability (*Henrot* 2010). For these reasons an interactive vegetation module as SimBA or others should be preferred to an asynchronously coupled model. Moreover, both climate and vegetation models may be physically not completely consistent. It could be that the vegetation model and the land surface scheme of the climate model are physically not completely consistent due to different parameterizations. This is actually the case for PlaSim and CARAIB (*Henrot* 2010): both models use different treatments of the surface radiation and the water budget. To provide a consistent linkage between atmosphere and biosphere, CARAIB should be fully incorporated into PlaSim, replacing the terrestrial component - however, it has not been possible to implement this until now (*Henrot* 2010).

6.4 Experiments

(a) European palaeovegetation

For the analysis of the European palaeovegetation, the fully coupled PlaSim as well as the vegetation model CARAIB are used. For the later calculation of the GDD evolution with *PlaSim*, output from the transient simulation presented in Chapter 4 is used, thus coupled to SimBA. As input data for *CARAIB*, output from a transient Holocene simulation with PlaSim, coupled to the LSG ocean, is used. Thus, this simulation is different in terms of the non-inclusion of the vegetation module SimBA. For SimBA, CARAIB is used instead. The PlaSim output is postprocessed as described in Section 6.3.3. From each 1000 yr time slice, a mean over the first 200 years, i.e. 9,999 to 9,800 yr BP, is used for each required variable to force an equilibrium simulation with CARAIB.

(b) Climate-vegetation interaction

For all these studies, PlaSim is used in the same configuration as in Chapter 3, regarding, for example, the model resolution and the prescription of both AMIP-SST and sea ice. Albeit, a more recent model version of PlaSim is used. Moreover, atmospheric CO_2 is set to 360 ppmv (if not stated otherwise) and the orbital parameters correspond to present-day conditions and are kept unchanged. The existence of vegetation is prescribed by four parameters in the land surface scheme (cf. Chapt. 2), which are the surface background albedo, the roughness length, the maximum water storage of the soil (bucket size) and the fraction of available soilwater, i.e. the ratio of actual and potential evapotranspiration. This study is based on the previous work by *Fraedrich et al.* (1999, 2005b) and *Kleidon et al.* (2000), who investigated the effects of vegetation extremes on the Earth's climate and the general circulation, either with the Hamburg climate model ECHAM4 (*Roeckner et al.* 1996) or with PlaSim alone or in combination with the Koeppen classification. In the experiments, the previously mentioned land surface parameters remain unchanged for a present-day control simulation of 100 years but are modified for all land points (except glaciers) according to *Fraedrich et al.* (2005b) for the specific setup of a "green planet" and a "desert world". Both the Koeppen climatology and the Budyko ratio are then applied

diagnostically to the control simulation as well as to the two scenarios. Although they are far away from being realistic, these setups are useful for studying the basics of the climate-vegetation-feedback, i.e. to estimate the effects of human-induced land cover changes, as it makes no difference whether these changes have a natural or anthropogenic origin. Similar setups of extreme boundary conditions have been used in various studies before (*Otterman et al.* 1984; *Claussen* 1994, 1997, 1998; *Kleidon et al.* 2000; *Brovkin et al.* 2009). The three simulations are then repeated under global warming conditions with a CO_2 concentration of 720 ppmv (i.e. 2×360 ppmv) to find out to what extent climate zones shift in a warmer climate, showing at the same time the sensitivity of both classifications to climate changes.

6.5 Results

6.5.1 European palaeovegetation (a)

As mentioned at the very beginning of this chapter, the intention of this part is to analyze the European vegetation evolution during the Holocene in terms of vegetation-related parameters and biome maps. The results are compared with results from other model studies and also with proxy-based reconstructions. The aim is clearly to discover general patterns throughout the whole Holocene. Therefore, both the fully coupled PlaSim and CARAIB are used for these analyses to yield a wide overview about the vegetation evolution and to use both models in the best feasible manner. It is explicitly underlined that no intercomparison between both models is made. The reason is the different usage in terms of the coupling procedure. SimBA is used interactively (synchronously) with PlaSim but with the version of CARAIB used here, neither an interactive simulation nor an asynchronous coupling is possible. The model can therefore only be used diagnostically (cf. Sect. 6.3.3) without any feedback on climate. Therefore, PlaSim-SimBA is used to obtain transient results and PlaSim-CARAIB to calculate biome maps at a very high resolution to make assumptions about the vegetation evolution. The intention is not to make any investigations on the differences resulting from the different coupling procedures.

Before analyzing the evolution of GDD over the Holocene, some general remarks about the parameter GDD are made. This includes the presentation of the present-day distribution of GDD0 and GDD5 in Figure 6.4, calculated with PlaSim-CARAIB. As this parameter illustrates the length of the growing season, the resulting pattern is as expected. A relatively strong gradient can be observed between regions where the climatic conditions, i.e. the temperature, enable a prolonged or a reduced growing period. There is thus a gradient from the southwestern to the northern parts of Europe. The high GDD values, i.e. a long growing season, are observed in desert regions where high temperatures prevail throughout the year. This yields desert types and thus a very sparse vegetation. Opposite to the very long growing season in the southern parts of Europe and North Africa, it is strongly reduced in the mountainous and cold regions at the high northern latitudes. The prevailing vegetation in those regions are tundra and forest types, clearly having a restricted growing period over the year, which is caused by lower temperatures. When now intercomparing GDD0 (Fig. 6.4 a) and GDD5 (Figure 6.4 b), the variations between both are striking. The growing season referred to the 0°C-threshold is characterized by constantly higher values and the regions with lower values of GDD0, i.e. below 2000 days, are clearly restricted to the Alps and the high northern latitudes (mainly Scandinavia). Moreover, the differences between GDD0 and GDD5 are most pronounced in the zone between 45°-55°N with values of more than 1000 days. Consequently, the parameter GDD is a good measure of how temperature is influencing vegetation. Changing temperatures are leading to variations in the lengths of the growing seasons and assumably to changes and shifts in the vegetation cover and vegetation types. Besides this, it may be shortly commented that temperature

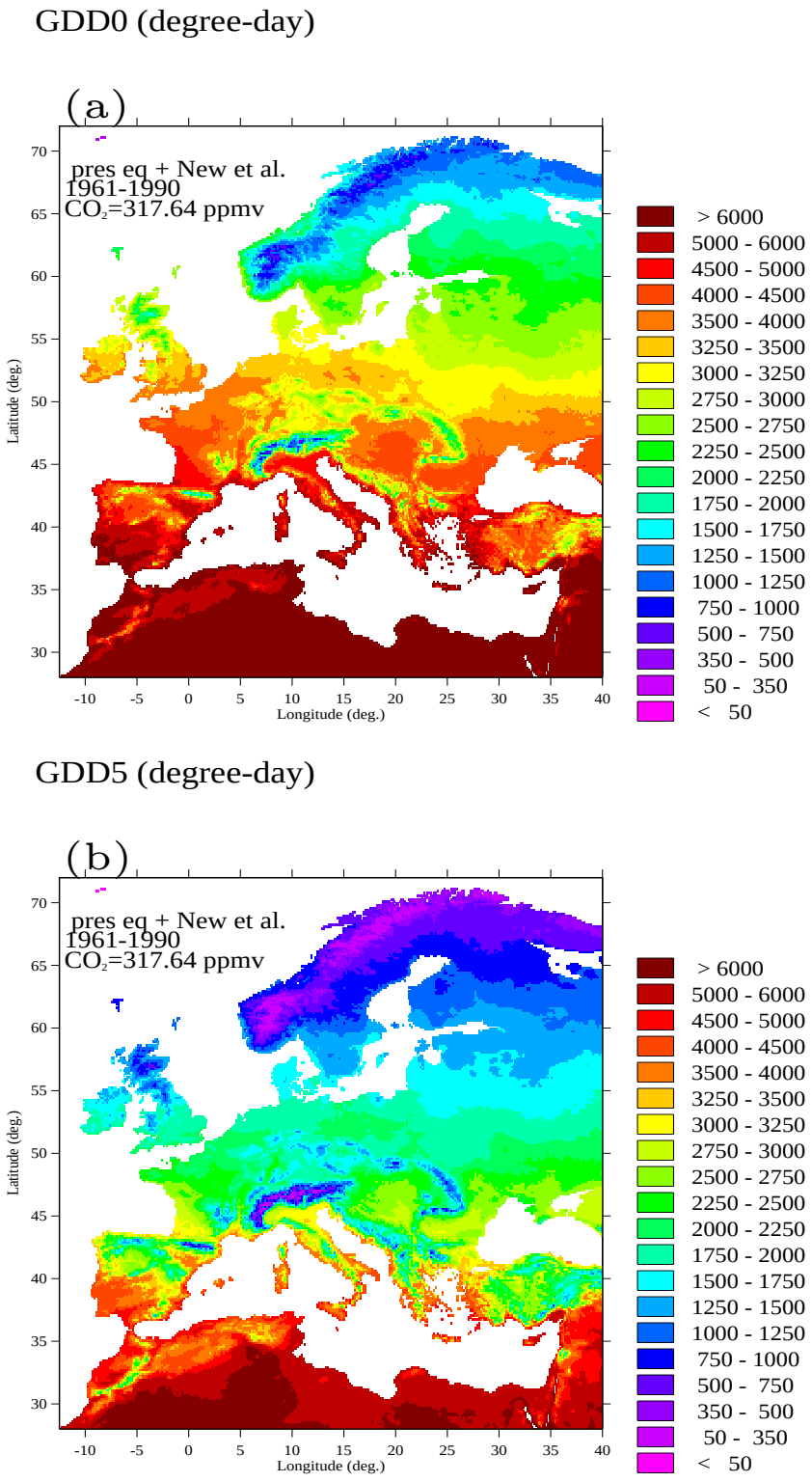

Figure 6.4: Present-day distribution of GDD0 (a) and GDD5 (b) calculated with PlaSim-CARAIB.

is of course not the only impact factor for vegetation (cf. Sect. 6.3.1), it is rather an interplay with other quantities, such as NPP and the conditions of moisture (precipitation, soil water availability).

After these more general remarks on the characteristics about the GDD, the evolution over the Holocene is analyzed. To enable a comparison with the results of other modelling studies, it is confined on the parameter GDD5 here. This is also one of the most distinctive parameters in the PFT and biome classification in CARAIB, which has been mentioned earlier. Thus, besides other characteristic quantities, every PFT and biome type has its own threshold of GDD5.

The Holocene evolution of GDD5 is presented in Figures 6.5 and 6.6. This representation, obtained with using CARAIB at the very high resolution, is rather unique and unprecedented - not only for GDD5 but also, and more decisive, for the biome distribution which is presented below. Although these results are not based on transient data, the full Holocene is covered with the long-term means of each time slice. The time slices for GDD5 and the later biome distributions are again presented reversely to be consistent to the climate reconstructions of the preceding sections. In this context, one short comment is made regarding the representation of the early Holocene. The 10k-time slice is not shown due to the missing land ice in PlaSim. The climate is slightly too warm, leading to an unrealistic GDD pattern. Moreover, changes between individual time slices are not discussed, as the differences may be very small. Instead, rather general and more striking variations over the whole Holocene are addressed.

Taking the time slices 9k, 6k and 0k as representatives for the early, mid- and late Holocene, some larger changes can be observed. Considering at first the high northern latitudes, a decrease in GDD5 can be constituted from the early to the late Holocene, i.e. the regions with very low GDD5 (less than 50 days) are growing compared to the 9k-time slice. The same trend can be observed in the eastern parts of Europe, between 55° and 60°N. Especially in the northern parts of Europe, this GDD5-trend is caused by the positive temperature anomaly during summer observed in those regions (Fig. 4.1 a, c) and which is induced by the enhanced summer insolation in the early Holocene. This decreasing pattern is also found in Figure 6.7, where the Holocene trend in GDD0 is shown for the area north of 60°N, as a deviation from the preindustrial mean. For preindustrial, again a 200 yr mean around the preindustrial year 1860 (≙ 90 yr BP) is chosen. This trend is calculated from the fully coupled transient PlaSim simulation (Chapt. 4) and is thus in line with the spatial changes of Holocene GDD5 in the regions to the north of 60°N (Fig. 6.5 and 6.6), obtained with PlaSim-CARAIB. Moreover, this decrease is very similar to the one shown by *Renssen et al.* (2005a), obtained with the ice-ocean-vegetation model ECBilt-CLIO-VECODE, who also found a reduction of around 200 days from 9k to the preindustrial as the authors left out the very early Holocene. In general terms, this decreasing trend is equivalent to a shortening of the growing season length over the Holocene and, at high latitudes, further implies a change in forest cover in those regions; this will be addresses again below when investigating the biome patterns. A decrease in GDD5 over the Holocene also occurs over the central and southeastern parts of Europe and around the Black Sea. More considerable changes can be further observed over the southwestern parts of France and the northern parts of Italy.

An opposite trend, i.e. an increase in GDD5 over the Holocene, can be guessed over the northwestern parts of Africa. The simulation of a reduced early and mainly mid-Holocene GDD indeed implies the existence of more "high-order" vegetation types in terms of for example shrubs. This feature points at the green Sahara (*Claussen and Gayler* 1997; *Claussen et al.* 1999; *de Noblet-Ducoudré et al.* 2000; *Renssen et al.* 2003, 2006a), caused by the assumed wetter conditions over the southern European regions (Fig. 4.2 b, d). The following growth of GDD is then consistent with an expansion of desert types and thus a decrease of vegetation cover, caused by the drying trend until the preindustrial (*Claussen et al.* 1999; *Renssen et al.* 2003, 2006a).

To sum up, a more or less European-wide reduction in GDD5 is detected with PlaSim-CARAIB.

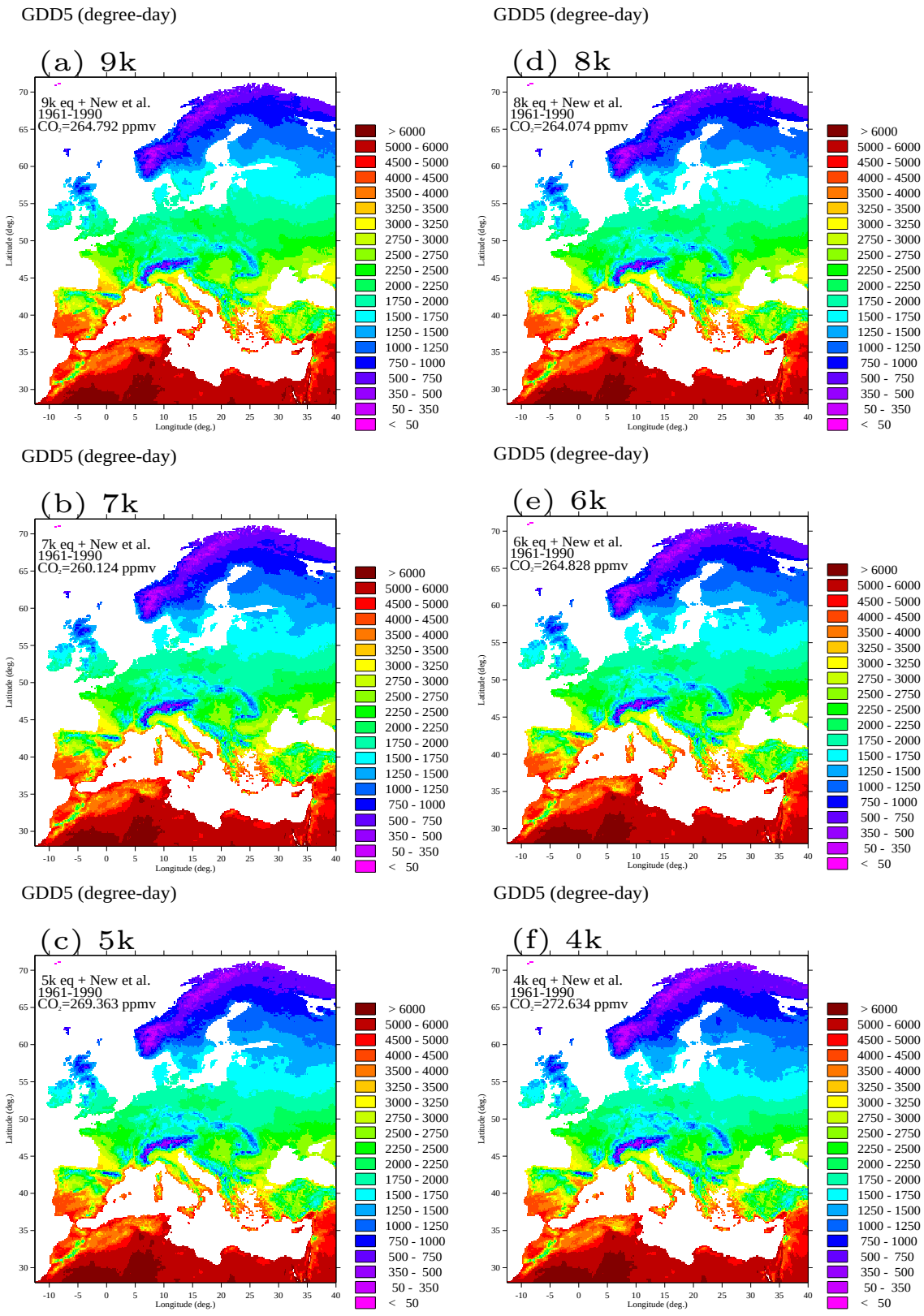

Figure 6.5: Time slice means of growing degree days (GDD5) over Europe, calculated with PlaSim-CARAIB for the time slices 9 to 4 kyr BP.

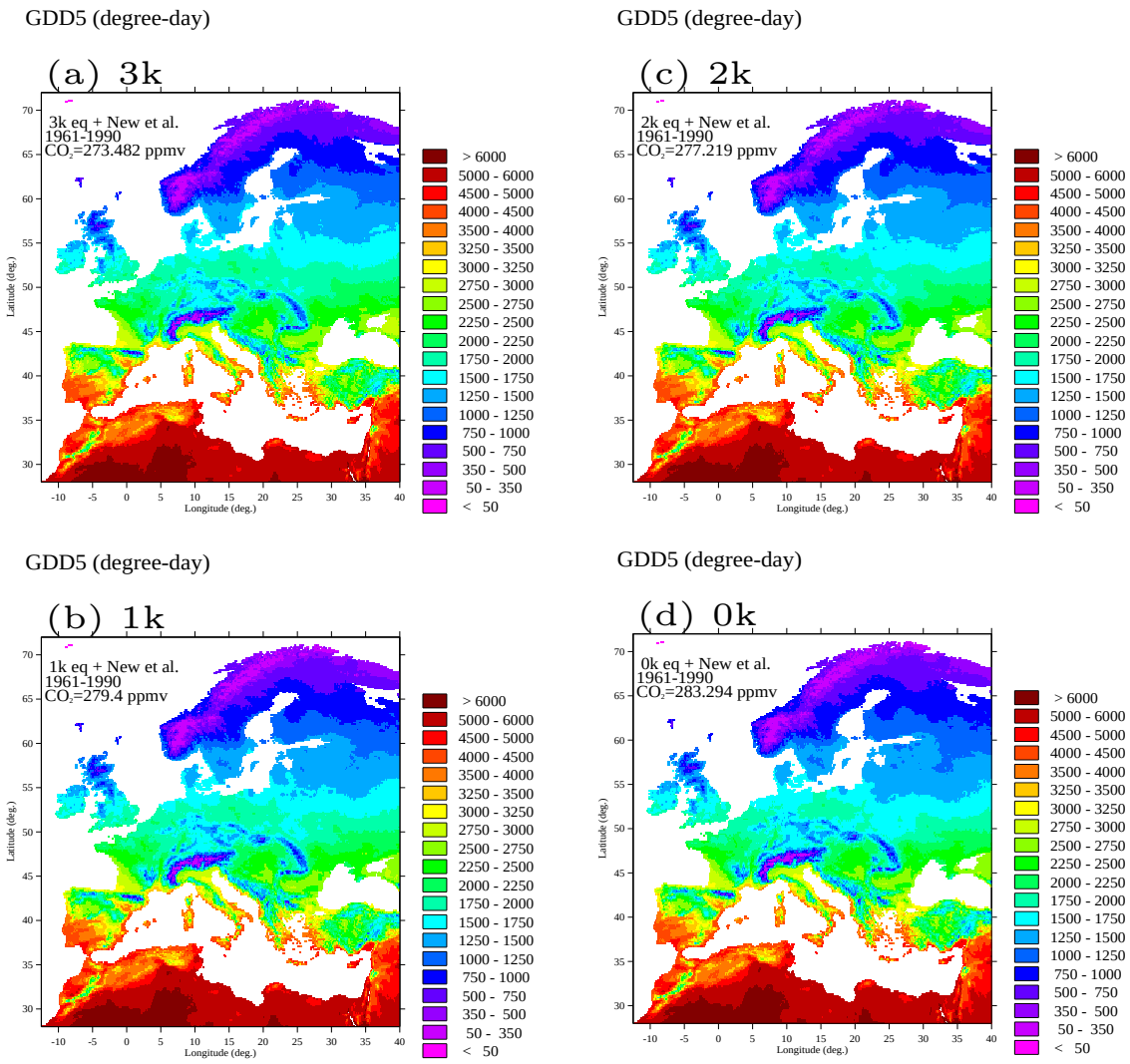

Figure 6.6: Figure 6.5 continued for the time slices 3 to 0 kyr BP.

Nevertheless, the GDD5 may be a bit overestimated at high northern latitudes due to the cooling impact of the persisting ice sheet (cf. Sect. 4.3.3), which cannot be captured by PlaSim due to the missing land ice. The GDD-results are at least partly consistent to the study by *Brewer et al.* (2007) - the author's GDD5 reconstruction on the basis of pollen data yields an alternating pattern of GDD anomalies for the mid-Holocene and the preindustrial from the southwestern to the northeastern parts of Europe: A positive anomaly occurs over western Spain, i.e. higher GDD at 6k, followed by a band of negative anomalies over eastern Spain and France. The central and northern parts of Europe, including Scandinavia and Finland, are characterized by a positive anomaly. The central eastern and southeastern parts are then again marked by a negative anomaly. Consequently, the results obtained with PlaSim-CARAIB slightly deviate from the palaeoreconstruction of *Brewer et al.* (2007), as the pattern is mostly determined by positive anomalies between the mid-Holocene and the preindustrial. Another study, which can be cited in this context is that of *Brewer et al.* (2009), where the authors intercompare simulated and observed European vegetation for the mid-Holocene. They use in total four different climate models together with CARAIB, which is thus very close to the approach here. Their model results on the GDD5 evolution

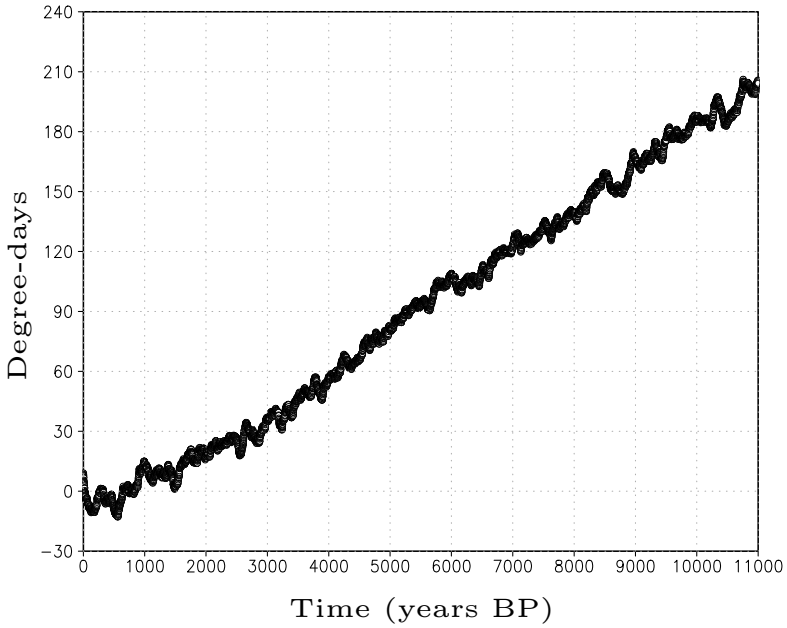

Figure 6.7: Holocene evolution of growing degree days (GDD0) as deviations from the preindustrial mean (today) for the area north of 60°N.

are very similar to the PlaSim-CARAIB outcome. Nearly all four models exhibit a positive anomaly over Europe. Only the southwestern parts of Europe (western Spain) and northern parts of Africa are characterized by a negative anomaly, i.e. an increase in GDD, which is consistent to the results here, at least over Africa. Finally, a mismatch between the cited model studies, including PlaSim-CARAIB, and the palaeoobservations (*Brewer et al.* 2007) is indeed apparent in this context. However, as *Brewer et al.* (2009) point out, a reliable data-model comparison seems to be a specific challenge if the climatic changes are rather small - which is the case during the Holocene over Europe - and thus much less pronounced as for other palaeoclimate periods, e.g. the Last Glacial Maximum.

It is now of interest, whether these changes in the growing season lengths also induce changes in the vegetation distribution. Therefore, the biome distribution for the time slices 9 to 0 kyr BP is presented in the Figures 6.8 and 6.9. The results for selected time slices at the early, mid- and late Holocene are also presented in *Haberkorn et al.* (2010a). Comparable to the analysis of the GDD evolution, again no changes in the vegetation distribution between individual time slices are discussed, as the differences may be very small. Instead, more general and more striking variations over the whole Holocene are addressed. Moreover, the 10k-time slice is again left out here due to the missing land ice problem. This may favor a deficient representation of the vegetation in terms of warmer types or still existent vegetation instead of ice.

In general, an evolution over the whole Holocene is obvious. The increased GDD5 at the early Holocene time slices which could be observed at high northern latitudes and which is induced by the positive summer insolation anomaly, goes together with a northward displacement of the treeline. This has also been detected by *Crucifix et al.* (2002) and *Renssen et al.* (2005a) in their model studies on the Holocene climate evolution, both showing a strong decrease in forest cover from 9k to the preindustrial. This northward shift of the treeline, i.e. the expansion of temperate forests and replacement of boreal forest and tundra, can be identified in the biome distribution of PlaSim-CARAIB (Fig. 6.8) for these early Holocene time slices. However, these warmer types may be slightly too well developed in PlaSim

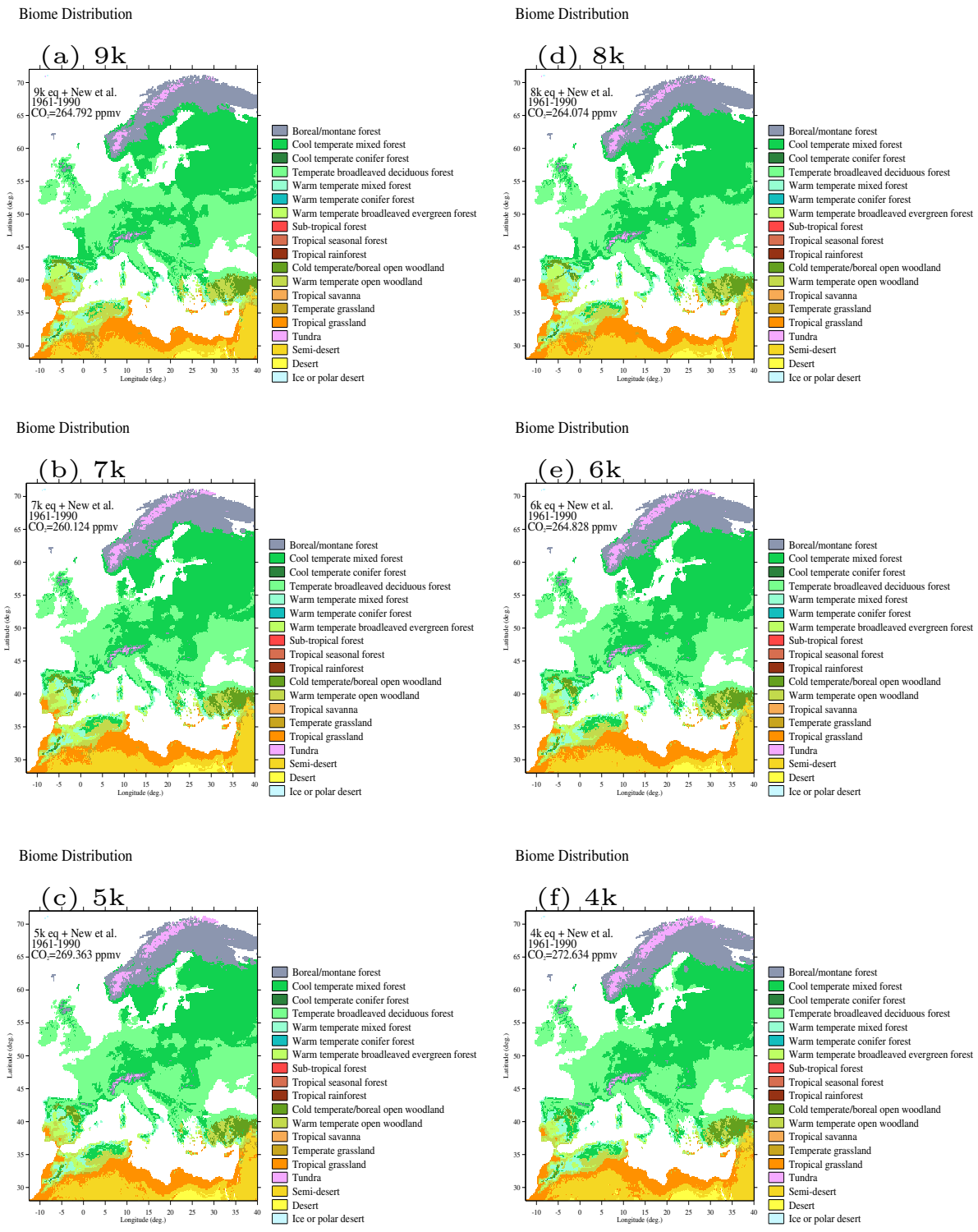

Figure 6.8: European biome distributions calculated with PlaSim-CARAIB for the time slices 9 to 4 kyr BP.

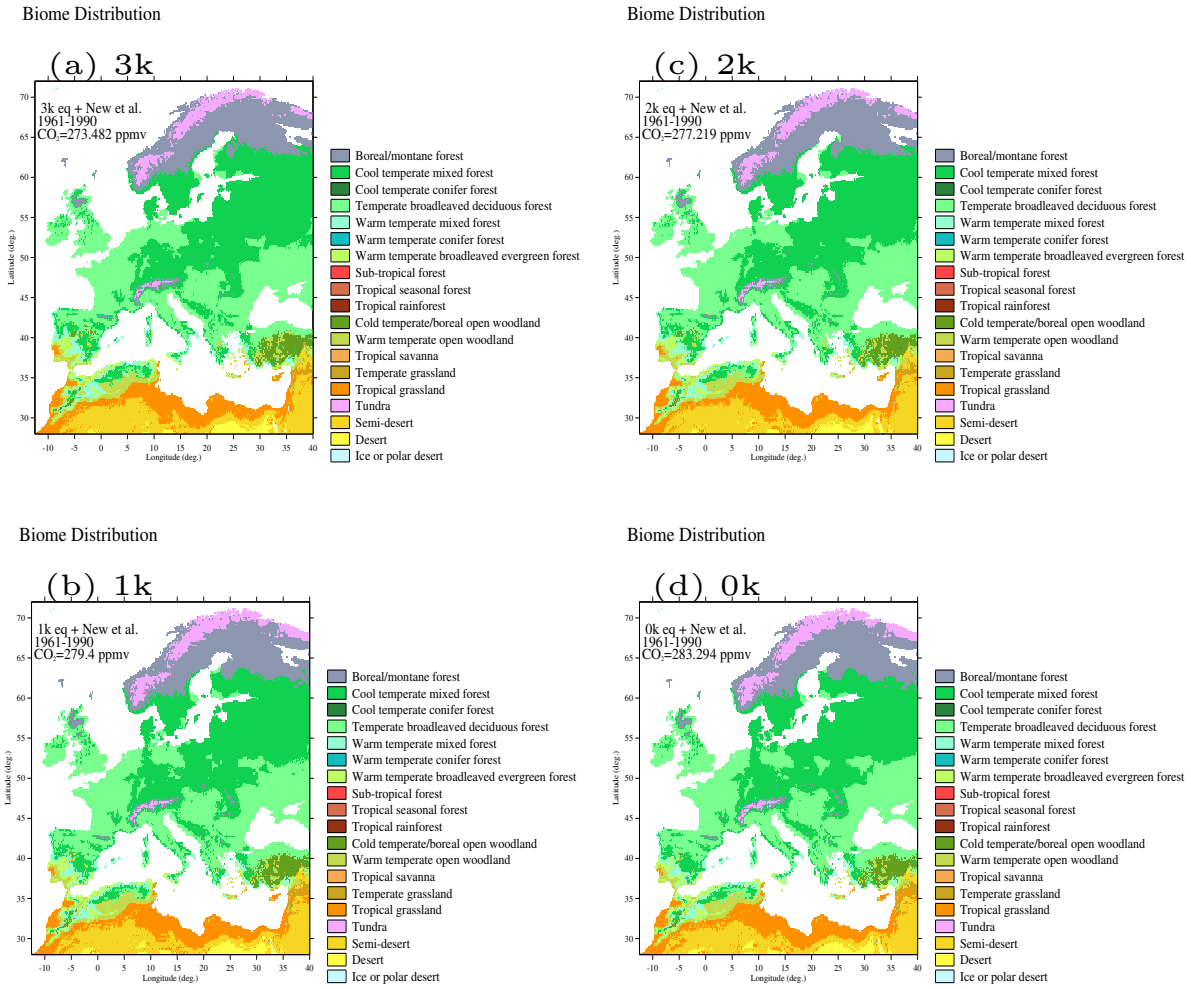

Figure 6.9: Figure 6.8 continued for the time slices 3 to 0 kyr BP.

resulting from the missing land ice and thus, the too warm conditions. With the declining insolation and the reduction in mainly the summer temperatures (Fig. 4.1 a, c), GDD decreases. At the same time, boreal/montane forests and tundra expand - at the expense of the temperate forest types, which require a longer growing season. With this, the treeline is relocated southwards again. Stronger changes also occur over the southern parts of Europe. The warmer and drier conditions during the early Holocene summer over SW-Europe (Fig. 4.1 b and 4.2 b) are leading to an expansion of tropical grassland and also woodland types (*Brewer et al.* 2009). Over the following millennia, these drier types are receding due to the increase in summer precipitation and the decreasing temperatures. Similar changes can be observed over SE-Europe, respectively western and central Turkey. In these regions, the warmer and drier summer conditions (Fig. 4.1 d and 4.2 d) during the early Holocene have also induced temperate open grassland types, which are decreasing in the subsequent time slices due to the increase in precipitation and the decrease in temperatures. In general, a rather variable pattern of types occurs over Spain and Turkey at the early Holocene, mainly at 8k and 9k, with a mixture of tropical grassland, temperate mixed forest and warm temperate open woodland. This is gradually diminishing to more temperate (deciduous) forest types existing in the late Holocene which is also indicative of a cooling and moistening trend in southern Europe during the Holocene.

Over central Europe, a development and expansion of cool temperate forest types can be constituted from the beginning to the late Holocene. This is also observed by *Brewer et al.* (2009). In contrast, broadleaved deciduous trees develop in western France at the expense of cool temperate forest, which occurred during the early Holocene time slices due to the prevailing wetter conditions in that region (Sect. 4.3.3 and *Guiot et al.* 1993). In the northern and eastern parts of Europe, needleleaved evergreen trees, thus cool temperate forest, can develop because of the cooling trend in those regions.

These results are partly verified by those of *Brewer et al.* (2009). The authors identify an expansion of boreal forest and tundra from the mid-Holocene to the preindustrial in their model-data intercomparison. Moreover, the authors also constitute a reduction of the drier grassland and woodland types over the southern parts of Europe.

6.5.2 Climate-vegetation interaction (b)

The results are presented separately in two parts to provide a various analysis of the impact of the extreme boundary conditions and the increased CO_2 concentration; the first one shows the rather physical outcome of these simulations, representing the dynamics and the hydrological cycle. As previous studies (*Claussen* 1994, 1997, 1998) identify two regions being especially sensitive to external perturbations, i.e. the northern parts of Africa and the high northern latitudes, the dynamical properties in the tropics and the mid-latitudes are investigated more closely, which are represented by the velocity potential and the zonally averaged zonal wind respectively. The two parameters precipitation and evaporation play an important role for the Budyko ratio (cf. Sect. 6.3.2), therefore, the difference between both, i.e. the precipitation minus evaporation ratio, is analyzed to account for the hydrological changes. The second part will then be made up by the two phenomenological quantities, the Koeppen climate classification and the Budyko dryness index. The focus is set at first on the results of a control run before analyzing sensitivity experiments, where either the biogeophysical boundary conditions alone are changed or in combination with the biogeochemical forcing, i.e. in terms of an increased CO_2 concentration.

Control run

Physical properties Before having a look at the climate classifications, the velocity potential is discussed which is presented in Figure 6.10 a for the 200 hPa-level near the tropopause. This quantity serves as a measure of large-scale divergence and convergence. Negative (positive) values are indicative of an upper level divergence (convergence) and a convergence (divergence) at the ground respectively, showing the characteristic dipole pattern of divergence and convergence.

Important features become apparent, when comparing the output of the control experiment to those of the extreme ones of the "green" and "desert world" (Fig. 6.13), which reveals significant differences between the three patterns. The divergence maxima at 200 hPa are located over the West Pacific, caused by a high convection over the warmer ocean. This is well shown in the control (Fig. 6.10 a) and the desert experiment (Fig. 6.13 b). This pattern is different in the forest experiment (Fig. 6.13 a) with a strong westward shift of the divergence maximum to the eastern parts of Africa. The convergence maxima (at 200 hPa) are more similar in the control and the forest simulation, whereas in the latter, the maximum is stronger and more shifted to the west. *Claussen* (1997) is showing that this is related to the enhanced convergence above the more vegetated Sahara, leading to the westward shift of both maxima. Another very important difference between the three experiments is the stronger convergence maximum in the desert simulation. This is related to the process of desertification (*Charney* 1975). The sandy soil

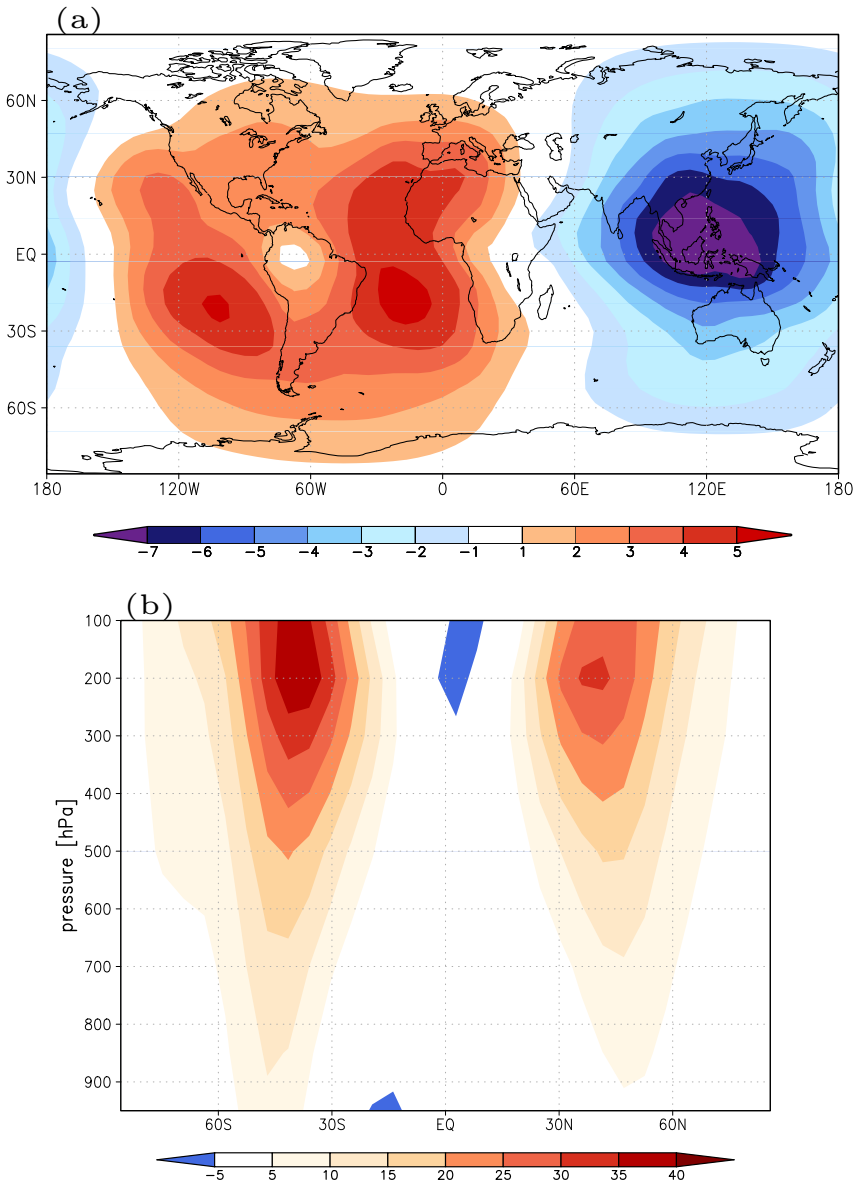

Figure 6.10: Annual mean velocity potential $[10^6 m^2/s]$ at 200 hPa (a) and annually and zonally averaged zonal wind $[m/s]$ (b) for PlaSim control.

has a much higher albedo, which causes relevant modifications in the local radiation budget, initiating enhanced sinking motions over the Sahara.

The zonally averaged zonal wind is shown in Figure 6.10 b. PlaSim reveals the typical pattern with mid-latitude westerlies and easterlies in the equatorial region. The subtropical jets are situated near 30°-35° with jetstream-axes located below the tropopause at 200 hPa in both hemispheres. In direct comparison to ERA (not shown here but see also *Haberkorn et al.* 2009b), PlaSim tends to slightly overestimate the jet maxima associated with a more upward and poleward location.

Some additional characteristics can be found, when the output of the control experiment is compared to those of the extreme ones of the "green" and "desert world". As the patterns of all three experiments look very similar at a first glance, the anomalies between the respective extreme scenario and the control experiment are presented (Fig. 6.13 c). The shaded areas (contour lines) designate the anomalies of the "green world" ("desert world") compared to the control simulation. In general, the SH winds are only very little affected by the extreme boundary conditions, merely leading to a small variation in the general patterns and the absolute values of the zonal wind velocity. These are mostly confined to the equatorial regions. These first remarks are consistent with the changes in the Koeppen classes which are described below. Stronger differences between the scenarios occur over the NH, forming an antipodal signal of positive and negative anomalies. This is especially obvious in the area between 0° to 35°N, where negative anomalies are observed for the "green world"- and positive for the "desert world"-anomaly. The decrease in the wind velocity in the forest scenario, leading to the negative anomaly, is due to the enhanced vegetation in those areas. Formerly desertic parts in the subtropics are replaced by vegetation, which induces a strong response in terms of a minimum wind anomaly at roughly 30°N. Further to the north, the opposite anomaly pattern occurs. As in these regions, only the type of vegetation is changing (according to the Koeppen classes), the response is much weaker, resulting in a positive anomaly, so higher zonal wind velocities here. The positive anomalies around the equator and at roughly 35°N for the "desert world" are caused by a decrease in the vegetation, so formerly vegetated areas are replaced by deserts, which is coherent with higher wind velocities due to a lower roughness length in those regions. Further to the north, again the opposite anomaly pattern occurs, as in the former case of the "green world". The reason is also similar, i.e. only a small change in the vegetation type occurs, inducing a much weaker signal in terms of lower zonal wind velocities, leading to a minimum in the anomaly. In general, the maxima and minima are stronger in the forest scenario, indicating a stronger response initiated by the extreme boundary condition of a "green world".

Phenomenology After the physical properties, the PlaSim climate is now expressed by means of two different classifications, which are the Koeppen classification and the Budyko-Lettau index of dryness respectively. Before having a closer look on how much the global vegetation distribution is influenced in the two extreme scenarios, the Koeppen climate zones for the control simulation are compared with those of ERA (Fig. 6.11 a, b). By doing so, one gets an insight of how the biomes are distributed globally in the "real world" and, in a second step, the differences can be found out which exist in the two extremes of a green and desert world. Moreover, the regions can be identified which react most sensitively to external perturbations.

The F-zone (ice climate) is stronger developed in PlaSim than in ERA which may be indicative of a too cold climate there. In opposite, the boreal E-zone, especially the continental part (E_c) seems to be slightly underestimated by PlaSim over Central Asia. The temperate D-zone is well represented by PlaSim, mainly over North America and the western parts of Asia. Over the central parts of Asia, it is overestimated or, the other way round, the dry B-zone, which is shown by ERA, is strongly underestimated by PlaSim. Additionally, the mountainous and the adjacent desert region in Asia, which

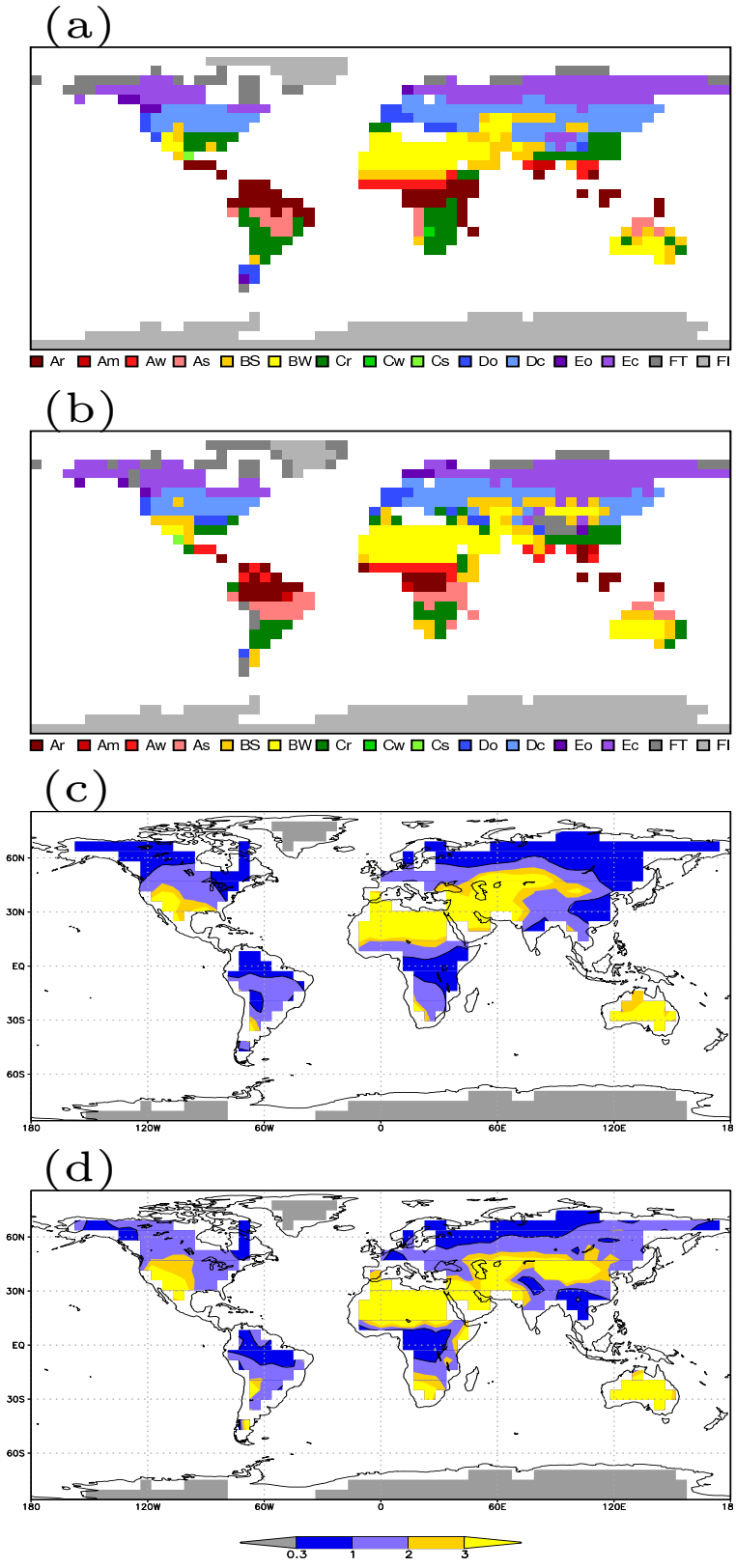

Figure 6.11: Koeppen climate classification and annual mean Budyko-Lettau dryness ratio for PlaSim control (a, c) and ERA (b, d).

should have an ice-and desert-climate respectively, as in ERA, are not shown by PlaSim. In contrast, the steppe-climate (BS) south of the Sahara is better represented in PlaSim than in ERA and more realistic when compared to *Fraedrich et al.* (2001) or *Kottek et al.* (2006) who both use observational data for calculating the Koeppen climates. Nevertheless it may be slightly shifted too far to the north, due to an overestimation of the precipitation in this region (cf. Fig. 3.4). One stronger difference is the distribution of the subtropical C-types which are overestimated by PlaSim in South America and the southern parts of Africa and shifted too far to the north. Again, the mountainous areas in South America are not shown by PlaSim. There is one peculiarity in both data sets in South America and in Central Africa, which affect the tropical A-types. Compared to the observations, there should be an A_r (permanent wet) and A_w (winter dry) region around the equator in Central Africa. Whereas the permanent wet area is shown very similarly to the observed, the winter dry type is represented correctly only to the north of the equator. The corresponding belt to the south (roughly 0° to 10°S) is not appearing. Instead of this, PlaSim simulates the permanent wet A_r-class and ERA shows the opposite A_s-type (summer type). In South America, between 0° and 20°S, both PlaSim and ERA show the summer dry (A_s-) type instead of the opposite winter dry type given by the observations. The winter dry-type is partly existing in ERA, but completely missing in PlaSim, simulating the permanent wet A_r-type instead. This rather false classification in PlaSim on the one side may be caused by an underestimated convection in PlaSim (*Haberkorn et al.* 2009b), leading to a deficient convective precipitation. On the other side, for ERA, it may be caused by an overestimation of precipitation (mainly the large-scale part) in the equatorial region of the tropics and the tropical oceans which has been addressed in Chapter 3.

Concerning the diagnosed Budyko index (Fig. 6.11 c, d), the characteristic patterns are shown by both PlaSim and ERA. Larger differences occur over the northern parts of North America and Asia and smaller parts of South America, where PlaSim shows a slightly lower dryness ratio than ERA, i.e. the region of humid savanna to forest is more extended than in ERA. The dryness ratio is equally underestimated by PlaSim over large parts of North Africa, Central Asia, Australia and smaller parts of North America, so that the desert is underrepresented there.

As a summary, the two classifications are now intercompared for the control simulation (Fig. 6.11 a and c), before further applying them in a composite study in the next section. Although both classifications are built on a different total number of classes, some similarities are clearly distinguishable as the general structures are pointed out by both Koeppen and Budyko. The desertic areas are a bit more pronounced in the dryness ratio, mainly over Asia and the southern parts of North America. The main deviation between both is caused by the forest-related classes in the tropics and in the temperate climate. They are clearly divided in the Koeppen scheme, for example tropical rain forests or the temperate D_o- and D_c-types, whereas no further distinction is made in the Budyko ratio. Moreover, the forest class, between 0.3 and 1, is even smaller and more restricted compared to the other classes, so changes in the forest fraction cannot be captured properly by the Budyko ratio. Further discrepancies may occur due to the temperature thresholds building most Koeppen classes (cf. Tables 6.2 and 6.3), but which are not the basis for the Budyko ratio, which depends on the energy and water fluxes.

Schreiber's equation By defining the classes by means of energy and water flux ratios, *Budyko* (1974) has set up a relationship which is based on two essential quantities of the climate system. Nevertheless, similar approaches have been subject of investigation already long before. At the beginning of the 20th century, *Schreiber* (1904) set up a semi-empirical relationship of the three hydrological parameters precipitation (P), evaporation (E) and runoff, stating the balancing of the water supply by the evaporation and the runoff, as a function of available energy. This equilibrium solution of the aridity-runoff relation is expressed by the formula

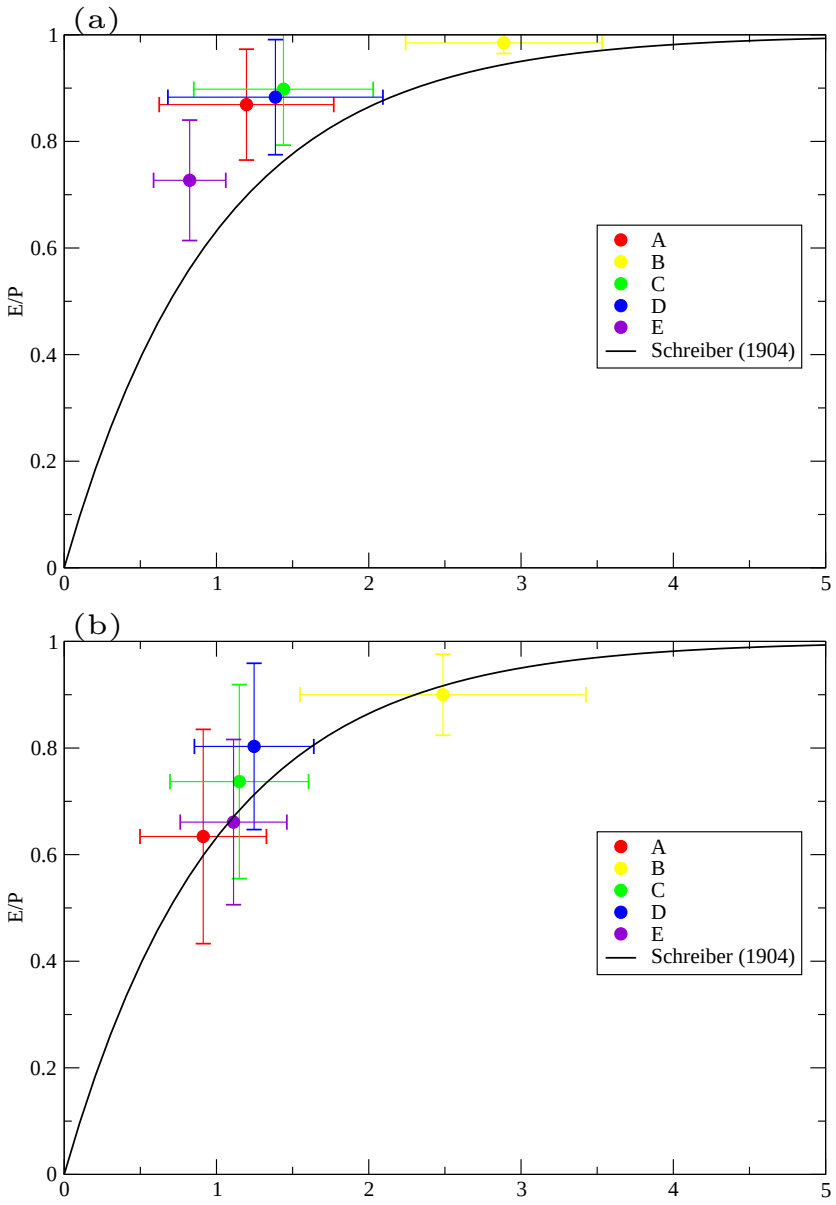

Figure 6.12: Koeppen-Budyko-composite with the E/P-ratio versus the Budyko dryness ratio for PlaSim control (a) and ERA (b), provided by F. Sielmann. The dots, horizontal and vertical lines are the sample means and the standard deviation of the respective ratio.

$$\frac{E}{P} = 1 - e^{-D} \tag{6.4}$$

representing the evaporation ratio E/P as a function of the aridity index, or dryness ratio, D. Due to its balancing function, this equation is comparable to an equation of state (*Fraedrich* 2010; *Fraedrich and Sielmann* 2011). As mentioned before (cf. Sect. 6.3.2), the dryness ratio characterizes evaporation in terms of the availability of water and energy, i.e. precipitation and net radiation respectively, with the

separation in the energy limited (D $<$ 1) and water limited (D $>$ 1) regimes. Applied to Equation (6.4), precipitation exceeds evaporation in the former case where available radiation energy is too small to balance the latent heat equivalent of precipitation. In the latter regime, low rainfall combined with a high level of radiative energy lead to a permanent and slight overbalance of precipitation by evaporation. Following these very first notions by *Schreiber* (1904), his original formula has been modified by several authors, with the studies of *Ol'dekop* (1911), *Turc* (1954), *Pike* (1964) and *Budyko* (1948, 1974) being the most frequently cited.

The relation between the different variables is shown in the solid curve in Figure 6.12, referring the evaporation ratio, i.e. the ratio of annual evapotranspiration to precipitation, to the rate of potential evaporation to precipitation which is the Budyko dryness index itself. This relationship can be used to evaluate models with respect to their representation of precipitation and available energy. The simple application of a model's output to this relation will lead to a scatter of data points, which is caused by regional variations influencing the evaporation (*Koster and Suarez* 1999). The PlaSim points (not shown here) are distributed along the solid curve, showing a clear increase of E/P with an increasing Budyko ratio. As E/P is a function of the dryness ratio only, a first estimate of the evaporation efficiency can be obtained already from the knowledge of the Budyko index alone (*Koster and Suarez* 1999). The discrepancies between the distribution of the PlaSim data points and Budyko's analysis are rather due to the model data than to a deficiency in the analysis itself (*Koster and Suarez* 1999).

A second step in this scheme, after the only empirical E/P-relationship, is a categorization of the PlaSim output in terms of the respective Koeppen classes. This inclusion of the Koeppen classes as a composite study is based on the work by *Hanasaki et al.* (2008). Therefore, Figure 6.12 serves as a kind of overview-scheme, connecting the parameters evaporation and precipitation as well as the Koeppen classification and the Budyko ratio to each other. This composite scheme provides a more profound analysis on the consistency of the physical E/P-ratio on the one side and the relation between the Koeppen climatology and the Budyko ratio on the other side. The Koeppen classes can be identified by the respective colors in Figure 6.12 and thus, can be clearly attributed to a specific E/P- and Budyko dryness index. As the dryness ratio isn't defined for negative available energy, it is thus not defined in the polar regions. For the same reason, the polar Koeppen class isn't considered here and it is further confined only on the main classes. The horizontal and vertical axes are centred on the sample-means and reflect the standard deviation (variability) of the respective (E/P and D-) ratios.

For PlaSim (Fig. 6.12 a), the Koeppen classes are well aligned around the E/P-curve, but all classes are located slightly above. The minimum (maximum) of the dryness ratio is represented by the boreal (desert) Koeppen class, belonging to the energy-limited (water-limited) regime. In between, the three other Koeppen classes can be found, all showing a dryness ratio between 1 and 2. As could be expected, the standard deviations increase with increasing E/P (vertical axis) or D (horizontal axis).

The corresponding composite for ERA (Fig. 6.12 b) gives a slightly different picture. In general terms, the Koeppen classes are disposed in closer distance to the empirical relation. The subtropical (C) and temperate (D) types show similar values of the dryness ratio than PlaSim (except the lower E/P-values). The location of the maximum, the desert class, is also comparable to PlaSim but has lower values of E/P and D and is hence located below the theoretical relationship. Its variability is much stronger as in PlaSim. Regarding the tropical (A)- and boreal (E)-types, ERA differs more strongly from PlaSim. The minimum in the E/P versus D-ratio is given by the tropical class in ERA instead of the boreal type as in PlaSim. In ERA, this cold forest type nearly shows the values which are predefined by the empirical relationship. The minimum for the tropical class may be caused by the already mentioned overestimated precipitation in the tropics which then leads to both a weaker E/P and dryness ratio.

Sensitivity studies-boundary conditions

In this section, the results for the two extreme scenarios are presented. The dynamical part, also for the extreme scenarios, has already been investigated in the previous section to highlight the differences to the control run. Instead of that, the hydrological cycle is investigated at this stage, in terms of the annual mean precipitation minus evaporation-fields, as the ratio of both variables is used for the Budyko index. For the control run, this has already been evaluated in comparison to ERA in Chapter 3 and it is referred to those remarks. However, for an easier comparison, the P-E field for the control run is included in Figure 6.14 a, as an annual mean value instead of daily rates in Figure 3.5.

As it has been the case for the velocity potential, some important features emerge when comparing the control run to those of the vegetation extremes (Fig. 6.14 b, c). The more vegetated Sahara in the "green world" scenario (Fig. 6.14 b) leads to an enhanced P-E ratio due to an increase in precipitation. In addition, the ratio also increases in the northeastern high latitudes of Asia which induces a shift in the climate classes as will be pointed out in the next paragraph. In contrast, the ratio over the Sahara is strongly reduced in the "desert world" (Fig. 6.14 c). In general, the absolute maxima slightly increase in the "green" world, whereas the minima intensify in the "desert world".

Phenomenology When now comparing the diagnosed Koeppen climate classes of the PlaSim control simulation (Fig. 6.11 a) to those of the extreme ones (Fig. 6.15 a, b), it becomes immediately obvious, that nearly the same pattern as in the control run has established in the two extreme scenarios. After 100 years of integration both have converged to the unperturbed state. Besides some smaller differences, for example in South America with a broadening of the tropical A_s-type in the "desert world" (Fig. 6.15 b) and in Australia, where dry types clearly expand (recede) in the "desert world" ("green world") compared to the control experiment, some stronger deviations occur, having a more relevant impact. In general, two regions can be identified, where the differences are still remarkable after the 100 years integration period. One is given by the northern high latitudes. Compared to the control run, there is a slight decline of the tundra, mainly over the Asian parts, in the "green world" (Fig. 6.15 a), i.e. the boreal taiga expands. Over North America, the temperate type (D_c) expands northwards, replacing the boreal types existing in the control experiment. So, in general, a spread of warmer types takes place, which is caused by an increased vegetation cover. This leads to a decrease in the albedo in those regions and, consequently, to a warmer climate.

In the "desert world" (Fig. 6.15 b), the opposite can be noticed. A strong expansion of the tundra (FT) occurs at the expense of boreal types which is indicative of a cooling due to the lower vegetation cover which induces an albedo increase. The other region, where stronger differences between the three different setups remain and which seems to be very sensitive to external perturbations, are the desert parts of Northern Africa and Arabia. In the "green world", the Saharan desert is significantly reduced, leading to an expansion of the steppe (BS-type) and also to an extension of the tropical permanent wet A_r-type and hence a northward shift of the winter dry A_w-type, compared to the control simulation. In addition, the desert-type has nearly completely disappeared in the Arabian realm and is displaced by subtropical C_r-types. In the "desert world", a strong expansion of the dry desert (BW-type) occurs. The Saharan desert expands north- and southward, completely replacing the permanent wet A_r-type. At the same time, summer dry A_s-types develop to the south of the desert, restricting the subtropical C_r-type which originally emerges in those regions, as it is shown in the control and "green world" simulation. In this context, the results of previous studies of *Claussen* (1994, 1997, 1998) become important, who investigate an asynchronously coupled atmosphere-biome model to find equilibrium solutions starting from different initial conditions. It is remarked that the combined model yields two equilibrium-states:

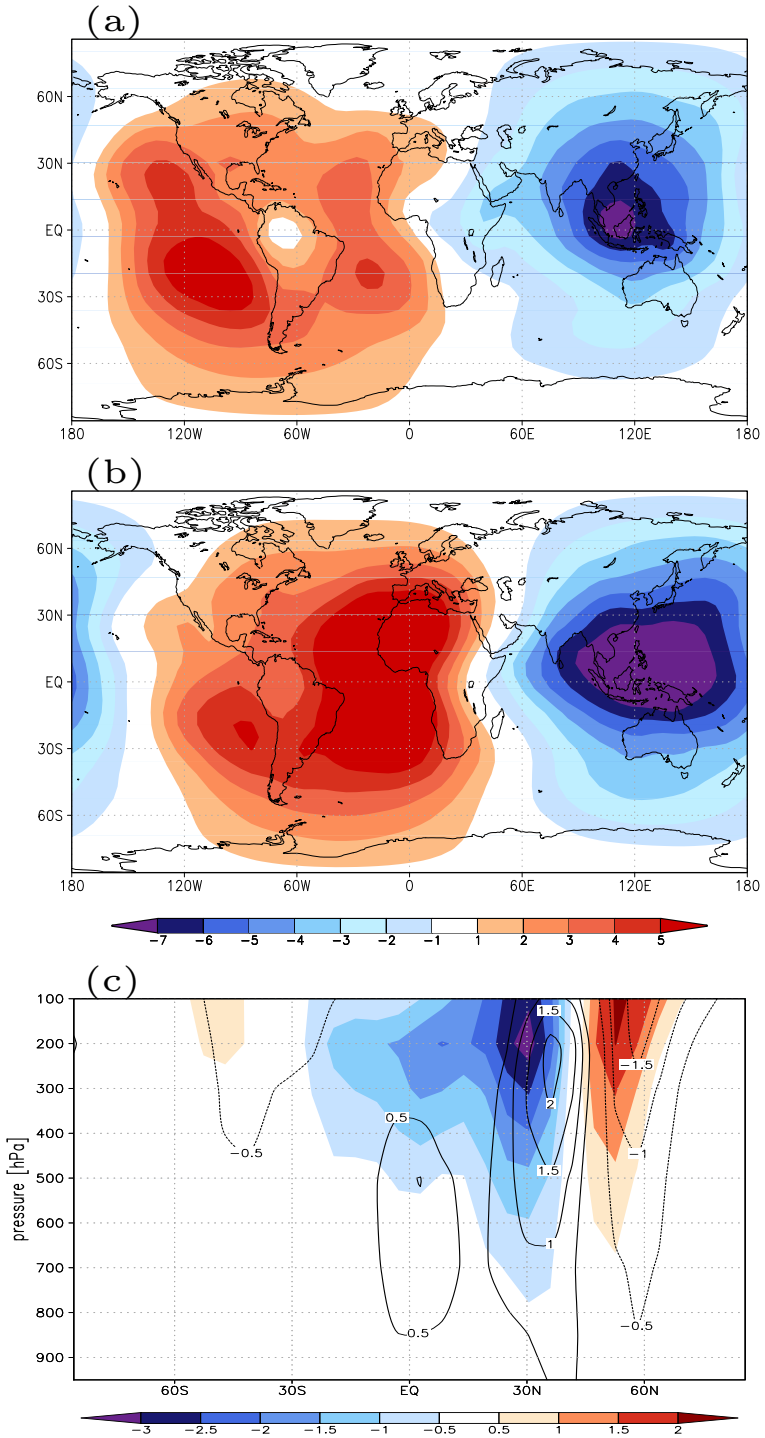

Figure 6.13: Annual mean velocity potential $[10^6 m^2/s]$ at 200 hPa, (a) forest and (b) desert; (c) Annually and zonally averaged zonal wind anomalies $[m/s]$ of the respective extreme scenario minus PlaSim control (forest: shaded, desert: contour lines).

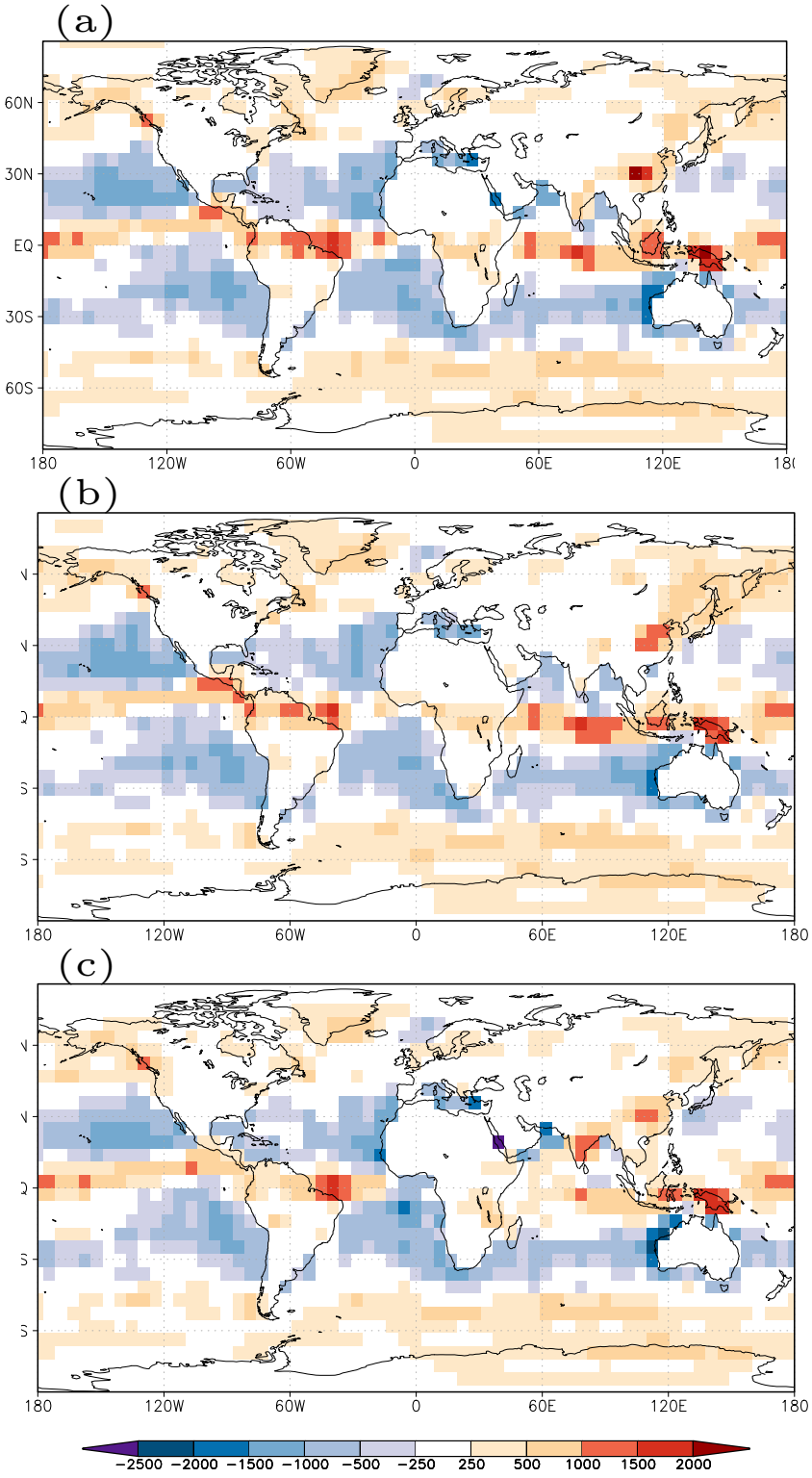

Figure 6.14: Annual mean precipitation minus evaporation [mm/year], (a) control, (b) forest, (c) desert.

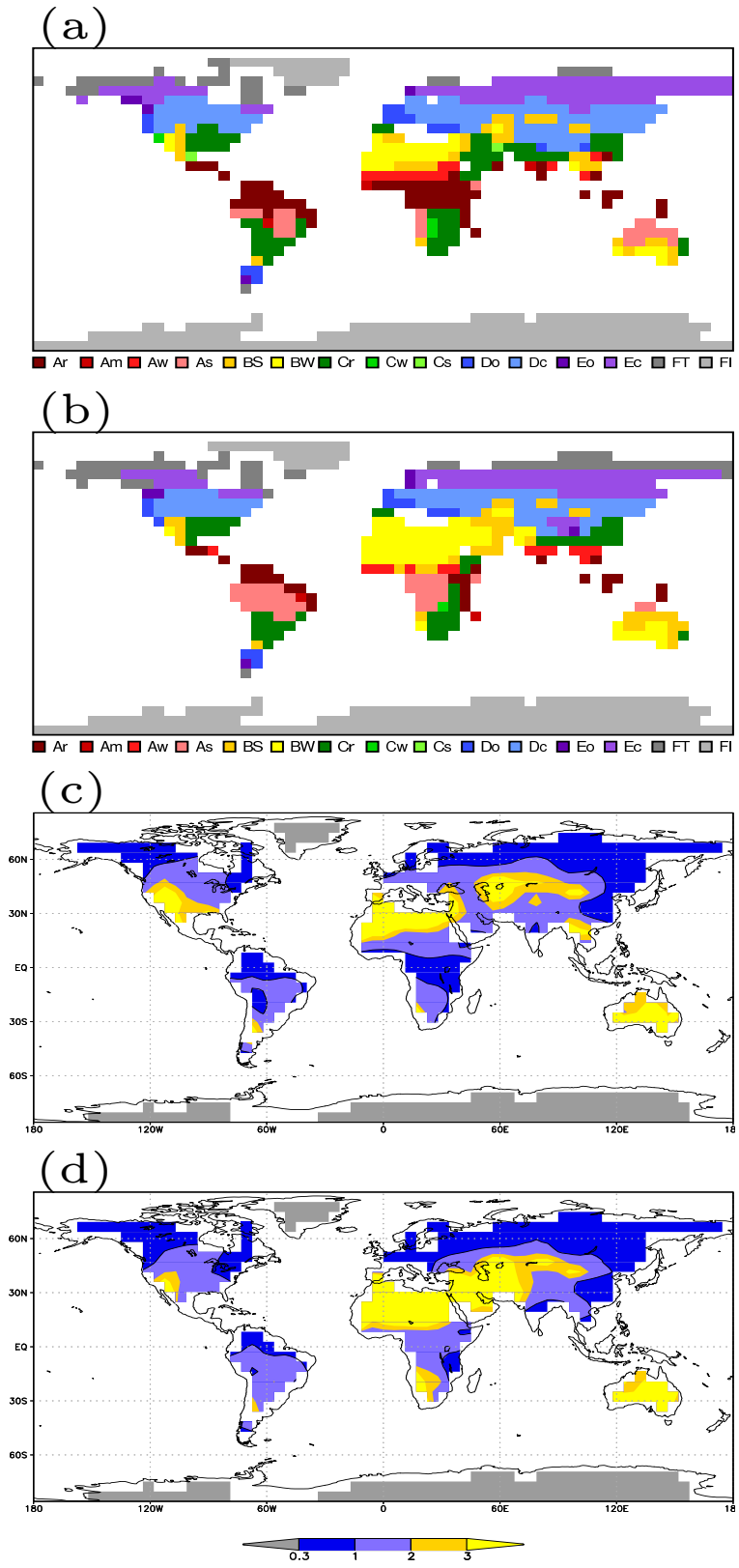

Figure 6.15: Koeppen climate classification and annual mean Budyko-Lettau dryness ratio for the forest (a, c) and desert world (b, d).

either a present-day distribution of vegetation and deserts or a modified distribution with smaller Saharan and Arabian deserts, keeping some vegetation in the southwestern Sahara. Although the investigation of the existence of different equilibria is beyond the scope of this study, the results can be seen as an addition in the larger context of those studies.

When comparing now the respective Budyko classes of the PlaSim control simulation (Fig. 6.11 c) with the "green" and "desert world" (Fig. 6.15 c, d), the strongest differences occur over the desert parts of the Sahara and Arabia, with the desert parts reduced, even strongly, in the control and mainly forest simulation compared to the "desert world". Over South America, humid savanna is declined in the "desert world" compared to the other two experiments with the expanded savanna-type being indicative of a higher net radiation due to the decreased vegetation. The same is found over the southern parts of Africa.

Sensitivity studies-global warming

Physical properties The possible effect of an enhanced greenhouse gas concentration on the hydrological cycle and the equilibrium climate-biome distribution is investigated in this section. For this, the same set of experiments is applied as for the previous studies but the CO_2 concentration is set to 720 ppmv.

In the annual mean P-E field for the control simulation (Fig. 6.16 a), there is a slight increase of the maxima over the tropical continents and mainly over Africa which is due to an enhanced precipitation in those regions. For the two extreme scenarios (Fig. 6.16 b, c), the basic features which have been mentioned before, i.e. an intensification of the maxima in the "green world" and of the minima in the "desert world", do not significantly change. Especially in the latter, the differences are very small.

Phenomenology To quantify, in a second step, whether the climate zones shift in a global warming simulation, the Koeppen classification and the Budyko index for the control simulation are presented in Figure 6.17. The overall changes due to enhanced CO_2 are very small for all three scenarios, therefore only the control results for Koeppen and Budyko are shown but all three simulations are discussed.

For the control run (Fig. 6.17 a) the changes are very small. At the northern high latitudes of North America, a slight warming is leading to an expansion of the boreal E_c-type. In the central parts of North America, the temperate D_c-type is growing at the expense of the subtropical C_r-type, which indicates a slight cooling. Further to the south, the dry steppe-type (BS) expands and removes the former subtropical C_r-type, which is due to a warming here. Small changes also occur in East Africa where precipitation seems to increase, leading to the permanent wet A_r-type instead of the subtropical C_r-type. In the southwestern parts of Asia, to the west of the Indian subcontinent, there is an indication of wetter conditions, as temperate and tropical types develop and remove the dry BS-type there. In the "green world" scenario, there is also a slight warming at the high latitudes of the North American continent, leading to the warmer boreal type there, which is similar to the control simulation. Other larger changes occur again in the northern parts of Africa. In the very northern part of Africa there seems to be a slight increase in precipitation with a change from the BW-type to the BS-type. A stronger increase occurs south of the Sahara, where the type is changing from BS to the tropical A_w-type. In the "desert world", a slight warming occurs at the high latitudes of Central Asia with an expansion of the boreal type E_c instead of tundra (FT). In Africa, the doubling of CO_2 leads to an increase of precipitation, as the climate class is changing from the dry steppe type (BS) to the winter dry A_w-type. In Asia, to the west of the Indian subcontinent, the classes change from the BW- to the BS-type, indicating wetter conditions there too.

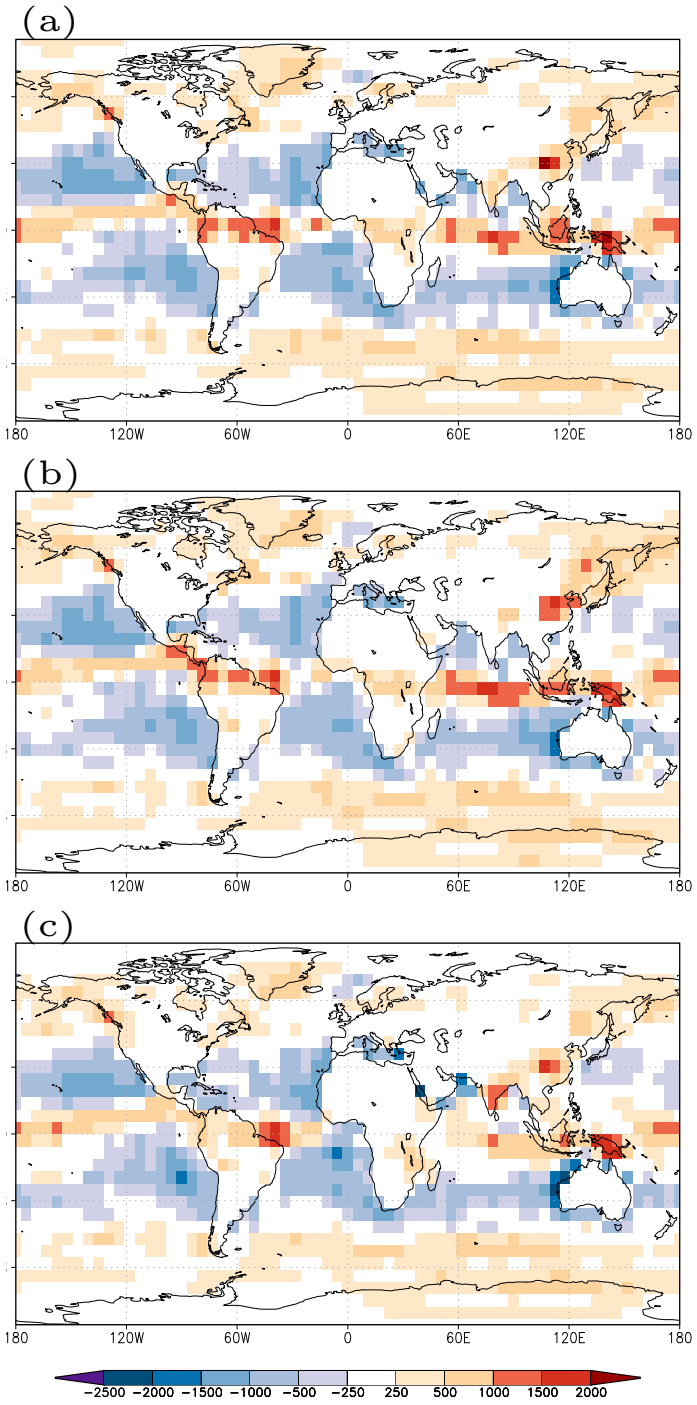

Figure 6.16: Annual mean precipitation minus evaporation [mm/year] for 2 × CO_2, (a) control, (b) forest, (c) desert.

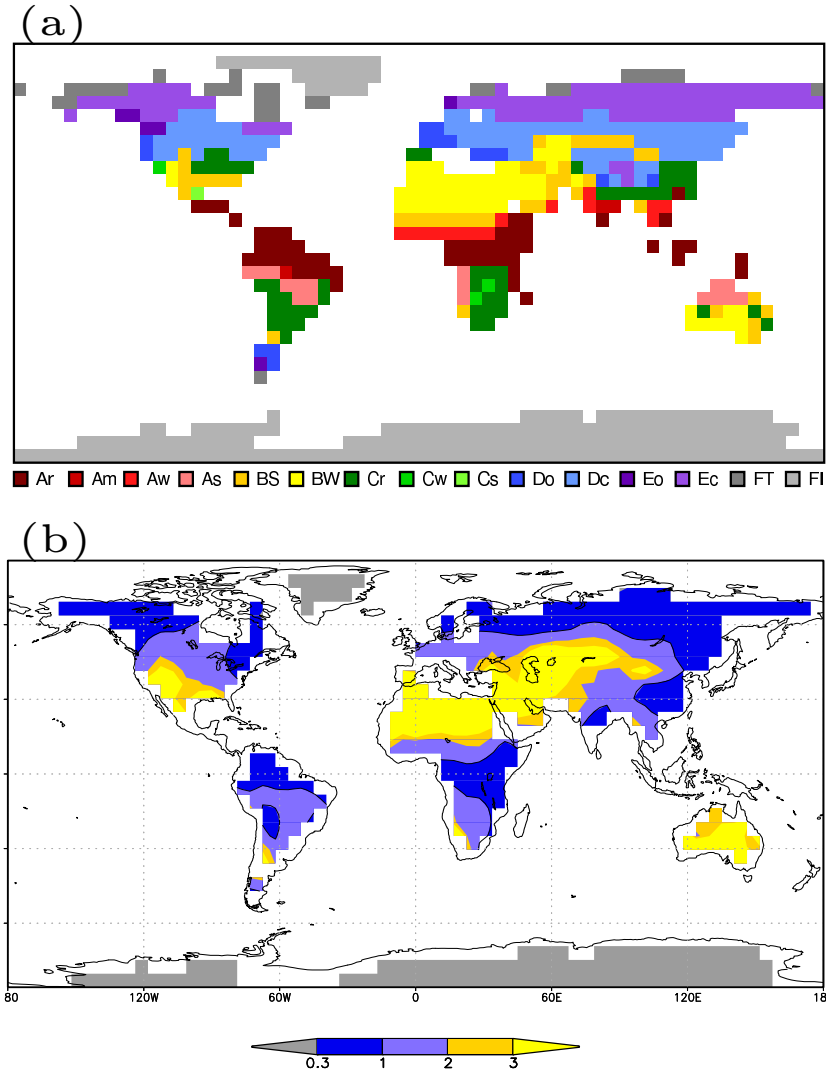

Figure 6.17: Koeppen climate classification (a) and annual mean Budyko-Lettau dryness ratio (b) for $2 \times CO_2$ for PlaSim control.

In contrast to the Koeppen zones, largest changes in the Budyko ratio of the control run (Fig. 6.17 b) occur over the western parts of Asia and Arabia, where the desert area is reduced, which is indicative of wetter conditions when the atmospheric CO_2 increases. The abovementioned changes in the Koeppen climates in the "green world" do not appear in the Budyko ratio, except the slight warming in North America which provokes an expansion of the desert-class. For the "desert world", only the changes over Arabia occur in the Budyko ratio as the desert class is diminishing, so wetter conditions are leading to the semi-desert type.

6.6 Summary and discussion

In this chapter, two different aspects related to vegetation are studied: Holocene changes of European vegetation and the interaction between climate and vegetation.

European palaeovegetation (a)

In the first part of this chapter, the European vegetation evolution during the Holocene is reconstructed using PlaSim and CARAIB. With the latter in a very high resolution, for the first time a very detailed overview is given for each time slice of the Holocene from 9 to 0 kyr BP. As a first parameter, the bioclimatic variable GDD, which reflects the length of the growing season, is analyzed. For present-day conditions, PlaSim is able to capture the characteristic pattern with a strong north-south gradient with high (low) values in the south (north). Over the Holocene, a general decreasing trend can be observed in the northern and eastern parts of Europe. The high GDD5-values during the early Holocene are caused by the positive temperature anomaly in those regions and thus by the enhanced insolation distribution. This pattern of the early Holocene is consistent with the northerly shift of the treeline in terms of warmer forest types. With the reduction in GDD5, the warmer types are replaced by the colder boreal forest and tundra. A prolonged growing season compared to the preindustrial is also detected in the southern parts of Europe. The opposite trend, i.e. an increase in GDD over the Holocene occurs over the northwestern parts of Africa. From this, enhanced vegetation cover until the mid-Holocene is inferred, where more summer precipitation has caused the "green Sahara". With decreasing precipitation until the preindustrial, also the vegetation cover is more and more diminishing, leading to the desert types of today. The results are verified by other model studies (*Brewer et al.* 2007, 2009) but show partly different trends to palaeoobservations which can be attributed to the model resolution which may be too large for a smaller region like Europe. Moreover, the climatic changes, leading to modifications in the GDD pattern, may be too small during the Holocene, so that they are not necessarily reflected in changes in the GDD pattern.

Regarding the distributions of the different biomes, a distinct northerly shift of the treeline is diagnosed, i.e. the expansion of warmer forest types and the instantaneous replacement of colder types is clearly shown by PlaSim-CARAIB. This process is a direct consequence of the increased insolation at the high northern latitudes. However, due to the missing land ice in the model, the distribution of the warmer types may be overestimated. With the weakening of the positive insolation anomaly in those regions, the GDD is decreasing and thus the temperate forest types. Consequently, the colder forest types and tundra can expand. Moreover, larger modifications occur over the warmer regions in southern Europe. Over the southwestern parts, mainly the warmer, but also drier, conditions during summer in the early Holocene lead to an expansion of grassland and woodland types which are receding until the preindustrial due to both the decrease in temperature and the increase in precipitation. Similar changes can also be observed over the southeastern part where grassland types are equally decreasing. Moreover, the general distribution of biomes in those southerly regions is revealing a rather variable pattern at the beginning of the

Holocene. This mixture of tropical grassland, temperate forest and woodland types is getting more and more uniform until the late Holocene which is also indicative of decreasing temperatures and increasing precipitation. In contrast, over the more central, northern and eastern parts of Europe, the distribution of forest types is changing according to the decreasing temperatures during the Holocene. In general, these studies are mostly in line with other model studies on this topic (*Crucifix et al.* 2002; *Renssen et al.* 2005a; *Brewer et al.* 2007, 2009). Nevertheless, further investigations may be required in terms of other model studies and/or vegetation reconstructions using proxies as mainly the early Holocene time slices are rather insecure. Also the already discussed inclusion of land ice into PlaSim plays a role in this context as well. Maybe, for an in-depth comparison and as proposed by *Henrot* (2010), one should compare the individual PFTs as they are more directly comparable to palaeobotanical or palynological data. As mentioned above, biome limits are rather imprecise and may vary according to the specific classification used here.

Climate-vegetation interaction (b)

These studies fit into the framework of the hitherto existing, vegetation-related studies on the Planet Simulator (*Fraedrich et al.* 2005c; *Kleidon et al.* 2007; *Dekker et al.* 2010; *Bathiany et al.* 2010). Whereas the latter three authors address the problem of existing multiple steady states in the atmosphere-biosphere-system, *Kleidon et al.* (2007) discussed this question, at least partly, in the context of the initial conditions of a vegetated and non-vegetated world.

Here, the issue is approached in terms of the effects of extreme boundary as well as global warming-conditions. Physical properties are investigated and, more decisive, these setups, characterized by vegetation-associated parameters, are linked to two independent vegetation classifications, the Koeppen climate classification and the Budyko-Lettau dryness index. For the Koeppen climatology, a modified version has been used.

The atmospheric variables clearly point out the modifications in the global circulation and the hydrological cycle under the effect of the two extremes, whereas the sensitivity to an increase in CO_2 is comparatively small. The results of the two climate classifications, which are both applied diagnostically, are indicative of two regions being most sensitive to external perturbations; these are the northern high latitudes and the desert parts of Northern Africa. Although both classifications only use a mean climate and give a mere static vegetation distribution, their results point into the direction of previous studies, which investigate the existence of different equilibria in the atmosphere, based on comparable boundary conditions.

Similar to the changes in the physical properties, the variations in the distribution of the two classifications in the global warming experiments are very small which supports the aforementioned statement that the sensitivity to the extreme boundary conditions is much stronger and that their influence is much more pronounced, although they do not persist over the whole simulation period due to the climatic influence. As shown, the changes in the Koeppen climate zones and the Budyko ratio in the global warming scenario are small but not completely identical, i.e. a shift in some Koeppen classes may not lead to a corresponding shift in the Budyko classes and vice versa. This may allow different interpretations of changes due to global warming and does not necessarily indicate a general deficiency of these classifications and is not entirely due to the different number of classes (15 in total for Koeppen and five for the Budyko ratio). Indeed, also deviations in the two classifications are detected for the control run, i.e. without any external perturbations, which must be very likely attributed to a coarser representation of the forest-related class in the Budyko scheme, so lately to the smaller number of classes, and to the fact that the Budyko classes are not built on temperature thresholds but on energy fluxes, which further impedes

the distinction of warm and cold biomes. If the different number of classes was the main reason, one would rather not expect changes in the Budyko classes which do not occur in the Koeppen classification. As this exacerbates a qualitative comparison of both classifications, a composite study is presented in terms of the Schreiber-Budyko-relation combining hydrological parameters and the Koeppen classes which are included by assigning them to their specific E/P- and dryness ratio. Through this, both classifications are related to each other which yields an overall and lately more consistent picture of how both the physical, in terms of the hydrological, and phenomenological properties, in terms of the two classifications, are located to each other.

Summarizing it can be said, that the described application of the two classifications, i.e. both individually and, more important, in their composite use, can provide valuable information on the current climate state, linking vegetation with energetic and hydrological features. It also improves the possibility to make a qualitative estimation and interpretation of the global response in a warmer climate and whether climate classes are shifting or not. Regarding the shifts due to global warming as a whole, they are only minor and the only static behavior of both classifications seem to lead to a low sensitivity to only small modifications in the climatic input. In addition, this may be partly due to the use of climatological SST instead of a free ocean or at least a mixed-layer ocean, so that the ocean and the atmosphere cannot freely interact. This leads to a strong dampening of the feedback between both systems. Although *Ganopolski et al.* (2001) and *Fraedrich et al.* (2005b) both show an intensification of the atmospheric response in their studies by using a mixed layer ocean, it still remains uncertain, whether this will lead to significant changes in both classifications. Moreover, the usage of a purely phenomenological classification scheme such as Koeppen, which has originally been established to reproduce the observations of the current climate, may not lead to representative results in a climate change scenario. Further concluding remarks on the results of this chapter are made in the very end of this study where the outcome is put into a wider context.

7 Summary and conclusion

7.1 Summary and conclusion

This present study is dedicated to set up the climatological and biospheric framework for a later and external more profound analysis of the early human-climate interaction during the Holocene. During this period in the past, a transition has taken place from hunting-gathering to farming societies, spreading from the East to the more western parts and also to Europe, which is in close relation to the climate being rather stable and thus beneficial for this human settlement. In turn, this transition has induced alterations of the land cover which itself had an impact on climate. Therefore, the aim of this study is to reconstruct the full Holocene climate and vegetation evolution over Europe, using two completely different approaches: a state-of-the-art fully coupled version, i.e. atmosphere-ocean-biosphere, of the general circulation model Planet Simulator (Chapt. 4) as well as proxy time series. The specific and unique approach characterizing this study is to use the latter not only for validation purposes of the simulation results but also, and explicitly, for assimilation purposes - thus, to force the climate model. For the aim to set up the climatological framework for the beginning of the settlement of the early human cultures, a climate simulation is required which is as realistic as possible. Hereby, the reliability is assumed to be provided by palaeoobservations. For the incorporation of the proxy time series into the climate model a novel methodology is developed and is presented in Chapter 5 of this study, together with in total three different applications. Concerning the palaeovegetation, the natural, and not anthropogenic, changes in the land cover composition, thus the biome distribution, are investigated using output from the fully coupled simulation as well as the dynamic vegetation module CARAIB (Chapt. 6 a). The impact of extreme land cover changes on the climate, which can be seen in the context of the early human-climate interaction, is estimated in Chapter 6 b, using two phenomenological classifications. Besides these chapters on palaeoclimate and (palaeo)vegetation, an essential prerequisite of the simulation of past climates is an evaluation of the model to the present-day climate (Chapt. 3).

To conclude this study, the main findings of each chapter are summarized here again. Afterwards, an outlook is given with possible directions of future research.

Evaluation of the Planet Simulator The focus of the validation is set on surface air temperature and precipitation, precipitation minus evaporation (P-E) as well as net radiation. Besides the first two, which are also analyzed in more detail over Europe, the presentation is in the global perspective and always in

comparison to the reanalysis data ERA-40. For the European temperature and the global precipitation respectively, two high-resolution climatologies (CRU and GPCP) are used in addition. P-E and the net radiation are considered only indirectly in the climate classifications. As surface air temperature and precipitation are used more directly and are reconstructed for the Holocene, only their results for the present-day are revisited at this stage. However, for all considered variables, the mean state is presented reasonably well by PlaSim. Concerning the surface air temperature, a cold bias can be observed over the high northern latitudes, which may be partly caused by the sea-ice mask and the cloud-parameterization in the model. This bias is also influencing the very northern regions of Europe, nevertheless PlaSim captures very similarly the general pattern given by CRU. For the precipitation, which is slightly overestimated over some regions and the global mean, a nevertheless satisfactory similarity, mainly to the climatology GPCP can be observed. These results are a good basis for the following palaeoclimate reconstructions.

Reconstruction of the Holocene climate In this chapter, the European climate over the Holocene is reconstructed using the fully coupled version of PlaSim. To account for the latitudinally different insolation distribution during the Holocene, Europe is sub-divided into four regions in total. As only anomalies (to the preindustrial) are considered here, the previously identified cold bias in the northern regions can be neglected.

Following the insolation changes over the Holocene, a strong cooling (slight warming) can be observed for all four regions during summer (winter). These results are very much in line in terms of trend and amplitude with those by other model studies. Stronger deviations are occurring compared to proxy reconstructions mainly over SW-Europe where a cooling trend by the models is opposing a warming trend in the data. This can be partly attributed to the resolution problem as well as to the model-specific representation of the insolation distribution.

The identification of the "correct" European precipitation evolution over the past 11,000 years is unequally more complicated compared to the temperature trend, which is rather well approved by both models and proxy data. The precipitation itself is a subject of uncertainty in models, even for present-day conditions due to its more complex behavior and the parameterized processes (cf. Chapt. 3). Besides this, stronger similarities between PlaSim and other reconstructions occur over the northern parts of Europe. In contrast, over the southern regions it seems again to be more complicated to capture the correct evolution. Moreover, the models are also differing in the seasonal distribution of the precipitation, i.e. which season is determining the annual mean trend. A variety of models and also PlaSim are in line with showing wetter conditions over the southern regions in winter and also in the annual mean, compared to the preindustrial. This seems to be associated with, on the one hand, drier early Holocene conditions over the northern parts and, on the other hand, lower temperatures during DJF over the whole Europe. This indicates that also model-specific properties, together with resolution problems, may contribute significantly to the representation of the precipitation patterns. Besides these similarities, these shortcomings are a motivation for the further, and most decisive part of this study, which is the assimilation of the proxy data.

Assimilation of proxy time series The motivation for this reconstruction refinement is to achieve a more realistic Holocene climate simulation which is as close as possible to proxy data. However, the approach is not to statistically assimilate the proxy data into the model, but to resimulate the trend which is given by the palaeoobservations. This process requires a preceding profound analysis and selection of the available proxy data, where the keywords are, amongst others, the temporal and spatial resolution, its reliability and dating uncertainty. For the real process of the resimulation of the proxy climate, i.e. the

adjustment of the model climate to the proxy, a new methodology has been implemented. This approach is built upon the oceanic conditions as one of the main drivers in the climate system, using a linear sensitivity relationship between the SST and the adjacent land temperatures. The methodology and the derivation of the sensitivity is introduced in detail in Chapter 5. Also in this context, the cold bias in the high northern latitudes doesn't play a role, as the climate is adjusted and, at a later stage, again only anomalies are considered. In total three alternatives are shown to reconstruct the Holocene climate on the basis of the Lake Ammersee proxy in southern Germany.

The first approach, aiming at the resimulation of three selected time slices during the Holocene, has shown the general applicability of this methodology. Albeit it is not able to capture the overall structure of the proxy including its variability pattern, a convergence of the simulated time slice means to the corresponding proxy means is achieved. Concerning the spatial pattern of the temperature evolution in Europe, based on the reconstruction to the Lake Ammersee climate, regionally differing responses are observed. These are partly in line with the observations, but also partly differing more strongly, which has also been discussed in the previous paragraph. As the aim is a full Holocene and transient reconstruction of the European climate, two modifications of the reconstruction approach are considered. The first is the adjustment based on millennial-scale time slice means and the second is based on the means of a climatological time scale of 40 years. Both are conceived to improve the overall pattern as well as, mainly through the latter, to ameliorate the variability structure. The second alternative clearly shows an enhanced convergence to the proxy mean in nearly all time slices. However, exceptions are found in those time slices, where a shift from a positive to a negative anomaly occurs between two millennia. In those cases, the adjustment is antipodal. Together with the less improved variability structure, this is a clear deficiency of this second alternative. The adjustment on shorter time scales is avoiding this misdirected adjustment, as the correction to the new SST conditions is occurring within the 40 years period. Thus, together with a slightly increased variability pattern, the model's time slice means are converging the proxy mean in all time slices, but in a very dampened manner. This causes only a very weak change in the overall trend for the full Holocene, which is thus very close to the reference. Instead, the trend induced by the millennial-scale reconstruction is much closer to the proxy given evolution.

To compare the results of this new methodology also to the results of the fully coupled simulation, the same representation with the four European regions is chosen. Further investigated is the precipitation pattern which is also subject to change when the SST is changing. Despite some still existing deficiencies in the representation of the regional patterns, clear improvements are achieved, as the results are much closer to those of the proxy data. This is even the case over the southern European region, where the fully coupled PlaSim simulation and several other models fail to capture the correct trends (cf. Chapt. 4).

Besides these achievements, the existing shortcomings of these reconstruction approaches could not have been neglected and required a reconsideration and further modifications. These are pointed out in the respective section and are targeted at an iteration procedure, where the *TS*-experiment is repeated in terms of the resimulation of the three selected time slices. The new aspect is that each time slice is split in segments of 100 years. For these, three to five iterations are carried out until PlaSim converges best to the proxy mean climate, in terms of a minimization of the cost function. If this is achieved, the next 100 years are simulated so that the climate of the whole time slice is reconstructed. The results are encouraging with PlaSim now capturing the major variations of the proxy. The overestimated influence of the preceding time slice, which has led to the misdirected adjustment as well as a temporal lag, can thus be eliminated.

This chapter is closing with a comparison between the simulated as well as the deviated PlaSim-SST and several SST-proxies from the Atlantic basin. The results, showing similar trends and also absolute values, are astonishing, considering the discussed limitations of the results as well as the model- and

proxy-dependent characteristics. This is thus a belated corroboration of the methodology in general.

Vegetation studies After determining the climatic conditions during the Holocene, the vegetation evolution needs to be assessed. The European palaeovegetation is mainly investigated using the dynamic vegetation model CARAIB in a very high resolution. Although only long-term climate means are used as input data, this approach, nevertheless covering the full Holocene, is unique. The changes in vegetation are diagnosed using on the one side the parameter GDD, which is a bioclimatic variable designating the length of the growing season during the year. This is enhanced over the early Holocene at the northern high latitudes - as a direct consequence of the positive insolation anomaly - and induces a northerly shift of the treeline in terms of warmer forest types. With the declining insolation, GDD is also decreasing in the northern and eastern parts of Europe, where, as a direct consequence, the warmer forest types are replaced by colder types and tundra. A longer growing season in the early Holocene is also detected in the warmer southern parts of Europe. However, an opposite trend in terms of an increase in GDD occurs over the northwestern parts of Africa. This is consistent with enhanced vegetation cover which can persist until the mid-Holocene, due to the favorable climatic conditions in terms of mainly an increased precipitation, which has caused the "green Sahara". With decreasing precipitation until the preindustrial, also the vegetation cover is gradually receding, resulting in the desert types of today. These results are in line with other model studies; however they vary slightly to palaeoobservations which can be attributed to the model resolution which may be too large for a smaller region like Europe.

On the other side, the biome distribution gives more insight into a potential change of types during the Holocene, which is already indicated by the climatic changes as well as the GDD variations. The northward shift of the treeline is also directly displayed by a change in the biomes in terms of an expansion of warmer forest types and the instantaneous replacement of colder types. However, due to the missing land ice in the model, the distribution of the warmer types may be overestimated. With the weakening of the positive insolation anomaly in those regions, colder forest types and tundra are expanding in the very northern parts of Europe and the warmer forest types are replaced southward. The southern parts of Europe seem to be very peculiar also in the biome distribution, which is in line to the change in the climatic conditions in these regions. Over SW-Europe, drier conditions during summer lead to an expansion of grassland and woodland types which are receding until the preindustrial as an increase in summer precipitation together with a general cooling are observed. A decline of grassland types is also observed over SE-Europe. In general terms, a mixture of different biome types is observed in those southerly regions at the beginning of the Holocene, which is getting more and more uniform until the late Holocene which is consistent to a moistening and cooling trend in those regions during summer. In general, these studies are mostly in line with other model studies on this topic but are partly diverging from the results given by proxy data. Moreover, especially the early Holocene time slices are an important issue of uncertainty which requires further analyses.

The second part of this chapter is dedicated to the investigation of the effects of extreme changes in the land cover composition on the present-day climate and the vegetation distribution. The latter is investigated using two phenomenological quantities, which are the Koeppen climate classification and the Budyko dryness index. Apart from the influence on the global dynamics and the hydrological properties, these modifications of the initial conditions induce changes in the climate classifications. Two regions are emerging to be most sensitive to the external perturbations which are the northern high latitudes and the desert parts of North Africa respectively. The fact that these changes can be identified with the static climate classifications may be rather advantageous for the future investigation of human-induced changes in land cover, which is revisited in the next paragraph.

7.2 Outlook

One important issue in the context of the fully coupled simulation can be seen in the inclusion of land ice, even in a prescribed form, to achieve an improved representation of the early Holocene climate. Insolation changes together with the changing glacial conditions over the first millennia of the Holocene had an enormous impact on the climate and vegetation evolution, partly also counteracting and outweighing. This could be seen in the temperature evolution of these time slices as well as the distribution of GDD and the biomes, where the too warm climate has led to deficiencies.

The more decisive part for the future is clearly the topic of the assimilation of the proxy time series, i.e. the resimulation of the proxy climate. The proposals are on the hand related to the remarks in Section 5.8 concerning the inclusion of several proxies as a reference; a feature, which should definitely be pursued. On the other hand, and even more essential, some effort should be dedicated to the remarks in Section 5.7 concerning the iteration procedure for the reconstruction of the Holocene climate. It is finally concluded and recommended at this stage, that this should be done in any case to avoid misleadings in the reconstruction as well as to achieve improved results for the European temperature and precipitation patterns. The strong similarity to the SST-proxies is a further motivation for reconsidering the methodology and the setup of new experiments with the modification in terms of the iteration procedure. However, this could not have been implemented into this study for the full Holocene but only for the three selected time slices. This may definitely be a feasible process of finding a synthesis between climate models and proxy data. In any case, the inclusion of proxy time series into climate models is an important issue of the palaeoclimate community and it would be of strong benefit to identify a feasible approach here. The next paragraph is suggesting another, more external, direction of potential future research activities.

Human-climate interaction

At these very final stages of this thesis, the very early paragraphs of this work are reconsidered concerning the larger framework this study is embedded in. With the results gathered in the preceding chapters on the climate and vegetation evolution during the Holocene, a profound basis is provided to further identify the linkages between climate and preindustrial cultures. Until now, only the climatic boundary conditions have been identified which can now be used by GLUES to analyze the early human migration. However, the mutual interaction has not been considered in this context yet, i.e. the influence of humans on climate. However, with the results of the preceding section on climate-vegetation-interaction, an alternative approach is conceived, which can be seen as an anticipatory remark of this interaction. As mentioned at the very early stages of this study (cf. Sect. 1.1.2) and as was shown before, an altered land cover composition has an enormous impact on climate. This has been diagnosed with the rather simple phenomenological quantity, the Koeppen climate classification. It thereby makes no difference whether these changes have a natural or anthropogenic origin (cf. Sect. 6.4). In this context, the rather sensitive behavior of the Koeppen climate classification, with respect to biogeophysical changes, seems to be feasible with respect to future studies of land use changes. In the already addressed modified version of the Koeppen climate classification, which has been used diagnostically here, an additional tool has been added which calculates, at each iteration, new global fields for the land surface parameters, mainly albedo and roughness length, which belong to the essential boundary conditions in the land surface scheme of PlaSim. After their recalculation, they can then be implemented into PlaSim for the next iteration. This procedure would then be a similar asynchronous coupling which has already been discussed for CARAIB in Section 6.3.3 and, moreover, it is also very close to the continuous replacement of the SST during the reconstruction of the Holocene climate presented in Chapter 5. The theory of a full-interaction approach

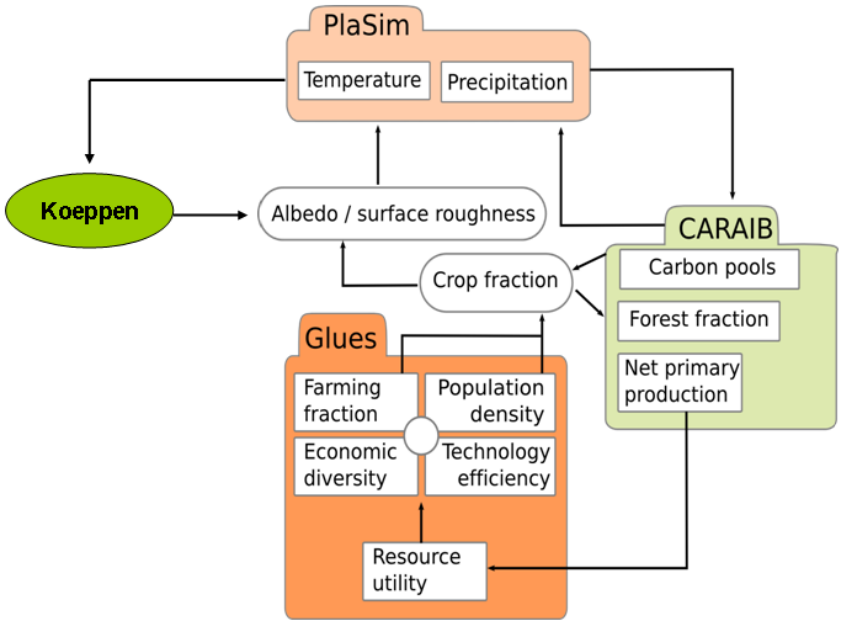

Figure 7.1: Schematic of the coupling of PlaSim and GLUES towards a "Human-Earth-System-Model", provided by C. Lemmen. The variables, obtained by the respective models, are given in circles and their interaction is illustrated with arrows.

is illustrated in Figure 7.1. The variables, provided by the respective models, are given in circles and their interaction is illustrated with arrows. Obtained with PlaSim, the climatic variables are used to calculate the specific vegetation-related parameters with CARAIB or Koeppen. These could then, in principle, be reimplemented into PlaSim, as natural changes in the land cover composition. The new and so far unprecedented part would now be to use the output of either PlaSim or PlaSim-CARAIB to force the model GLUES, which then calculates the anthropogenic influence in terms of crop fraction. This is then transformed into fields for the land surface parameters albedo and surface roughness which can then be, in turn, reimplemented into PlaSim. The natural and anthropogenic part of the land cover changes thereby can of course be combined or rather should be considered together to achieve a more detailed analysis.

This will now round out the whole picture of the linkages between climate and preindustrial cultures and would lead, in the end, to a new "creation" of a model, thus a

"Human-Earth-System-Model".

In fact, there are of course other studies existing which are quantifying the anthropogenic effect on climate. These have already been tackled in Section 1.1.2. In this context, the work by *Kleidon* (2006) with PlaSim-SimBA can also be stated where the author tries to simulate the human impact on climate through modifications of the land surface. His approach is to use the parameter "Human appropriated net primary productivity" HANPP (references in *Kleidon* 2006) which represents the human consumption of the NPP of the biosphere. Assuming different intensities of human NPP, the author tries to quantify the climate sensitivity in terms of global entropy production.

Nevertheless and to now conclude finally, this mutual interaction between climate and humans, respectively its consideration and thus simulation with GLUES, would be a completely new approach in the scientific community. However, it should be said, that up to now, it is only about a theory and outlook for a possible new and interesting direction of future research; indeed, the execution completely goes beyond the scope of this study. Nevertheless, some related studies have already been carried out and presented in *Haberkorn et al.* (2010b). If this multisided approach, i.e. the combination of climate and vegetation reconstructions as well as of human activities, which is also concluded by *Dearing* (2006) as the compulsory tool for a complete understanding of the causes of earth system changes, can be further proceeded, also for other regions in the world, this will very likely lead to fundamentally new insights into the history of climate-culture interaction.

Bibliography

Adler, R. F., G. J. Huffman, A. Chang, R. Ferraro, P.-P. Xie, J. Janowiak, B. Rudolf, U. Schneider, S. Curtis, D. Bolvin, A. Gruber, J. Susskind, P. Arkin, and E. Nelkin, The Version-2 Global Precipitation Climatology Project (GPCP) Monthly Precipitation Analysis (1979-Present), *J. Hydrometeor.*, *4*, 1147–1167, 2003.

Ágústsdóttir, A. M., Abrupt climate changes and the effects of North Atlantic deepwater formation: results from the GENESIS global climate model and comparison with data from the Younger Dryas event and the event at 8200 years BP and the present, Ph.D. thesis, The Pennsylvania State University, University Park, Pennsylvania, USA., 1998.

Alefs, J., Feinstratigraphie und Diatomeensukzession in den Profundalsedimenten des Ammersees und Starnberger Sees (Oberbayern), Ph.D. thesis, Fak. f. Chem., Biol. und Geowiss. der Tech. Univ. München, Munich, Germany, 1997.

Alley, R. B., and A. M. Ágústsdóttir, The 8k event: cause and consequences of a major Holocene abrupt climate change, *Quatern. Sci. Rev.*, *24*, 1123–1149, 2005.

Alley, R. B., P. A. Mayewski, T. Sowers, M. Stuiver, K. C. Taylor, and P. U. Clark, Holocene climatic instability: A prominent, widespread event 8200 yr ago, *Geology*, *25 (6)*, 483–486, 1997.

Asselin, R., Frequency filter for time integration, *Mon Wea. Rev.*, *100*, 487–490, 1972.

Avila, F. B., A. J. Pitman, M. G. Donat, L. V. Alexander, and G. Abramowitz, Climate model simulated changes in temperature extremes due to land cover change, *J. Geophys. Res.*, *117 (D4)*, D04,108, doi:10.1029/2011JD016382, 2012.

Ball, J. T., I. E. Woodrow, and J. A. Berry, A model predicting stomatal conductance and its contribution to the control of photosynthesis under different environmental conditions., *Progress in Photosynthesis Research*, *4:221*, 1987.

Bathiany, S., M. Claussen, V. Brovkin, T. Raddatz, and V. Gayler, Combined biogeophysical and biogeochemical effects of large-scale forest cover changes in the MPI earth system model, *Biogeosciences*, *7*, 1383–1399, doi:10.5194/bg-7-1383-2010, 2010.

Bathiany, S., M. Claussen, and K. Fraedrich, Implications of climate variability for the detection of multiple equilibria and for rapid transitions in the atmosphere-vegetation system, *Clim. Dyn.*, 2011.

Bauer, E., and A. Ganopolski, Simulation of the cold climate event 8200 years ago by meltwater outburst from Lake Agassiz, *Paleoceanography*, *19*, PA3014, doi:10.1029/2004PA001030, 2004.

Beck, C., J. Grieser, M. Kottek, F. Rubel, and B. Rudolf, Characterizing global climate change by means of Köppen Climate Classification, Climate Status Report 2005, Deutscher Wetterdienst, p. 139-149, 2006.

Bendle, J. A. P., and A. Rosell-Melé, High-resolution alkenone sea surface temperature variability on the North Icelandic Shelf: implications for Nordic Seas paleoclimatic development during the Holocene, *The Holocene*, *17 (1)*, 19–24, doi:10.1177/0959683607073269, 2007.

Berger, A., Long-term variations of daily insolation and quarternary climatic change, *J. Atmos. Sci.*, *35*, 2362–2367, 1978b.

Berner, K. S., N. Koç, D. Divine, F. Godtliebsen, and M. Moros, A decadal-scale Holocene sea surface temperature record from the subpolar North Atlantic constructed using diatoms and statistics and its relation to other climate parameters, *Paleoceanography*, *23*, PA2210, doi:10.1029/2006PA001339, 2008.

Betts, R. A., P. M. Cox, S. E. Lee, and F. I. Woodward, Contrasting physiological and structural vegetation feedbacks in climate change simulations, *Nature*, *387*, 796–799, 1997.

Blunier, T., J. Chappellaz, , J. Schwander, B. Stauffer, and D. Raynaud, Variations in atmospheric methane concentration during the Holocene epoch, *Nature*, *374 (6517)*, 46–49, 1995.

Boer, G. J., and B. Yu, Climate sensitivity and response, *Clim. Dyn.*, *20*, 415–429, 2003.

Bond, G., W. Showers, M. Cheseby, R. Lotti, P. Almasi, P. deMenocal, P. Priore, H. Cullen, I. Hajdas, and G. Bonani, A pervasive millennial-scale cycle in North Atlantic Holocene and glacial climates, *Science*, *278*, 2157–1266, 1997.

Bousquet, P., P. Ciais, P. Peylin, M. Ramonet, and P. Monfray, Inverse modeling of annual atmospheric CO_2 sources and sinks 1. Method and control inversion, *J. Geophys. Res.*, *104 (D21)*, 26,161–26,178, 1999a.

Bousquet, P., P. Peylin, P. Ciais, M. Ramonet, and P. Monfray, Inverse modeling of annual atmospheric CO_2 sources and sinks 2. Sensitivity study, *J. Geophys. Res.*, *104 (D21)*, 26,179–26,193, 1999b.

Braconnot, P., B. Otto-Bliesner, S. Harrison, S. Joussaume, J.-Y. Peterchmitt, A. Abe-Ouchi, M. Crucifix, E. Driesschaert, T. Fichefet, C. D. Hewitt, M. Kageyama, A. Kitoh, A. Laîné, M.-F. Loutre, O. Marti, U. Merkel, G. Ramstein, P. Valdes, S. L.Weber, Y. Yu, and Y. Zhao, Results of PMIP2 coupled simulations of the mid-Holocene and Last Glacial Maximum - Part 1: experiments and large-scale features, *Clim. Past*, *3*, 261–277, 2007a.

Braconnot, P., B. Otto-Bliesner, S. Harrison, S. Joussaume, J.-Y. Peterchmitt, A. Abe-Ouchi, M. Crucifix, E. Driesschaert, T. Fichefet, C. D. Hewitt, M. Kageyama, A. Kitoh, M.-F. Loutre, O. Marti, U. Merkel, G. Ramstein, P. Valdes, S. L.Weber, Y. Yu, and Y. Zhao, Results of PMIP2 coupled simulations of the mid-Holocene and Last Glacial Maximum - Part 2: feedbacks with emphasis on the location of the ITCZ and mid- and high latitudes heat budget, *Clim. Past*, *3*, 279–296, 2007b.

Bradley, R. S., *Paleoclimatology: Reconstructing Climates of the Quaternary*, 2. ed., Academic Press, San Diego, Calif., 1999.

Brewer, S., J. Guiot, and F. Torre, Mid-Holocene climate change in Europe: a data-model comparison, *Clim. Past*, *3*, 499–512, 2007.

Brewer, S., L. M. François, R. Cheddadi, J.-M. Laurent, and E. Favre, Comparison of simulated and observed vegetation for the mid-Holocene in Europe, *Clim. Past Discuss.*, *5*, 965–1011, 2009.

Brovkin, V., A. Ganopolski, and Y. Svirezhev, A continuous climate-vegetation classification for use in climate-biosphere studies, *Ecological modelling*, *101 (2-3)*, 251–261, 1997.

Brovkin, V., M. Claussen, V. Petoukhov, and A. Ganopolski, On the stability of the atmosphere-vegetation system in the Sahara/Sahel region, *J. Geophys. Res.*, *103 (D24)*, 31,613–31,624, 1998.

Brovkin, V., A. Ganopolski, M. Claussen, C. Kubatzki, and V. Petoukhov, Modelling climate response to historical land cover change, *Global Ecology and Biogeography*, *8*, 509–517, 1999.

Brovkin, V., J. Bendtsen, M. Claussen, A. Ganopolski, C. Kubatzki, V. Petoukhov, and A. Andreev, Carbon cycle, vegetation, and climate dynamics in the Holocene: Experiments with the CLIMBER-2 model, *Global Biogeochem. Cycl.*, *16 (4)*, 1139, 2002.

Brovkin, V., S. Levis, M.-F. Loutre, M. Crucifix, M. Claussen, A. Ganopolski, C. Kubatzki, and V. Petoukhov, Stability analysis of the climate-vegetation system in the northern high latitudes, *Climatic Change*, *57*, 119–138, 2003.

Brovkin, V., M. Claussen, E. Driesschaert, T. Fichefet, D. Kicklighter, M. F. Loutre, H. D. Matthews, N. Ramankutty, M. Schaeffer, and A. Sokolov, Biogeophysical effects of historical land cover changes simulated by six Earth system models of intermediate complexity, *Clim. Dyn.*, *26 (6)*, 587–600, 2006.

Brovkin, V., T. Raddatz, C. Reick, M. Claussen, and V. Gayler, Global biogeophysical interactions between forest and climate, *Geophys. Res. Lett.*, *36 (7)*, L07,405, doi:10.1029/2009GL037543, 2009.

Budyko, M. I., Evaporation under natural conditions, Gidrometeorizdat, Leningra, English translation by IPST, Jerusalem, 1948.

Budyko, M. I., The heat balance of the earth‘s surface, U.S. Dept of Commerce, Washington, 1958.

Budyko, M. I., *Climate and Life*, Academic Press, N. Y., 1974.

Büntgen, U., W. Tegel, K. Nicolussi, M. McCormick, D. Frank, V. Trouet, J. O. Kaplan, F. Herzig, K.-U. Heussner, H. Wanner, J. Luterbacher, and J. Esper, 2500 Years of European Climate Variability and Human Susceptibility, *Science*, *331*, 578–582, 2011.

Burke, A., O. Marchal, L. I. Bradtmiller, J. F. McManus, and R. François, Application of an inverse method to interpret ^{231}Pa/^{230}Th observations from marine sediments, *Paleoceanography*, *26*, PA1212, doi:10.1029/2010PA002022, 2011.

Cacho, I., J. O. Grimalt, M. Canals, L. Sbaffi, N. J. Shackleton, J. Schönfeld, and R. Zahn, Variability of the western Mediterranean Sea surface temperature during the last 25,000 years and its connection with the Northern Hemisphere climatic changes, *Paleoceanography*, *16 (1)*, 40–52, 2001.

Calvo, E., J. Grimalt, and E. Jansen, High-resolution U_{37}^K sea surface temperature reconstruction in the Norwegian Sea during the Holocene, *Quat. Sci. Rev.*, *21*, 1385–1394, 2002.

Carter, T. R., R. N. Jones, X. Lu, S. Bhadwal, C. Conde, L. O. Mearns, B. C. O'Neill, M. D. A. Rounsevell, and M. B. Zurek, *Climate Change 2007: Impact, Adaptation and Vulnerability. Contribution of Working Group II to the Fourth Assessment Report of the Intergovernmental Panel on Climate Change*, chap. New Assessment Methods and the Characterisation of Future Conditions (2), pp. 133–172, Cambridge University Press, Cambridge, UK, 2007.

Casely, A. F., and A. J. Dugmore, Good for glaciers, bad for people? Archaeologically relevant climate models developed from reconstructions of glacier mass balance, *Jounal of Archaeological Science*, *34*, 1763–1773, 2007.

Charney, J. G., Dynamics of deserts and droughts in the Sahel, *Quart. J. Roy. Meteorol. Soc.*, *101 (428)*, 193–202, 1975.

Claussen, M., On coupling global biome models with climate models, *Clim. Research*, *4*, 203–221, 1994.

Claussen, M., Modeling bio-geophysical feedback in the African and Indian monsoon region, *Clim. Dyn.*, *13*, 247–257, 1997.

Claussen, M., On multiple solutions of the atmosphere-vegetation system in present-day climate, *Global Change Biology*, *4*, 549–559, 1998.

Claussen, M., and V. Gayler, The greening of the Sahara during the mid-Holocene: results of an interactive atmosphere-biome model, *Global Ecology and Biogeography Letters*, *6*, 369–377, 1997.

Claussen, M., C. Kubatzki, V. Brovkin, A. Ganopolski, P. Hoelzmann, and H.-J. Pachur, Simulation of an abrupt change in Saharan vegetation in the mid-Holocene, *Geophys. Res. Lett.*, *26*, 2037–2040, 1999.

Claussen, M., V. Brovkin, and A. Ganopolski, Biogeophysical versus biogeochemical feedbacks of large-scale land cover change, *Geophys. Res. Letters*, *28 (6)*, 1011–1014, 2001.

Claussen, M., L. A. Mysak, A. J. Weaver, M. Crucifix, T. Fichefet, M.-F. Loutre, S. L. Weber, J. Alcamo, V. A. Alexeev, A. Berger, R. Calov, A. Ganopolski, H. Goosse, G. Lohmann, F. Lunkeit, I. I. Mokhov, V. Petoukhov, P. Stone, and Z. Wang, Earth system models of intermediate complexity: closing the gap in the spectrum of climate system models , *Clim. Dyn.*, *18*, 579–586, 2002.

Clement, A. C., R. Burgman, and J. R. Norris, Observational and model evidence for positive low-level cloud feedback, *Science*, *325*, 460–463, 2009.

Collatz, J. G., M. Ribas-Carbo, and A. J. Berry, Coupled photosynthesis-stomatal conductance model for leaves of C_4 plants, *J. Plant. Physiol.*, *19*, 519–538, 1992.

Cramer, W., A. Bondeau, F. I. Woodward, I. C. Prentice, R. A. Betts, V. Brovkin, P. M. Cox, V. Fisher, J. A. Foley, A. D. Friend, C. Kucharik, M. R. Lomas, N. Ramankutty, S. Sitch, B. Smith, A. White, and C. Young-Molling, Global response of terrestrial ecosystem structure and function to CO2 and climate change: results from six dynamic global vegetation models, *Global change biology*, *7 (4)*, 357–373, 2001.

Crowley, T. J., and S. K. Baum, Effect of vegetation on an ice-age climate model simulation, *J. Geophys. Res.*, *102 (14)*, 443–480, 1997.

Crucifix, M., M. Loutre, P. Tulkens, T. Fichefet, and A. Berger, Climate evolution during the Holocene: a study with an Earth system model of intermediate complexity, *Clim. Dyn.*, *19*, 43–60, 2002.

Cullen, H. M., P. B. deMenocal, S. Hemming, G. Hemming, F. H. Brown, T. Guilderson, and F. Sirocko, Climate change and the collapse of the Akkadian empire: Evidence from the deep sea, *Geology*, *28*, 379–382, 2000.

Czymzik, M., P. Dulski, B. Plessen, U. von Grafenstein, R. Naumann, and A. Brauer, A 450 year record of spring-summer flood layers in annually laminated sediments from Lake Ammersee (southern Germany), *Water Resour. Res.*, *46 (11)*, W11,528, doi:10.1029/2009WR008360, 2010.

D'Andrea, W. J., Y. Huang, S. C. Fritz, and N. J. Anderson, Abrupt Holocene climate change as an important factor for human migration in West Greenland, *Proc. Nat. Acad. Sci.*, *108 (24)*, 2011.

Dansgaard, W., Stable isotopes in precipitation, *Tellus*, *16 (4)*, 436–468, 1964.

Davis, B., S. Brewer, A. Stevenson, J. Guiot, and D. Contributors, The temperature of Europe during the Holocene reconstructed from pollen data, *Quatern. Sci. Rev.*, *22*, 1701–1716, 2003.

Davis, B. A. S., and S. Brewer, Orbital forcing and role of the latitudinal insolation/temperature gradient, *Clim. Dyn.*, *32*, 143–165, 2009.

de Noblet, N. I., I. C. Prentice, S. Joussaume, D. Texier, A. Botta, and A. Haxeltine, Possible role of atmosphere-biosphere interactions in triggering the last glaciation, *Geophys. Res. Lett.*, *23 (22)*, 3191–3194, 1996.

de Noblet-Ducoudré, N., M. Claussen, and I. C. Prentice, Mid-Holocene greening of the Sahara: first results of the GAIM 6000 year BP Experiment with two asynchronously coupled atmosphere/biome models, *Clim. Dyn.*, *16 (9)*, 643–659, 2000.

Dearing, J. A., Climate-human-environment interactions: resolving our past, *Clim. Past*, *2*, 187–203, 2006.

Dee, D. P., S. M. Uppala, A. J. Simmons, P. Berrisford, P. Poli, S. Kobayashi, U. Andrae, M. A. Balmaseda, G. Balsamo, P. Bauer, P. Bechtold, A. C. M. Beljaars, L. van de Berg, J. Bidlot, N. Bormann, C. Delsol, R. Dragani, M. Fuentes, A. J. Geer, L. Haimberger, S. B. Healy, H. Hersbach, E. V. Hólm, L. Isaksen, P. Kållberg, M. Köhler, M. Matricardi, A. P. McNally, B. M. Monge-Sanz, J.-J. Morcrette, B.-K. Park, C. Peubey, P. de Rosnay, C. Tavolato, J.-N. Thépaut, and F. Vitart, The ERA-Interim reanalysis: configuration and performance of the data assimilation system, *Q. J. R. Meteorol. Soc.*, *137 (656)*, 553–597, 2011.

Dekker, S. C., H. de Boer, V. Brovkin, K. Fraedrich, M. J. Wassen, and M. Rietkerk, Biogeophysical feedbacks trigger shifts in the modelled vegetation-atmosphere system at multiple scales, *Biogeosciences*, *7*, 1237–1245, 2010.

deMenocal, P. B., Cultural responses to climate change during the late Holocene, *Science*, *292*, 667–673, 2001.

deMenocal, P. B., J. Ortiz, T. Guilderson, J. Adkins, M. Sarnthein, L. Baker, and M. Yarusinsky, Abrupt onset and termination of the African Humid Period: rapid climate responses to gradual insolation forcing, *Quaternary science reviews*, *19*, 347–361, 2000a.

deMenocal, P. B., J. Ortiz, T. Guilderson, and M. Sarnthein, Coherent High- and Low-Latitude Climate Variability during the Holocene Warm Period, *Science*, *288*, 2198–2202, 2000b.

Diamond, J., *Guns, germs and steel - The fates of human societies*, W. W. Norton & Company, Inc., 500 Fifth Avenue, New York, NY 10110, 1997.

Diamond, J., *Collapse - How societies choose to fail or succeed*, Penguin Books, 2006.

Diaz, H. F., and J. K. Eischeid, Disappearing "alpine tundra" Köppen climate type in the western United States, *Geophys. Res. Lett.*, *34*, L 18,707, doi:10.1029/2007GL031253, 2007.

Donohue, R. J., M. L. Roderick, and T. R. McVicar, On the importance of including vegetation dynamics in Budyko's hydrological model, *Hydrol. Earth Syst. Sci.*, *11*, 983–995, 2007.

Drysdale, R., G. Zanchetta, J. Hellstrom, R. Maas, A. Fallick, M. Pickett, I. Cartwright, and L. Piccini, Late Holocene drought responsible for the collapse of Old World civilizations is recorded in an Italian cave flowstone, *Geology*, *34*, 101–104, 2006.

Eliasen, E., B. Machenhauer, and E. Rasmussen, On a numerical method for integration of the hydrodynamic equations with a spectral representation of the horizontal fields, *report*, Copenhagen, Denmark, 1970.

Emeis, K. C., and A. Dawson, Holocene palaeoclimate records over Europe and the North-Atlantic, *The Holocene*, *13 (3)*, 305–309, doi:10.1191/0959683603hl622ed, 2003.

Emeis, K.-C., U. Struck, T. Blanz, A. Kohly, and M. Voss, Salinity changes in the Central Baltic Sea (NW Europe) over the last 10,000 years, *The Holocene*, *13 (3)*, 413–423, 2003.

Evensen, G., Sequential data assimilation with a nonlinear quasi-geostrophic model using Monte Carlo methods for forecast error statistics, *J. Geophys. Res.*, *10*, 10,143–10,162, 1994.

Evensen, G., Advanced data assimilation for strongly nonlinear dynamics, *Mon. Wea. Rev.*, *125 (6)*, 1342–1354, 1997.

Evensen, G., The Ensemble Kalman Filter: theoretical formulation and practical implementation, *Ocean Dyn.*, *53*, 343–367, 2003.

Farquhar, G. D., S. van Caemmerer, and J. A. Berry, A biogeochemical model of photosynthetic CO_2 assimilation on leaves of C_3 species, *Planta*, *149*, 78–90, 1980.

Favre, E., L. M. François, T. Utescher, J.-P. Suc, A.-J. Henrot, and K. H. an R. Cheddadi, Improving the classification of plant functional types in dynamic vegetation modelling for the Neogene, *Geophys. Res. Abstr.*, *12:EGU2010-3429,3*, 2010.

Feynman, J., and A. Ruzmaikin, Climate stability and the development of agricultural societies, *Clim. Change*, *84*, 295–311, doi:10.1007/s10584-007-9248-1, 2007.

Findell, K. L., E. Shevliakova, P. C. D. Milly, and R. J. Stouffer, Modeled Impact of Anthropogenic Land Cover Change on Climate, *J. Climate*, *20*, 3621–3634, 2007.

Fischer, N., and J. H. Jungclaus, Effects of orbital forcing on atmosphere and ocean heat transports in Holocene and Eemian climate simulations with a comprehensive Earth system model, *Clim. Past*, *6*, 155–168, 2010.

Fischer, N., and J. H. Jungclaus, Evolution of the seasonal temperature cycle in a transient Holocene simulation: orbital forcing and sea-ice, *Clim. Past*, *7*, 1139–1148, doi:10.5194/cp-7-1139-2011, 2011.

Foley, J. A., S. Levis, I. C. Prentice, D. Pollard, and S. L. Thompson, Coupling dynamic models of climate and vegetation, *Global change biology*, *4 (5)*, 561–579, 1998.

Foley, J. A., S. Levis, M. H. Costa, W. Cramer, and D. Pollard, Incorporating dynamic vegetation cover within global climate models, *Ecological Applications*, *10 (6)*, 1620–1632, 2000.

Fraedrich, K., A parsimonious stochastic water reservoir: Schreiber's 1904 Equation, *Notes and Correspondence*, *11*, 575–578, doi:10.1175/2009JHM1179.1, 2010.

Fraedrich, K., A suite of user-friendly global climate models: Hysteresis experiments, *Eur. Phys. J. Plus*, *127*, doi:10.1140/epjp/i2012-12053-7, 2012.

Fraedrich, K., and F. Lunkeit, Diagnosing the entropy budget of a climate model, *Tellus A*, *60*, 921–931, 2008.

Fraedrich, K., and F. Sielmann, An equation of state for land surface climates, *International Journal of Bifurcation and Chaos*, *21 (12)*, 3577–3587, doi:10.1142/S021812741103074X, 2011.

Fraedrich, K., A. Kleidon, and F. Lunkeit, A green planet versus a desert world: estimating the effect of vegetation extremes on the atmosphere, *J. Climate*, *12*, 3156–3163, 1999.

Fraedrich, K., F.-W.-Gerstengarbe, and P. C. Werner, Climate shifts during the last century, *Clim. Change*, *50*, 405–417, 2001.

Fraedrich, K., E. Kirk, U. Luksch, and F. Lunkeit, Ein Zirkulationsmodell für Forschung und Lehre, *Promet*, *29*, 34–48, 2003.

Fraedrich, K., H. Hansen, E. Kirk, U. Luksch, and F. Lunkeit, The Planet Simulator: Towards a user friendly model, *Meteorol. Z.*, *14*, 299–304, doi:10.1127/0941-2948/2005/0043, 2005a.

Fraedrich, K., H. Hansen, E. Kirk, and F. Lunkeit, The Planet Simulator: Green planet and desert world, *Meteorol. Z.*, *14*, 305–314, doi:10.1127/0941-2948/2005/0044, 2005b.

Fraedrich, K., E. Kirk, U. Luksch, and F. Lunkeit, The Portable University Model of the Atmosphere (PUMA): Strom track dynamics and low frequency variability, *Meteorol. Z.*, *14*, 735–745, doi:10.1127/0941-2948/2005/0074, 2005c.

François, L. M., C. Delire, P. Warnant, and G. Munhoven, Modelling the glacial-interglacial changes in the continental biosphere, *Global Planet. Change*, *16-17*, 37–52, 1998.

François, L. M., Y. Goddéris, P. Warnant, G. Ramstein, N. de Noblet, and S. Lorenz, Carbon stocks and isotopic budgets of the terrestrial biosphere at mid-Holocene and last glacial maximum times, *Chemical Geology*, *159*, 163–189, 1999.

François, L. M., M. Ghislain, D. Otto, and A. Micheels, Late Miocene vegetation reconstruction with the CARAIB model, *Palaeogeography, Palaeoclimatology, Palaeoecology*, *238*, 302–320, doi:10.1016/j.palaeo.2006.03.034, 2006.

François, L. M., T. Utescher, E. Favre, A.-J. Henrot, P. Warnant, A. Micheels, B. Erdei, J.-P. Suc, R. Cheddadi, and V. Mosbrugger, Modelling Late Miocene vegetation in Europe: Results of the CARAIB model and comparison with palaeovegetation data, *Palaeogeogr., Palaeoclimatol., Palaeoecol.*, *304*, 359–378, doi:10.1016/j.palaeo.2011.01.012, 2011.

Gaillard, M.-J., S. Sugita, F. Mazier, A.-K. Trondman, A. Broström, T. Hickler, J. O. Kaplan, E. Kjellström, U. Kokfelt, P. Kuneš, C. Lemmen, P. Miller, J. Olofsson, A. Poska, M. Rundgren, B. Smith, G. Strandberg, R. Fyfe, A. B. Nielsen, T. Alenius, L. Balakauskas, L. Barnekow, H. J. B. Birks, A. Bjune, L. Björkman, T. Giesecke, K. Hjelle, L. Kalnina, M. Kangur, W. O. van der Knaap, T. Koff, P. Lagerås, M. Latałowa, M. Leydet, J. Lechterbeck, M. Lindbladh, B. Odgaard, S. Peglar, U. Segerström, H. von Stedingk, and H. Seppä, Holocene land-cover reconstructions for studies on land cover-climate feedbacks, *Clim. Past*, *6*, 483–499, doi:10.5194/cp-6-483-2010, 2010.

Galy, V., L. François, C. France-Lanord, P. Faure, H. Kudrass, F. Palhol, and S. K. Singh, C4 plants decline in the Himalayan basin since the Last Glacial Maximum, *Quaternary Science Reviews*, *27*, 1396–1409, 2008.

Ganopolski, A., V. Petoukhov, S. Rahmstorf, V. Brovkin, M. Claussen, A. Eliseev, and C. Kubatzki, Climber-2: a climate system model of intermediate complexity. Part II: model sensitivity, *Clim. Dyn.*, *17*, 735–751, 2001.

Garreta, V., P. A. Miller, J. Guiot, C. Hély, S. Brewer, M. T. Sykes, and T. Litt, A method for climate and vegetation reconstruction through the inversion of a dynamic vegetation model, *Clim. Dyn.*, *35*, 371–389, 2010.

Gates, W. L., AMIP: The Atmospheric Model Intercomparison Project, *Bull. Amer. Meteor. Soc.*, *73*, 1962–1970, 1992.

Ghent, D., J. Kaduk, J. Remedios, J. Ardö, and H. Balzter, Assimilation of land surface temperature into the land surface model JULES with an ensemble Kalman filter, *J. Geophys. Res.*, *115 (D19)*, D19,112, 2010.

Gibson, J., P. Kållberg, S. Uppala, A. Hernandez, A. Nomura, and E. Serrano, ERA Description, *Tech. Rep. 1*, ECMWF Re-Analysis Project Report Series, 1997.

Gnanadesikan, A., and R. J. Stouffer, Diagnosing atmosphere-ocean general circulation model errors relevant to the terrestrial biosphere using the Köppen climate classification, *Geophys. Res. Lett.*, *33 (22)*, L22,701, doi:10.1029/2006GL028098, 2006.

Göckede, M., A. M. Michalak, D. Vickers, D. P. Turner, and B. E. Law, Atmospheric inverse modeling to constrain regional-scale CO_2 budgets at high spatial and temporal resolution, *J. Geophys. Res.*, *115 (D15)*, D15,113, doi:10.1029/2009JD012257, 2010a.

Göckede, M., D. P. Turner, A. M. Michalak, D. Vickers, and B. E. Law, Sensitivity of a subregional scale atmospheric inverse CO_2 modeling framework to boundary conditions, *J. Geophys. Res.*, *115 (D24)*, D24,112, doi:10.1029/2010JD014443, 2010b.

Good, P., J. M. Gregory, and J. A. Lowe, A step-response simple climate model to reconstruct and interpret AOGCM projections, *Geophys. Res. Lett.*, *38 (1)*, L01,703, doi:10.1029/2010GL045208, 2011.

Goosse, H., H. Renssen, A. Timmermann, R. S. Bradley, and M. E. Mann, Using paleoclimate proxy data to select optimal realisations in an ensemble of simulations of the climate of the past millennium, *Clim. Dyn.*, *27*, 165–184, 2006.

Goosse, H., E. Crespin, A. de Montety, M. E. Mann, H. Renssen, and A. Timmermann, Reconstructing surface temperature changes over the past 600 years using climate model simulations with data assimilation, *J. Geophys. Res.*, *115 (D9)*, D09,108, doi:10.1029/2009JD012737, 2010.

Green, A. E. S., Attenuation by ozone and the earth's albedo in the middle ultraviolet, *Appl. Opt.*, *3*, 203–208, 1964.

Gregory, J. M., W. J. Ingram, M. A. Palmer, G. S. Jones, P. A. Stott, R. B. Thorpe, J. A. Lowe, T. C. Johns, and K. D. Williams, A new method for diagnosing radiative forcing and climate sensitivity, *Geophys. Res. Lett.*, *31*, L03,205, doi:10.1029/2003GL018747, 2004.

Gronenborn, D., *Die Anfänge der Landwirtschaft und die frühe Gesellschaftsentwicklung zwischen Orient und Europa*, Zeitreise Heldenberg-geheimnisvolle Kreisgräben, Berger Horn, Wien, 2005.

Grootes, P. M., M. Stuiver, J. W. C. White, S. Johnsen, and J. Jouzel, Comparison of oxygen isotope records from the GISP2 and GRIP Greenland ice cores, *Nature*, *366*, 552–554, 1993.

Grosfeld, K., G. Lohmann, and N. Rimbu, The impact of Atlantic and Pacific Ocean sea surface temperature anomalies on the North Atlantic multidecadal variability, *Tellus*, *60A (4)*, 1–14, 2008.

Guetter, P. J., and J. E. Kutzbach, A modified Köppen classification applied to model simulations of glacial and interglacial climates, *Clima. Change*, *16 (2)*, 193–215, 1990.

Guiot, J., S. P. Harrison, and I. C. Prentice, Reconstruction of Holocene precipitation patterns in Europe using pollen and lake-level data, *Quatern. Res.*, *40*, 139–149, 1993.

Guiot, J., F. Torre, D. Jolly, O. Peyron, J. J. Boreux, and R. Cheddadi, Inverse vegetation modeling by Monte Carlo sampling to reconstruct paleoclimates under changed precipitation seasonality and CO_2 conditions: application to glacial climate in Mediterranean region, *Ecol. Model.*, *127*, 119–140, 2000.

Guiot, J., H. B. Wu, V. Garreta, C. Hatté, and M. Magny, A few prospective ideas on climate reconstruction: from a statistical single proxy approach towards a multi-proxy and dynamical approach, *Clim. Past*, *5*, 571–583, 2009.

Haberkorn, K., R. Blender, F. Lunkeit, and K. Fraedrich, Reconstructing Holocene climate using a climate model: Model strategy and preliminary results, Geophysical Research Abstracts, EGU General Assembly 2009, Vol. 11, EGU2009-9058, 2009a.

Haberkorn, K., F. Sielmann, F. Lunkeit, E. Kirk, A. Schneidereit, and K. Fraedrich, Planet Simulator Climate, *Scientific report*, Hamburg, Germany, available from http://www.mi.uni-hamburg.de/Downloads-un.245.0.html[accessed 2011-09-05], 2009b.

Haberkorn, K., K. Fraedrich, A.-J. Henrot, L. François, P. Warnant, M. Dury, E. Favre, and G. Munhoven, European vegetation evolution during the Holocene simulated by Planet Simulator and CARAIB, Geophysical Research Abstracts, EGU General Assembly 2010, Vol. 12, EGU2010-8204-1, 2010a.

Haberkorn, K., C. Lemmen, R. Blender, F. Lunkeit, and K. Fraedrich, Reconstructing socially relevant Holocene climate using proxy records and a climate model, Abstract PP41B-1643, presented at 2010 Fall Meeting, AGU, San Francisco, Calif., 13-17 Dec, 2010b.

Haberkorn, K., C. Lemmen, R. Blender, and K. Fraedrich, Iterative land proxy based reconstruction of SST for the simulation of terrestrial Holocene climate, *Earth Syst. Dynam. Discuss.*, *3*, 149–200, doi:10.5194/esdd-3-149-2012, 2012.

Hagemann, S., K. Arpe, and L. Bengtsson, Validation of the hydrological cycle of ERA-40, *ERA-40 Project Report Series 24*, ECMWF, workshop on Re-analysis, Reading, United Kingdom, ECMWF, 2005.

Hanasaki, N., S. Kanae, T. Oki, K. Masuda, K. Motoya, N. Shirakawa, Y. Shen, and K. Tanaka, An integrated model for the assessment of global water resources Part 1: Model description and input meteorological forcing, *Hydrol. Earth Syst. Sci.*, *12*, 1007–1025, 2008.

Hartmann, D. L., M. E. Ockert-Bell, and M. K. Michelsen, The effect of cloud type on Earth's energy balance: Global analysis, *J. Clim.*, *5*, 1281–1304, 1992.

Hegerl, G. C., F. W. Zwiers, P. Braconnot, N. P. Gillett, Y. Luo, J. A. M. Orsini, N. Nicholls, J. E. Penner, and P. A. Stott, *Climate Change 2007: The Physical Science Basis. Contribution of Working Group I to the Fourth Assessment Report of the Intergovernmental Panel on Climate Change*, chap. Understanding and attributing climate change (9), pp. 664–745, Cambridge University Press, Cambridge, United Kingdom and New York, NY, USA, 2007.

Henderson-Sellers, A., Continental vegetation as a dynamic component of a global climate model - a preliminary assessment, *Clim. Change*, *23 (4)*, 337–377, 1993.

Hendl, M., *Das Klimasystem der Erde*, chap. Globale Klimaklassifikation, pp. 218–266, Dt. Verlag d. Wiss., Berlin, 1991.

Henrot, A.-J., Modelling climate and vegetation interactions. Application to the study of paleoclimates and paleovegetation, Ph.D. thesis, Université de Liège, Faculté des Sciences, 2010.

Henrot, A.-J., L. François, S. Brewer, and G. Munhoven, Impacts of land surface properties and atmospheric CO_2 on the Last Glacial Maximum climate: a factor separation analysis, *Clim. Past*, *5*, 183–202, 2009.

Henrot, A.-J., L. François, E. Favre, M. Butzin, M. Ouberdous, and G. Munhoven, Effects of CO_2, continental distribution, topography and vegetation changes on the climate at the Middle Miocene: a model study, *Clim. Past*, *6*, 675–694, 2010.

Herbert, T. D., and J. D. Schuffert, History of sea surface temperature variations in Cariaco Basin over a full glacial-interglacial cycle, *Scientific Results*, *165*, 239–347, 2000.

Hoskins, B. J., and A. J. Simmons, A multi-layer spectral model and the semi-implicit method, *Quart. J. Roy. Meteorol. Soc.*, *101*, 637–655, 1975.

Hubert, B., L. François, P. Warnant, and D. Strivay, Stochastic generation of meteorological variables and effects on global models of water and carbon cycles in vegetation and soils, *J. Hydrol.*, *212-213*, 318–334, 1998.

Imbrie, J., E. A. Boyle, S. C. Clemens, A. Duffy, W. R. Howard, G. Kukla, J. Kutzbach, D. G. Martinson, A. McIntyre, A. C. Mix, B. Molfino, J. J. Morley, L. C. Peterson, N. G. Pisias, W. L. Prell, M. E. Raymo, N. J. Shackleton, and J. R. Toggweiler, On the structure and origin of major glaciation cycles: 1. Linear responses to Milankovitch forcing, *Paleoceanography*, *7*, 701–738, 1992.

Indermühle, A., T. F. Stocker, F. Joos, H. J. Smith, M. Wahlen, B. Deck, D. Mastroianni, J. Tschumi, T. Blunier, R. Meyer, and B. Stauffer, Holocene carbon-cycle dynamics based on CO_2 trapped in ice at Taylor Dome, Antarctica, *Nature*, *398*, 121–126, 1999.

Istanbulluoglu, E., T. Wang, O. M. Wright, and J. D. Lenters, Interpretation of hydrologic trends from a water balance perspective: The role of groundwater storage in the Budyko hypothesis, *Water Resour. Res.*, *48 (0)*, W00H16, 2012.

Jansen, E., J. Overpeck, K. R. Briffa, J.-C. Duplessy, F. Joos, V. Masson-Delmotte, D. Olago, B. Otto-Bliesner, W. R. Peltier, S. Rahmstorf, R. Ramesh, D. Raynaud, D. Rind, O. Solomina, R. Villalba, and D. Zhang, *Climate Change 2007: The Physical Science Basis. Contribution of Working Group I to the Fourth Assessment Report of the Intergovernmental Panel on Climate Change*, chap. Palaeoclimate (6), pp. 433–498, Cambridge University Press, Cambridge, United Kingdom and New York, NY, USA, 2007.

Jimenez-Moreno, G., Progressive substitution of a subtropical forest for a temperate one during the middle Miocene climate cooling in Central Europe according to palynogical data from cores Tengelic-2 and Hidas-53 (Pannonian Basin, Hungary, *Rev. Palaeobot. Palynol.*, *142*, 1–14, 2006.

Jimenez-Moreno, G., S. Fauquette, and J.-P. Suc, Vegetation, climate and palaeoaltitude reconstructions of the Eastern Alps during the Miocene based on pollen records from Austria, Central Europe, *J. Biogeogr.*, *35*, 1638–1649, 2008.

Jones, J., and M. Widmann, Reconstructing large-scale variability from paleoclimatic evidence by means of data assimilation through upscaling and nudging (DATUN), in *The KIHZ project: towards a synthesis of Holocene proxy data and climate models*, edited by H. Fischer, G. Lohmann, G. Flöser, H. Miller, H. von Storch, and J. F. Negendank, Springer, Berlin, 2003.

Jones, P. D., and M. E. Mann, Climate over past millennia, *Rev. Geophys.*, *42*, RG2002, 2004.

Jones, P. D., T. J. Osborn, and K. R. Briffa, Estimating sampling errors in large-scale temperature averages, *J. Clim.*, *10*, 2548–2568, 1997.

Jones, P. D., K. R. Briffa, T. P. Barnett, and S. F. B. Tett, High-resolution palaeoclimatic records for the last millennium: interpretation, integration and comparison with General Circulation Model control-run temperatures, *Holocene*, *8 (4)*, 455–471, 1998.

Joussaume, S., and P. Braconnot, Sensitivity of paleoclimate simulation results to season definitions, *J. Geophys. Res.*, *102 (D2)*, 1943–1956, 1997.

Joussaume, S., K. E. Taylor, P. Braconnot, J. F. B. Mitchell, J. E. Kutzbach, S. P. Harrison, I. C. Prentice, A. J. Broccoli, A. Abe-Ouchi, P. Bartlein, C. Bonfils, B. Dong, J. Guiot, K. Herterich, C. D. Hewitt, D. Jolly, J. W. Kim, A. Kislov, A. Kitoh, M. F. Loutre, V. Masson, B. McAvaney, N. McFarlane, N. de Noblet, W. R. Peltier, J. Y. Peterschmitt, D. Pollard, D. Rind, J. F. Royer, M. E. Schlesinger, J. Syktus, S. Thompson, P. Valdes, G. Vettoretti, R. S. Webb, and U. Wyputta, Monsoon changes for 6000 years ago: Results of 18 simulations from the Paleoclimate Modeling Intercomparison Project (PMIP), *Geophysical Res. Lett.*, *26 (7)*, 859–862, 1999.

Kållberg, P., P. Berrisford, B. Hoskins, A. Simmons, S. Uppala, S. Lamy-Thépaut, and R. Hine, ERA-40 Project report series. 19. ERA-40 Atlas, ECMWF, workshop on Re-analysis, Reading, United Kingdom, ECMWF, 2005.

Kalnay, E., M. Kanamitsu, R. Kistler, W. Collins, D. Deaven, L. Gandin, M. Iredell, S. Saha, G. White, J. W. Y. Zhu, A. Leetmaa, R. Reynolds, M. Chelliah, W. Ebisuzaki, W.Higgins, J. Janowiak, K. C. Mo, C. Ropelewski, J. Wang, R. Jenne, and D. Joseph, The NCEP/NCAR 40-Year Reanalysis Project, *Bull. Amer. Meteorol. Soc.*, *77*, 437–471, 1996.

Kalvová, J., T. Halenka, K. Bezpalcová, and I. Nemešová, Köppen Climate types in observed and simulated climates, *Stud. Geophys. Geod.*, *47*, 185–202, 2003.

Kaplan, J. O., K. M. Krumhardt, E. C. Ellis, W. F. Ruddiman, C. Lemmen, and K. Klein Goldewijk, Holocene carbon emissions as a result of anthropogenic land cover change, *The Holocene*, *21*(5), 775–791, doi:10.1177/0959683610386983, 2011.

Keigwin, L. D., and E. A. Boyle, Detecting Holocene changes in thermohaline circulation, *PNAS*, *97 (4)*, 1343–1346, 2000.

Keigwin, L. D., J. P. Sachs, Y. Rosenthal, and E. A. Boyle, The 8200 year BP event in the slope water system, western subpolar North Atlantic, *Paleoceanography*, *20*, PA2003, doi:10.1029/2004PA001074, 2005.

Kim, J.-H., and R. R. Schneider, GHOST global database for alkenone-derived Holocene sea-surface temperature records, http://www.pangaea.de/Projetcs/GHOST, 2004.

Kim, J.-H., N. Rimbu, S. J. Lorenz, G. Lohmann, S.-I. Nam, S. Schouten, C. Rühlemann, and R. R. Schneider, North Pacific and North Atlantic sea-surface temperature variability during the Holocene, *Quartern. Sci. Rev.*, *23*, 2141–2154, 2004.

Kim, J. H., H. Meggers, N. Rimbu, G. Lohmann, T. Freudenthal, P. J. Müller, and R. R. Schneider, Impact of the North Atlantic gyre circulation on Holocene climate off Northwest Africa, *Geology*, *35*, 387–390, 2007.

Kleidon, A., The climate sensitivity to human appropriation of vegetation productivity and its thermodynamic characterization, *Global and planetary change*, *54 (1-2)*, 109–127, 2006.

Kleidon, A., K. Fraedrich, and M. Heimann, A green planet versus a desert world: estimating the maximum effect of vegetation on the land surface climate, *Climatic Change*, *44*, 471–493, 2000.

Kleidon, A., K. Fraedrich, E. Kirk, and F. Lunkeit, Maximum entropy production and the strength of boundary layer exchange in an atmospheric general circulation model, *Geophys. Res. Lett.*, *33*, L06,706, 2006.

Kleidon, A., K. Fraedrich, and C. Low, Multiple steady-states in the terrestrial atmosphere-biosphere system: a result of a discrete vegetation classification, *Biogeosciences*, *4*, 707–714, 2007.

Klitgaard-Kristensen, D., H. P. Sejrup, H. Haflidason, S. Johnsen, and M. Spurk, A regional 8200 cal. yr BP cooling event in northwest Europe, induced by final stages of the Laurentide ice-sheet deglaciation?, *Journal of Quaternary Science*, *13 (2)*, 165–169, 1998.

Klocke, D., Assessing the uncertainty in climate sensitivity, Ph.D. thesis, University of Hamburg, 2011.

Klocke, D., P. Pincus, and J. Quaas, On constraining the effect of climate sensitivity with present-day observations through model weighting, *J. Clim.*, *24*, 6092–6099, 2011.

Kohfeld, K. E., and S. P. Harrison, How well can we simulate past climates? Evaluating the models using global palaeoenvironmental datasets, *Quaternary Science Reviews*, *19*, 321–346, 2000.

Köppen, W., *Das geographische System der Klimate*, *C*, vol. Bd. 1, Handbuch der Klimate, 1936.

Koster, R. D., and M. J. Suarez, A simple framework for examining the interannual variability of land surface moisture fluxes, *J. Climate*, *12*, 1911–1917, 1999.

Kottek, M., J. Grieser, C. Beck, B. Rudolf, and F. Rubel, World Map of the Köppen-Geiger climate classification updated, *Meteorol. Zeitschrift*, *15 (3)*, 259–263, doi:10.1127/0941-2948/2006/0130, 2006.

Kuo, H., On formation and intensification of tropical cyclones through latent heat release by cumulus convection, *J. Atmos. Sci.*, *22*, 40–63, 1965.

Kuo, H., Further studies of the parameterization of the influence of cumulus convection on large-scale flow, *J. Atmos. Sci.*, *31*, 1232–1240, 1974.

Kutzbach, J. E., and B. L. Otto-Bliesner, The sensitivity of the African-Asian monsoon climate to orbital parameter changes for 9000 years BP in a low-resolution general circulation model, *J Atmos Sci*, *39*, 1177–1188, 1982.

Lacis, A. A., and J. E. Hansen, A parameterization for the absorption of solar radiation in the Earth‘s atmosphere, *J. Atmos. Sci.*, *31*, 118–133, 1974.

Laepple, T., and G. Lohmann, Seasonal cycle as template for climate variability on astronomical timescales, *Paleoceanography*, *24*, PA4201, doi:10.1029/2008PA001674, 2009.

Laurent, J.-M., A. Bar-Hen, L. François, M. Ghislain, and R. Cheddadi, Refining vegetation simulation models: From plant functional types to bioclimatic affinity groups of plants, *J. Veg. Sci.*, *15 (6)*, 739–746, 2004.

Laurent, J.-M., L. François, A. Bar-Hen, L. Bel, and R. Cheddadi, European bioclimatic affinity groups: Data-model comparisons, *Global and Planetary Change*, *91*, 28–40, 2008.

Laursen, L., and E. Eliasen, On the effect of the damping mechanisms in an atmospheric general circulation model, *Tellus*, *41*, 385–400, 1989.

Lea, D. W., D. K. Pak, L. C. Peterson, and K. A. Hughen, Synchroneity of tropical and high-latitude Atlantic temperatures over the last glacial termination, *Science*, *301*, 2003.

Leduc, G., R. Schneider, J.-H. Kim, and G. Lohmann, Holocene and Eemian sea surface temperature trends as revealed by alkenone and Mg/Ca paleothermometry, *Quaternary science reviews*, *29 (7-8)*, 989–1004, 2010.

Leemans, R., and W. Cramer, The IIASA database for mean monthly values of temperature, precipitation and cloudiness on a global terrestrial grid, *Tech. Rep. IIASA-report RR-91-18*, International Institute for Applied System Analyses, 1991.

Lehman, S. J., and L. D. Keigwin, Sudden changes in North Atlantic circulation during the last deglaciation, *Nature*, *356*, 757–762, 1992.

Lemmen, C., World distribution of land cover changes during Pre- and Protohistoric Times and estimation of induced carbon releases, *Géomorphologie*, *4*, 303–312, 2009.

Lemmen, C., and K. W. Wirtz, *The Spread of the Neolithic to Central Europe*, chap. Socio-technological revolutions and migration waves re-examining early world history with a mathematical model, RGZM Tagungen, 2010.

Lemmen, C., D. Gronenborn, and K. W. Wirtz, A simulation of the Neolithic transition in Western Eurasia, *J. Archaol. Science*, *38*, 3459–3470, doi:10.1016/j.jas.2011.08.008, 2011.

Lettau, H., Evapotranspiration climatonomy: I. A new approach to numerical prediction of monthly evapotranspiration, run-off and soil moisture storage, *Mon. Wea. Rev.*, *97 (10)*, 691, 1969.

Li, B., D. W. Nychka, and C. M. Ammann, The Value of Multiproxy Reconstruction of Past Climate, *Journal of the American Statistical Association*, *105*, 883–895, doi:10.1198/jasa.2010.ap09379, 2010.

Li, W., C. E. Forest, and J. Barsugli, Comparing two methods to estimate the sensitivity of regional climate simulations to tropical SST anomalies, *J. Geophys. Res.*, *117 (D20)*, D20,103, doi:10.1029/2011JD017186, 2012.

Ljungqvist, F. C., P. J. Krusic, G. Brattström, and H. S. Sundqvist, Northern Hemisphere temperature patterns in the last 12 centuries, *Clim. Past*, *8*, 227–249, doi:10.5194/cp-8-227-2012, 2012.

Lohmann, G., Meteorologische Interpretation geologischer Daten-Neue Wege in der Paläoklimaforschung, *Promet*, *28*, 147–152, 2002.

Lohmann, G., M. Pfeiffer, T. Laepple, G. Leduc, and J.-H. Kim, A model-data comparison of the Holocene global sea surface temperature evolution, *Clim. Past Discuss.*, *8*, 1005–1056, doi:10.5194/cpd-8-1005-2012, 2012.

Lohmann, U., R. Sausen, L. Bengtsson, U. Cubasch, J. Perlwitz, and E. Roeckner, The Köppen climate classification as a diagnostic tool for general circulation models, *Clim. Res.*, *3*, 177–193, 1993.

Löptien, U., and E. Ruprecht, Effect of synoptic systems on the variability of the North Atlantic Oscillation, *Mon. Wea. Rev.*, *133*, 2894–2904, 2005.

Lorenz, S. J., and G. Lohmann, Acceleration technique for Milankovitch type forcing in a coupled atmosphere-ocean circulation-model: method and application for the Holocene, *Clim. Dyn.*, *23*, 727–743, 2004.

Lorenz, S. J., J.-H. Kim, N. Rimbu, R. R. Schneider, and G. Lohmann, Orbitally driven insolation forcing on Holocene climate trends: Evidence from alkenone data and climate modeling, *Paleoceanography*, *21 (1)*, PA1002, doi:10.1029/2005PA001152, 2006.

Louis, J.-F., A parametric model of vertical eddy fluxes in the atmosphere, *Boundary-Layer Meteorology*, *17*, 187–202, 1979.

Louis, J.-F., M. Tiedke, and J.-F. Geleyn, *Proceedings of the ECMWF Workshop on Planetary Boundary Layer Parameterization, Reading, 25-27 Nov. 1981*, in , pp. 59–80, 1982.

Lucarini, V., K. Fraedrich, and F. Lunkeit, Thermodynamic analysis of snowball earth hysteresis experiment: efficiency, entropy production, and irreversibility, *Q. J. R. Meterol. Soc.*, *136 (646)*, 2–11, 2010.

Lunkeit, F., M. Böttinger, K. Fraedrich, H. Jansen, E. Kirk, A. Kleidon, and U. Luksch, Planet Simulator, Reference Manual, Version 16.0, available from http://www.mi.uni-hamburg.de/Downloads-un.245.0.html [accessed 2010-08-24], 2010.

Luterbacher, J., D. Dietrich, E. Xoplaki, M. Grosjean, and H. Wanner, European seasonal and annual temperature variability, trends, and extremes since 1500, *Science*, *303*, 1499–1503, 2004.

Lyell, C., *Principles of Geology, An attempt to explain the former changes of the Earth's surface, by reference to causes now in operation*, vol. 1-3, 1830.

Lynch, A. H., A. R. Rivers, and P. J. Bartlein, An assessment of the influence of land cover uncertainties on the simulation of global climate in the early Holocene, *Clim. Dyn.*, *21 (3-4)*, 243–256, 2003.

Maier-Reimer, E., U. Mikolajewicz, and K. Hasselmann, Mean circulation of the Hamburg LSG OGCM and its sensitivity to the thermohaline surface forcing, *J. Phys. Oceanogr.*, *23 (4)*, 731–757, 1993.

Mann, M. E., S. Rutherford, E. Wahl, and C. Ammann, Testing the fidelity of methods used in proxy-based reconstructions of past climate, *J. Climate*, *18*, 4097–4107, 2005.

Mann, M. E., S. Rutherford, E. Wahl, and C. Ammann, Robustness of proxy-based climate field reconstruction methods, *J. Geophys. Res.*, *112*, D12,109, 2007.

Mann, M. E., Z. Zhang, M. K. Hughes, and R. S. Bradley, Proxy-based reconstructions of hemispheric and global surface temperature variations over the past two millennia, *Proc. Nat. Acad. Sci.*, *105 (36)*, 13,252–13,257, 2008.

Mann, M. E., G. A. Schmidt, S. K. Miller, and A. N. LeGrande, Potential biases in inferring Holocene temperature trends from long-term borehole information, *Geophys. Res. Lett.*, *36 (5)*, L05,708, doi: 10.1029/2008GL036354, 2009.

Marchal, O., I. Cacho, T. F. Stocker, J. O. Grimalt, E. Calvo, B. Martrat, N. Shackleton, M. Vautravers, E. Cortijo, S. van Kreveld, C. Andersson, N. Koç, M. Chapman, L. Sbaffi, J.-C. Duplessy, M. Sarnthein, J.-L. Turon, J. Duprat, and E. Jansen, Apparent long-term cooling of the sea surface in the

northeast Atlantic and Mediterranean during the Holocene, *Quaternary Science Reviews*, *21*, 455–483, 2002.

Martrat, B., J. O. Grimalt, N. J. Shackleton, L. de Abreu, M. A. Hutterli, and T. F. Stocker, Four climate cycles of recurring deep and surface water destabilizations on the Iberian Margin, *Science*, *27*, 502–507, 2007.

Marzin, C., and P. Braconnot, Variations of Indian and African monsoons induced by insolation changes at 6 and 9.5 kyr BP, *Clim. Dyn.*, *33*, 215–231, 2009.

Masson, V., R. Cheddadi, P. Braconnot, S. Joussaume, D. Texier, and P. participants, Mid-Holocene climate in Europe: What can we infer from PMIP model data comparisons?, *Clim. Dyn.*, *15*, 163–182, 1999.

Matthews, H. D., A. J. Weaver, K. J. Meissner, N. P. Gillett, and M. Eby, Natural and anthropogenic climate change: incorporating historical land cover change, vegetation dynamics and the global carbon cycle, *Clim. Dyn.*, *22 (5)*, 461–479, 2004.

Mayewski, P. A., E. E. Rohling, J. C. Sager, W. Karlén, K. A. Maasch, L. Meeker, E. A. Meyerson, F. Gasse, S. van Kreveld, K. Holmgren, J. Lee-Thorp, G. Rosqvist, F. Rack, M. Staubwasser, R. R. Schneider, and E. J. Steig, Holocene climate variability, *Quat. Res.*, *62*, 243–255, 2004.

Melillo, J. M., A. D. McGuire, D. W. Kicklighter, B. Moore, C. J. Vorosmarty, and A. L. Schloss, Global climate chnage and terrestrial net primary production, *Nature*, *363*, 234–235, 1993.

Micheels, A., and M. Montenari, A snowball Earth versus a slushball Earth: Results from Neoproterozoic climate modeling sensitivity experiments, *Geosphere*, *4 (2)*, 401–410, 2008.

Micheels, A., A. Bruch, and V. Mosbrugger, Miocene climate modelling sensitivity experiments for different CO_2 concentrations, *Palaeontologia Electronica*, *12 (2)*, 2009a.

Micheels, A., J. Eronen, and v. Mosbrugger, The Late Miocene climate response to a modern Sahara desert, *Global and Planetary Change*, *67*, 193–204, 2009b.

Milankovitch, M., *Mathematische Klimalehre und Astronomische Theorie der Klimaschwankungen*, Gebrüder Borntraeger, 1930.

Mitchell, J. F. B., N. S. Grahame, and K. J. Needham, Climate simulations for 9000 years before present - Seasonal Variations and effect of the Laurentide Ice-Sheet, *J. Geophys. Res.*, *93 (7)*, 8283–8303, 1988.

Mitchell, T. D., and P. D. Jones, An improved method of constructing a database of monthly climate observations and associated high-resolution grids, *International Journal of Climatology*, *25 (6)*, 693–712, 2005.

Moberg, A., D. M. Sonechkin, K. Holmgren, N. M. Datsenko, and W. Karlén, Highly variable Northern Hemisphere temperatures reconstructed from low-and high-resolution proxy data, *Nature*, *433*, 613–619, 2005.

Monserud, R. A., N. M. Tchebakova, and R. Leemans, Global vegetation change predicted by the modified Budyko model, *Clim. Change*, *25*, 59–83, 1993.

Mosbrugger, V., and T. Utescher, The coexistence approach-a method for quantitative reconstructions of Tertiary terrestrial palaeoclimate data using plant fossils, *Palaeogeogr., Palaeoclimatol., Palaeoecol.*, *134*, 61–86, 1997.

Nemry, B., L. M. François, P. Warnant, F. Robinet, and J.-C. Gérard, The seasonality of the CO_2 exchange between the atmosphere and the land biosphere: A study with a global mechanistic vegetation model, *J. Geophys. Res.*, *101 (D3)*, 7111–7125, 1996.

New, M., D. Lister, M. Hulme, and I. Makin, A high-resolution data set of surface climate over global land areas, *Clim. Res.*, *21*, 1–25, 2002.

Oglesby, R. J., T. L. Sever, W. Saturno, D. J. E. III, and J. Srikishen, Collapse of the Maya: Could deforestation have contributed?, *J. Geophys. Res.*, *115 (D12)*, D12,106, 2010.

Ol'dekop, E. M., On evaporation from the surface of river basins, Trans. Met. Obs., lur-evskogo, Univ. Tartu 4 in Russian, 1911.

Olofsson, J., and T. Hickler, Effects of human land-use on the global carbon cycle during the last 6,000 years, *Vegetation history and archaeobotany*, *17 (5)*, 605–615, 2008.

Olson, J. S., J. A. Watts, and L. J. Allison, Carbon in live vegetation of major world ecosystems, ORNL-5862, Oak Ridge National Laboratory, Oak Ridge, TN, 1983.

Olsson, F., M.-J. Gaillard, G. Lemdahl, A. Greisman, P. Lanos, D. Marguerie, N. Marcoux, P. Skoglund, and J. Wäglind, A continuous record of fire covering the last 10,500 calendar years from southern Sweden - The role of climate and human activities, *Palaeogeography, Palaeoclimatology, Palaeoecology*, *291*, 128–141, doi:10.1016/j.palaeo.2009.07.013, 2010.

Onogi, K., J. Tsutsui, H. Koide, M. Sakamoto, S. Kobayashi, H. Hatsushika, T. Matsumoto, N. Yamazaki, H. Kamahori, K. Takahashi, S. Kadokura, K. Wada, K. Kato, R. Oyama, T. Ose, N. Mannoji, and R. Taira, The JRE-25 Reanalysis, *Journal of the Meteorological Society of Japan*, *85 (3)*, 369–432, 2007.

Orszag, S. A., Transform Method for calculation of vector coupled sums, *J. Atmos. Sci.*, *27*, 890–895, 1970.

Otterman, J., M.-D. Chou, and A. Arking, Effects of nontropical forest cover on climate, *J. Clim. appl. Met.*, *23*, 762–767, 1984.

Otto, D., D. Rasse, J. Kaplan, P. Warnant, and L. François, Biospheric carbon stocks reconstructed at the Last Glacial Maximum: comparison between general circulation models using prescribed and computed sea surface temperatures, *Global and Planetary Change*, *33*, 117–138, 2002.

Pachauri, R. K., and A. Reisinger (Eds.), *IPCC, 2007: Climate Change 2007: Synthesis Report. Contribution of Working Groups I, II and III to the Fourth Assessment Report of the Intergovernmental Panel on Climate Change*, p. pp 104, IPCC, Geneva, Switzerland, 2007.

Pailler, D., and E. Bard, High-frequency paleoceanographic changes during the past 140,000 years recorded by the organic matter in sediments off the Iberian Margin, *Palaeogeography,Palaeoclimatology and Palaeoecology*, *181*, 431–452, 2002.

Peltier, W., Global Glacial Isostasy and the Surface of the Ice-Age Earth: The ICE-5G (VM2) Model and GRACE, *Ann. Rev. Earth and Planet. Sci.*, *32*, 111–149., 2004.

Perlwitz, J., M. Hoerling, J. Eischeid, T. Y. Xu, and A. Kumar, A strong bout of natural cooling in 2008, *Geophys. Res. Lett.*, *36*, L23,706, doi:10.1029/2009GL041188, 2009.

Petit, J. R., J. Jouzel, D. Raynaud, N. I. Barkov, J. M. Barnola, I. Basile, M. Bender, J. Chappellaz, M. Davis, G. Delaygue, M. Delmotte, V. M. Kotlyakov, M. Legrand, V. Y. Lipenkov, C. Lorius, L. Pepin, C. Ritz, E. Saltzman, and M. Stievenard, Climate and atmospheric history of the past 420,000 years from the Vostok ice core, Antarctica, *Nature*, *399*, 429–436, 1999.

Pike, J. P., The estimation of annual runoff from meteorological data in a tropical climate, *J. Hydrol.*, *2*, 116–123, 1964.

Pongratz, J., C. Reick, T. Raddatz, and M. Claussen, A reconstruction of global agricultural areas and land cover for the last millenium, *Global Biogeochemical Cycles*, *22*, 2008.

Pongratz, J., T. Raddatz, C. H. Reick, M. Esch, and M. Claussen, Radiative forcing from anthropogenic land cover change since A.D. 800, *Geophys. Res. Lett.,*, *36 (2)*, L02,709, 2009a.

Pongratz, J., C. H. Reick, T. Raddatz, and M. Claussen, Effects of anthropogenic land cover change on the carbon cycle of the last millennium, *Global Biogeochem. Cycles*, *23 (4)*, GB4001, 2009b.

Pongratz, J., C. H. Reick, T. Raddatz, and M. Claussen, Biogeophysical versus biogeochemical climate response to historical anthropogenic land cover change, *Geophys. Res. Lett.*, *37 (8)*, L08,702, 2010.

Prentice, I. C., W. Cramer, S. P. Harrison, R. Leemans, R. A. Monserud, and A. M. Solomon, A global biome model based on plant physiology and dominance, soil properties and climate, *J. Biogeogr.*, *19 (2)*, 117–134, 1992.

Prentice, I. C., J. Guiot, B. Huntley, D. Jolly, and R. Cheddadi, Reconstructing biomes from palaeoecological data: a general method and its application to European pollen data at 0 and 6 ka, *Clim. Dyn.*, *12 (3)*, 185–194, 1996.

Raymo, M. E., and K. Nisancioglu, The 41 kyr world: Milankovitch's other unsolved mystery, *Paleoceanography*, *18 (1)*, 1011, doi:10.1029/2002PA000791, 2003.

Reason, C. J. C., and H. M. Mulenga, Relationships between South African rainfall and SST anomalies in the SW Indian Ocean, *Int. J. Climatol.*, *19*, 1651–1673, 1999.

Reichert, B. K., L. Bengtsson, and O. Åkesson, A statistical modeling approach for the simulation of local paleoclimatic proxy records using general circulation model output, *Journal Geophys. Res.*, *104 (D16)*, 19,071–19,083, 1999.

Reichle, R. H., R. D. Koster, J. Dong, and A. A. Berg, Global soil moisture from satellite observations, land surface models, and ground data: Implications for data assimilation, *Journal of Hydrometeorology*, *5 (3)*, 430–442, 2004.

Renssen, H., H. Goosse, T. Fichefet, and J.-M. Campin, The 8.2 kyr BP event simulated by a global atmosphere-sea-ice-ocean model, *Geophys. Res. Lett.*, *28*, 1567–1570, 2001.

Renssen, H., H. Goosse, and T. Fichefet, Modeling the effect of freshwater pulses on the early Holocene climate: The influence of high-frequency climate variability, *Paleoceanography*, *17 (1020)*, doi:10.1029/2001PA000649, 2002.

Renssen, H., V. Brovkin, T. Fichefet, and H. Goosse, Holocene climate instability during the termination of the African Humid Period, *Geophysical Res. Lett.*, *30 (4)*, 1184, 2003.

Renssen, H., H. Goosse, T. Fichefet, V. Brovkin, E. Driesschaert, and F. Wolk, Simulating the Holocene climate evolution at northern high latitudes using a coupled atmosphere-sea ice-ocean-vegetation model, *Clim. Dyn.*, *24*, 23–43, 2005a.

Renssen, H., H. Goosse, T. Fichefet, V. Masson-Delmotte, and N. Koç, Holocene climate evolution in the high-latitude Southern Hemisphere simulated by a coupled atmosphere-sea ice-ocean-vegetation model, *The Holocene*, *15 (7)*, 951–964, 2005b.

Renssen, H., V. Brovkin, T. Fichefet, and H. Goosse, Simulation of the Holocene climate evolution in Northern Africa: The termination of the African Humid Period, *Quaternary international*, *150 (1)*, 95–102, 2006a.

Renssen, H., H. Goosse, and R. Muscheler, Coupled climate model simulation of Holocene cooling events: oceanic feedback amplifies solar forcing, *Clim. Past*, *2*, 79–90, 2006b.

Renssen, H., H. Seppä, O. Heiri, D. M. Roche, H. Goosse, and T. Fichefet, The spatial and temporal complexity of the Holocene thermal maximum, *Nature Geoscience*, *513*, 1–4, 2009.

Rimbu, N., G. Lohmann, S. J. Lorenz, and J. H. Kim, Holocene climate variability as derived from alkenone sea surface temperature and coupled ocean-atmosphere model experiments, *Clim. Dyn.*, *23*, 215–227, 2004.

Rind, D., D. Peteet, W. Broecker, A. McIntyre, and W. Ruddiman, The impact of cold North Atlantic sea surface temperatures on climate: implications for the Younger Dryas cooling (11-10k), *Clim. Dyn.*, *1*, 3–33, 1986.

Robert, A. J., A stable numerical integration scheme for the primitive meteorological equations, *Atmos. Ocean*, *19*, 35–46, 1981.

Rodrigues, T., J. O. Grimalt, F. G. Abrantes, J. A. Flores, and S. M. Lebreiro, Holocene interdependences of changes in sea surface temperature, productivity, and fluvial inputs in the Iberian continental shelf (Tagus mud patch), *Geochem. Geophys. Geosyst.*, *10*, Q07U06, doi:10.1029/2008GC002367, 2009.

Rodwell, M. J., D. P. Rowell, and C. K. Folland, Oceanic forcing of the wintertime North Atlantic Oscillation and European climate, *Nature*, *398*, 320–323, 1999.

Roe, G. H., and M. Baker, Why is climate sensitivity so unpredictable?, *Science*, *318*, 629–632, 2007.

Roeckner, E., K. Arpe, and L. Bengtsson, Simulation of present-day climate with the ECHAM model: Impact of model physics and resolution, *Tech. rep.*, 93, Max -Planck-Institut, Hamburg, Germany, 1992.

Roeckner, E., K. Arpe, L. Bengtsson, M. Christoph, M. Claussen, L. Dümenil, M. Esch, M. Giorgetta, U. Schlese, and U. Schulzweida, The Atmospheric General Circulation Model ECHAM-4: Model Description and Simulation of Present-Day Climate, *Tech. Rep. 218*, Max-Planck-Institut fuer Meteorologie, 1996.

Rohling, E. J., P. A. Mayewski, R. H. Abu-Zied, J. S. L. Casford, and A. Hayes, Holocene atmosphere-ocean interactions: records from Greenland and the Aegean Sea, *Clim. Dyn.*, *18*, 587–593, 2002.

Romanova, V., G. Lohmann, and K. Grosfeld, Effect of land albedo, CO_2, orography, and oceanic heat transport on extreme climates, *Clim. Past*, *2*, 31–42, 2006.

Romero, O. E., J.-H. Kim, and B. Donner, Submillennial-to-millennial variability of diatom production off Mauritania, NW Africa, during the last glacial cycle, *Paleoceanography*, *23*, PA3218, 2008.

Rozanski, K., L. Araguás-Araguás, and R. Gonfiantini, Relation between long-term trends of oxygen-18 isotope composition of precipitation and climate, *Science*, *258*, 981–985, 1992.

Ruddiman, W. F., *Earth's Climate: past and future*, W. H. Freeman and Company, 2000.

Ruddiman, W. F., The anthropogenic greenhouse era began thousands of years ago, *Clim. Change*, *61*, 261–293, 2003.

Rudloff, W., Weltklimate, *Naturwiss. Rdsch.*, *34*, 443–450, 1981.

Rühlemann, C., S. Mulitza, P. J. Müller, G. Wefer, and R. Zahn, Warming of the tropical Atlantic Ocean and slowdown of thermohaline circulation during the last deglaciation, *Nature*, *402*, 511–514, 1999.

Rutherford, S., M. E. Mann, T. J. Osborn, R. S. Bradley, K. R. Briffa, M. K. Hughes, and P. D. Jones, Proxy-based Northern Hemisphere surface temperature reconstructions: Sensitivity to method, predictor network, target season, and target domain , *J. Climate*, *18*, 2308–2329, 2004.

Sachs, J. P., Cooling of Northwest Atlantic slope waters during the Holocene, *Geophys. Res. Lett.*, *34*, L03,609, doi:10.1029/2006GL028495, 2007.

Sarnthein, M., S. van Kreveld, H. Erlenkeuser, P. M. Grootes, M. Kucera, U. Pflaumann, and M. Schulz, Centennial-to-millenial-scale periodicities of Holocene climate and sediment injections off the western Barents shelf, 75°N, *Boreas*, *32 (3)*, 447–461, 2003.

Sasamori, T., The radiative cooling calculation for application to general circulation experiments, *J. Appl. Meteor.*, *7*, 721–729, 1968.

Sausen, R., S. Schubert, and L. Dümenil, A model of river runoff for use in coupled atmosphere-ocean models, *J. Hydrol.*, *155*, 337–352, 1994.

Schmittner, A., T. A. M. Silva, K. Fraedrich, E. Kirk, and F. Lunkeit, Effects of mountains and ice sheets on global ocean circulation, *J. Climate*, *24*, 2814–2829, 2011.

Schneider, B., G. Leduc, and W. Park, Disentangling seasonal signals in Holocene climate trends by satellite-model-proxy integration, *Paleoceanography*, *25 (4)*, PA4217, doi:10.1029/2009PA001893, 2010.

Schreiber, P., Über die Beziehungen zwischen dem Niederschlag und der Wasserführung der Flüsse in Mitteleuropa, *Meteor. Z.*, *21*, 441–452, 1904.

Semtner, A. J. J., A Model for the Thermodynamic Growth of Sea Ice in Numerical Investigations of Climate, *J. Physic. Oceanogr.*, *3*, 379–389, 1976.

Seppä, H., A. E. Bjune, R. J. Telford, H. J. B. Birks, and S. Veski, Last nine-thousand years of temperature variability in Northern Europe, *Clim. Past*, *5 (3)*, 523–535, 2009.

Siegenthaler, U., and H. Oeschger, Correlation of δ^{18}O in precipitation with temperature and altitude, *Nature*, *285*, 314–317, 1980.

Simmons, A., and J. Gibson, ERA-40 Project report series. 1. ERA-40 Project Plan, ECMWF, workshop on Re-analysis, Reading, United Kingdom, ECMWF, 2000.

Simmons, A. J., B. Hoskins, and D. Burridge, Stability of the semi-implicit method of time integration, *Mon. Wea. Rev.*, *106*, 405–412, 1978.

Slingo, A., and J. M. Slingo, Response of the National Center for Atmospheric Research community climate model to improvements in the representation of clouds, *J. Geophys. Res.*, *96*, 341–357, 1991.

Stephens, G. L., Radiation profiles in extended water clouds. II: Parameterization schemes, *J. Atmos. Sci.*, *35*, 2123–2132, 1978.

Stephens, G. L., S. Ackermann, and E. A. Smith, A shortwave parameterization revised to improve cloud absorption, *J. Atmos. Sci.*, *41*, 687–690, 1984.

Sujatta, M., Snowball Earth experiments with the Planet Simulator, Master's thesis, Meteorological Institute, University of Hamburg, 2011.

Sundqvist, H. S., Q. Zhang, A. Moberg, K. Holmgren, H. Körnich, J. Nilsson, and G. Brattström, Climate change between the mid- and late Holocene in northern high latitudes – Part 1: Survey of temperature and precipitation proxy data, *Clim. Past*, *6*, 591–608, 2010.

Sutton, R. T., and D. L. R. Hodson, Influence of the Ocean on North Atlantic climate variability 1871-1999, *J. Climate*, *16*, 3296–3313, 2003.

Sutton, R. T., and D. L. R. Hodson, Atlantic ocean forcing of North American and European summer climate, *Science*, *309*, 115–118, 2005.

Taylor, K. E., D. Williamson, and F. Zwiers, *PCMDI Report Series*, in , 60, Program for Climate Model Diagnosis and Intercomparison, University of California, Lawrence Livermore National Laboratory, Livermore, CA, USA, 2000.

Tingley, M. P., P. F. Craigmile, M. Haran, B. Li, E. Mannshardt, and B. Rajaratnam, Piecing together the past: statistical insights into paleoclimatic reconstructions, *Quatern. Sci. Rev.*, *35*, 1–22, doi:10.1016/j.quascirev.2012.01.012, 2012.

Trewartha, G. T., *An Introduction to Climate*, 5th edn. ed., McGraw-Hill Book Co., New York, London, p. 437, 1980.

Turc, L., Le bilan d'eau des sols. Relation entre la précipitation, l'évaporation et l'écoulement, *Ann. Agron.*, *5*, 491–569, 1954.

Uppala, S. M., P. W. Kållberg, A. J. Simmons, U. Andrae, V. da Costa Bechtold, M. Fiorino, J. K. Gibson, J. Haseler, A. Hernandez, G. A. . Kelly, X. Li, K. Onogi, S. Saarinen, N. Sokka, R. P. Allan, E. Andersson, K. Arpe, M. A. B. lmaseda, A. C. M. Beljaars, L. van de Berg, J. Bidlot, N. Bormann, S. Caires, F. Chevallier, A. Dethof, M. Dragosavac, M. Fisher, M. Fuentes, S. Hagemann, E. Hólm, B. J. Hoskins, L. Isaksen, P. A. E. M. Janssen, R. Jenne, A. P. McNally, J.-F. Mahfouf, J.-J. Morcrette, N. A. Rayner, R. W. Saunders, P. Simon, A. Sterl, K. E. Trenberth, A. Untch, D. Vasiljevic, P. Viterbo, and J. Woollen, The ERA-40 re-analysis, *Quart. J. Roy. Meteor. Soc.*, *131*, 2961–3012, 2005.

Utescher, T., B. Erdei, L. M. François, and V. Mosbrugger, Tree diversity in the Miocene forests of Western Eurasia, *Palaeogeogr., Palaeoclimatol., Palaeoecol.*, *253*, 226–250, 2007.

van de Wal, R. S. W., B. de Boer, L. J. Lourens, P. Köhler, and R. Bintanja, Reconstruction of a continuous high-resolution CO_2 record over the past 20 million years, *Clim. Past*, *7*, 1459–1469, doi: 10.5194/cp-7-1459-2011, 2011.

van Wijk, V. M., S. Dekker, W. Bouten, F. Bosveld, W. Kohsiek, K. Kramer, and G. Mohren, Modeling daily gas exchange of a douglas-for forest: comparison of three stomatal conductance models with and without a soil water stress function, *Tree Physiol.*, *20*, 115–122, 2000.

von Grafenstein, U., H. Erlenkeuser, J. Müller, P. Trimborn, and J. Alefs, A 200 year mid-European air temperature record preserved in lake sediments: An extension of the $\delta^{18}O_p$-air temperature relation into the past, *Geochim. Cosmochim. Ac.*, *60 (21)*, 4025–4036, 1996.

von Grafenstein, U., H. Erlenkeuser, J. Müller, J. Jouzel, and S. Johnsen, The cold event 8200 years ago documented in oxygen isotope records of precipitation in Europe and Greenland, *Clim. Dyn.*, *14 (2)*, 73–81, 1998.

von Grafenstein, U., H. Erlenkeuser, A. Brauer, J. Jouzel, and S. J. Johnsen, A mid-European decadal isotope-climate record from 15,500 to 5000 years B.P., *Science*, *4 (284)*, 1654–1657, 1999.

von Grafenstein et al., U., Ammersee Ostracod Oxygen Isotope Data, IGBP PAGES/World Data Center for Paleoclimatology. Data Contribution Series. NOAA/NGDC Paleoclimatology Program, Boulder, CO, USA., 2003.

von Storch, H., E. Zorita, J. M. Jones, Y. Dimitriev, F. González-Rouco, and S. F. B. Tett, Reconstructing past climate from noisy data, *Science*, *306*, 679–682, 2004.

Wang, M., and J. E. Overland, Detecting arctic climate change using Köppen climate classification, *Clim. Change*, *67*, 43–62, 2004.

Wanner, H., J. Beer, J. Bütikofer, T. J. Crowley, U. Cubasch, J. Flückiger, H. Goosse, M. Grosjean, F. Joos, J. O. Kaplan, M. Küttel, S. A. Müller, I. C. Prentice, O. Solomina, T. F. Stocker, P. Tarasov, M. Wagner, and M. Widmann, Mid- to Late Holocene climate change: an overview, *Quatern. Sci. Rev.*, *27 (19-20)*, 1791–1828, 2008.

Warnant, P., Modélisation du cycle du carbone dans la biosphère continentale à l'échelle globale, Ph.D. thesis, Université de Liège, 1999.

Warnant, P., L. M. François, D. Strivay, and J.-C. Gérard, CARAIB: A global model of terrestrial biological productivity, *Global Biogeochem. Cycles*, *8 (3)*, 255–270, 1994.

Weldeab, S., R. R. Schneider, and P. Müller, Comparison of Mg/Ca-and alkenone-based sea surface temperature estimates in the fresh water-influenced Gulf of Guinea, eastern equatorial Atlantic, *Geochemistry, Geophysics, Geosystems*, *8 (5)*, Q05P22, doi:10.1029/2006GC001360, 2007.

Werner, M., P. M. Langebroek, T. Carlsen, M. Herold, and G. Lohmann, Stable water isotopes in the ECHAM5 general circulation model: Toward high-resolution isotope modeling on a global scale, *J. Geophys. Res.*, *116 (D15)*, D15,109, 2011.

Widmann, M., H. Goosse, G. van der Schrier, R. Schnur, and J. Barkmeijer, Using data assimilation to study extratropical Northern Hemisphere climate over the last millennium, *Clim. Past*, *6*, 627–644, 2010.

Wiersma, A. W., and H. Renssen, Model-data comparison for the 8.2 ka BP event: confirmation of a forcing mechanism by catastrophic drainage of Laurentide Lakes, *Quatern. Sci. Rev.*, *25*, 63–88, 2006.

Wilks, D. S., *Statistical methods in the atmospheric sciences, 2nd edition*, Academic Press, San Diego, 2006.

Wilson, R., E. Cook, R. D'Arrigo, N. Riedwyl, M. Evans, A. Tudhope, and R. Allan, Reconstructing ENSO: the influence of method, proxy data, climate forcing and teleconnections, *JQS*, *25 (1)*, 62–78, doi:10.1002/jqs.1297, 2010.

Wirtz, K. W., and C. Lemmen, A global dynamic model for the neolithic transition, *Clim. Change*, *59*, 333–367, 2003.

Wirtz, K. W., G. Lohmann, K. Bernhardt, and C. Lemmen, Mid-Holocene regional reorganization of climate variability: Analyses of proxy data in the frequency domain, *Palaeogeography, Palaeoclimatology, Palaeoecology*, *298*(3–4), 189–200, doi:10.1016/j.palaeo.2010.09.019, 2010.

Woodward, F. I., M. R. Lomas, and C. K. Kelly, Global climate and the distribution of plant biomes, *Phil. Trans. R. Soc. London Ser. B*, *359*, 1465–1476, 2004.

Wu, H., J. Guiot, S. Brewer, and Z. Guo, Climatic changes in Eurasia and Africa at the last glacial maximum and mid-Holocene: reconstruction from pollen data using inverse vegetation modelling, *Clim. Dyn.*, *29*, 211–229, 2007.

Xia, Y., K. Mitchell, M. Ek, B. Cosgrove, J. Sheffield, L. Luo, C. Alonge, H. Wei, J. Meng, B. Livneh, Q. Duan, and D. Lohmann, Continental-scale water and energy flux analysis and validation for North American Land Data Assimilation System project phase 2 (NLDAS-2): 2. Validation of model-simulated streamflow, *J. Geophys. Res.*, *117 (D3)*, D03,110, 2012a.

Xia, Y., K. Mitchell, M. Ek, J. Sheffield, B. Cosgrove, E. Wood, L. Luo, C. Alonge, H. Wei, J. Meng, B. Livneh, D. Lettenmaier, V. Koren, Q. Duan, K. Mo, Y. Fan, and D. Mocko, Continental-scale water and energy flux analysis and validation for the North American Land Data Assimilation System project phase 2 (NLDAS-2): 1. Intercomparison and application of model products, *J. Geophys. Res.*, *117 (D3)*, D03,109, 2012b.

Yurtsever, Y., Worldwide survey of stable isotopes in precipitation: Reports section isotope hydrology, *Tech. rep.*, International Atomic Energy Agency, 1975.

Zhang, Q., H. S. Sundqvist, A. Moberg, H. Körnich, J. Nilsson, and K. Holmgren, Climate change between the mid- and late Holocene in northern high latitudes - Part 2: Model-data comparisons, *Clim. Past*, *6*, 609–626, 2010.

Zhao, M., N. Beveridge, N. J. Shackleton, M. Sarnthein, and G. Eglinton, Molecular stratigraphy of cores off northwest Africa: sea surface temperature history over the last 80 ka, *Paleoceanography*, *10*, 661–675, 1995.

List of Figures

List of Tables

A Appendix

Additional figures of the interactive reconstruction

In Figure A.1, the individual *ITS*-time slices are again merged to give a complete overview of the Holocene temperature trend (cf. Fig. 5.4 and Fig. 5.15).

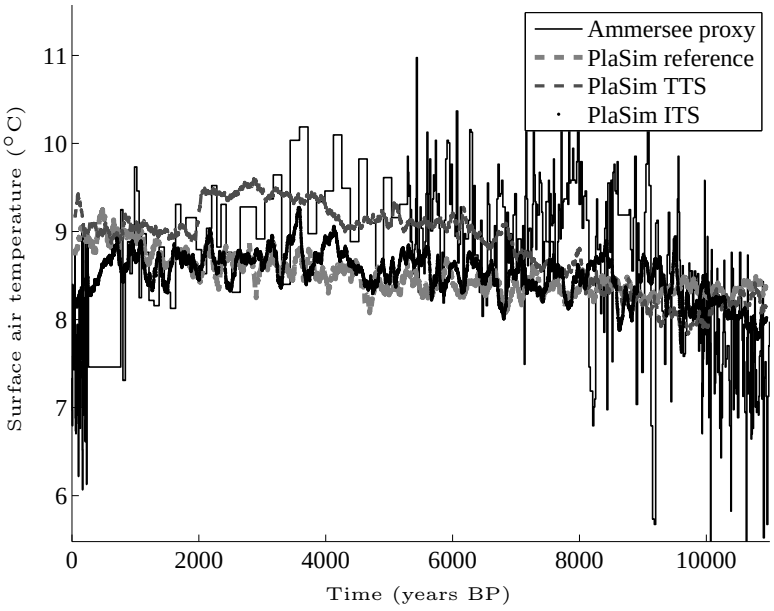

Figure A.1: Reconstructed annual mean surface air temperature [°C] for the Lake Ammersee proxy (solid black stairs) and the respective PlaSim time series (100 year running means) from 0 to 11 kyr BP; light gray: reference, medium gray: PlaSim *TTS*, black: PlaSim *ITS*.

The overall pattern confirms which has been indicated by the individual time slice means. Although each time slice mean could be slightly improved with regard to an approximation to the proxy mean, which was not always the case in the *TTS*-experiment, an only very reduced response caused by the interactive reconstruction and no significant improvement of the overall trend has to be asserted. The complete time series of this experiment and the reference are thus very close to each other and not at all capturing the Holocene climate optimum which is indicated by the proxy. The slight improvements which could be achieved in each time slice and thus no misdirecting adjustments are too weak to cause a corrected representation over the full Holocene.

Biome classification in the modified version of the Koeppen climate classification

In Table A.1, an overview is given of the biome classification used in the modified version of the Koeppen climate classification. Also included are the land surface parameters, i.e. albedo, roughness length, vegetation and forest cover, which are assigned to each individual biome.

Vegetation type	Koeppen class	alb	z0	c_v	c_f
Tropical rain forest	Ar	0.12	2.0	0.96	1.0
Tropical seasonal forest	Am	0.12	2.0	0.81	0.9
Savanna	Aw	0.15	0.361	0.6	0.6
Savanna	As	0.15	0.361	0.6	0.6
Warm grass/shrub	BS	0.20	0.10	0.29	0.0
Hot desert	BW	0.28	0.004	0.08	0.0
Warm mixed forest	Cr	0.15	0.716	0.83	0.8
Warm mixed forest and xerophytic woods/shrub	Cw	0.165	0.4135	0.715	0.5
Warm mixed forest and xerophytic woods/shrub	Cs	0.165	0.4135	0.715	0.5
Cool mixed forest and temperate deciduous forest	Do	0.155	1.0	0.55	1.0
Cool conifer forest	Dc	0.13	1.0	0.96	1.0
Cold mixed forest	Eo	0.15	1.0	0.51	1.0
Taiga	Ec	0.14	0.634	0.68	0.9
Tundra	FT	0.17	0.033	0.39	0.1
Polar desert	FI	0.15	0.001	0.0	0.0

Table A.1: Land surface parameters of the modified Koeppen climate classification, adapted to the study by *Claussen* (1994): albedo (alb), roughness length (z0), vegetation cover (c_v), forest cover (c_f).

Acknowledgments

At this stage I have the pleasure to acknowledge all people who supported me during the creation of my thesis. Unfortunately, I cannot name all of them.

At the very first place, I would like to thank my supervisor Klaus Fraedrich for giving me the opportunity to work in the Theoretical Meteorology department, providing me with his scientific advises and guidance. I am thankful for his time, his interest and his ongoing support throughout the last years. Moreover, I deeply acknowledge the continuous support of my co-advisor Richard Blender, for his helpful and always motivating discussions. This was sometimes surely not easy, especially during the last months due to several disappointing moments.

Special thanks also to Kai Wirtz for giving me the opportunity to work in his group at the HZG and also to Carsten Lemmen for providing the proxy data and for his ongoing support.

I gratefully thank Frank Lunkeit, Edilbert Kirk and Frank Sielmann for answering all my questions and problems related to model mysteries as well as their technical support when the computers decided to stop working. Many thanks also to the entire Theoretical Meteorology group for the nice working atmosphere during the past years.

I also like to thank Louis François for enabling me to spend several weeks in his group at the University of Liège and to work with the model CARAIB. In this context I would also like to thank Alexandra-Jane Henrot for her continuous support with the model, her help during my stay and the nice cooperation. Moreover, many thanks also to Guy Munhoven for his support and for proofreading parts of this thesis.

I also very much appreciate the financial support for this thesis, which was provided by the priority program INTERDYNAMIK of the German Research Foundation (DFG). In this context I want to give my thanks to the ECMWF for providing the reanalysis data.

On a more personal level, my very special thanks are also given to Andrea Schneidereit - thank you Johann for letting your mum proofread my thesis - and to Eileen Dahms, Anne Dallmeyer, Kathrin Riemann-Campe as well as Silke Schubert for their support and the enjoyable atmosphere inside and outside the office. It was always a lot of fun.

Finally, and most important, my very special thanks belong to my family and my friends. Many thanks to my parents and Martina for their ongoing material and non-material support, for always believing in me and encouraging me. I don't know what I would have done without you. I am deeply grateful for the special motivation skills of you, Luca, Kilian, Kolja and Alicia. Thank you for always being just yourself, which is the best recreation ever. Without all of you, this would

not have been possible and the thesis would have never ever come to an end.

Furthermore, on a completely other level, I thank whomsoever to make responsible for providing me with the abilities and passion for an activity that completely fulfills me, giving me the necessary balance from work and providing me to regain my motivation and enthusiasm. It has finally been through my running that I learnt to keep focussed and to never give up.

Anima sana in corpore sano

(mit freundlicher Genehmigung der ASICS Deutschland GmbH)